COLLEGE DOCTORAL PAYS DE LA LOIRE

ED EDUCATION, COGNITION, LANGAGES, INTERACTIONS, SANTE

Nantes Université

THESE DE DOCTORAT

NANTES UNIVERSITE

ECOLE DOCTORALE N° 603
Education, Cognition, Langages, Interactions, Santé
Spécialité : Sciences et Techniques des Activités Physiques et Sportives

Par
Valentin GOREAU

Non-invasive estimation of synaptic inputs to human spinal α-motoneurons: effects of joint position and central nervous system injury

Thèse présentée et soutenue **à Nantes, le 5 juin 2026**
Unité de recherche : **UR 4334, Laboratoire Motricité, Interactions, Performance**

Rapporteurs avant soutenance :

Véronique MARCHAND-PAUVERT - *Directrice de recherche, INSERM, Paris*
Stéphane BAUDRY - *Professeur, Université Libre de Bruxelles, Belgique*

Composition du Jury :

Présidente : Véronique MARCHAND-PAUVERT - *Directrice de recherche, INSERM, Paris*

Examinateurs : Gregory PEARCEY - *Assistant Professor, Memorial University of Newfoundland, Canada*
Påvel LINDBERG - *Directeur de recherche, INSERM, Paris*

Dir. de thèse : Raphaël GROSS - *Professeur, Nantes Université*

Co-dir. de thèse : Thomas CATTAGNI - *Maître de conférences, Nantes Université*
Guillaume LE SANT - *Enseignant-chercheur, Nantes Université*

Invité : François HUG - *Professeur, Université Côte d'Azur*

The work presented in this thesis is not the result of the efforts of a single individual. I would like to thank all those whose help and support have been invaluable.

First and foremost, I would like to express my gratitude to the members of my thesis committee. Professor Véronique Marchand-Pauvert and Professor Stéphane Baudry, thank you for agreeing to evaluate my work. I also thank Dr Greg Pearcey and Professor Pâvel Lindberg for serving as examiners on my committee. My thanks therefore go to all members of the committee for your time, your travel (sometimes from very far away), and for sharing your expert perspective on this work.

I would like to thank the members of my thesis monitoring committee, Professor David Gasq and Dr Sydney Grosprêtre, for your time, your insightful feedback, and your encouragement.

A special thank you to all the participants in the studies that make up this work. This included friends, family, colleagues, curious volunteers, and of course patients. Particular thanks go to the latter, whose lives have been marked by hardship yet who were willing to give out of pure generosity.

This work would not have been possible without the funding provided by IFM3R. I therefore thank this institution for its trust and for the opportunity to conduct research while teaching. Thank you to all colleagues for your welcome, your commitment to your work, and your kindness. Special mention goes to its two directors, Blandine Coadic and Myriam Thual, for their support, good humour, coffee, and chocolate. Thanks also to Yann Le Lay for his insights and his keen understanding of what my work entailed.

The work comprising this thesis was carried out within the Motricité, Interactions, Performance laboratory (UR 4334) at Nantes Université and is the result of a collective and collaborative effort. I will try to remain concise and therefore may not be able to fully express my gratitude to this laboratory and its “occupants”. Please know that every day of these five years at MIP was a pleasure, working alongside you, learning, laughing, and exercising together.

Above all, thank you to my supervisors.

Raphaël, despite your ministerial schedule, you managed to convey what mattered most: your trust. I knew I could move forward and that, if needed, you would be there. Thank you also for all the organisation surrounding the hospital-based studies, which, those who know, know, is no small task.

Guillaume, thank you for making this thesis possible and for ensuring that it unfolded under good conditions. Thank you for your kindness and your encouraging feedback. This thesis has taken a different direction from what was initially intended, but the journey is not over: Renfexc must go on.

Thomas, what years we have shared! We went through disappointments like the first failed attempt at securing funding; stressful moments, from “there are no patients at the hospital” to “they’re doing the same thing as us, we need to move fast”; and plenty of joy: successes, of course, but above all the daily exchange of ideas and testing them. In short, we were never bored. Thank you for sharing your knowledge as well as your doubts, for giving me a great deal of autonomy while never being far away, and for providing an ideal framework in which to grow.

François, you are not officially listed as a supervisor, but we will leave that to administration. Thank you for the time you spent correcting, refining, critiquing, and guiding this work. Thank you for your critical thinking and your talent for storytelling. Your feedback was always thorough and highly instructive. I fully appreciate how fortunate I have been to work with you and to learn from you.

Thank you to all the other members of MIP.

To my office 202 companions: Titouan, the “T”, Moriiiin; fortunately you were always in the corridors, otherwise it might have taken me two more years to finish this thesis. A PhD is about good humour, and muscular hypertrophy… at least in intention. Juliette, the “J”, research assistant and colour critic of figures, sharer of both successes and difficulties. A PhD is about sharing. Thanks to those who were there at the beginning, Julien and Iris, and to the next generation, Emma and Baptiste.

To my fellow PhD companions Hugo and Tristan, from the biomechanics–climbing–laughing office. To my younger PhD colleagues Yohan, Titouan M and Quentin, you are brilliant. To my recently graduated doctor friends Julian, Antoine F and Raphaël H, such dedication and kindness among the three of you; thank you for showing the way. To my faithful experimental partner Thomas L, what a struggle it would have been without you. To François D, I look forward to continuing to travel the world and ideas with you.

To those by whose offices I often found myself lingering, asking for scientific advice, or a game of padel, tennis, or a beer. Thank you to the “big brothers” Ricardo, Valentin D and Simon.

To the academic staff, who despite their status are more than approachable: thank you for the good humour and intellectual stimulation Sylvain, Lilian, Robin, Marion, Ricardo, Valentin R, Angèle, Julie, Benoît and our dear director Antoine N.

To those who make everything else easier: thank you Aurélie, Eva, and Gwen for your help.

To the (then) students who were invaluable to this work. Quentin, Louis, Anthony, and all the others, this work is yours as well.

Thank you also to all those who enabled me to reach this PhD. From the EFOM physiotherapy school, special thanks to Edson Gendrey, Alexandre Cazenoves, Thomas Osinski, Thomas Davergne, Céline Bonnyaud and Karine Langlois for their teaching. Thank you to the brilliant Bruno Falissard, whom I hope not to disappoint by choosing biology over statistics (though one can do both). Thank you Matthieu Guemman and Lilian Lacourpaille for opening the doors of research to me and confirming that this was where I belonged.

Thank you to my family and friends for supporting me and, at times, helping me forget about science. Thank you Maman for doing everything so that I could study in peace (this year was the last one).

The life of a researcher is probably not always easy, I guess. As for me, I have my novia Mar. Thank you for your help with this work: figures, proofreading, questions… Be aware that this person is capable of sending me scientific articles on MY research topic in the middle of the night. Thank you for your unwavering support and your love.

Thank you to everyone who takes the time to read this work. May the PICs be with you.

And finally, in French… Merci à tous !

THIS WORK HAS BEEN THE SUBJECT OF THE FOLLOWING PUBLICATIONS AND COMMUNICATIONS

Publications in peer-reviewed international scientific journals

Goreau, V., Morvan Q., Hug, F., Le Sant, G., Gross, R., & Cattagni, T. (2025). Muscle-length modulation of persistent inward currents in alpha motoneurons mediated by inhibitory inputs. *Journal of Neurophysiology*

Articles under review or in preparation

Goreau, V., Hug, F., Simon, L., Le Sant, G., Gross, R., & Cattagni, T. (2026). Disrupted Inhibitory-Excitatory Balance Underlies Spinal Motoneuron Dysfunction in Incomplete Spinal Cord Injury. *bioRxiv*, 2026-02.

Goreau, V., Cattagni, T., Hug, F., Le Sant, G., Gross, R. Reduced motoneuron rate coding after stroke is associated with increased inhibitory inputs despite increased neuromodulatory inputs. *In preparation.*

Oral presentations at international conferences

Goreau V, Hug F, Gross R, Le Sant G, Cattagni T. Incomplete Spinal Cord Injury: lost flexible control of Persistent Inward Currents? *International Motoneuron Society congress (St John's 2025)*

Goreau V, Morvan Q, Hug F, Gross R, Le Sant G, Cattagni T. Estimates of persistent inward currents in α-motoneurons of the gastrocnemius medialis and soleus muscles decrease with muscle lengthening positions. *International Motoneuron Society congress (Bordeaux 2024)*

Goreau V. Quand les Neurones Délibèrent: L'Art de l'équilibre entre Excitation et Inhibition Musculaire. *Journées francophones de kinésithérapie (Montpellier 2025)*

Publications in peer-reviewed international scientific journals not related to the PhD thesis

Goreau, V., Hug, F., Jannou, A., Dernoncourt, F., Crouzier, M., & Cattagni, T. (2023). Estimates of persistent inward currents in lower limb muscles are not different between inactive, resistance-trained and endurance-trained young males. *Journal of Neurophysiology*.

Le Sant, G., Lecharte, T., **Goreau, V**., Nordez, A., Gross, R., & Cattagni, T. (2023). Motor performance, motor impairments, and quality of life after eccentric resistance training in neurological populations: A systematic review and meta-analysis. *NeuroRehabilitation*

Oral presentations at international conferences not related to the PhD thesis

Goreau, V, Hug, F, Jannou, A, Dernoncourt, F, Crouzier, M, & Cattagni, T. Estimates of persistent inward currents in lower limb muscles are not different between inactive, resistance-trained and endurance-trained young males. *European Congress of Sport Science (Paris 2023)*

LIST OF ABREVIATIONS

SCI	Spinal Cord Injury
EMG	Electromyography
HDsEMG	High Density Surface Electromyography
GM	Gastrocnemius medialis
SOL	Soleus
TA	Tibialis Anterior
MUAP	Motor Unit Action Potential
MVT	Maximal Voluntary Torque
MVC	Maximal Voluntary Contraction
PICs	Persistent Inward Currents
5-HT	Serotonin
NE	Noradrenaline
GPCR	G protein–coupled receptors
RMS	Root Mean Square
PCA	Principal Component Analysis
EPSP	Excitatory Postsynaptic Potential
IPSP	Inhibitory Postsynaptic Potential
CST	Corticospinal Tract
RST	Reticulospinal Tract
CNS	Central Nervous System

TABLE OF CONTENTS

INTRODUCTION

Movement requires the contraction of muscles, which generate forces on bones and ultimately move joints. The human body comprises hundreds of joints and muscles, enabling a high degree of movement complexity. This diversity of movement relies on a highly complex "system of command": the central nervous system and its almost 100 billions of neurons. Damage to the central nervous system disrupts this command and leads to significant movement impairments, as observed after stroke and spinal cord injury (SCI), the two conditions investigated in this thesis.

How can we make sense of damage affecting several billion neurons, all more or less interconnected and linked to the rest of the nervous system? In particular, where should we look within the central nervous system to explain the limited motor behaviour observed after injury? A wide range of methodological approaches address how brain and spinal networks are altered. However, translating this knowledge into understanding of behavioural impairment requires to describe how information from these networks is integrated into a coordinated motor output.

All motor commands ultimately converge on motoneurons, which ultimately drive muscle contraction (Heckman & Enoka, 2012). Accordingly, spinal motoneurons that innervate muscle fibres (α-motoneurons, referred to simply as a motoneuron in this thesis) have been referred to as the "final common pathway" of the motor system (Liddell & Sherrington, 1925). This raises the question of how a lesion of the central nervous system, affecting massive and interconnected networks, translates into specific output alterations. Thus, motoneurons constitute a special site for quantifying alterations that underlie motor impairments. The assessment of motoneurons has a history spanning more than a century. However, a methodological shift occurred in the 2010s with the advent of electromyographic decomposition of individual motoneuron behaviour from high-density recording (Farina & Holobar, 2016; Negro, 2016). This approach now enables the non-invasive assessment of the activity of tens of motoneurons, opening up the possibility of population-level analyses of motoneurons.

Beyond improving quantification of motoneurons behaviour, access to large populations of motoneuron activity provides indirect insight into motor command organisation. Indeed, the different types of inputs converging onto the motoneuron leave specific signatures in motoneuron behaviour. This makes it possible to infer key aspects of the synaptic inputs and to determine

how the inputs shaping motoneuron firing behaviour differ between individuals with stroke or SCI and those of healthy controls (Beauchamp, Pearcey, et al., 2023; Chardon et al., 2024; Johnson et al., 2017; Powers & Heckman, 2017). Therefore, this perspective begins at the final stage of the motor system and moves upstream towards the inputs underpinning it. Although not exhaustive of the processes leading to motor output, it uniquely informs on the final effective inputs influencing motoneurons.

The "types of inputs" referred to here are the three categories of synaptic inputs that determine whether and how motoneurons discharge. The first, and historically the earliest identified, are excitatory and inhibitory inputs. Excitatory inputs are required to activate motoneurons and their intensity further regulates the level of motoneuron activity. Conversely, inhibitory inputs oppose excitatory inputs by restraining motoneuron activity. Both of these influences are driven by multiple motor pathways. The third category comprises neuromodulatory inputs. Although originating from a single descending pathway, these inputs alter the input–output relationship of motoneurons and are therefore critical for integrating synaptic inputs into motoneuron output. Importantly, neuromodulatory inputs leave identifiable signatures in motoneuron discharge, facilitating the inference of synaptic command from motoneuron activity (Chardon et al., 2024). This framework now provides a unique opportunity to investigate how alterations in motor pathways following central nervous system damage reorganise the synaptic inputs received by motoneurons during voluntary contractions, thereby constraining motor output.

The overall aim of this thesis was to improve understanding of synaptic input organisation in individuals with stroke and SCI during voluntary contraction in plantar flexor muscles, with particular emphasis on muscle length.

This document includes four main sections. The first section presents a literature review on: (1) movement impairments after SCI and stroke, with emphasis on paresis and muscle length; (2) the descending and spinal control of motoneurons in health and after SCI and stroke; and (3) synaptic inputs to motoneurons and their integration. The second section describes the overall experimental methods used in the experimental studies. The third includes the three experimental studies conducted during the PhD. The fourth section provides a general discussion of the findings, their implications, and future directions for research in this field.

◥ PART 1: MOVEMENT IMPAIRMENTS AFTER SCI AND STROKE WITH EMPHASIS ON PARESIS AND MUSCLE LENGTH

1. Essentials on epidemiology, pathophysiology and classification

1.A. SCI

1.A.1 Definition and epidemiology

The term SCI refers to damage to the spinal cord. SCI can cause paralysis, sensory disorders, pain, bladder and bowel dysfunction, respiratory impairment and troublesome dysautonomia, with subsequent disability and impact on quality of life. SCI can have traumatic or non-traumatic causes. By definition, traumatic causes result in acute onset, whereas non-traumatic causes may present with acute, subacute, or chronic onset. Traumatic causes include motor vehicle accidents (36–48%), violence (5–29%), falls (17–21%), and recreational activities (7–16%) (Kang et al., 2017; McDonald & Sadowsky, 2002). Non-traumatic causes include degeneration (e.g., spinal stenosis), infection, transverse myelitis, tumour compression, and vascular ischaemia (McDonald & Sadowsky, 2002).

In developed countries, and depending on the study, the incidence for traumatic SCI ranges from 13.1 to 163.4 per million population, the prevalence from 490 to 526 per million, and mortality from 3.1% to 22.2% (Kang et al., 2018). Some estimates suggest that the prevalence of non-traumatic spinal cord injuries is more than four times that of traumatic injuries, but it remains difficult to measure because of heterogeneous aetiologies (McDonald & Sadowsky, 2002). SCI imposes substantial economic costs. For example, the average lifetime cost per person with traumatic spinal-cord injury is between US$500 000 and $2 million, depending on factors such as extent and location of injury; and total direct costs of caring for individuals with spinal-cord injury exceed $7 billion per year in the USA (DeVivo, 1997).

A recent study conducted in France and benefiting from the The French Public Health Insurance database allowed precise estimation of different features (Duchaine et al., 2024). In 2019, 140 000 persons were living with SCI in France, 20 000 being confirmed as post-traumatic SCI (and up to 55 000 but with a certain degree of uncertainty) of whom 70 % were paraplegics and 30

% tetraplegics; 44.2 % were women and median age was 57 [IQR 44–70]. The age at first identification of a SCI showed 3 peaks for 3 clusters of subpopulations (around 0; 20; and 50 years old). Regarding the etiology, the most important category was the acquired non-traumatic subgroup (n=62 561, 46.7%), followed by the symptomatic (i.e., no defined etiology) subgroup (n=34 590, 25.8%), and traumatic (n=21 459, 16.0%). Congenital, genetic and tumours accounted respectively for 6.6%, and 2% each of the overall population. Women prevailed over men in congenital and tumoral categories (57 and 54% respectively) and men were largely overrepresented in the traumatic category (67%) (Fig. 1).

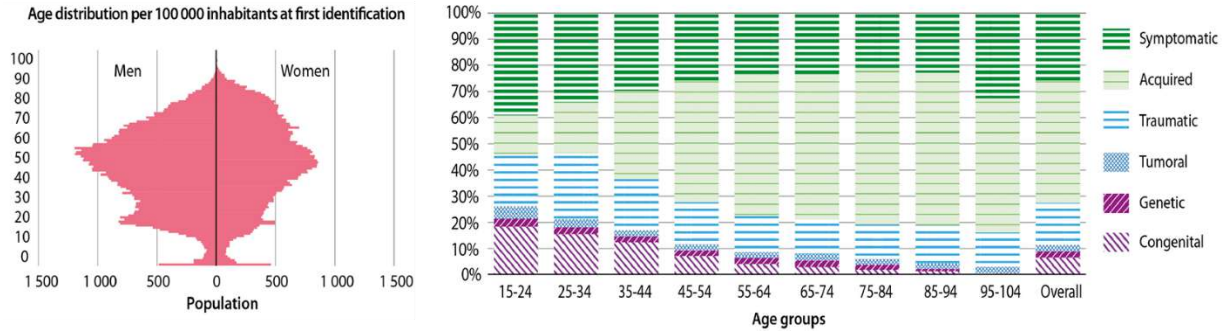

Figure 1. Epidemiology of SCI. *Age and sex repartitions at first identification within the time-period 2012–2019 by the algorithm (left) and age repartition of the SCI population by cause (right). Adapted from Duchaine et al. (2024).*

1.A.2 Pathophysiology

Initial mechanical trauma includes traction and compression forces. Direct compression of neural elements by fractured and displaced bone fragments, disc material, and ligaments injures both the central and peripheral nervous systems. Blood vessels are damaged, axons disrupted, and neural-cell membranes broken. Microhaemorrhages occur within minutes in the central grey matter and spread radially and axially over the next few hours. In case of extended initial damage, within minutes, the spinal cord swells to occupy the entire diameter of the spinal canal at the injury level. Secondary ischaemia, potentially extensive, results when cord swelling exceeds venous blood pressure. Autoregulation of blood flow ceases, and spinal neurogenic shock leads to systemic hypotension, thus exacerbating ischaemia. Ischaemia, release of toxic chemicals from disrupted neural membranes, and electrolyte shifts trigger a secondary injury cascade that substantially compounds initial mechanical damage by harming or killing neighbouring cells (McDonald & Sadowsky, 2002). Secondary injury involves cell death through excitotoxicity, a phenomenon from which knowledge comes largely from stroke and will thus be described in the pathophysiology of stroke section.

The spinal cord is composed of neurons (motoneurons, interneurons) that notably receive inputs from descending centres (corticospinal, reticulospinal – detailed in Part 2). These descending inputs remain intact above the lesion, but are reduced at the lesion epicentre due to axon disruption and/or demyelination (Fig. 2). Spinal segments below the injury may receive no descending inputs or a more or less preserved inputs, leading to paresis. At the damaged spinal levels, motoneuron death will induce denervation, although axons of functional or paralysed motor units may sprout to recover muscle innervation. Ascending input is often intact below the lesion. Spinal segments above the lesion and supraspinal structures receive less or no ascending input (Thomas et al., 2014).

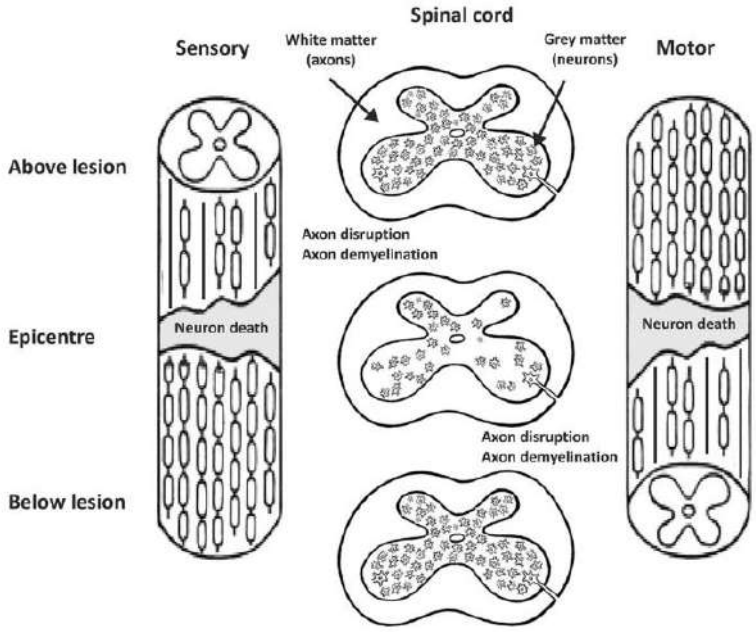

Figure 2. Schematic physiopathology of spinal cord injury. *Motor function remains intact above the lesion (right). At the lesion epicentre, there is disruption and demyelination of axons (white matter), as well as neuron death (grey matter). This reduces or eliminates descending (Motor) inputs to the lesion epicentre and lower spinal segments, and ascending inputs (Sensory) to segments above the lesion and supraspinal structures. Function of muscles innervated from damaged spinal levels will largely depend on the fraction of motor units that remain under voluntary control vs. paralysed (partially paralysed muscles, right). Adapted from Thomas et al. (2014).*

1.A.3 Classification

For standardisation purposes, the American Spinal Injury Association introduced the ASIA Impairment Scale (AIS) (Steeves et al., 2007). This scale includes sensory testing in twenty-eight dermatomes, assessment of ten key muscles of the upper and lower limbs bilaterally, as well as the assessment of motor and sensory anal function. It yields a five-grade classification, from

AIS A (most severe, complete lesions) to AIS E (recovery of normal function) (Table 1). Motor-complete injuries (AIS A or B) are more frequent in traumatic SCI, whereas motor-incomplete injuries (AIS C or D) predominate in non-traumatic SCI (Kang et al., 2018). Patients with AIS grades A and D have the lowest (8.3%) and highest (97.3%) probability, respectively, of walking independently one year after injury (EM-SCI Study Group et al., 2009).

The AIS notably defined (1) the sensory level, which is the most caudal dermatome with normal function for both pin prick (sharp/dull discrimination) and light touch sensation; (2) the motor level, which is the lowest key muscle function that has a grade of at least 3/5 (on manual muscle testing) and all segments above that level are 5/5; and (3) the neurological level of injury, which is the most cranial segment of the left and right sensory and motor level determined (Rupp et al., 2021).

Table 1. ASIA impairment scale

Grade	Description
A	Complete; no sensory or motor function preserved in the sacral segments S4-S5
B	Incomplete; sensory but not motor function preserved below the neurological leveland extending through the sacral segment S4-S
C	Incomplete; motor function preserved velow the neurological level; most key muscles have a grade < 3
D	Incomplete; motor function preserved velow the neurological level; most key muscles have a grade > 3
E	Normal motor and sensory function

Incomplete SCI gives rise to distinct syndromes depending on the transverse localisation of the lesion. Two such syndromes, identified in some participants of the PhD studies, are anterior cord syndrome and Brown-Séquard syndrome. Anterior cord syndrome is characterised by damage to the anterior two-thirds of the spinal cord (Fig. 3), typically due to reduced or absent blood supply, often following flexion injuries (Rupp et al., 2021). The corticospinal and spino-thalamic tracts are compromised, resulting in loss of motor function, pain, and temperature sensation at and below the level of injury (Rupp et al., 2021). Light touch and joint position sense are preserved. Brown-Séquard syndrome results from unilateral damage of the spinal cord. It presents with ipsilateral loss of proprioception, vibration, and motor control at and below the lesion, sensory loss at the level of the lesion, and contralateral loss of pain and temperature sensation below the neurological level of injury.

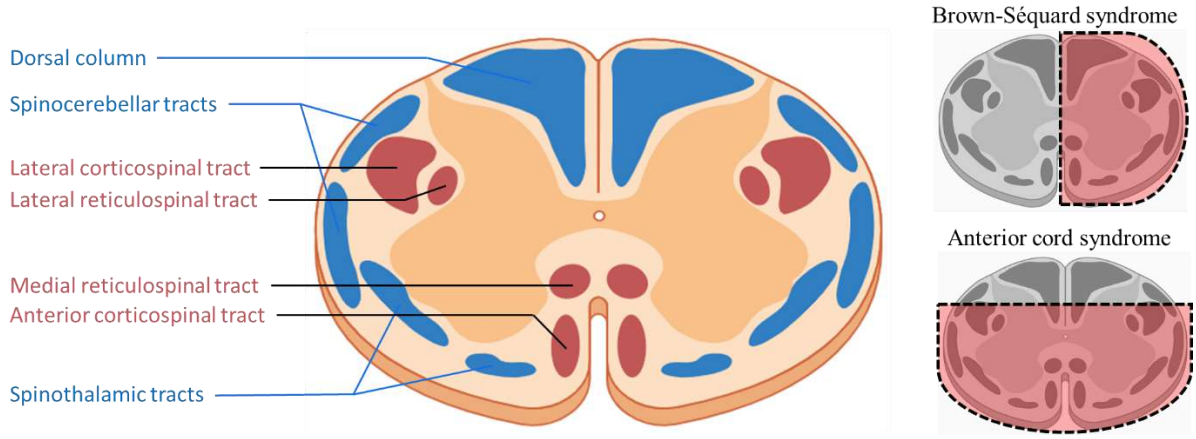

Figure 3. Major ascending and descending pathways. *Cross-sectional spinal cord diagram illustrating the main ascending and descending pathways (left) and specific SCI syndromes (right).*

1.B. Stroke

1.B.1 Definition and epidemiology

The World Health Organisation defines stroke as a "neurological deficit of cerebrovascular cause that persists beyond 24 hours or is interrupted by death within 24 hours". The 24-hour threshold distinguishes stroke from transient ischaemic attack, a related syndrome in which symptoms resolve completely within 24 hours (Donnan et al., 2008).

Strokes are classified as ischaemic or haemorrhagic. The most common type is ischaemic stroke, caused by interruption of blood flow to a specific brain region, and it accounts for approximately 80% of acute strokes (Thrift et al., 2001). The TOAST classification system identifies the mechanism leading to vessel occlusion (cardioembolic, artery-to-artery embolism, or in-situ small-vessel [lacunar] disease) (Adams et al., 1993). In haemorrhagic stroke, the most frequent mechanism is hypertensive small-vessel disease, leading to lipohyalinotic aneurysm formation and subsequent rupture (Donnan et al., 2008). Because management differs substantially between subtypes, their rapid clinical differentiation is a critical step in acute stroke care.

Stroke is the second leading cause of death worldwide, with an age-standardised mortality rate of 75.9 deaths (67.8–83.5) per 100,000 population in 2023 (GBD 2023 – Naghavi et al., 2025). The global prevalence is 93.8 million individuals, with an incidence of 11.9 million events per year (GBD 2021 – (Feigin et al., 2024)). The major modifiable risk factors are hypertension, diabetes mellitus, tobacco smoking, and hyperlipidemia, as well as lifestyle factors, such as obesity, poor diet/nutrition, and physical inactivity (Guzik & Bushnell, 2017). Stroke induces

large costs. For example, the average lifetime cost per person of first strokes occurring is around US$100 000 across all stroke subtypes and the corresponding aggregate lifetime cost associated was $40.6 billion.

1.B.2 Pathophysiology

Interruption of blood flow with ischaemic stroke leads to a loss of blood supply to part of the brain and induces primary cell death followed by secondary injury events, reactive tissue progenitor responses, and formation of new neuronal circuits (Fig. 4). This progression is radial: the tissue that suffers the infarct and secondary injury radiates signals out to the surrounding tissue, including free radicals, inflammatory cytokines, and synchronised electrical activity. Thus, stroke can be conceived as a site of complete cellular death surrounded by zones of damage and of tissue reorganisation. In addition to the radial diffusion of signals from the injured region to surrounding intact tissue, damage signals in stroke are relayed through neuronal connections. This is because dying tissue includes both the axons of distant neurons that projected to that tissue and the projections of neuronal cell bodies located within the dying area. This means that dying neurons relay signals of their death through their degenerating connections to distant sites like ipsilesional motor cortical areas, basal ganglia, brainstem, and thalamus or even spinal cord (Carmichael, 2016).

The initial cell death is due to neuronal excitotoxicity. Neurons devote a substantial amount of energy to maintain ion gradients through the sodium/potassium pump, for this gradient is needed to fire action potentials. When ischaemia depletes adenosine triphosphate (ATP), neurons cannot maintain this sodium/potassium gradient, which results in depolarisation that opens voltage-dependent calcium channels. Excessive calcium in the cell leads to dysfonction of mitochondria, proteolysis, lipolysis and DNA degradation, ultimately resulting in cell death. This process is called neuronal excitotoxicity and is quickly irreversible (Carmichael, 2016). However, the tissue around the infarct core has reduced blood flow but is not yet irreversibly damaged. Tissue repair and recovery depend in large part on what happens adjacent to the stroke core and preserving this area is a main objective in the emergency stroke care (Rosso & Samson, 2014). In this context, the ischaemic penumbra designates the brain tissue that is not initially damaged by stroke but will progress to infarction over time if therapy is not initiated. Importantly, secondary injury cascades occur in the penumbra with a paradoxical effect: signals that mediate cell death during the acute stage of stroke might in fact promote repair during the recovery phase through neurogenesis, axonal sprouting and new connections (Lo, 2008).

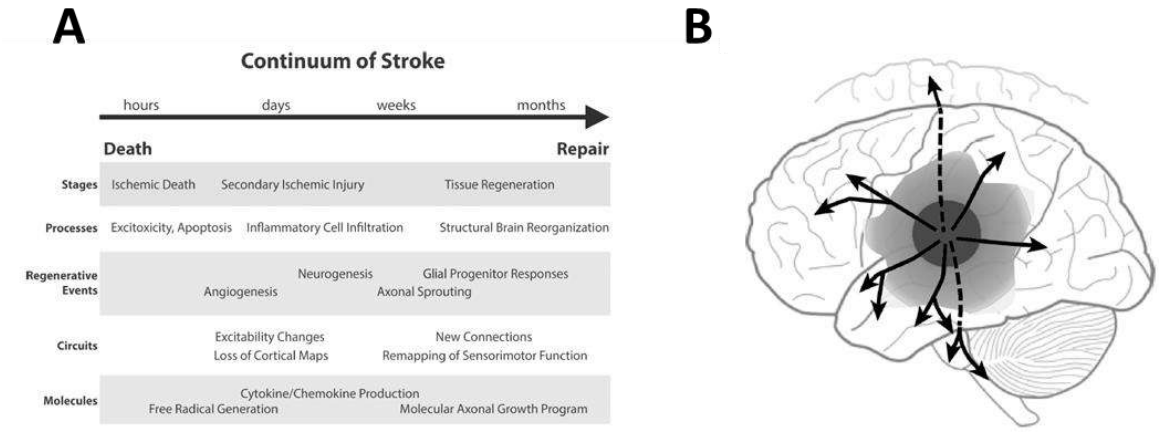

Figure 4. Schematic physiopathology of stroke. *(A) The events from damage to repair can be conceived as a continuum. Below the arrow, each horizontal row progresses, from top to bottom, to an increasingly small scale of event, from stages of tissue responses down to molecules within these responses, and organises these along a timeline. All events can be organised on a macro scale into stages of initial damage, secondary damage, and repair. At the other end of the spectrum, distinct classes of molecules participate in each point along the time continuum of stroke. (B) Stroke damage and secondary injury is relayed from the stroke core in a radial manner into peri-infarct tissue. Stroke kills not only neurons in the stroke core but also their axons, which means that degenerating axons and lost synaptic contacts occur in the brain areas and more distantly connected areas, including the spinal cord. Adapted from Krakauer & Carmichael (2017).*

Haemorrhagic stroke can also cause primary and secondary brain injury. The immediate effects, such as hematoma expansion and the consequent increase in intracranial pressure, lead to primary injury, whereas subsequent effects, such as inflammation, contribute to secondary injury. Inflammation is characterised by the accumulation and activation of inflammatory cells and mediators within the haemorrhagic brain. Intracerebral haemorrhage allows the immediate infiltration of blood components, including red blood cells, leukocytes, macrophages, plasma proteins into the injury site. The inflammatory response that follows this infiltration involves inflammatory mediator release, protease activation, microglia and astrocyte activation, brain tissue breakdown, and repair (Li et al., 2010).

1.B.3 Classification

The human brain can be subdivided into a mosaic of anatomically and functionally distinct, spatially contiguous areas (Glasser et al., 2016). Consequently, strokes present as stereotyped clinical syndromes reflecting reduced blood flow to specific brain regions that correspond to neurological findings. As this thesis focuses on distal lower-limb muscles, only a limited number of stroke locations are relevant to such paresis (Fig. 5). The primary motor cortex

representation of the lower limb is located on the medial surface of the frontal lobe, within the paracentral lobule. This region is supplied predominantly by the anterior cerebral artery. However, lower-limb muscles may also be affected by extension of infarction in another vascular territory, typically the middle cerebral artery, either through involvement of the ischaemic penumbra (Lo, 2008) or expansion of a haematoma in haemorrhagic stroke. In addition, limb muscles may be affected by subcortical lesions, particularly of the internal capsule, through which descending corticospinal fibres pass. Lesions of the left hemisphere produce right-sided lower-limb deficits, and vice versa. Deficits typically affect one side of the body, referred to as hemiparesis, in contrast to spinal cord injuries, which are often bilateral, reflecting the anatomical narrowness of the spinal cord.

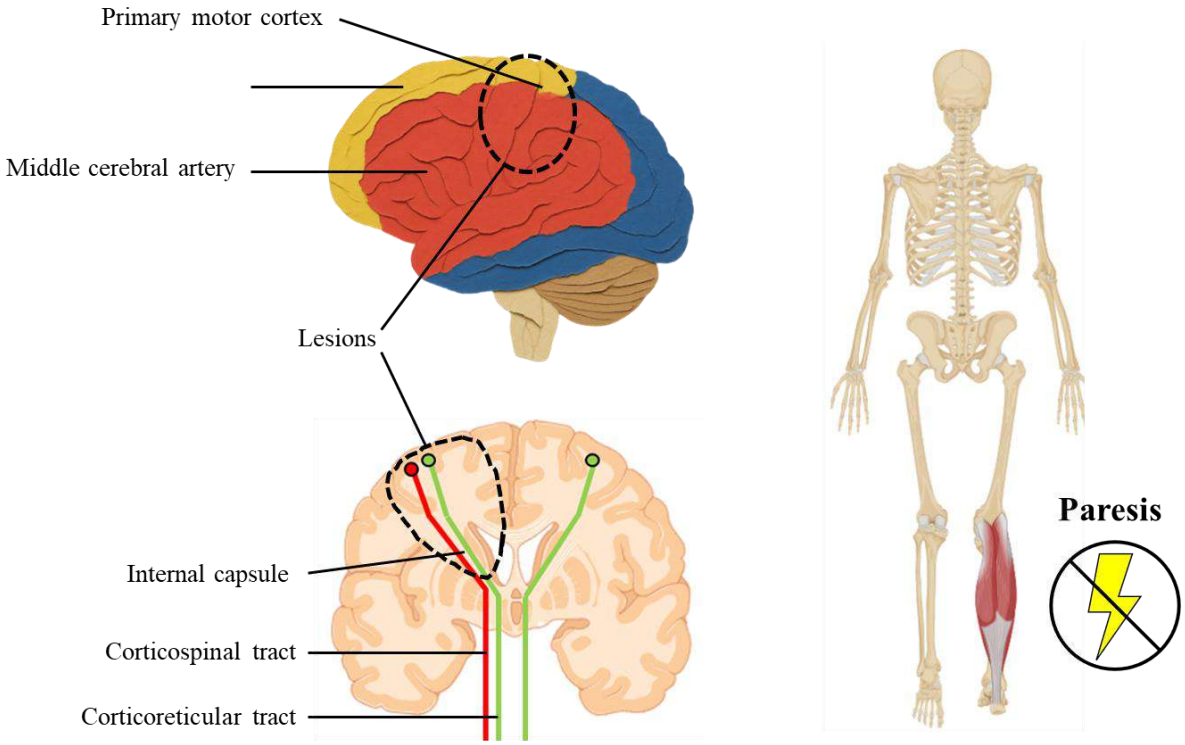

Figure 5. Main regions associated with plantar flexor paresis following stroke. *Paresis of the plantar flexors can result from stroke in the anterior cerebral artery, which supplies the lower-limb representation of the primary motor cortex, or from extension of infarction into another vascular territory, typically the middle cerebral artery. In addition, stroke affecting the internal capsule, through which descending pathways such as the corticospinal and corticoreticular tracts pass, can also lead to plantar flexor paresis.*

2. Voluntary movement impairment after SCI and stroke

As separate entities, SCI and stroke have been presented independently. However, they share several common features related to impairments in voluntary movement and will therefore be addressed together below.

2.A. Definition of movement impairment

The World Health Organisation, in collaboration with the International Society of Physical and Rehabilitation Medicine, developed the International Classification of Functioning, Disability and Health in 2001 (Leonardi et al., 2022). At the highest level, the classification distinguishes between functioning and disability. These are complementary terms: one emphasises gains and the other losses across three hierarchical levels: impairment, activity limitation, and participation restriction. Impairment refers to problems in body structure or function. Activity limitation denotes reduced ability to perform a task or action. Participation restriction, which replaced the term handicap, refers to reduced involvement in social situations. Following stroke or SCI, muscle weakness may be compensated for by use of the less affected limb or assistive devices, thereby limiting activity restriction. Activity limitation may in turn restrict participation; however, compensatory strategies (e.g., wheelchair use) may mitigate participation restriction. In contrast, repair and reorganisation mechanisms primarily operate at the impairment level, which is the focus of this thesis.

2.B. Weakness

In motor impairment following SCI or stroke, deficits include reduced force generation (weakness) and impaired motor control such as speed, accuracy or coordination. Weakness is arguably the most prominent component of the motor phenotype. For example, in the NIH Stroke Scale (NIHSS), motor items primarily assess strength rather than control; the same applies to the ASIA assessment for SCI. Several arguments support this emphasis. Methodologically, weakness is straightforward to quantify, which favours its clinical use. In addition, weakness is the dominant contributor to movement impairment in the acute phase, whereas motor control deficits often emerge later, alongside plastic reorganisation (Hiersemenzel et al., 2000; Levin et al., 2009). Moreover, motor control presupposes sufficient force production; without strength, coordination cannot be meaningfully expressed. Weakness therefore constitutes the foundation of other dimensions of movement impairment. Notably, plantarflexion weakness, which is the

focus of this thesis, leads to a substantial loss of forward propulsion during walking and is commonly observed in both pathologies (Dorsch et al., 2016; Moore et al., 2015; Williams et al., 2019).

2.B.1 Paresis

Weakness results primarily from impairment of upper motor neurons, which limits muscle activation. To characterise the deficit in voluntary muscle activation, we use the term "paresis". The most appropriate method to quantify the neural component of weakness (i.e., paresis) is the application of supramaximal electrical stimulation during maximal voluntary contraction (twitch interpolation). The ratio of peak voluntary torque to peak superimposed torque provides an estimate of voluntary activation (%), which is distinct from intrinsic muscle strength. This assessment has been performed in individuals with incomplete SCI, showing substantial deficits in plantar flexors, with voluntary activation levels of 53 ± 6% on the less affected side and 36 ± 8% on the more affected side (Jayaraman et al., 2006). Similar findings have been reported for the knee extensors (Jayaraman et al., 2006; H. E. Kim et al., 2015) and the flexor carpi radialis (Lin et al., 2012). In stroke plantar flexors, voluntary activation on the paretic side has been reported as 48.5 ± 36.9% (range 0–92%), compared with 96.8 ± 1.9% on the non-paretic side (Klein et al., 2010a). Deficits appear less severe in the knee extensors (Hsiao, 2001; Miller et al., 2009). Notably, Hsiao (2001) assessed bilateral quadriceps activation and strength during the first six months following stroke and observed significant improvements in strength, whereas gains in activation, therefore in paresis, were modest and not statistically significant.

2.B.2 Changes in mechanical properties

Weakness may also be exacerbated by changes in mechanical properties of muscle and tendon secondary to denervation and inactivity (Ng & Shepherd, 2000). These include alterations in the determinants of strength in the agonist muscle or increased resistance to movement due to antagonist contracture (Gracies, 2005a). In stroke, weakness is associated with reduced muscle mass, shorter fibre length, smaller pennation angle, and increased tendon compliance (Gray et al., 2012). An increased proportion of type II fibres has also been reported, possibly reflecting a compensatory adaptation (Jakobsson et al., 1992). These structural adaptations are less extensively studied in SCI; however, muscle atrophy is likely to contribute substantially (Moore et al., 2015). Given that many of these changes are related to disuse, similar adaptations are likely to occur following SCI.

2.C. Selectivity of motor command

In addition to paresis, another neural mechanism limiting joint force production is unwanted contraction of the antagonist muscle (i.e., excessive co-activation). Altered co-activation is well documented after stroke (Gracies, 2005a; Lamontagne et al., 2000), whereas it appears less prominent after SCI (Thomas et al., 1998). However, altered contraction is not limited to antagonist cocontraction. More generally, the term synergy refers either to systematic coupling or coarticulation across different joints, or to a fixed pattern of muscle coactivation. The notion of synergy in pathological contexts differs from its usage in healthy movement, where it represents a form of dimensionality reduction to simplify the degrees of freedom to control. The term synkinetic is also often used in clinical context and refers to the classical observation of involuntary coordination patterns across joints that limit the ability of patients to precisely control the proximal and distal limb.

One way to conceptualise abnormal joint synergies after central nervous system lesions is as a loss of degrees of freedom, or repertoire, due to neural damage (Krakauer & Carmichael, 2017). In healthy individuals, the capacity of the nervous system is often assumed to be effectively unlimited, and synergies are proposed as a means to exploit and resolve redundancy. In contrast, lesions of the central nervous system alter its selectivity and may require new synergies to accomplish the task. Accordingly, an observed synergy may reflect both loss of repertoire and adoption of a compensatory pattern based on the remaining circuitry. On the one hand, it may correspond to a hard synergy, with constraints imposed by the residual neural networks. One likely hard synergy is the flexion synergy pattern in the upper limb after stroke, which will be detailed in Part 2 in relation to a possible reticulospinal compensation. On the other hand, habits (soft synergies) can coexist, as illustrated by persistent inefficient asymmetric gait after stroke, even when split-belt treadmill adaptation has transiently restored greater symmetry (Reisman et al., 2013). This raises the question of whether a patient performs poorly out of habit, or whether this represents the best achievable performance given the remaining neural (and mechanical) constraints.

2.D. Other factors underlying voluntary motor impairments

Both weakness and motor control may be influenced by factors beyond motor execution. By affecting the brain, stroke may also cause apraxia, reflecting a higher-level disturbance (i.e., cognitive) of motor control (Goldenberg, 2013). Apraxia differs from other motor symptoms of

unilateral brain damage in that symptoms are often bilateral despite unilateral lesions. Lesions are predominantly located in the left hemisphere, particularly when premotor and parietal regions are involved, and apraxia is frequently associated with aphasia. Ideomotor apraxia, the most common form after stroke, is a disorder of skilled action not attributable to weakness, incoordination, or elementary sensory or motor deficits; motor execution per se is preserved**.** When apraxia coexists with motor execution deficits, diagnosis becomes challenging. Nevertheless, it should be considered a potential contributor to movement impairment. In addition, pain is common after both stroke and SCI and may inhibit motor output (Le Pera et al., 2001). More complex interactions between motor and pain systems have also been proposed; for example, sensorimotor cortex reorganisation may occur to limit the development of neuropathic pain (Jutzeler et al., 2015).

2.E. Importance of muscle length

The deforming spastic paresis syndrome (Gracies, 2005a) offers a comprehensive, unified view on the importance of muscle length following central nervous system lesions. On one hand, the muscle following central nervous system injuries undergoes numerous changes, notably resulting in a loss of extensibility. This emphasises that non-neural factors contribute substantially to muscle resistance and, ultimately, to voluntary movement impairment. On the other hand, it emphasises the length dependence of paresis, corresponding to reduced central drive to the agonist at shorter muscle lengths, aggravated by the antagonist stretch (Vinti et al., 2015). Notably, compared with controls, patients exhibit lower voluntary activation during concentric than during isometric and eccentric contractions (Kim et al., 2015). Finally, antagonist cocontraction is aggravated by antagonist stretch (Vinti et al., 2013), limiting joint torque production by the agonists. In the terminology of Gracies et al., (2024), the term “spastic” refers to length dependence; thus, there is “spastic coactivation,” denoting stretch-enhanced coactivation, as well as “spastic paresis”. A striking feature resulting from lost extensibility, spastic paresis, and spastic cocontraction is the production of a reversed movement (negative torque) relative to movement intended, particularly when the antagonist is stretched and the agonist is shortened (Vinti et al., 2015).

3. Involuntary movement impairment after SCI and stroke

3.A. Overactivity signs

3.A.1 Spasticity

Lesions of the brain and spinal cord do not produce purely motor deficits. One predominant clinical sign illustrating this is spasticity, defined as a velocity-dependent increase in tonic stretch reflexes (i.e., a sensorimotor deficit), detected and measured at rest (Baude et al., 2019). Spasticity has occupied a central place in the history of central nervous system lesions. It represents the principal "positive sign", in contrast to "negative signs", which include loss of voluntary contraction. However, experimental studies have shown that reflex measurements obtained at rest have limited relevance for understanding how sensory input from muscle stretch receptors is integrated during movement (Ibrahim et al., 1993; J. B. Nielsen et al., 2005). Accordingly, motor performance impairments have been shown to be poorly related to the presence of spasticity (Beer et al., 2000; Zackowski, 2004). As Landau (2004) stated in arguing against an excessive focus on treating spasticity, "Because it is there constitutes neither scientific nor ethical rationale for the reflex temptation to treat this reflex". Nonetheless, spasticity highlights profound sensorimotor alterations and may even represent a functionally useful adaptation to corticospinal pathway injury.

3.A.2 Dystonia

Dystonia is an involuntary muscle activity at rest, in the absence of phasic stretch or voluntary effort but sensitive to tonic stretch (Baude et al., 2019). By maintaining the muscle in a short length, it may lead, surimposing on altered muscle properties, to deformity in the limbs of individual with central nervous system lesions, with stroke in particular (Gracies, 2005a).

3.A.3 Spasms

Spasms can manifest as multi-joint and crossed muscle activation. They are usually triggered by brief innocuous sensory stimuli and often last for several seconds but can be spontaneous (Adams & Hicks, 2005; Li et al., 2004). Muscle spasms may negatively influence quality of life through restricting activities of daily living, inhibiting effective walking and selfcare, causing pain and fatigue, and disturbing sleep (Adams & Hicks, 2005). As with spasticity and dystonia, spasms vary with muscle length, as evidenced by extensor spasms being larger when the

hip is placed in a more extended position. This emphasises the role of proprioceptors and their integration in the initiation of extensor spasms (Wu et al., 2005).

3.B. Specificity of SCI and stroke

The clinical spasticity syndrome following stroke is characterised in large part by excess dystonia and spasticity (especially in arm flexors and leg extensors) and a relative absence of spasms, whereas the clinical spasticity syndrome following SCI is characterised by less muscle tone and, instead, flexor and extensor muscle spasms triggered by cutaneous stimulation are the hallmark (Macht & Kuhn, 1948). However, spasticity is a common feature after SCI (Sangari & Perez, 2022) and, while the literature is mixed on the subject, increased coactivation has also been reported in SCI (Cremoux et al., 2016; Thomas et al., 1998). Change in muscle properties is a fundamental part of spasticity disorder after stroke (Dietz & Sinkjaer, 2007; Gracies, 2005a), which is not or less the case after SCI (Bennett, 2008).

4. Interpretation of motor impairments within motor control theories

4.A. Spastic movement disorder within optimal feedback control

In a similar attempt to that of Gracies, described above, to move beyond a reductionist focus on spasticity, other authors have introduced the concept of spastic movement disorder (Dietz & Sinkjaer, 2007; J. B. Nielsen et al., 2020). The perspective of Nielsen and colleagues complements that of Gracies. Both recognise the central roles of paresis and muscle alterations in limiting force production. However, Nielsen et al. (2020) integrate the adaptive "spastic" component differently. They propose that weakness compromises postural stability and may be counteracted by antagonist co-activation (Nielsen et al., 1994). In this view, co-activation is not solely pathological but may represent an adaptive strategy developed by the injured nervous system to achieve functional stability in the presence of weak and poorly timed muscle activation. At the whole-body level, a stiff, reduced-range and slow gait may therefore constitute an adaptive solution rather than a simple deficit. Nevertheless, these interpretations must address the mechanisms of motor plasticity. For example, recruitment of alternative descending pathways may be more diffuse, inherently promoting co-contraction while attempting to compensate for paresis; this issue is discussed in Part 2.

The view proposed by Nielsen (2020) is grounded in prevailing theories of sensorimotor control in the intact nervous system. These posit that the nervous system uses sensory feedback and

efference copies of motor commands to ensure that movement conforms to predictions generated by internal models (Shadmehr & Krakauer, 2008; Wolpert & Flanagan, 2016). Within this framework, sensory feedback (for instance the stretch reflex – altered after brain or spinal lesions) is integrated as an expected consequence of motor output (Fig. 6). Deviations from predicted sensory feedback generate an error signal, which updates the motor programme to refine future performance. Lesions affecting descending or ascending pathways disrupt the stable coupling between motor commands and sensory consequences, thereby impairing the formation of accurate internal predictions. Movement may then become random guesses. In response to such uncertainty, spastic movement disorder may reflect the nervous system's attempt to control excessive degrees of freedom under conditions of unreliable somatosensory input. The delayed emergence of hyperexcitability after central lesions (Katoozian et al., 2018) may represent gradual upregulation of somatosensory gain to improve the signal-to-noise ratio and facilitate internal model formation. A strategy based on co-contraction around joints may therefore minimise degrees of freedom and stabilise movement (Franklin & Granata, 2007; Heald et al., 2018). Consistent with this view, initial paresis predicts later spasticity (Picelli et al., 2014), suggesting that spastic movement disorder may represent a learned compensation for weakness.

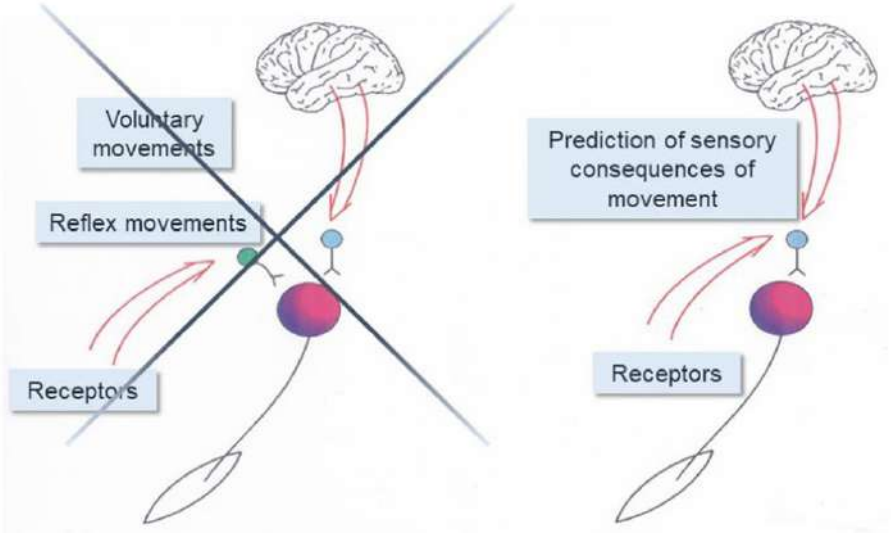

Figure 6. Schematic illustration of the changing view of the role of sensory information during voluntary movement and in relation to spastic movement disorder. *The idea that it is possible to separate reflexes and voluntary movements into separate entities has been abandoned a long time ago in the realisation that descending motor pathways and sensory afferents converge on the same premotoneuronal neurons (left side of figure). Sensory information may instead be seen as an integrated part of central motor commands, if the nervous system optimises movements by minimising the error between the predicted and the actual sensory consequences of movements (right side of figure). It follows that spastic movement disorder may be seen as the consequence of an inadequate prediction of the sensory consequences of movements. From Nielsen et al. (2020).*

4.B. Spastic movement disorder within the referent control hypothesis

An alternative theory of motor control also places sensory integration at its core and explicitly incorporates the stretch reflex into voluntary movement. This framework, the threshold position control theory, is based on the concept that voluntary activation results from central modulation of the spatial stretch reflex threshold, defined as the muscle length (or joint angle) at which stretch elicits muscle activity (Feldman, 2015; Fig. 7). Within this model, spasticity reflects impaired ability to increase spatial stretch reflex threshold in affected muscles, thereby preventing inappropriate activation during passive stretch (Levin & Feldman, 1994; Musampa et al., 2007). Importantly, spatial stretch reflex threshold modulation also underlies voluntary movement control. A muscle inactive at a given length can be activated by shifting its threshold below that length. Reduced capacity to modulate spatial stretch reflex thresholds may therefore contribute simultaneously to spasticity, paresis and co-activation. This framework offers an integrative view of the various motor signs observed after central nervous system lesions, centred on the regulation of the stretch reflex.

Both optimal feedback control and the referent control hypothesis have been debated and contrasted for decades (Mangalam & Stergiou, 2026), and alternative frameworks have also been proposed (e.g., Adams et al., 2013). Despite their specificities, they converge on the central role of sensory information and muscle length, whether considered as error signals, predictive variables, or drivers of motor output. This is particularly relevant in the context of CNS lesions, where altered sensory processing profoundly affects the organisation of motoneuron inputs, as detailed in Part 2 and Part 3. Overall, this highlights the importance of analysing movement impairments in relation to muscle length, which is closely associated with substantial sensory information.

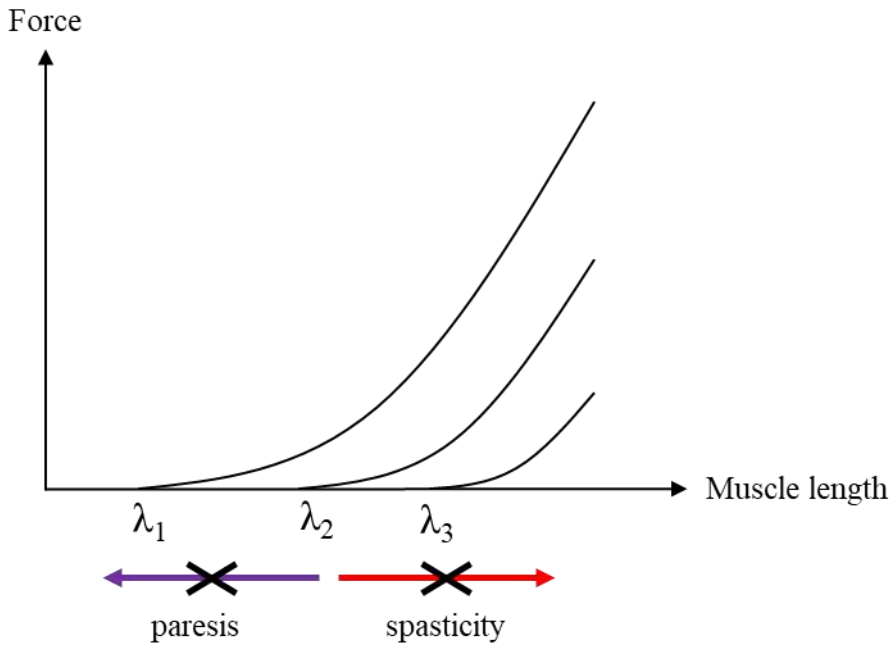

Figure 7. Schematic illustration of spasticity and paresis within the referent control hypothesis. *The referent control hypothesis is centered on the spatial stretch reflex threshold (λ), defined as the muscle length at which stretch elicits muscle activity. Note that the stereotypical relationship between force and muscle length was obtained in the decerebrate cat (Matthews 1959), thus without descending control. Therefore, this relationship is not observable under physiological conditions, but the referent control hypothesis posits that the threshold of the tonic stretch reflex (λ) is controlled by the central nervous system to produce movement. For example, by shifting from λ2 to λ1, force increases at a given muscle length. Conversely, force decreases when shifting from λ2 to λ3. Failure to appropriately adjust λ would lead to paresis and spasticity, respectively, which may occur following central nervous system injuries.*

Key points

SCI and stroke represent major public health issues, notably due to the motor impairments they induce. While they affect the central nervous system through different mechanisms and at different anatomical locations, both conditions lead to overlapping motor impairments.

One major feature of motor impairment in these pathologies is weakness, primarily driven by paresis, which is the focus of this thesis, and which may be accompanied by alterations in mechanical properties. In addition, motor impairments include other deficits in voluntary control, such as impaired command selectivity, as well as involuntary motor impairments characterised by overactivity, including spasticity, dystonia, and spasms.

All these deficits are either demonstrated or suggested to be modulated by changes in muscle length, which therefore constitutes a key factor for understanding these impairments. Furthermore, most current motor control theoretical frameworks emphasise the role of muscle length and sensory information in explaining motor deficits following central nervous system lesions. Thus, changes in muscle length will form a central theme of this thesis.

The next part details the motor system in both healthy conditions and after stroke and SCI, in order to characterise motor impairments in terms of underlying circuit alterations and reorganisation.

◥ PART 2: DESCENDING AND SPINAL CONTROL OF MOTONEURONS IN HEALTH AND AFTER STROKE AND SCI

In Part 1, we considered the motor consequences of stroke and SCI. In Part 2, the emphasis is placed on the descending and spinal circuits acting on motoneurons, and on how these circuits are altered by the lesions. Notably, the following description focuses on the corticospinal tract (CST) and the corticoreticulospinal tract, which are of primary importance for force generation and motor control in humans (Glover & Baker, 2022) and are the most extensively studied in relation to stroke and recovery. Furthermore, among extrapyramidal tracts, the rubrospinal tract appears vestigial in human adults (Onodera & Hicks, 2010) and the vestibulospinal tract has been comparatively less investigated, although this does not preclude functional relevance (Cleland & Madhavan, 2021).

1. Descending control of motoneurons in health

1.A. Cortical control

Since the pioneering work of Penfield, the primary motor cortex has been thought to control movements of different body parts from somatotopically organised cortical territories, corresponding to a 'point-for-point correspondence of an area of the body to a specific cortical point'. Work in humans based on cortical stimulation of small patches of primary motor cortex continues to show isolated and stereotyped movements in response, suggesting that stimulated neurons in the primary motor cortex represent specific movements or groups of agonist muscles involved in a movement (Roux et al., 2020). Notably, this somatotopy echoes clinical findings that limited lesions of the precentral gyrus cause focused paralysis of specific body parts (Foerster, 1936; Celebisoy et al. 2007).

However, recordings at the scale of neurons during natural movement from the 1980s onwards revealed far more complex mechanisms within the motor cortex. Rather than being specified solely by a somatotopic map, specific movements appear to be encoded by neuronal populations distributed throughout the motor cortex (Schieber & Hibbard, 1993). In the same line of research, using single-unit recordings, Georgopoulos et al. (1982) demonstrated that neural activity is broadly tuned to movement direction, with individual neurons exhibiting preferred directions. Subsequent investigations, including population-level analyses of single-unit recordings, revealed that the summed neuronal activity predicts instantaneous velocity and trajectory with

high accuracy throughout movement (Georgopoulos et al., 1988; Michaels et al., 2016). Thus, the motor cortex appears to encode movement kinematics, whereas the details of muscle activation patterns are generated by subcortical or spinal processing mechanisms. Notably, these approaches have been highly successful in motor cortical prosthetic control (Collinger et al., 2013), offering promise for compensatory strategies after paralysis following central nervous system lesions.

However, a profusion of hypotheses exists regarding the level of control exerted by the motor cortex. Some argue for a more 'low-level' control of movement dynamics, such as torque representation (Scott & Kalaska, 1997) or cooperative muscle "synergies" (d'Avella & Bizzi, 2005). Importantly, the motor cortex is composed of different types of neurons with distinct projections. Among these are corticomotoneuronal neurons, which form monosynaptic connections with alpha motoneurons and for which substantial evidence supports a role in controlling low-level parameters such as EMG and muscle force (Omrani et al., 2017). It is plausible that while the "old" motor cortex contributes to motor output by providing activation drives for the spinal modules, the "new" motor cortex further sculpts the activations of specific muscles by bypassing the spinal mechanisms through the corticomotoneuronal cells (Bizzi & Cheung, 2013).

The motor cortex is also involved in a variety of higher-level control functions that depend heavily on sensory signals from the periphery for robust and precise operation. These functions include motor skill learning, motor planning, sensory guidance of manipulative movements, modulation of movement patterns, initiation and termination of low-level pattern generators operating largely at the spinal or brainstem level, and mental simulation of movements (Omrani et al., 2017). The presence of sensory feedback in the motor cortex has been argued to play an essential role in motor control (Scott, 2004; Todorov & Jordan, 2002), or to update motor plans when movement dynamics do not match expectations (Diedrichsen et al., 2005; Wolpert & Ghahramani, 2000). In this line, it has recently been shown that sensory expectations shape neural population dynamics, including in motor cortical areas (Michaels et al., 2025). Notably, these findings reflect the rich interconnectivity and extensive convergence within the motor cortex, including cortico-cortical projections and inputs from the basal ganglia, cerebellum, and other subcortical structures (Georgopoulos & Carpenter, 2015).

1.B. Corticospinal tract

The CST originates from multiple cortical areas and terminates in distinct regions of the spinal grey matter (Fig. 8). Recent quantification in humans indicates that primary sensory and motor cortex, supplementary motor area, and premotor cortex contribute approximately 37%, 32%, 25%, and 7% of CST axons, respectively (Seo & Jang, 2013). Each subdivision exhibits a specific termination pattern within the spinal grey matter, reflecting distinct functional roles. CST projections from primary motor cortex are crucial for voluntary movement; those from premotor areas contribute to sensory guidance; supplementary motor area projections support planning and coordination of movement sequences; and cingulate motor areas are implicated in the emotional aspects of movement (Lemon, 2008; Lemon & Griffiths, 2005).

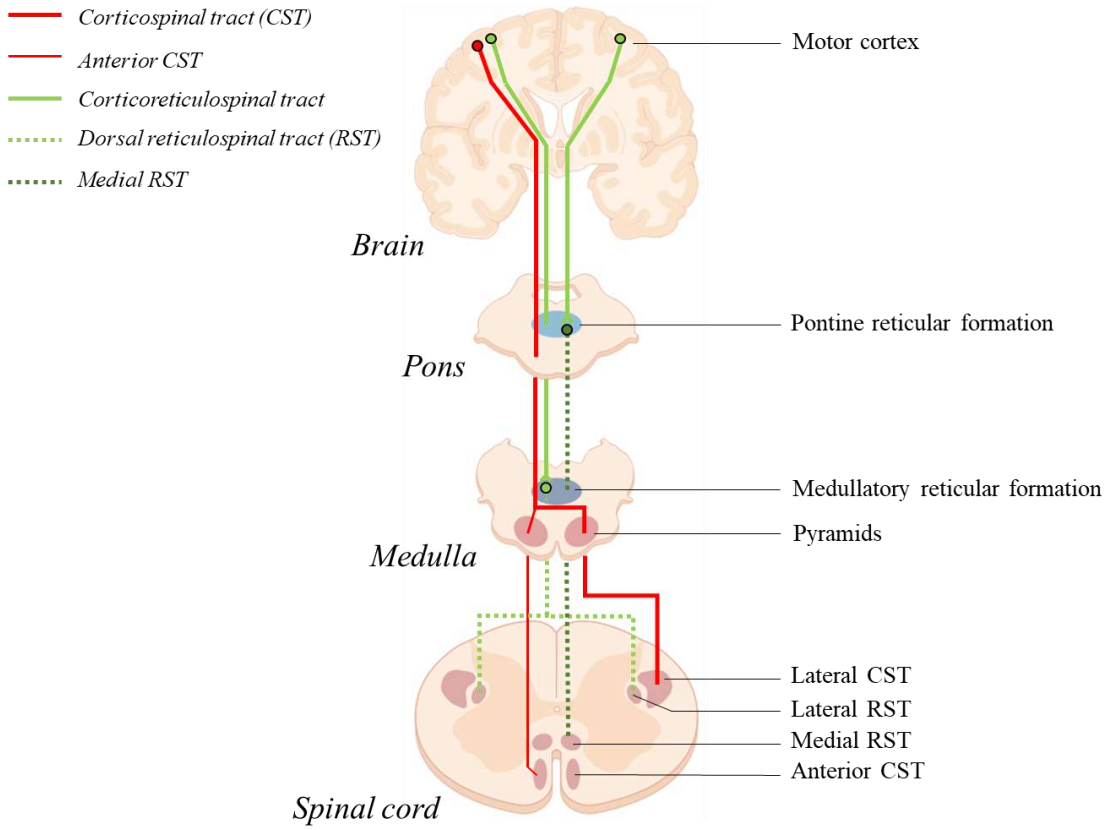

Figure 8. Schematic anatomy of the corticospinal and corticoreticulospinal tracts. *Transverse sections of the spinal cord, medulla, and pons, and a frontal section of the brain. The corticospinal tract originates from the cortex, decussates at the level of the pyramids to form the lateral corticospinal tract, while the remaining portion does not decussate and forms the anterior corticospinal tract. The corticoreticulospinal tracts are composed of corticoreticular projections, which give rise to the medial and lateral reticulospinal tracts, projecting ipsilaterally and bilaterally, respectively.*

1.C. Reticulospinal tract

The corticoreticulospinal tract represents a major extrapyramidal motor pathway and comprises the corticoreticular tract and the reticulospinal tract (RST) (Jang & Lee, 2019). The RST originates from the reticular formation and is organised bilaterally: single reticulospinal axons terminate bilaterally in the spinal cord, mainly onto interneurons but also monosynaptically onto motoneurons, over multiple segmental levels with minimal ipsilateral predominance (Kuypers, 1964; Sakai et al., 2009). Cortical input to the pontomedullary reticular formation arises bilaterally from primary motor cortex, premotor cortex, cingulate, and supplementary motor area (Keizer & Kuypers, 1989). The RST plays a central role in recovery and adaptation after stroke and SCI. However, understanding its role after stroke and SCI requires anatomical and physiological clarification. The reticular formation is a diffuse brainstem network comprising heterogeneous neuronal populations organised into nuclei. It extends through the mesencephalon, pons, and medulla and is classically divided into median, medial, and lateral columns. Neurons in the lateral column and mesencephalic reticular formation contribute primarily to ascending pathways, notably the ascending reticular activating system, which regulates arousal and sleep–wake cycles (Fig. 9).

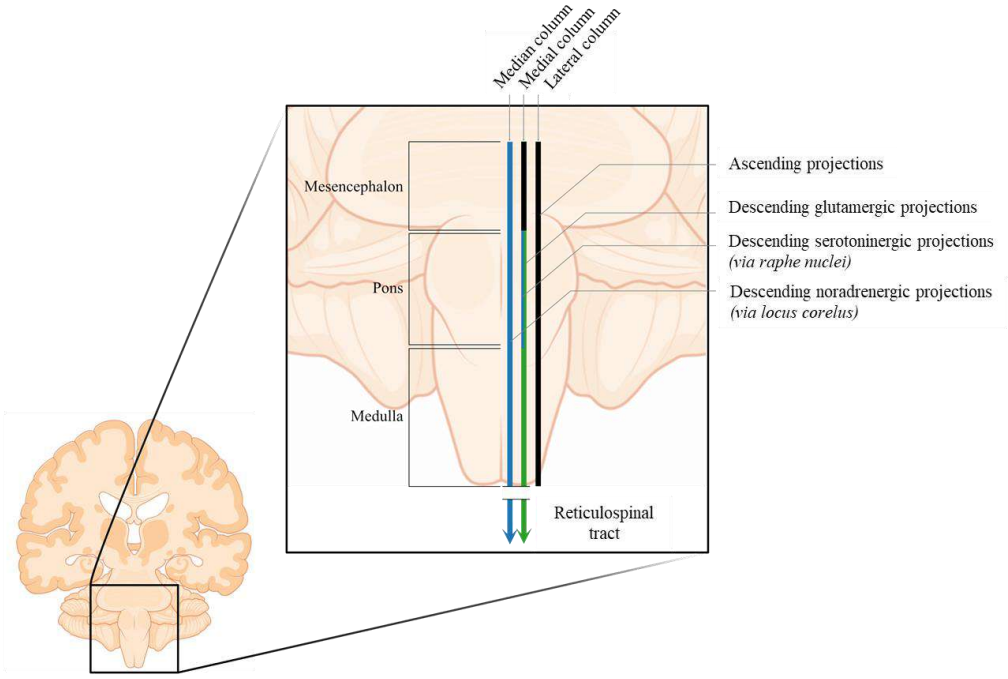

Figure 9. Schematic anatomy and projections of the reticular formation. *The reticulospinal tract originates largely from nuclei located in the pons and medulla, within the median and medial columns. Monoaminergic projections of the reticulospinal tract arise from all three levels of the median column and from the pons within the medial column (blue). Glutamatergic projections originate from the pons and medulla within the medial column (green). Nuclei located in the mesencephalon of the medial column and at the three levels of the lateral column primarily give rise to ascending projections (black).*

The descending motor component is the reticulospinal tract. It comprises glutamatergic reticulospinal neurons arising mainly from the medial column of the pons and medulla, as well as monoaminergic neurons from the median column (raphe nuclei) (Hochman et al., 2001). These neuronal populations exert distinct effects on spinal circuits. Glutamatergic reticulospinal neurons convey relatively fast specific (although spatially diffuse) motor commands. In contrast, monoaminergic projections exert a neuromodulatory, or excitability, command by altering the input-output properties of motoneurons (Heckman et al., 2003). This neuromodulatory influence, which modifies motoneuronal gain rather than providing specific movement commands, constitutes a central focus of this thesis. As will be described in the next section, both of these commands seem to be implicated in various motor impairments after stroke and SCI.

The raphe nuclei and the locus coeruleus are the dominant sources of serotonin and noradrenaline, respectively, for the central nervous system. Accordingly, it is common to speak about serotonergic and noradrenergic systems (Heckman et al., 2009a). Notably, these systems are closely related to the emotional systems of the brain (Holstege & Kuypers, 1987). The locus coeruleus and associated nuclei, which are the source of noradrenaline-containing axons in the spinal cord and elsewhere in the brain, have long been known to play a fundamental role in attention and arousal (Aston-Jones et al., 2001). In this line, recent evidence suggests that the level of neuromodulation to spinal motoneurons is decreased during relaxation (Mesquita et al., 2022). More direct evidence supports a link between the serotonergic system and motor behaviour: neurons of the raphe nuclei fire least during sleep and most during tonic motor outputs such as locomotion, with firing rate increasing with locomotor speed (Jacobs et al., 2002). Importantly, monoaminergic systems are diffuse in topology but organised in a highly structured manner, with different subnuclei projecting preferentially to distinct targets. This organisation warrants caution when transposing context-dependent influences observed in higher functions to motor function, as there may be a functional selectivity in projections (Esposito et al., 2014). Thus, behaviour associated with descending monoaminergic projections remains partly speculative.

Serotonergic fibres project throughout the spinal cord grey matter (Hochman et al., 2001). Raphespinal serotonergic neurons located in the more rostral medulla tend to lack neuropeptides and project to the dorsal horn, whereas more caudal raphespinal neurons co-contain neuropeptides and project to the ventral horn (Hökfelt et al., 2000). These neuropeptides, notably substance P and thyrotropin-releasing hormone, have been shown to strongly excite motoneurons

(Bédard et al., 1987), suggesting that ventral horn projections are particularly designed to enhance motor activity. It is also known that the ventral horn of the spinal cord receives a rich noradrenaline input (Heckman et al., 2003).

2. Descending control of motoneurons after stroke and SCI

2.A. Stroke

2.A.1 Cortical control

Stroke induces loss of brain tissue. Spontaneous reactions to this loss occur already within a few minutes after ischaemia, initiating a complex cascade of cellular and molecular processes not only in the peri-lesional tissue but also in remote brain regions (Schallert et al., 2000). These processes include inflammation, altered gene transcription and translation, growth factor secretion, changes in neurotransmitter receptors, synaptogenesis, and axonal sprouting (Cramer, 2008). They ultimately promote the establishment of new connections with surrounding tissue (Carmichael et al., 2001). At the level of cortical organisation, human studies using positron emission tomography and functional magnetic resonance imaging have consistently demonstrated overactivity during reorganisation (Grefkes & Ward, 2014). After stroke, activity increases in the contralesional primary motor cortex and bilaterally in the ventral premotor cortex and supplementary motor area compared with healthy controls (Rehme et al., 2012). Longitudinal studies indicate that this cortical overactivity does not occur immediately at stroke onset but reflects a time-dependent reorganisation process. Early increases are associated with better functional recovery, suggesting a supportive role of contralesional motor areas during this phase. However, successful long-term recovery is associated with a subsequent normalisation of initially enhanced cortical activity (Grefkes & Ward, 2014).

2.A.2 Corticospinal and reticulospinal tracts

The functional relevance of this reorganisation depends critically on which descending pathways are recruited. Potential mechanisms include engagement of uncrossed corticospinal projections from the contralesional cortex, interhemispheric connections between motor cortical areas, or recruitment of alternative pathways such as the corticoreticulospinal tract. The recruitment of the corticoreticulospinal tract remains one of the most prominent hypotheses and is of fundamental importance in this thesis.

Motor impairment after stroke is strongly associated with ipsilesional CST damage (Byblow et al., 2015; Soulard et al., 2020; Swayne et al., 2008). Stroke may disproportionately affect the CST because of its predominantly unilateral organisation and relatively focal cortical origin, thus limiting redundancy compared with other descending pathways (Krakauer & Carmichael, 2017).

The diffuse organisation of corticoreticular projections may have important implications for recovery following strokes that preferentially damage the more focal and predominantly contralateral CST (Fisher et al., 2021). In primates, pyramidal tract lesions induce upregulation of the RST within six months (Zaaimi et al., 2012). In patients with stroke, cortical overactivity, including enhanced contralesional connectivity, suggests similar RST upregulation during recovery. Notably, Cho and colleagues (Jang & Cho, 2022, for review) have associated recovery, particularly of walking capacity (Seo & Jang, 2013), with increased tract volume of the contralesional corticoreticular tract (Fig. 10). In addition, recovery of ipsilesional and contralesional CST integrity, as well as the ipsilesional corticoreticulospinal pathway, has been positively associated with functional improvement (Soulard et al., 2020).

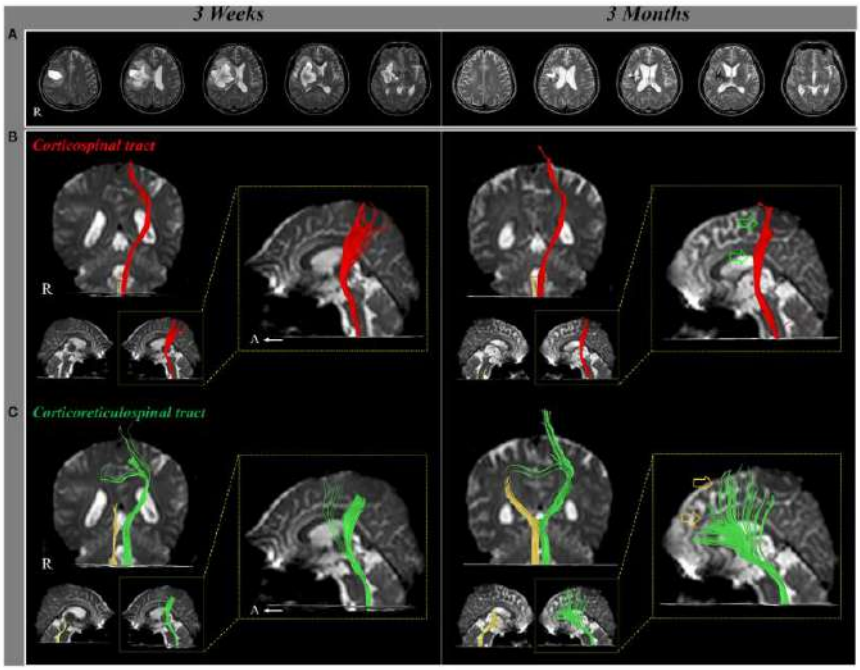

Figure 10. Contralesional corticoreticular tract plasticity after stroke. *(A) T2-weighted MR images show a putaminal haemorrhage in the right hemisphere at 3 weeks and 3 months after onset. (B) Result of diffusion tensor tractography (DTT), the right corticospinal tract (CST) shows discontinuation at the brainstem on both 3-week and 3-month DTT. By contrast, on 3-month DTT, the left CST has become thinner (green arrow) compared with 3-week DTT. (C) The right corticoreticulospinal tract (CRT) shows discontinuation below the lesion on both 3-week and 3-month DTT. On 3-month DTT, the left CRT has become thicker (yellow arrow) compared with 3-week DTT, revealing CRT reorganisation. From Jang & Lee (2017).*

Importantly, several motor impairments may reflect increased RST influence. Dewald and colleagues proposed that flexion synergy after stroke results from progressive substitution of corticospinal output by ipsilateral (i.e., same side as the motor impairments) reticulospinal projections as force demands increase (Ellis et al., 2009). Activation of shoulder abductors in the paretic arm induces involuntary elbow, wrist, and finger flexion, termed flexion synergy, linked to task-dependent recruitment of contralesional cortex and excessive ipsilateral reticulospinal drive. Because reticulospinal projections lack the capacity for finely fractionated control, their increased contribution promotes stereotyped flexor patterns. This may represent an adaptive strategy preserving residual force at the expense of fine motor control (Ellis et al., 2009, 2012; McPherson, Chen, et al., 2018). Further support of this hypothesis derives from involuntary finger movements in the passive hand during attempted movement of a single finger of the paretic hand, consistent with bilateral monosynaptic reticulospinal projections to finger flexors (Baker, 2011). Interactions between residual CST and corticoreticulospinal tract pathways remain debated and likely involve complex recovery-dependent dynamics (Hammerbeck et al., 2021).

2.B. SCI

2.B.1 Cortical control

In a review of motor cortex reorganisation after SCI, Urbin et al. (2019) concluded that motor maps reorganise to some extent following injury, although the precise locus of adaptation remains uncertain. Lundell et al. (2011) reported a pattern of cortical over-activation similar to that observed after stroke: during simple ankle movements, individuals with SCI exhibited bilateral activation of primary motor, premotor, and supplementary motor cortices. This widespread activation may reflect compensatory recruitment associated with abnormal muscle synergies after SCI.

2.B.2 Corticospinal and reticulospinal tracts

Evidence for CST involvement in SCI derives primarily from electrophysiological studies. Motor evoked potential latencies are prolonged, likely reflecting demyelination of corticospinal axons, and stimulation thresholds are increased, suggesting reduced numbers of functional corticospinal projections reaching spinal motoneurons (Oudega & Perez, 2012). In animal models, CST axons exhibit spontaneous sprouting (i.e., axon growth from new or existing collaterals) rostral and caudal to the lesion, establishing indirect connections below the injury, potentially

via propriospinal interneurons (Bareyre et al., 2004; Fouad et al., 2001). These interneurons integrate convergent motor and sensory inputs and modulate spinal circuits, including via long propriospinal projections. Although CST sprouting is well documented in animals (Oudega & Perez, 2012; Rosenzweig et al., 2010), human evidence remains limited (Oudega & Perez, 2012). Recent trials suggest that corticospinal recovery contributes to functional improvement in humans with SCI (Jo & Perez, 2020). Similarly, the injured RST can form new connections, including via propriospinal relays, accompanied by locomotor improvements (Filli et al., 2014; May et al., 2017). Indirect human evidence also supports RST contributions to motor function and spasticity after SCI (Baker & Perez, 2017; Sangari & Perez, 2019).

3. Spinal control of motoneurons in health

SCI and stroke primarily affect the descending pathways described above. These pathways project information to spinal targets. For the generation of purposeful movements, target interneurons and motoneurons must integrate this information with inputs from other pathways and from propriospinal and segmental inputs. Importantly, as Lemon (2008) put it, descending pathways do not simply telegraph commands for movement to the spinal apparatus; rather, the spinal cord functions as part of the brain, not as its servant. Indeed, the spinal cord has a largely integrative role, likely reflecting the complex parameters that must be controlled in spinal neurons, such as firing threshold, rate coding, and synaptic gain, as will be described in Part 3 (Pierrot-Deseilligny, 2012). Among all spinal neurons, of particular importance for movement are motoneurons, which project to contractile muscle fibres, ultimately leading to muscle contraction and movement. In the following section, we describe the main spinal pathways that participate in the control of motoneurons, as well as how SCI and stroke affect these pathways. Of note, we use the terms excitation and inhibition of motoneurons, the underlying mechanisms of which will be detailed in Part 3.

Different populations of interneurons act as relays between descending projections and motoneurons, and the field aimed at characterising these populations has recently progressed substantially, notably through whole central nervous system imaging in rodent models and single-cell transcriptomic analyses (Squair et al., 2025). For parsimony, we will only present one group of interneurons that does not primarily project directly onto motoneurons: propriospinal interneurons, which have fundamental motor roles and have proven highly relevant to the functional impact and recovery after SCI and stroke. The remaining interneurons discussed are the main ones projecting directly to motoneurons, with either excitatory or inhibitory influences.

3.A. Propriospinal interneurons in health

Propriospinal interneurons receive inputs from descending locomotor pathways and propagate motor commands rostrocaudally to locomotor circuits via short or long, ipsilateral, or commissural axons. Extensive evidence supports their locomotor role, although they are also essential for dexterous forelimb movements (Azim et al., 2014). Their locomotor role is specifically linked to innervating or participating in the locomotor central pattern generator, ultimately coordinating forelimb and hindlimb networks by integrating sensory information (Laliberte et al., 2019).

3.B. Excitation by motor synergy encoder interneurons in health

As briefly evoked earlier, when discussing the role of the motor cortex in movement generation, substantial evidence supports the view that voluntary movement relies on a complex pathway linking the motor cortex to spinal interneurons. Through this circuitry, the cortex selects and combines appropriate spinal interneuronal modules and provides them with temporal patterns of activation suited to the behaviour being executed (Bizzi & Cheung, 2013). In this context, an important group of interneurons has been described as motor synergy–encoding interneurons (Levine et al., 2014; Ronzano et al., 2021). They may represent a central node in the neural pathways underlying voluntary and reflexive movement. This population receives direct input from the motor cortex and sensory pathways and, in turn, provides monosynaptic output to spinal motoneurons. Importantly, they may underlie motor synergies by shaping the coordinated activity of motoneurons within and between muscles (Levine et al., 2014; Ronzano et al., 2021). They potentially constitute motor primitives that manage redundant degrees of freedom at muscles and joints and may therefore be considered building blocks of motor control (Hug et al., 2023).

3.C. Monosynaptic Ia excitation of motoneurons in health

3.C.1 Muscle spindle, related afferents and the monosynaptic reflex

Muscle spindles are the major sensory receptors that inform kinaesthesia, the ability to sense position and movement (Proske & Gandevia, 2012). Each spindle contains specialised intrafusal fibres oriented parallel to the force-producing extrafusal fibres. At both ends, intrafusal fibres are connected either to extrafusal fibres or to tendinous ligaments. Thus, when extrafusal fibres change length, intrafusal fibres are stretched or shortened accordingly. The receptor

consists of primary and secondary sensory endings. Primary endings respond, by changing firing frequency, to both the magnitude and velocity of muscle length change (Matthews, 1981). They therefore contribute to the sense of limb position and movement. Secondary endings lack pronounced velocity sensitivity and signal only length change, thus contributing primarily to position sense (Proske & Gandevia, 2012). Axons of primary endings belong to group Ia afferents, whereas those of secondary endings belong to group II afferents. Importantly, Ia afferents make excitatory synapses with (α-)motoneurons, forming a monosynaptic reflex such that muscle lengthening can lead to contraction of the lengthened muscle (Fig. 11).

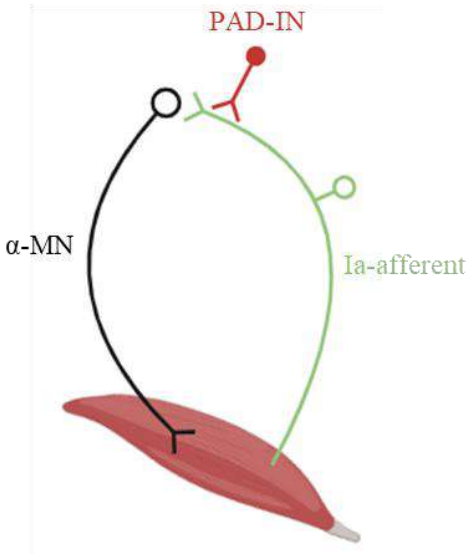

Figure 11. Monosynaptic Ia excitation of motoneurons. *Ia afferents originate from muscle spindles and form excitatory synapses with motoneurons (α-MN). These excitatory inputs are notably modulated by primary afferent depolarisation interneurons (PAD-IN), which reduce the amplitude of action potentials in Ia afferents. This mechanism is regulated by descending pathways.*

3.C.2 Gamma innervation

Unlike other peripheral mechanoreceptors, spindle organs possess their own motor supply via γ ('fusimotor') neurons (Matthews, 1981). This innervation is substantial: approximately 30% of spinal motor neurons are γ neurons, supplying muscle spindles exclusively and controlled by descending commands and peripheral afferent input (Burke et al., 1976). The classical explanation for human spindle control is based on 'α–γ co-activation' (Vallbo, 1970), whereby γ neurons are activated simultaneously with α-motoneurons to prevent spindle slack during contraction, thereby maintaining stretch sensitivity. However, several findings point to a more complex role, including independent and goal-directed tuning of muscle spindles (Papaioannou & Dimitriou, 2021). Consequently, new hypotheses propose that human spindle control facilitates

sensorimotor performance according to task demands, rather than merely encoding posture and movement (Dimitriou, 2022).

3.C.3 Presynaptic inhibitions

The excitatory effect of Ia afferents on motoneurons is regulated by two mechanisms termed presynaptic, as they occur at the afferent, i.e., before the synapse. Importantly, these mechanisms are specific to Ia afferents, unlike postsynaptic inhibition acting directly on motoneurons. The first, homosynaptic post-activation depression, consists of a frequency-dependent decrease in excitation due to neurotransmitter depletion. Of note, this phenomenon is not confined to the Ia-motoneuron synapse and it might be argued that it is not a « true » presynaptic inhibition, contrary to the second mechanism (Burke et al., 2013).

The second mechanism, 'true' presynaptic inhibition, is mediated by primary afferent depolarisation interneurons. An excitatory synapse near the presynaptic terminal releases γ-aminobutyric acid (GABA), inducing sustained depolarisation of the afferent membrane and reducing action potential amplitude. Because neurotransmitter release depends on action potential amplitude, this reduces transmitter release into the synaptic cleft. Of note, the precise anatomy of primary afferent depolarisation interneurons remains under investigation (Hari et al., 2022).

3.D. Synaptic inhibition of motoneurons in health

Besides excitation, motoneurons also receive inhibition via interneurons (Fig. 12). These neurons have multiple roles, including coordinating large neuronal networks in the spinal cord that shape coherent patterns of movement (Goulding et al., 2014). Below, the focus is placed on interneurons located close to motoneurons in the ventral horn of the spinal cord, which directly influence them.

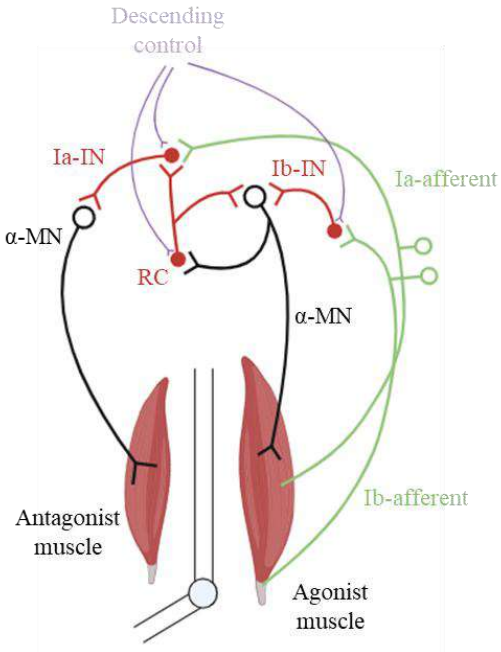

Figure 12. Main spinal inhibitory pathways to motoneurons. *Motoneurons (α-MN) receive inhibitory inputs from Ia interneurons (Ia-IN), Renshaw cells (RC), and Ib interneurons (Ib-IN), all under the influence of descending pathways. Motoneurons are shown in black, while excitatory afferents are shown in green and inhibitory interneurons in red. Circles represent the soma of the neurons and are filled to indicate inhibitory neurons.*

3.D.1 Disynaptic reciprocal Ia inhibition

Other pathways directly inhibit motoneuron membranes, reducing responsiveness to excitatory inputs. A key example is disynaptic reciprocal Ia inhibition. Here, Ia afferents act via Ia interneurons to inhibit motoneurons innervating antagonist muscles (Laporte & Lloyd, 1952). Thus, stretch of an agonist increases Ia activity, which activates inhibitory interneurons and suppresses antagonist motoneurons. In this functional description, the « muscle stretch » is the primary stimulus activating Ia afferents. Notably, disynaptic reciprocal Ia inhibition is often referred to as mediating reciprocal inhibition on the basis that antagonist alpha motoneuron inhibition is evoked by agonist muscle contraction. However, concentric contractions (muscle shortening) would produce the opposite effect. Therefore, the final behaviour - reciprocal antagonist activity - must be partially distinct from disynaptic reciprocal Ia inhibition. This distinction likely resides in the descending control of Ia interneurons (Jankowska, 1992). Consistent with this, reciprocal Ia inhibition from ankle dorsiflexors onto plantar flexors appears 50 ms before the onset of tibialis anterior contraction (Crone et al., 1987), supporting the supraspinal initiation of this inhibition in humans. However, it should be noted that whether

muscle spindles are primarily sensitive to muscle length or other factors, such as force, remains an ongoing debate (e.g., Blum et al., 2017).

3.D.2 Renshaw inhibition

The axon collaterals of motoneurons diverge within the ventral horns to form excitatory synapses with specialised interneurons termed Renshaw cells (Fig 12). Renshaw cell axons project back to motoneuron somata to form inhibitory synapses (Niyo et al., 2024). This inhibition spreads over the entire motoneuron pool (i.e., other motoneurons innervating the same muscle) and may also involve motoneurons innervating synergistic muscles. Thus, motoneuron output excites cells that subsequently inhibit the same motoneurons. This scheme, known as recurrent inhibition, was first demonstrated by Renshaw, (1941).

3.D.3 Ib inhibition

Muscle spindles are not the only sensory receptors within the muscle-tendon unit. Golgi tendon organs are force-sensitive receptors responding to active and passive tension. They are situated in series with muscle fibers at the musculotendinous junction. Ib afferents from Golgi tendon organs are primarily excited by muscle tension and participate in pathways that inhibit motoneurons projecting to synergists (Fig. 12) while facilitating those projecting to antagonists (Knikou, 2008).

4. Spinal control of motoneurons after stroke and SCI

4.A. Propriospinal interneurons after stroke and SCI

Regarding propriospinal interneurons, their position within the spinal cord and their central role in locomotor generation make them well suited to propagate supraspinal commands to motor systems below the level of an SCI. This concept underpins some of the most promising results in restoring motor function (Lorach et al., 2023), particularly through the formation of new connections from supraspinal neurons to propriospinal interneurons (Bareyre et al., 2004) and the establishment of "detour" circuits around lesions (Courtine et al., 2008). Propriospinal pathways are also thought, although far less studied, to provide an alternative route for transmitting motor commands after stroke (Stinear & Byblow, 2004; Tohyama et al., 2017; Urbin, 2025).

4.B. Motor synergy encoder interneurons after stroke and SCI

The motor synergy encoder network is thought to be highly "eloquent", that is, a region which, if lesioned, impairs functional recovery more severely than other areas. These regions may account for the "neuroanatomical–functional paradox", whereby similarly located lesions produce differing effects (Fouad et al., 2001). The fundamental role of these neurons has been exploited using epidural electrical stimulation of the dorsal spinal cord in SCI to engage functional muscle synergies, ultimately leading to partial locomotor recovery (Wenger et al., 2016).

4.C. Monosynaptic Ia Excitation of motoneurons after stroke and SCI

This reflex underlies the tendon tap reflex, which produces a brief muscle stretch followed by contraction. An increased tendon tap reflex is a typical sign of central nervous system lesions, and is therefore observed after SCI and stroke, at least after the initial 'flaccid' period. An electrophysiological equivalent is the H-reflex, elicited by electrical stimulation of Ia fibres. The H-reflex, and thus the monosynaptic reflex, is increased at rest compared with healthy individuals in both SCI (Chen & Perez, 2022) and stroke (Aymard, 2000).

Studies in triceps surae and forearm extensors found no evidence of increased background fusimotor drive or abnormal stretch responsiveness post-stroke (Hagbarth et al., 1973; Wilson et al., 1999). Similarly, in SCI, recordings from peroneal nerve muscle spindle afferents showed no differences in ongoing firing rate, discharge variability, or passive stretch responses compared with intact individuals (Macefield, 2013). However, in mice, muscle spindles have been shown to be essential for locomotor recovery after SCI by shaping rearrangements of descending circuits (Takeoka et al., 2014).

A decrease in homosynaptic post-activation depression is an invariant finding after stroke and SCI and is one of the very few mechanisms that correlate to the degree of spasticity (Aymard, 2000; Grey et al., 2008; Lamy et al., 2009). After SCI and stroke, presynaptic inhibition is decreased, although the reduction appears modest in stroke (Faist et al., 1994; Lamy et al., 2009).

4.D. Synaptic inhibition of motoneurons after stroke and SCI

In plantar flexors post-stroke and SCI, reciprocal Ia inhibition has been reported to be replaced by facilitation (Crone, 2003), although facilitation may originate from Ib pathways. Recurrent

inhibition is increased at rest in patients with stroke and SCI (Katz & Pierrot-Deseilligny, 1982; Shefner et al., 1992). Group Ib inhibition is reportedly replaced by facilitation in patients with stroke (Delwaide & Oliver, 1988), whereas results in SCI remain contradictory (Knikou, 2005; Morita et al., 2006). Importantly, all spinal circuits are under the control of descending inputs, which are altered after stroke and SCI, as detailed in the following paragraph.

4.E. Descending control of spinal neurons and implication for natural movement

Following SCI and stroke, descending control of spinal circuits is altered, providing the primary explanation for the aforementioned changes in spinal circuitry. Crucially, these results derive from assessments performed at rest, whereas supraspinal control of interneurons is fundamental during movement. As stated by Burke et al. (2013) regarding upper motoneuron syndrome, « during movement, the supraspinal control of all testable spinal circuits is defective ». For example, spinal loop excitability is higher at rest after SCI compared with healthy individuals but increases in a much lesser manner during muscle activity (Chen & Perez, 2022). Thus, the clinical utility of resting-state results may be limited in explaining behaviour during actual movement. Notably, descending control of spinal interneurons is mainly excitatory; however, it can activate both excitatory and inhibitory interneurons to modulate the motor command (Jankowska, 1992). Recent studies continue to highlight the critical importance of descending control. For example, animal models demonstrate that the acquisition of mature behaviour during postnatal development correlates with the maturation of supraspinal projections. Conversely, removing descending input during the postnatal period severely disrupts spinal circuit development and ultimately leads to the monosynaptic reflex hyperexcitability observed in SCI and stroke (Smith et al., 2017).

4.F. Interpreting the role of spinal circuits and changes after SCI and stroke

Only a subset of spinal circuits has been presented above, specifically the simpler monosynaptic and disynaptic pathways. Yet, complexity emerges alongside a lack of unambiguous function. Indeed, numerous functions have been proposed for each of these circuits, with notably the possibility that they may serve several roles depending on the behavioural goal (Krakauer & Carmichael, 2017; Windhorst, 1996). Below, we do not discuss all proposed functions in detail, but present these circuits within the context of a general theory of motor control: the referent control hypothesis, presented earlier. In this framework, a primary common feature of these circuits is that they are all posture-stabilising mechanisms. When motoneurons are activated,

the antagonist muscle lengthens, increasing reciprocal inhibition and thereby deactivating the activated motoneurons, which ultimately resists the original agonist shortening. Similarly, when motoneurons activate, Renshaw cells are concurrently activated and, in return, diminish motoneuron activity. In addition, Renshaw cells inhibit Ia interneurons mediating reciprocal Ia inhibition to antagonist motoneurons, thereby increasing the resistive effects of reciprocal inhibition. Furthermore, contraction increases Ib inhibition activity, which also diminishes the activity of the motoneurons responsible for the original contraction. All these pathways would act as posture-stabilising mechanisms. Interestingly, they highlight a posture-movement paradox: « how can an active movement occur without triggering the resistance of these posture-stabilising mechanisms? ». The referent control hypothesis addresses this by assuming that central control structures shift physiological variables associated with muscle activation thresholds (λ, threshold of tonic stretch reflex) and reset posture-stabilising mechanisms to a new posture, thereby transforming them into movement-producing mechanisms (Feldman, 1986). One of the most appealing aspects of this hypothesis in the context of SCI and stroke is that it unifies exaggerated muscle reflexes and poor voluntary control into a single framework. These are often considered separately, as illustrated by the classical classification of negative signs (paresis) and positive signs (spasticity, co-contraction, dystonia) (Levin et al., 2000).

Key points

Motor command relies primarily on the motor cortex, descending pathways, and spinal circuits. The motor cortex is composed of distributed neuronal populations encoding high-level movement parameters, such as kinematics, and is integrated with higher-order functions, including planning, learning, sensory integration, and prediction.

Multiple brain regions contribute to the formation of descending pathways. Notably, the CST serves as the principal pathway for voluntary and fine motor control, whereas the RST is bilateral and diffuse, contributing to posture, gross movements, and monoaminergic neuromodulation.

Stroke and SCI induce a reorganisation of descending control. Key features include cortical overactivity and a shift from corticospinal to reticulospinal contribution, which may constrain the repertoire of movement (e.g., flexion synergy after stroke).

The spinal cord acts as an active integrative centre, composed of diverse interneuronal networks that structure motor output. After stroke and SCI, alterations in these interneuronal circuits are observed, including increased monosynaptic reflex excitability, reduced presynaptic inhibition, and disrupted inhibitory pathways, collectively suggesting impaired regulation by descending inputs.

Together, these changes indicate that the net synaptic input to motoneurons may be altered, in terms of excitatory, inhibitory, and neuromodulatory components. However, this organisation remains poorly characterised, particularly during voluntary contraction

◥ PART 3: SYNAPTIC INPUTS TO MOTONEURONS AND THEIR INTEGRATION

In the previous Part, we considered the anatomical and functional organisation of the central nervous system with respect to motor output, with an emphasis on the consequences of SCI and stroke. Moving from these circuit-level alterations towards an understanding of behavioural impairment requires describing the organisation and integration of motoneuron inputs. This will be addressed in this Part, in both the healthy state and after stroke and SCI.

1. Regulation of motoneuron activity

1.A. Motoneuron structure

Neurons are cells specially endowed with the ability to communicate precisely and rapidly with other cells at distant sites in the body. Two features give neurons this ability. First, they have a high degree of morphological and functional asymmetry. Neurons have receptive dendrites at one end and a transmitting axon at the other. This arrangement is the structural basis for unidirectional neuronal signalling. Second, neurons are both electrically and chemically excitable. The cell membrane of neurons contains specialised proteins, ion channels and receptors, that facilitate the flow of specific inorganic ions, thereby redistributing charge and creating electrical currents that alter the voltage across the membrane. These changes in charge can produce a wave of depolarisation in the form of action potentials along the axon, the usual way a signal travels within the neuron (Kandel et al., 2021).

Motoneurons have their cell body in the ventral horn of the spinal cord (Fig. 13). Their axon travels from the ventral horn to the skeletal muscle to form a contact called the neuromuscular junction (or endplate). At this site, they lose their myelin sheath and divide into several fine branches. At their ends, these fine branches form multiple expansions or varicosities called synaptic boutons from which the axon releases its transmitter acetylcholine (Ach) which binds to and opens the ACh receptor-channels in the end-plate membrane, leading to depolarisation of the post-synaptic membrane and ultimately to an action potential, which then propagates along the muscle fiber, resulting in muscle fibre contraction. Importantly, innervation is organised in a precise manner. One motoneuron innervates several muscle fibers through its axon and the assembly of one motoneuron and the muscle fibers it innervates is called a motor unit (Heckman & Enoka, 2012).

An action potential of a motoneuron leads to the genesis of a unique action potential on the muscle cell membrane because more transmitter is not available in the synapse to attach to the receptors in sufficient quantities until another motoneuron action potential occurs. Thus, there is a 1 : 1 ratio between action potentials on the neuronal and muscle cell membranes, which is a fundamental property that allows the recording of the activity of motoneurons through muscle activity recording (see Method section) (Kandel et al., 2021).

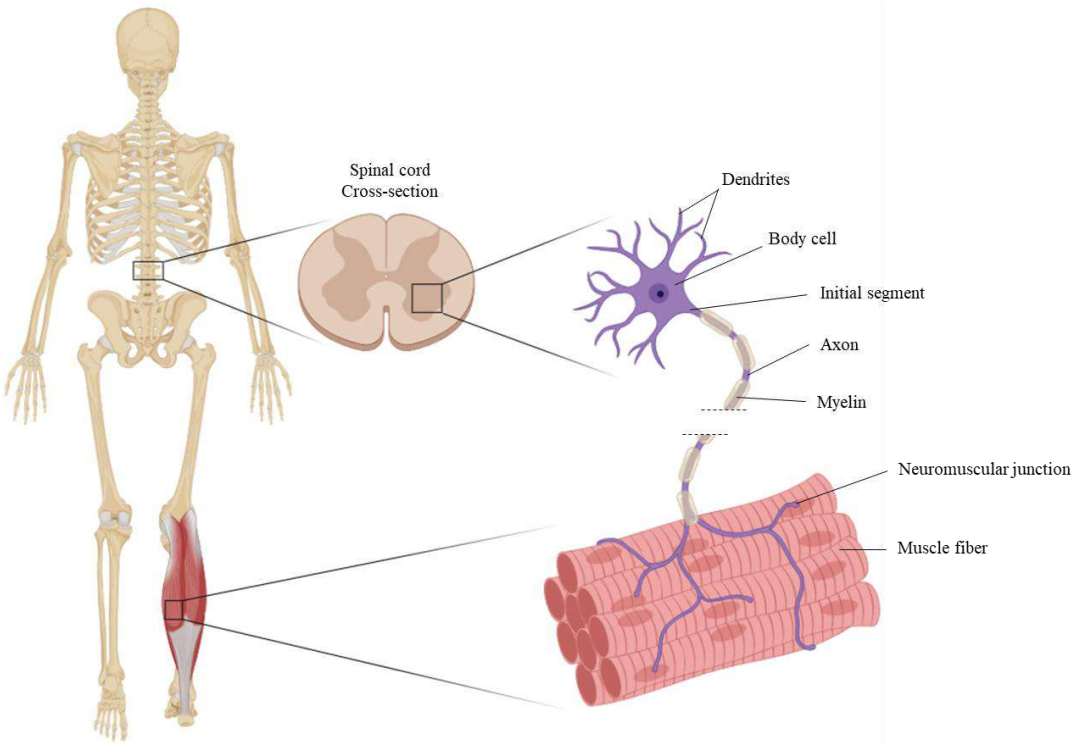

Figure 13. Structure of motoneurons. *Motoneurons have their cell bodies located in the ventral horn of the spinal cord. Their axons project along peripheral motor nerves to innervate the skeletal muscle fibres they supply.*

1.B. The resting membrane potential

An action potential is a rapid change in membrane potential. Thus, understanding the generation of an action potential first requires detailing the mechanisms that regulate the resting membrane potential (Fig. 14). Inside and outside the cell are ions, both positive (cations) and negative (anions). Differences in charge between the extracellular and cytoplasmic surfaces of the membrane give rise to the membrane potential (V_m), defined as the electrical potential difference across the membrane ($V_m = V_{in} - V_{out}$), where V_{in} is the intracellular potential and V_{out} is the extracellular potential. The resting membrane potential (V_r), is equal to V_{in}, since by convention the extracellular potential is defined as zero. Its typical range is −60 to −70 mV. Regulation of

the membrane potential is mediated by specialised membrane pores called ion channels, a class of integral membrane proteins present in all cells. Ion channels selectively recognise specific ions and conduct them across the membrane. Their opening may be either non-gated or gated, and both types contribute to the resting membrane potential (Kandel et al., 2021).

Potassium (K^+) ions are the major contributors to the resting membrane potential. Their concentration is much higher in the cytoplasm than in the extracellular fluid. They therefore diffuse out of the cell down their chemical concentration gradient. However, the efflux of K^+ is self-limiting. As K^+ leaves the cell, it generates an electrical potential difference (positive outside, negative inside). Because K^+ is positively charged, the increasing negative intracellular potential opposes further efflux. This simplified example illustrates the two forces driving ions across the membrane: (1) a chemical driving force, determined by the concentration gradient, and (2) an electrical driving force, determined by the membrane potential. The membrane potential at which these forces balance is called the equilibrium potential ($E_K \approx -90$ mV for K^+), and is determined by the Nernst equation (Equation 1), where R is the gas constant, T the absolute temperature, z the valence of the ion, F the Faraday constant, and $[X]_o$ and $[X]_i$ the extracellular and intracellular ion concentrations (Kandel et al., 2021).

$$Ex = \frac{RT}{zF}\, ln \frac{[X]o}{[X]i}$$

Equation (1)

If neuronal membranes were permeable only to K^+, then E_K would determine V_m (i.e. $E_K = V_m$). If Vm were more positive than E_K, the electrochemical force on K^+ would drive it outward and reduce V_m; conversely, if V_m were more negative, inward movement would occur. However, neurons at rest are also permeable to notably sodium (Na^+) and chloride (Cl^-) ions. Thus, K^+, Na^+ and Cl^- fluxes together determine the resting membrane potential by biasing V_m towards their respective equilibrium potentials. The resting membrane potential is therefore described by the Goldman equation (Equation 2), which incorporates the relative membrane permeability (P) to each ion. Permeability, expressed in cm/s, reflects the number of open channels for a given ion. Because the membrane is far more permeable to K^+ than to other ions, V_m lies closer to E_K (V_m typically around −65 mV) (Kandel et al., 2021).

$$Vm = \frac{RT}{F}\, ln \frac{P_k[K^+]_o + P_k[Na^+]_o + P_{Cl}[Cl^-]_i}{P_k[K^+]_i + P_k[Na^+]_i + P_{Cl}[Cl^-]_o}$$

Equation (2)

The resting membrane potential does not equal the equilibrium potential of any single ion. Consequently, without active mechanisms, ionic gradients would dissipate over time and V_m would decline. This dissipation is prevented by the sodium–potassium pump (Na^+/K^+-ATPase), which transports Na^+ out of the cell and K^+ into the cell against their electrochemical gradients. This process requires energy derived from adenosine triphosphate ATP hydrolysis. Thus, at rest, the cell is not at equilibrium but in a steady state: passive Na^+ influx and K^+ efflux through resting channels are exactly balanced by the activity of the Na^+/K^+ pump. Other active transporters also contribute, such as the Ca^{2+} pump. In addition, some active transport mechanisms do not directly use ATP but rely on cotransporters, which move one ion against its electrochemical gradient by exploiting the energy stored in the gradient of another ion. Because these mechanisms depend indirectly on ATP-driven pumps, they are termed secondary active transporters (Kandel et al., 2021).

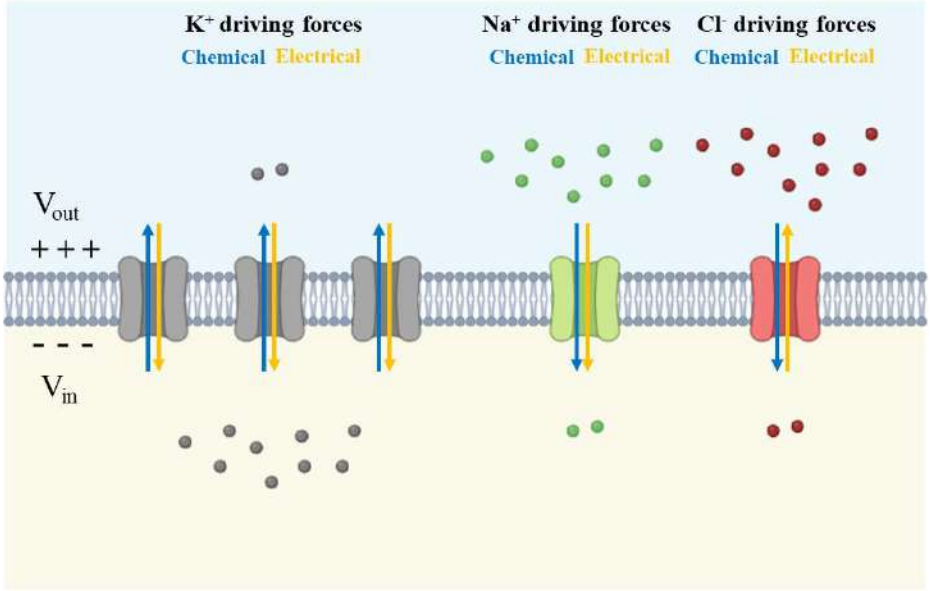

Figure 14. Ion channels determining the resting membrane potential. *The resting potential of a motoneuron is determined by the proportions of different types of ion channels that are open, together with the value of their equilibrium potentials. Potassium (K^+), sodium (Na^+), and chloride (CL^-) channels are illustrated in a simplified cell membrane, with arrows indicating the associated chemical and electrical driving forces.*

1.C. Neurotransmitters and synaptic integration

Motoneurons communicate with other neurons by chemical synaptic transmission. A presynaptic action potential triggers the release of a chemical transmitter from the presynaptic cell via

exocytosis. Transmitter molecules then rapidly diffuse across the synaptic cleft and bind to receptors on the postsynaptic cell. There are two major classes of transmitter receptors: ionotropic and metabotropic receptors. Ionotropic receptors are ligand-gated ion channels. Binding of transmitter to an extracellular site induces a conformational change that opens the channel pore, generating an ionic current that either excites (depolarises) or inhibits (hyperpolarises) the postsynaptic cell, depending on the receptor type. Thus, the action of a transmitter depends on the properties of the postsynaptic receptor rather than on the transmitter itself (Kandel et al., 2021).

Depolarisation of the motoneuron is referred to as an excitatory postsynaptic potential (EPSP). The unitary EPSP produced by a single sensory input depolarises an extensor motoneuron by less than 1 mV, typically 0.2–0.4 mV, well below the threshold for action potential generation. Reaching threshold generally requires a depolarisation of approximately 10 mV. Consequently, action potential generation in a motoneuron requires near-synchronous activation of multiple excitatory inputs. Conversely, hyperpolarisation is termed an inhibitory postsynaptic potential (IPSP), which counteracts EPSPs and prevents the membrane potential from reaching threshold (Kandel et al., 2021).

Neurons that release glutamate typically activate receptors that generate EPSPs. Glutamate receptor activation usually opens ligand-gated channels permeable to Na^+ and K^+. The equilibrium potentials are approximately $E_{Na} \approx +60$ mV and $E_K \approx -90$ mV, creating electrochemical driving forces for Na^+ influx and K^+ efflux, respectively. The net effect of these opposing fluxes is determined by the reversal potential (E_{rev}), defined as the membrane potential at which Na^+ influx equals K^+ efflux and net current is zero. For these non-selective cation channels, E_{rev} is close to 0 mV, representing a weighted average of E_{Na} and E_K, given by the Goldman equation (Equation 3). Given a resting membrane potential of approximately −65 mV, opening these channels produces a strong depolarising inward current driving Vm towards 0 mV. As the electrochemical driving force ($V_m - E_{rev}$) decreases during depolarisation, the current rapidly declines. This reduction in driving force, together with the brief opening of synaptic channels and the activation of opposing conductances, explains the small amplitude of a single EPSP (Kandel et al., 2021).

$$Erev = \frac{RT}{F}\, ln \frac{P_{Na}[Na^+]_o + P_k[K^+]_o}{P_{Na}[Na^+]_i + P_k[K^+]_i} = 0$$

Equation (3)

IPSPs are generated by neurons releasing GABA or glycine. For example, the GABAa receptor is an ionotropic receptor that opens Cl^- channels. Because these channels are primarily permeable to Cl^-, the reversal potential approximates the Cl^- equilibrium potential ($E_{Cl} \approx -70$ mV). If ECl is slightly more negative than the resting potential (e.g., Vr ≈ −65 mV), opening Cl^- channels produce a hyperpolarising current ($V_m - E_{Cl} > 0$). Even when E_{Cl} is close to the resting membrane potential and little hyperpolarisation occurs, the opening of Cl^- channels still inhibits the neuron from firing by holding the membrane near its resting potential, which is called a shunting inhibition effect (Kandel et al., 2021).

Motoneurons receive synaptic inputs from many other neurons, some excitatory and others inhibitory. These inputs are coordinated through neuronal integration. This integration of excitatory and inhibitory inputs depends on several factors, including the location, size and geometry of synapses. The final output is binary: the neuron either generates an action potential or it does not. Action potential initiation occurs at the axon initial segment. Neuronal integration therefore involves the summation of synaptic potentials that spread to this site. Temporal summation refers to the addition of successive synaptic potentials in the same postsynaptic neuron. This property exists because the change in current does not translate instantaneously into a change in membrane potential, leaving time for summation. This property is determined by the membrane time constant. The other type of summation is called spatial summation and refers to the process by which inputs from many presynaptic neurons acting at different sites on the postsynaptic neuron must be added together at the initial segment. This property reflects the degree to which the EPSP decreases as it spreads passively from a synapse along the length of the dendrite to the cell body and axon initial segment. It is related to the length constant property of the neuron (Kandel et al., 2021).

1.D. Action potential generation

At the axon initial segment, the depolarisation required to reach the action potential threshold (−55 mV) is approximately 10 mV from a resting level of −65 mV. When summation of EPSPs and IPSPs brings the membrane potential close to this threshold, voltage-gated Na^+ channels, distinct from chemically ligand-gated channels, open rapidly (Fig. 15). The resulting depolarisation triggers the opening of additional voltage-gated Na^+ channels, producing a further influx of Na^+ and accelerating depolarisation. This regenerative positive feedback cycle develops explosively, driving the membrane potential rapidly almost toward the Na+ equilibrium potential of +55 mV (Kandel et al., 2021).

When the depolarisation is maintained for some time, the Na+ channels begin to close, leading to a decrease of inward current. This process, termed inactivation, renders the channel temporarily non-responsive to further depolarisation. Recovery from inactivation requires repolarisation to the resting membrane potential and defines the absolute refractory period. Although a small subthreshold depolarisation increases inward Na^+ current, it also enhances outward K^+ current by increasing the electrochemical driving force on K^+ ($E_K \approx -90$ mV). Closure of voltage-gated K^+ channels is slower than that of Na^+ channels, and several milliseconds are required for them to return to the closed state. As a result, the membrane potential transiently becomes more negative than its resting value as V_m approaches E_K. This phenomenon, termed afterhyperpolarisation, limits the maximal firing rate of a neuron, defined as the number of action potentials generated per unit time. Firing rate is a fundamental parameter in neuronal communication and, in the present context, in the transmission of signals from motoneurons to muscle fibers (Kandel et al., 2021).

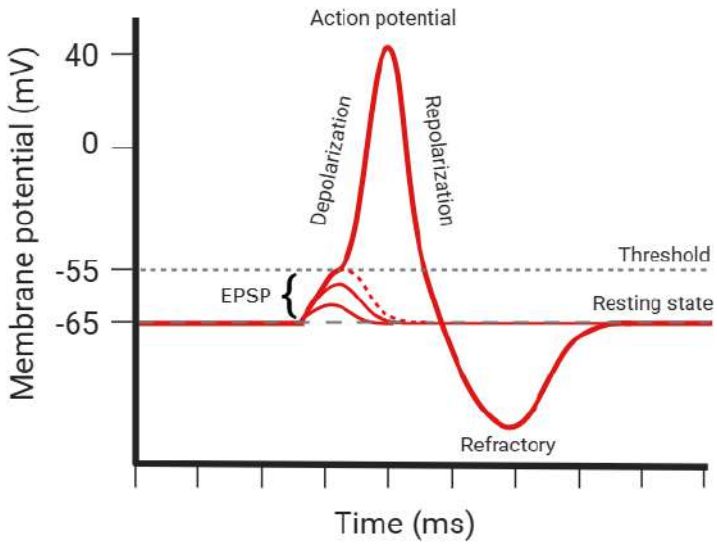

Figure 15. Action potential. *Excitatory postsynaptic potentials (EPSPs) depolarise the membrane from its resting potential (−65 mV). If this depolarisation reaches the threshold (−55 mV), a stereotyped action potential is triggered, consisting of a rapid depolarisation, followed by repolarisation and a refractory period during which the membrane potential falls below the resting level.*

1.E. Metabotropic receptors and persistent inward current

As mentioned previously, in addition to ionotropic receptors, motoneurons are also regulated by metabotropic receptors. In contrast to ionotropic receptors, which directly control ion flux, metabotropic receptors act through intracellular biochemical cascades that ultimately lead to the indirect modulation of ion channels. A major family of metabotropic receptors is the G

protein–coupled receptors (GPCRs), which have been extensively studied and exert significant effects in motoneurons. Here, we focus on their actions on voltage-sensitive channels (Fig. 16). Of note, several terms have been used to describe these inputs: neuromodulatory (as they alter neuronal properties), G protein–coupled (because most neuromodulatory inputs act via GPCRs), metabotropic (as the intracellular cascades are considered part of neuronal metabolism), and slow synaptic transmission (reflecting the slower time course compared with fast ionotropic transmission) (Heckman et al., 2009a). Consistent with the majority of studies on human motoneurons, we use the term neuromodulation, although this represents only one aspect of GPCR function, which is fundamental to numerous physiological processes.

Current evidence indicates that the principal neuromodulatory effects on spinal motoneurons arise from serotonin (5-HT) and noradrenaline (NE), two monoamines that exert similar effects on spinal neurons (Heckman et al., 2009a). Their brainstem origins were described in Part 2. As with ionotropic receptors, the effects of 5-HT and NE depend on the receptor subtypes expressed by the target neuron. For example, both monoamines can depolarise the resting membrane potential, probably via 5-HT6 or 5-HT7 receptors (Harvey et al., 2006). In contrast, 5-HT1 receptors exert inhibitory actions at the initial segment, which may contribute to central fatigue during prolonged 5-HT release reaching this region (J. Perrier & Cotel, 2008). Overall, however, descending 5-HT and NE inputs strongly enhance motoneuron intrinsic excitability. This effect is primarily mediated by persistent inward currents (PICs) activated via 5-HT2 and NE α1-receptors (Harvey et al., 2006; J.-F. Perrier & Hounsgaard, 2003). GPCRs act through second-messenger signaling cascades, which are fully characterised only for selected pathways in the nervous system. Ultimately, activation of 5-HT2 and α1 receptors promotes the opening of two channel types that generate PICs: L-type Ca^{2+} channels (CaV1.3) and persistent Na^{+} channels (molecular subtype unidentified), located predominantly on dendrites (Lee & Heckman, 1999; Y. Li et al., 2004). Because PIC channels are voltage-gated, they require membrane depolarisation for activation. Importantly, their contribution to synaptic processing depends critically on descending monoaminergic drive: greater monoaminergic input produces larger PICs (Lee & Heckman, 2000).

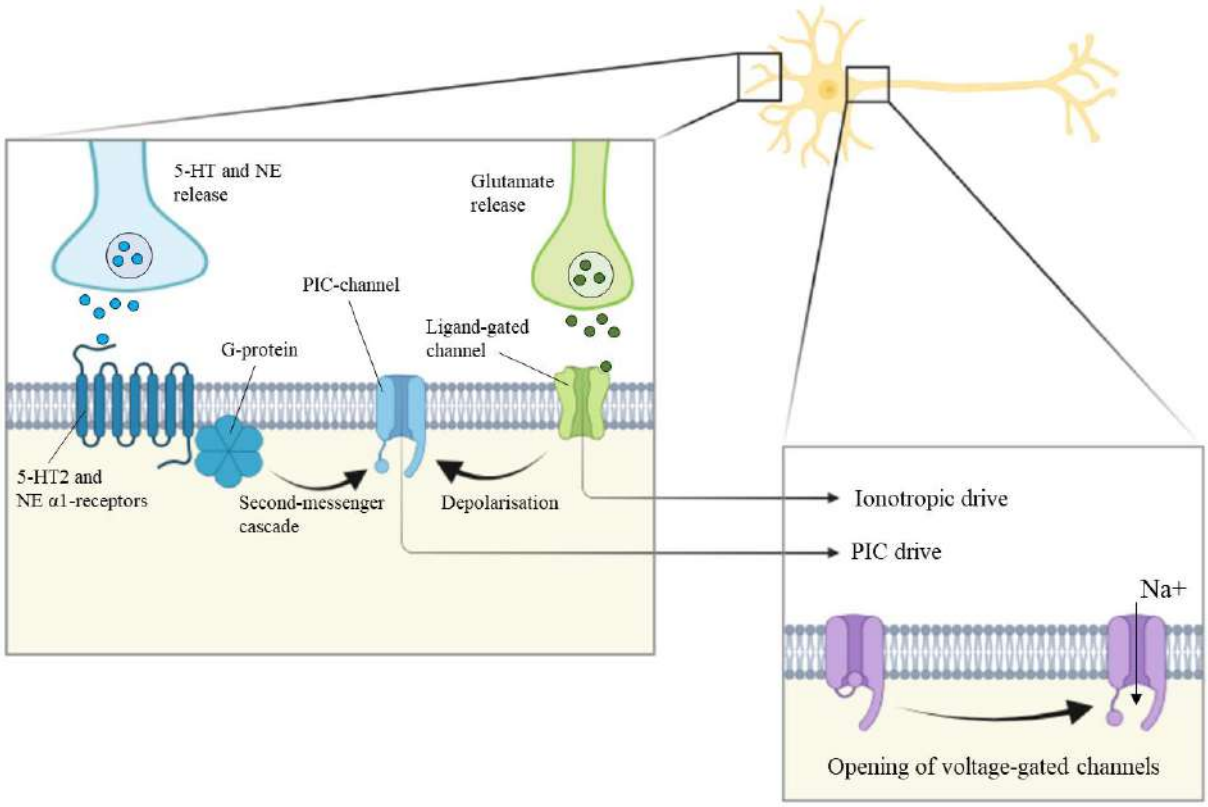

Figure 16. Generation of PIC drive. *Serotonin (5-HT) and noradrenaline (NE), originating from the brainstem, activate metabotropic G protein–coupled receptors (GPCRs), which act via second-messenger signaling cascades to ultimately activate persistent inward current (PIC) channels. Because PIC channels are voltage-gated, they also require membrane depolarisation for activation, thereby acting as an amplifier of synaptic input. Similar to potentials generated by ionotropic inputs, PIC-mediated depolarisations are transmitted to the axon initial segment and contribute to the firing behaviour of motoneurons.*

PICs are characterised by two prominent effects on firing rate. First, they produce a high acceleration (i.e., rate of increase) of firing rate in response to injected current, reflecting amplification of synaptic input (Hultborn et al., 2003; Lee & Heckman, 2000). Second, they generate bistability, whereby a brief excitatory input can trigger self-sustained firing that is terminated only by inhibitory input (Hounsgaard et al., 1988; Schwindt & Crill, 1980). These phenomena correspond to amplification and prolongation effects of synaptic inputs mediated by PICs (Fig. 17). The Na^+-mediated PIC (NaPIC) contributes primarily to amplification but not prolongation, as it inactivates within seconds (Powers & Binder, 2001). In contrast, the Ca^{2+}-mediated PIC (CaPIC) underlies both acceleration and prolongation of motoneuron firing (Harvey et al., 2006; Kuo et al., 2006). These two aspects are inextricably linked by the inherent persistence of the channels mediating the PIC (Heckman et al., 2009b). Most evidence derives from animal models, using voltage-clamp techniques to directly characterise PICs in motoneurons. In the

following sections, we discuss their influence on motoneuron firing during natural behaviour in humans; accordingly, we refer to the effects of PICs on motoneuron firing output, rather than on synaptic input per se. Although not addressed in detail here, PICs are also essential for repetitive firing by reducing afterhyperpolarisation (Harvey et al., 2006; Kuo et al., 2006). In summary, PICs profoundly reshape α-motoneuron integration by modifying the input–output relationship.

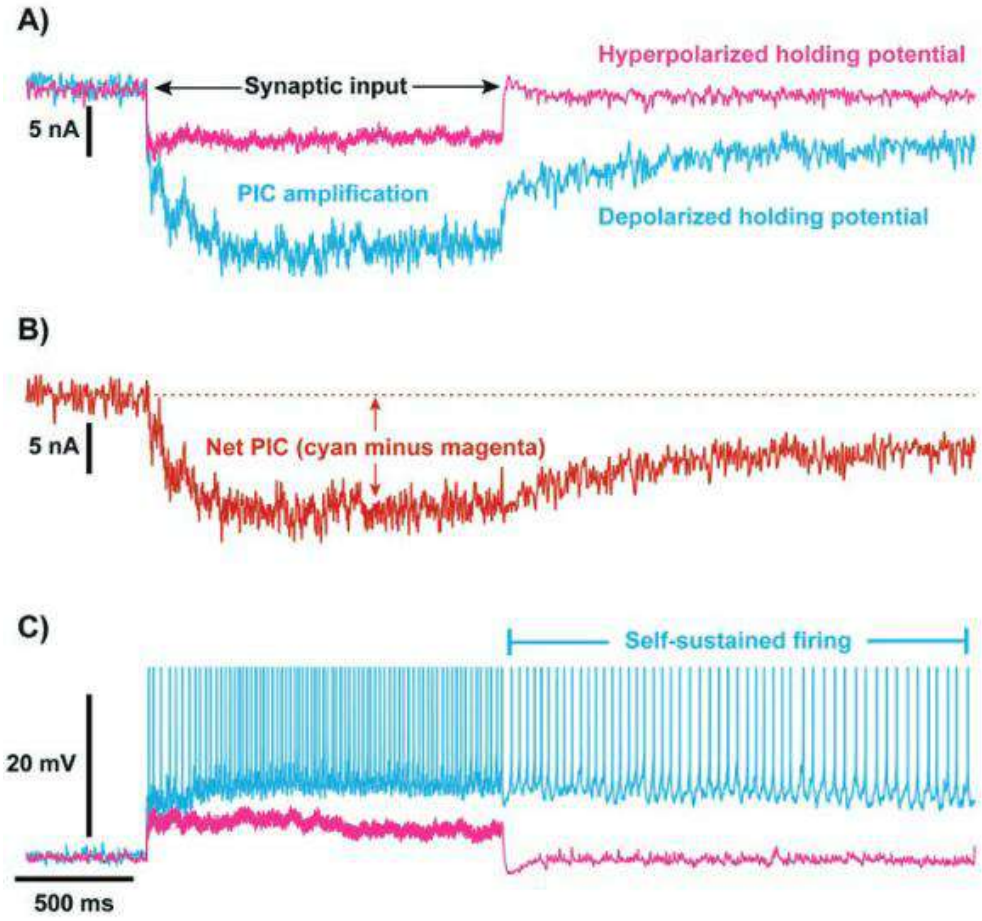

Figure 17. PIC amplification and prolongation of synaptic inputs. *In (a), a low threshold motoneuron is voltage clamped to either −90 mV (magenta trace) or −55 mV (cyan trace). At a hyperpolarised holding potential (i.e. −90 mV) activation of homonymous Ia afferents resulted in a steady current response with a sharp onset and offset that matched temporal parameters of the input. At a depolarised holding potential (i.e. −55 mV), the same input was amplified and prolonged, highlighting the voltage dependence of the PIC. In (b), the net PIC (red trace) is the difference between the motoneuron current response at a depolarised and at a hyperpolarised holding potential from (a). In (c), the motoneuron is unclamped. At a hyperpolarised level (~ −90 mV; magenta trace), synaptic input does not reach the threshold for repetitive firing. By contrast, at a more depolarised level (~ −70 mV; cyan trace), the same input evokes repetitive firing that is sustained well after the input is turned off, albeit at a lower firing rate. From Khurram et al. (2022).*

1.F. Three types of inputs integrated by motoneurons

Summarising the preceding sections, motoneurons receive (i) excitatory inputs that induce excitatory postsynaptic potentials, driving the membrane potential toward the action potential threshold; (ii) inhibitory inputs that induce inhibitory postsynaptic potentials, preventing the membrane potential from reaching threshold; and (iii) neuromodulatory (metabotropic) inputs that enhance intrinsic excitability through PICs, thereby modulating the input–output gain of motoneurons. These three types of inputs are mediated by glutamate (excitation), GABA and glycine (inhibition), and serotonin (5-HT) and noradrenaline (NE) for neuromodulation. The pathways mediating these inputs are summarised in Figure 18. Overall, motoneurons integrate these inputs to determine their recruitment and firing behaviour, as detailed in the following sections.

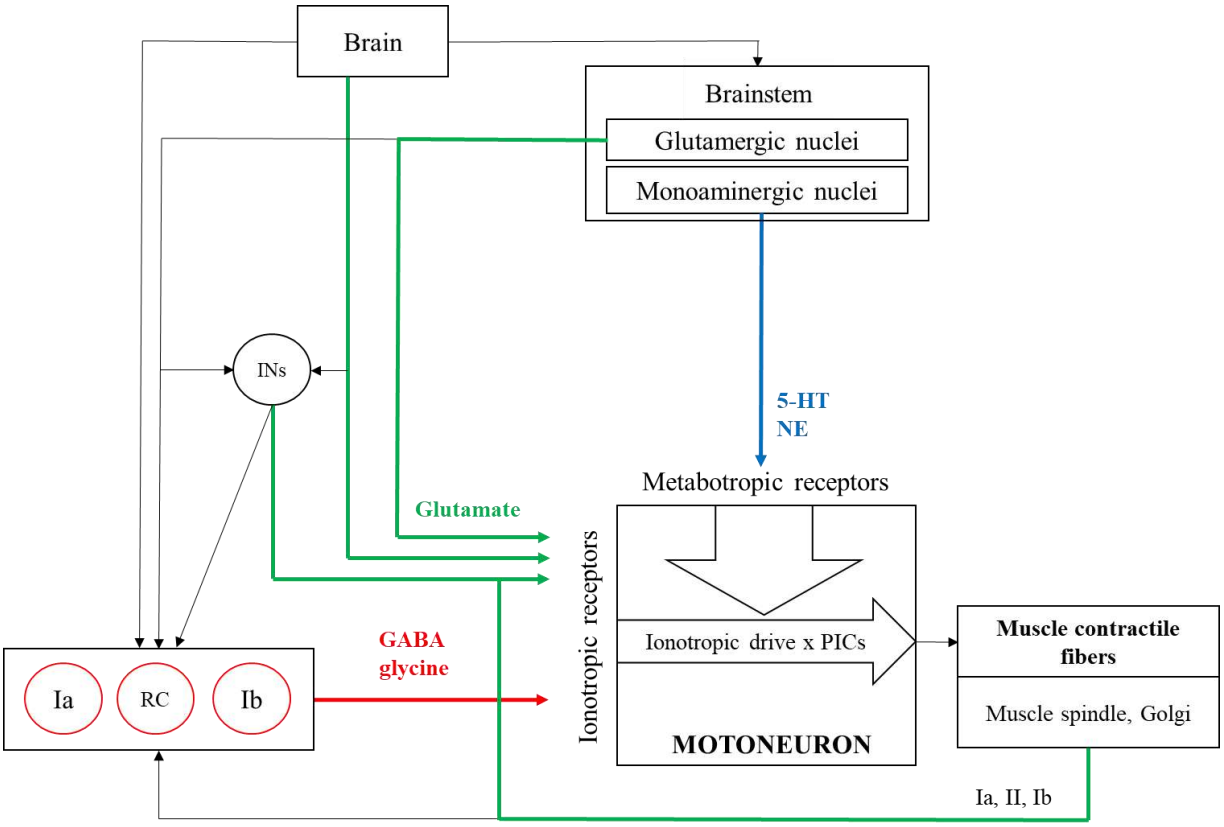

Figure 18. Overview of motoneuron inputs. *Motoneuron inputs can be classified into three main types: excitatory (green), inhibitory (red), and neuromodulatory (blue), with the underlying pathways illustrated. Excitatory inputs primarily arise from the brain, particularly the motor cortex, from glutamatergic nuclei in the brainstem, from spinal interneurons (INs), and from peripheral afferents. Inhibitory inputs primarily arise from specialised spinal interneurons, including Ia interneurons (Ia), Ib interneurons (Ib), and Renshaw cells (RC). Neuromodulatory inputs arise from monoaminergic nuclei in the brainstem, notably serotonergic (5-HT) and noradrenergic (NE) pathways, which modulate motoneuron excitability* via metabotropic receptors, ultimately resulting in amplification and prolongation of the ionotropic drive.

2. Motoneuron pool organisation

2.A. Motoneuron role in force generation

So far, we have considered motoneurons through various aspects: their descending and spinal inputs, and how these inputs regulate their activity. However, the central role of motoneurons is defined by their projections to skeletal muscle. The number of motor units per muscle is typically a few hundred, with large variation across muscles (Heckman & Enoka, 2012). The innervation ratio, the number of muscle fibers innervated by a single motoneuron, also displays large variability both between and within muscles (Heckman & Enoka, 2012). Importantly for central nervous system force control, muscle units exhibit high mechanical heterogeneity, with a 100-fold range in force production across motor units, primarily due to the innervation ratio (Heckman & Enoka, 2012). As detailed below, motor units determine muscle force through two mechanisms: the number of motor units recruited and the force produced by each unit, which depends on the motoneuron firing rate and the number of muscle fibres innervated.

2.B. Motoneuron recruitment

The recruitment threshold of a motoneuron is determined by two primary factors: (1) its relative share of the synaptic input and (2) its intrinsic threshold (Heckman & Binder, 1993). In the cat medial gastrocnemius, motoneuron thresholds range from approximately 3 nA to over 30 nA (Heckman & Binder, 1991). This 10-fold range is largely attributable to differences in input resistance, which is inversely proportional to motoneuron surface area; consequently, smaller neurons reach threshold with less current. Conversely, it is unlikely that total ionotropic synaptic current is ten times greater in high-threshold units than in low-threshold units (Heckman & Binder, 1993; Powers & Binder, 2001), despite evidence that certain descending inputs preferentially target high-threshold motoneurons (Fig. 19).

Ultimately, the recruitment sequence is governed by these differences in input resistance, leading to Henneman's size principle. This principle dictates that motor units are recruited in an orderly fashion from small to large. This sequence corresponds to the progressive activation of slow-twitch, low-force, fatigue-resistant units (low threshold), followed by progressively larger, faster, and more fatigable units (high threshold) (Henneman & Mendell, 1981). While neuromodulatory inputs can shift motoneuron thresholds, these effects are generally insufficient to override the substantial threshold differences imposed by input resistance (Heckman et al.,

2009b). The upper limit of motor unit recruitment typically occurs below maximal voluntary contraction (MVC); for instance, soleus motor units are recruited up to approximately 90% MVC (Oya et al., 2009).

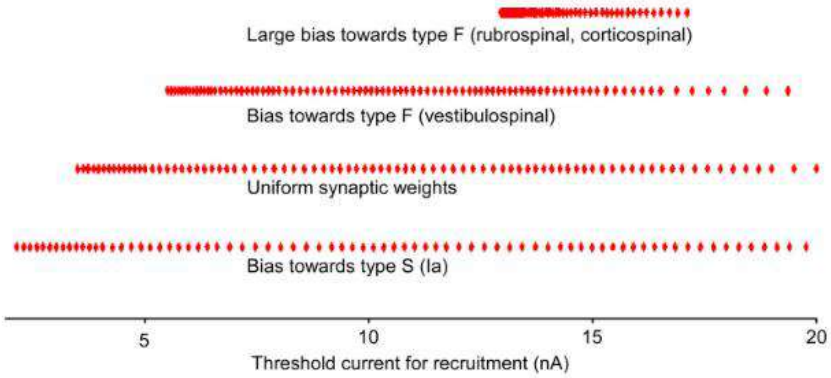

Figure 19. Schematic of the distribution of synaptic inputs across motoneuron types shows that synaptic sources are not uniformly distributed. *Additionally, synaptic sources do not have a uniform effect on each type of motoneuron (S vs. F). Cortical and rubrospinal inputs produce much greater (up to 9 times) effects in F motoneurons than they do in S motoneurons. Vestibular inputs are about twice as strong in F motoneurons than in S. Ia inputs have the strongest effect in S motoneurons, being about twice that in F motoneurons.*

2.C. Motoneuron rate coding

A historical perspective is insightful for understanding the mechanisms underlying motor unit rate coding. Early attempts (1950s–1980s) to link synaptic current to firing rate via intracellular recordings (reviewed in Khurram et al., 2022) revealed a relatively simple linear input-output relationship. However, this model failed to account for firing patterns observed during voluntary contractions in humans, which are characterised by: (1) an initial acceleration creating a steep slope in rate modulation; (2) a rapid transition to a significantly lower slope; and (3) a relatively linear decline in firing rate as input decreases, with derecruitment occurring at a much lower input level of current injection than recruitment (Johnson et al., 2017; Fig. 20)

This discrepancy arose because early input-output functions were derived from anaesthetised preparations, which suppressed the neuromodulatory drive from the brainstem. Conversely, decerebrate cat preparations, used to study the effects of serotonin 5-HT and norepinephrine, revealed discharge patterns strikingly similar to those observed in humans (Heckman et al., 2009b). As discussed, monoaminergic drive induces PICs that modulate the voltage-sensitive channels responsible for action potential generation. It is now clear that PICs fundamentally shape rate coding by inducing marked initial acceleration and onset-offset hysteresis (Fig. 20).

These PIC-mediated effects, visible during natural human behaviour, are believed to be closely linked to the amplification and prolongation of synaptic inputs. Recent studies further confirm that neuromodulatory input from the brainstem is a fundamental component of normal motor behaviour. For example, in vivo antagonism of 5-HT2 receptors attenuates the self-sustained firing of human motor units, confirming that serotonergic neuromodulation is a key facilitator of motoneuron discharge (Goodlich et al., 2024).

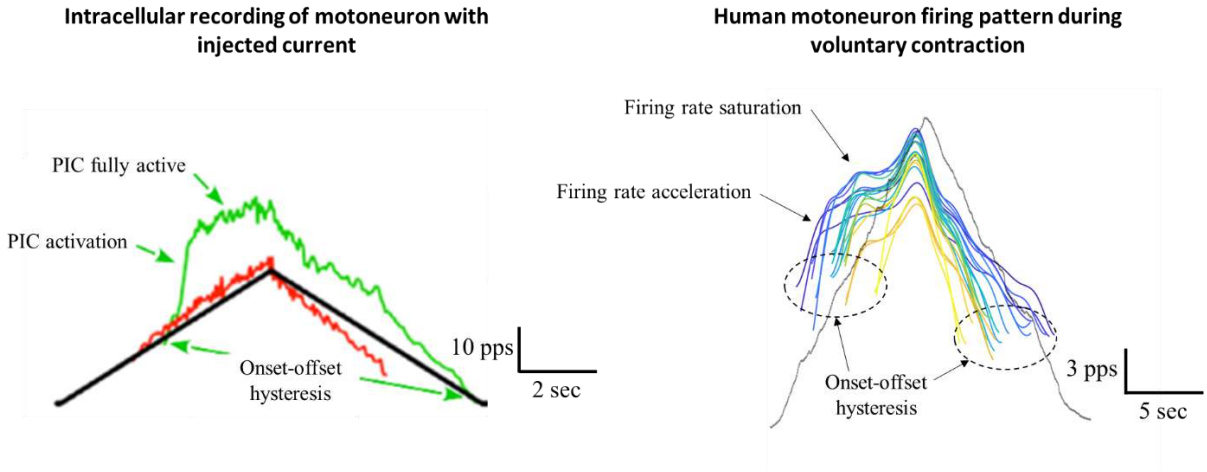

Figure 20. **Similarity of firing patterns between intracellular recordings with PICs and human motoneuron firing.** On the left, a triangular current ramp is injected via an intracellular electrode into a motoneuron of a decerebrate cat. In the absence of persistent inward currents (PICs; low neuromodulatory state), the change in firing frequency is linear and follows the injected current (red trace). When PICs are present (high neuromodulatory state), the firing behaviour becomes non-linear, with marked initial acceleration, saturation, and pronounced onset–offset hysteresis (green trace). On the right, representative human motoneuron firing rate patterns are shown during a linear increase and decrease in torque, mimicking the injected current ramp. These firing patterns exhibit similar features, including strong initial acceleration, saturation, and onset–offset hysteresis, consistent with intracellular recordings under high neuromodulatory conditions. This supports a fundamental contribution of PICs to human motoneuron firing behaviour. Adapted from Johnson et al. (2017).

While PICs increase motoneuron excitability, they also enhance the capacity of inhibitory synaptic activity to reduce that excitability (Hultborn et al., 2003; Kuo et al., 2003). There are two primary mechanisms by which PICs amplify inhibitory synaptic inputs. First, membrane hyperpolarisation can deactivate the inward current; the subsequent loss of this depolarising current is effectively equivalent to adding a hyperpolarising current. Second, the activation of inward currents depolarises the membrane, thereby increasing the reversal (driving) potential for inhibitory synapses. The first mechanism, unlike the second, alters the time course of inhibitory postsynaptic currents (IPSCs) and requires higher-amplitude IPSCs (Bui et al., 2008). Furthermore, the interaction between dendritic PIC channels and synaptic inhibition is location-

dependent. Renshaw cells, for instance, exert a potent inhibitory effect due to their projection's location (Bui et al., 2008), whereas the mechanism underlying the efficacy of reciprocal Ia inhibition remains unclear (Hyngstrom et al., 2007). Of note, while the studies discussed above focus on how PICs modulate inhibition, conversely, human studies often emphasise the « dampening effect » of inhibition on PICs. This highlights that the interaction is bidirectional and can be characterised from either perspective.

In humans, motoneurons likely receive substantial tonic inhibition during normal motor behaviour, evidenced by high levels of spontaneous activity in premotor spinal interneurons (many of which are inhibitory) in awake primates (Prut & Perlmutter, 2003). The decerebrate cat preparation similarly exhibits significant tonic inhibition (Hyngstrom et al., 2007; Johnson et al., 2012). This steady background allows for several distinct temporal patterns of inhibition relative to excitation: (1) constant inhibition while excitation varies; (2) a « push-pull » pattern, where inhibition decreases as excitation increases; or (3) « proportional » inhibition, where excitation and inhibition covary. A fundamental study for this thesis, Chardon et al., (2024), demonstrated through simulations (details will be provided in the Method section) that these distinct inhibitory patterns are associated with specific firing behaviours (Fig. 21). For instance, at a constant neuromodulatory level, a push-pull pattern enhances PIC acceleration and prolongation effects on the firing; whereas a proportional pattern tends to suppress them, reflecting the dampening effect of inhibition on PICs. Notably, the push-pull pattern is supported by spinal circuit architecture, such as the organisation of Ia afferents and Ia inhibitory interneurons (Johnson et al., 2012), and aligns with firing patterns observed in healthy humans (Chardon et al., 2024). Furthermore, a push-pull pattern is required for reaching high firing rates during high-force contractions (Škarabot et al., 2025) and is more pronounced in trained versus untrained individuals (Škarabot et al., 2026). While proportional patterns are common throughout the central nervous system (Berg et al., 2019), spinal circuits may modulate these inhibitory strategies based on the task. Importantly, whether these inhibitory patterns are altered after SCI and stroke remains a critical question.

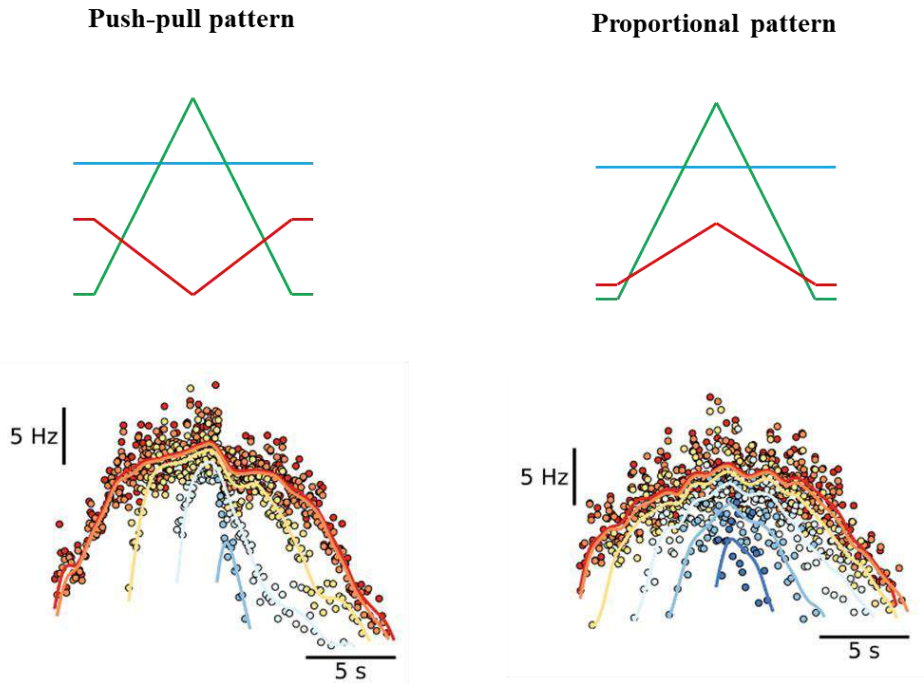

Figure 21. Impact of inhibitory pattern on firing rate pattern. *A motoneuron pool model receives a constant neuromodulatory input (blue trace) but different inhibitory patterns. A push-pull inhibitory pattern, which corresponds to a decrease in inhibitory conductance (red trace) during increase in excitatory conductance (green trace), or a proportional pattern, which corresponds to a co-increase of excitatory and inhibitory conductances, leading to different firing patterns. Adapted from Chardon et al. (2024)*

2.D. Synaptic inputs: functionnal considerations

A central question in neuroscience is how neurons, despite their limited bandwidth, encode signals spanning several orders of magnitude. In the motor system, this problem can be reformulated as follows: how can accuracy be maintained across a wide range of force outputs? To illustrate this issue, Wei et al. (2014) proposed the following example. Consider a transmission system (e.g. motoneurons to muscles) capable of transmitting only a limited number of spikes within a relevant interval, with force assumed to be proportional to spike count. Suppose the system can generate a maximum of 10 spikes. In Situation A, forces between 0 and 1 N are required, whereas in Situation B, forces between 0 and 10 N are needed. With a fixed gain, the system must operate at 1 N per spike to accommodate the maximal force in Situation B. A lower gain would fail to produce the required peak force. However, under this constraint, Situation A would allow only integer force values, leading to errors of up to 0.5 N, as the maximum error equals half the step size. Thus, without gain modulation, the capacity to generate high forces necessarily compromises precision at low forces. In contrast, a context-dependent gain would

allow a gain of 0.1 N per spike in Situation A and 1 N per spike in Situation B. Under these conditions, maximal error in Situation A would be reduced to 0.05 N, substantially decreasing output variability while preserving performance in Situation B. In motoneurons, gain can be regulated by PICs and the pattern of inhibition described above. PICs increase gain through their amplification effect and a push–pull inhibitory organisation provides the central nervous system with a further mechanism for increasing motoneuron gain in a paradoxical manner: increasing background inhibition to enhance disinhibition and thereby increase effective gain (Johnson et al., 2012).

While the adaptation of motoneuron gain by PICs is a crucial component of motor control, it presents a potential problem. Monoaminergic projections driving PICs are diffuse and lack apparent somatotopy. Consequently, they are not motor pool specific (Johnson & Heckman, 2014; Skagerberg et al., 1982). As a result, their profound effect could potentially lead to involuntary activation across multiple motor pools, including agonists and antagonists acting at multiple joints. The interaction between inhibition and PICs has been proposed as the solution to this issue (Hyngstrom et al., 2007). Inhibition provides the capacity for "sculpting" specific movement patterns from the diffuse background of neuromodulation generated by descending monoaminergic tracts (Hyngstrom et al., 2007). This hypothesis is often summarised as « diffuse descending neuromodulation, focused local inhibition » (Heckman et al., 2008), which highlights the crucial role of inhibition and the risks associated with the dysregulated inhibition that follows SCI and stroke.

2.E. Common and independent inputs

So far, we have presented the synaptic command characterised through three components acting on motoneurons: inhibitory and excitatory (ionotropic), and neuromodulatory (metabotropic) inputs. Another fundamental distinction between types of synaptic inputs concerns the portion of input correlated across the motoneuron pool, termed common synaptic input, and the remaining portion, termed independent input (Fig. 22; Farina et al., 2014). The fundamental properties of common synaptic input are: (1) despite the non-linear properties of individual motoneurons (described above), the motoneuron pool linearises the relationship between common synaptic input and the neural drive to the muscle. This likely provides a mechanism for the central nervous system to execute smooth movements using non-linear elements with high synaptic noise; (2) within the frequency bandwidth relevant for force generation (typically <10 Hz due to muscle contractile characteristics), the motoneuron pool filters out signals sent independently to

each neuron and transfers only the common components with pure scaling. This makes common input the primary driver of force modulation (Farina, et al., 2014). This line of research thus focuses on understanding functional connectivity. Beyond these features, questions remain regarding the organisational level of common input across muscles and behavioural contexts (i.e., motoneuron functional synergies) (Hug et al., 2023).

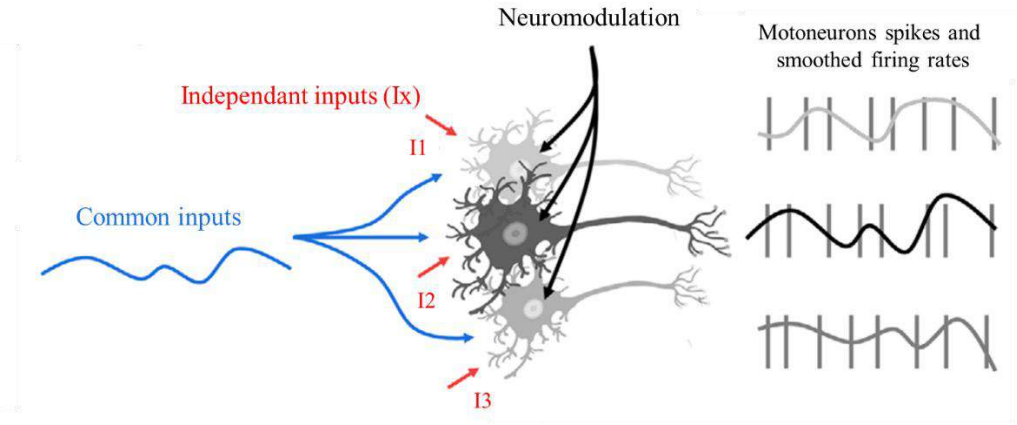

Figure 22. Common and independent inputs to motoneurons. *Motoneurons receive a proportion of inputs that are shared across the motoneuron pool (common inputs), originating from multiple sources, as well as independent inputs (Ix). Neuromodulatory inputs project diffusely across motoneuron pools. Theses input structure the firing bahaviour of groups of motoneurons. Adapted from Hug et al. (2023).*

3. Motoneuron inputs and behaviour after stroke and SCI

3.A. SCI

SCI results in muscle-dependent changes in motoneuron recruitment and rate coding. While no global differences compared to controls were observed in the triceps brachii (Wiegner et al., 1993), significantly lower firing rates have been reported in the first dorsal interosseous, biceps brachii, and tibialis anterior (Debenham et al., 2024; Kizyte et al., 2025; Thomas et al., 2014). Within plantar flexor muscles, the SOL was assessed by (Kizyte et al. (2025), who reported no significant differences in motoneuron mean discharge rates between SCI and control individuals.

Changes in recruitment thresholds remain difficult to quantify in humans. Available evidence focuses on the maximal relative force at which the highest-threshold motoneurons are recruited. For example, thenar motoneurons are recruited at forces up to 72% maximal voluntary contraction torque (MVT), compared to controls, which typically saturate below 30% MVT (Thomas

et al., 2014). Experiments have also started to explore motoneuron synergies after SCI, suggesting that some reorganisation may occur (Duan et al., 2026). Generally, synaptic input to motoneurons during voluntary contraction has received minimal attention, likely due to the technical challenges of using intramuscular EMG to isolate individual motor unit behaviour. Conversely, animal models and involuntary contractions have been more extensively explored regarding synaptic input commands.

Animal models of SCI demonstrate that increased PICs play a primary role in the development of muscle spasms and spasticity (Li & Bennett, 2003). Crucially, increased PICs after complete lesions are due to the compensatory emergence of constitutively active 5-HT2 and NA α1 receptors; these provide neuromodulatory excitation independent of monoaminergic drive (D'Amico et al., 2014; Murray et al., 2010). Importantly, the transition from acute spinal shock to the recovery of excitability, marked by increased residual force and signs of overactivity, parallels the re-emergence of motoneuron PICs in animal experiments (Li et al., 2004).

In humans with chronic SCI, the contribution of PICs is suggested by the reduced synaptic drive required to maintain firing in paired motor unit analysis during spasms (Gorassini, 2004). Beyond the evidence linking PICs to spasms, recent findings suggest that spasms also arise from a global reduction in synaptic inhibition, which disrupts the regulation of PIC magnitude. Consequently, both disinhibition and heightened intrinsic excitability contribute to spasm generation (Mahrous et al., 2024). This decreased inhibition would be primarily driven by the disfacilitation of interneurons following the loss of descending pathways and the downregulation of the chloride transporter KCC2, which depolarises the chloride reversal potential (normally E_{Cl} ~ -70 mV), reducing the inhibition effect (Boulenguez et al., 2010). Importantly, these mechanisms likely differ from those underlying paresis, as evidenced by findings that spinal excitation is increased at rest in SCI but fails to appropriately scale (i.e., increase) during voluntary contractions (Chen & Perez, 2022; Vastano & Perez, 2020).

In this thesis, the firing behaviour of motoneurons will be assessed during voluntary contractions using large populations of recorded motoneurons, and synaptic inputs will be estimated for the first time in humans after SCI, in terms of excitatory, inhibitory, and neuromodulatory components (Study 2).

3.B. Stroke

Previous studies assessing motoneuron firing rates have consistently revealed a systemic reduction in paretic muscles post-stroke. Specifically, this has been observed during submaximal contractions in the biceps brachii (Gemperline et al., 1995; Mottram et al., 2014), the first dorsal interosseous (Hu et al., 2015; Li et al., 2015), and the tibialis anterior (Chou et al., 2013). One striking feature identified in some motoneurons is "negative rate modulation", which is a decrease in firing rate despite an increase in torque, and thus presumably an increase in net synaptic input (Mottram et al., 2014).

Pharmacological attenuation of the monoaminergic drive in stroke survivors reduces the flexion synergy typically associated with chronic stroke, suggesting that monoamines contribute to these motor adaptations (Beauchamp et al., 2022; McPherson, et al., 2018). Accordingly, various methodologies addressing whether neuromodulation is increased post-stroke suggest that it may contribute to signs of overactivity, alongside ionotropic changes (McPherson et al., 2008; Mottram et al., 2010). However, estimates of neuromodulatory level during voluntary contraction have revealed mixed results compared to controls (Beauchamp, et al., 2023; Mottram et al., 2009). Mottram et al., (2009) argue that their results support distinct mechanisms for overactivity signs in stroke versus SCI, with PICs being less altered post-stroke. While these comparisons are legitimate, given that SCI and stroke differ in their clinical presentation (e.g., prevalence of spasms versus spasticity), we maintain that the confounding factor of state (voluntary contraction versus rest) is crucial. This distinction limits the validity of extrapolating results from rest to active movement, particularly across populations where standardised, comparative assessments are lacking.

Overall, few studies have attempted to estimate synaptic input commands after stroke. Mottram et al. (2009) used the paired motor unit approach, which has been shown to be highly dependent on inhibitory inputs, thereby limiting conclusions regarding neuromodulatory levels. The study by Beauchamp et al. (2023) used a more recent approach, the same as that employed in this thesis (see Methods), but focused on the biceps brachii, comparing it to the contralateral side, and was conducted on a relatively small sample (n = 11). *Thus, in this thesis, motoneuron firing behaviour has been assessed during voluntary contractions using large populations of recorded motoneurons for the first time in plantar flexor muscles, with healthy individuals as controls (Study 3).*

4. Modulation of motoneuron inputs and behaviour with muscle length and antagonist tendon vibration

4.A. Modulation of motoneuron inputs and behaviour with muscle length in healthy individuals

Movement necessitates changes in joint kinematics, which are accompanied by both neural and mechanical modifications. As joint position shifts, muscles may be stretched, increasing the activity of various afferents (primarily Ia, II, and Ib). This provides the central nervous system with sensory feedback that regulates the spinal mechanisms, as described in Part 2. In the muscles investigated in this thesis (SOL and GM), lengthening enhances torque-generating capacity, following their curvilinear and consistently positive force-length relationship (Hoffman et al., 2012; Maganaris, 2001). Consequently, less muscle activation is required to produce the same absolute torque at longer muscle length.

How the central nervous system adapts synaptic commands to these shifting neural and mechanical properties remains largely unexplored. To date, this question has primarily been addressed through pathway-specific approaches. For example, homosynaptic postactivation depression increases with muscle length (Colard et al., 2025). However, the length-dependence of neuromodulatory, inhibitory, and excitatory inputs in humans remains unknown. A fundamental study, in the decerebrate cat model, revealed that changing joint position substantially modulates PICs via reciprocal inhibition (Hyngstrom et al., 2007). Nevertheless, these findings may differ from the physiological state during active movement in humans for two reasons: (1) Ib afferent-mediated inhibition increases at longer muscle lengths and is likely more influential during voluntary contractions than in paralysed animal models; and (2) key descending systems that modulate sensory-driven inhibition are absent in the decerebrate cat (Hyngstrom et al., 2007). *Thus, the length-dependence of neuromodulatory, inhibitory, and excitatory inputs in humans remains to be determined, which has been the focus of the Study 1 of this thesis. Specifically, this study primarily aimed to test the hypothesis that PIC-mediated prolongation is modulated by changes in muscle length through changes in inhibitory inputs.*

4.B. Modulation of motoneuron inputs and behaviour with muscle length in SCI and stroke

As proposed in Part 1, muscle length is central to the physiological and sensorimotor impairments observed after stroke and SCI. Notably, a « stretch-sensitive paresis » has been described

(Vinti et al., 2015). However, that study quantified activation via EMG amplitude, which is not a reliable indicator of neural drive. Factors such as biased spatial sampling of motor units and variable volume conductor effects across joint positions alter the relationship between neural drive and EMG amplitude (Besomi et al., 2020). Addressing this through individual motor unit activity is necessary to verify this hypothesis. While position-dependent alterations in torque are evident - particularly in stroke, where patients may produce reversed (negative) torque - this phenomenon could be explained by abnormal co-activation alone.

Whether PICs are altered after stroke and SCI remains unclear. However, it is established that several spinal pathways mediating postsynaptic inhibition are dysfunctional in both conditions (as detailed in Part 2). Beyond altering the net synaptic input to motoneurons, impaired inhibitory control may also disrupt PIC regulation via the « dampening effect » (Heckman et al., 2009b). Consequently, inhibitory system dysfunction could lead to severe motor deficits, as poorly controlled PICs would amplify the detrimental consequences of altered inhibitory inputs. The interaction between inhibitory inputs and PICs has notably been tested using antagonist tendon vibration (Mesquita et al., 2022), which reduces PICs, likely via activation of the reciprocal Ia inhibition pathway (Burke et al., 1976). Additionally, vibration may, via sensory afferent stimulation, increase the responsiveness of raphe serotonergic neurons (Moolenaar et al., 1976), thereby enhancing PICs. Consequently, vibrations of the antagonist tendon provide an excellent experimental paradigm for manipulating inhibition and evaluating the interaction between different synaptic inputs. *Both change of muscle length and tibialis anterior vibration were used in Study 2 and Study 3 to experimentally manipulate inhibitory inputs to plantar flexor motoneurons, providing insights into the role of inhibitory inputs in shaping motoneuron behaviour.*

Key points

Motoneurons are the final integrators of the motor command, translating neural signals into force through the innervation of muscle fibers. This innervation is organised into motor units, whereby one motoneuron innervates multiple muscle fibers via its axon.

Motoneuron function depends on the membrane potential, defined by the charge difference between extracellular and intracellular compartments. The membrane potential can undergo a stereotyped, rapid change known as the action potential, which transmits discrete discharges to muscle fibers.

The membrane potential of motoneurons is determined by electrochemical driving forces, which are strongly influenced by synaptic inputs from other neurons. These inputs act on ion channels, generating ionic currents that either depolarise or hyperpolarise the membrane. Ultimately, motoneurons integrate these inputs to determine their output behaviour.

In addition to excitatory and inhibitory ionotropic inputs, motoneuron behaviour is critically modulated by neuromodulatory inputs, which activate PICs and result in amplification and prolongation of synaptic inputs. In this way, neuromodulation reshapes the input–output relationship of motoneurons.

Muscle force is determined by both the number of active motor units (recruitment) and their discharge rates (rate coding). These features are shaped by the three types of inputs, resulting in input-specific firing patterns.

Motoneuron firing behaviour has been studied in selected muscles following stroke and SCI, and has generally revealed alterations. However, it has rarely been investigated in lower limb muscles, particularly using large populations of motor unit recordings. Regarding synaptic inputs, current knowledge is largely limited to animal models in SCI and to upper limb muscles in stroke.

Finally, the dependence of excitatory, inhibitory, and neuromodulatory inputs on muscle length, in both healthy and pathological conditions, remains unknown. This also represents a key experimental paradigm, along with antagonist tendon vibration, which allow manipulation of inhibitory inputs in vivo in humans.

Objectives & hypotheses

Regulation of muscle force depends on both the number of recruited motor units and the force produced by each unit, which in turn is determined by motoneuron firing rate and the number of innervated muscle fibers. Recruitment and rate coding depend on the three types of synaptic inputs: excitatory, inhibitory, and neuromodulatory. In functional contexts, motor output must continuously adapt to changing mechanical and sensory conditions. Movements of daily life notably involve variations in joint position, which modify muscle mechanical properties through the force–length relationship, thereby requiring corresponding adjustments in synaptic inputs. In parallel, changes in joint position alter sensory feedback to motoneurons, which must be integrated to ensure appropriate regulation of motoneuron pool behaviour. Consequently, the central nervous system must coordinate these multiple constraints to produce effective motor output. Increasing force production, adapting to mechanical demands, and integrating sensory inputs all require complex neural computations. Ultimately, the three synaptic input commands must be coherently integrated by motoneurons to generate appropriate motor behaviour. Regarding stroke and SCI, it is unclear how synaptic inputs are organised to support residual force production, and how these inputs adapt to changes in joint position or sensory feedback.

The global objective of this thesis is to better define the organisation of synaptic inputs to motoneurons during voluntary contraction after stroke and SCI, and to determine how these inputs adapt to changes in inhibitory inputs in both health and disease. The experimental work is structured into three studies.

Specifically, Study 1 aimed to investigate changes in synaptic inputs during voluntary contractions in humans. We hypothesised that PIC estimates would decrease as plantar flexor muscle length increases, regardless of whether absolute or relative torque is maintained constant across ankle positions. This would suggest that muscle length, rather than muscle tension, primarily drives PIC modulation. We further hypothesised that this decrease would be mainly attributable to increased inhibitory input, whereas neuromodulatory input would remain relatively stable during these tasks.

Studies 2 and 3 aimed to determine how synaptic inputs shape motoneuron rate coding in individuals with incomplete chronic SCI and chronic stroke, respectively. First, we compared the relative contributions of inhibitory and neuromodulatory inputs to motoneuron firing rates in plantar flexor muscles between individuals with pathology and healthy controls, using specific

firing features to estimate synaptic inputs. We then experimentally manipulated inhibitory input through changes in muscle length and antagonist tendon vibration, to further characterise the role of inhibition in shaping motoneuron behaviour.

What allowed us to address these questions for the first time was the following experimental framework, common to all three studies. Participants performed isometric plantarflexion tasks, while high-density EMG signals were recorded and decomposed into individual motoneuron firing patterns. Then, synaptic inputs were inferred from the characteristic signatures observed in these firing patterns (Fig. 23).

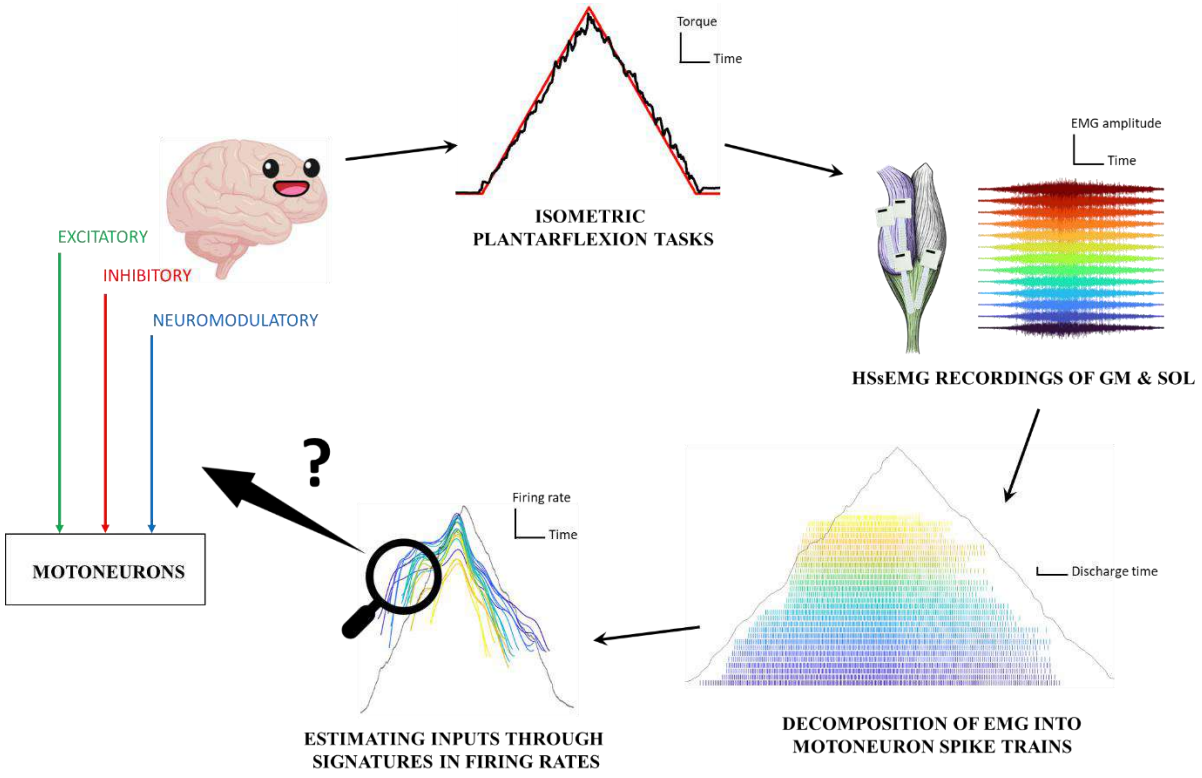

Figure 23. Thesis method overview. *Participants performed isometric plantarflexion consisting of a linear increase and decrease in torque, while high-density surface electromyography (HDsEMG) was recorded from the gastrocnemius medialis (GM) and soleus (SOL). EMG signals were then decomposed into individual motoneuron spike trains and converted into continuous firing rates. Specific firing rate features were quantified and served as "signatures" of distinct synaptic inputs, which allowed estimation of the contributions of excitatory, inhibitory, and neuromodulatory inputs to motoneuron firing.*

METHOD

In each study included in this thesis, analyses are based on the activity of motoneurons from the gastrocnemius medialis (GM) and the soleus (SOL). As detailed previously, impairments of these muscles are common after stroke and SCI and have important functional consequences. Additionally, these muscles are superficial, which allows the decomposition of EMG signals into the activity of individual motoneurons.

The following sections detail (i) the experimental setup and protocol common to all studies in this thesis, (ii) the method used to decompose EMG signals into individual motoneuron activity, (iii) the motoneuron firing rate-related metrics used in the experiments, and (iv) the validation of the metrics used to infer motoneuron inputs.

◥ EXPERIMENTAL SET UP AND PROTOCOL

For all the studies, participants were seated on an isokinetic dynamometer (HUMAC NORM, CMSI, Stoughton, MA, USA), with their foot securely attached to the footplate (Fig. 24). Inextensible straps were tightened to immobilise their torso, pelvis, and thigh of the tested leg. The lateral malleolus was aligned with the dynamometer's axis of rotation. The participant's position was adjusted to ensure a hip angle of 80° (hip extended = 0°) and a knee angle of 10° (leg extended = 0°). The ankle position was set to either 20° of plantar flexion or 0° (neutral ankle position). A third position was set to 20° of dorsiflexion (referred to as -20°) in Study 1, or 10° of dorsiflexion (referred to as -10°) in Studies 2 and 3. Torque signal was digitised at 2048 Hz (Quattrocento, 400-channel EMG amplifier; OT Bioelettronica, Torino, Italia).

For all the studies, participants began with a standardised warm-up consisting of two 5-second contractions at 50%, 70%, and 90% of their self-estimated maximal contraction intensity, with a 20 s rest period between contractions. After a 2-minute rest, they performed two 5-second plantarflexion MVTs at each of the three ankle angles in Study 1, separated by a 2-minute rest period. In Studies 2 and 3, MVTs were recorded only at 20° of plantarflexion and 0° because of limited possibility for participants to repeat contractions and/or to reach the position of -10° of dorsiflexion. If the difference between the two contractions exceeded 5%, an additional MVT was performed. Participants received real-time visual feedback of the torque signal during each effort, and strong verbal encouragement was provided. Peak MVT torque was considered as the

maximal value obtained from a moving average window of 100 ms and was subsequently used to determine submaximal plantarflexion targets. The same procedure was performed to determine dorsiflexion MVTs. After the warm-up and MVT assessments, participants performed a set of isometric submaximal plantarflexion contractions that varies depending on the studies. Accordingly, the rest of the experimental procedure is detailed in the 'Materials and Methods' section of each study in this thesis.

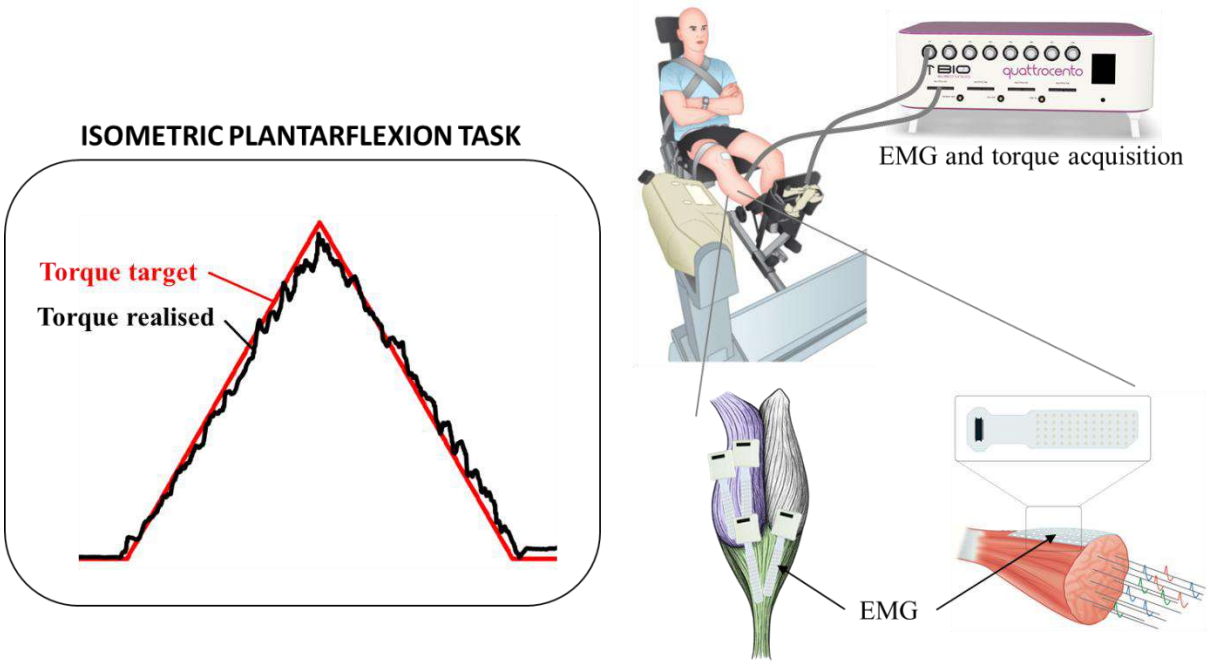

Figure 24. Set up. *Participants were seated in an isokinetic dynamometer and performed isometric plantarflexion consisting of a linear increase and decrease in torque, while high-density surface electromyography (HDsEMG) was recorded from the gastrocnemius medialis (GM) and soleus (SOL). Two EMG grids were used for the GM (in purple) and the SOL (in green).*

High-density surface electromyograms (EMG) were recorded using two 64 electrode grids per muscle (13 x 5 gold-coated electrodes, with one electrode absent in a corner; 4 mm interelectrode distance; OT Bioelettronica, Torino, Italy) placed over the muscle bellies of both the GM, SOL and TA. The GM and SOL muscles were selected because they are strongly affected by both paresis and signs of hyperexcitability in individuals with incomplete SCI (Jayaraman et al., 2006), whereas the TA was assessed to control for the level of coactivation. The electrode grids were attached using disposable bi-adhesive foam layers (SpesMedica, Battipaglia, Italy), and the cavities in the adhesive were filled with conductive paste (SpesMedica, Battipaglia, Italy). A reference electrode (Kendall Medi-Trace, Canada) was placed over the patella, and a ground electrode (strap dampened with water) was placed around the ankle of the tested leg.

The EMG signals were recorded in monopolar mode, bandpass filtered (10–500 Hz), and digitised at a sampling rate of 2048 Hz (EMG-Quattrocento, 400 channel EMG amplifier; OT Bioelettronica, Torino, Italy). The data were acquired using OT BioLab+ software (OT Bioelettronica, Torino, Italy).

◥ DECOMPOSITION OF EMG SIGNAL INTO MOTONEURONS ACTIVITY

1. EMG

Electromyography measures the electrical signal generated by a muscle during contraction (Merletti & Muceli, 2019). This electrical activity originates from action potentials propagating along active muscle fibers. As described earlier, muscle fibers are grouped into motor units, which constitute the basic control unit of muscle contraction. Each action potential discharged by a motoneuron activates all the muscle fibers it innervates. As multiple motoneurons discharge concomitantly, the EMG signal is an interference signal representing the sum of the action potentials of the active motor units (Day & Hulliger, 2001). However, the amplitude of surface EMG is also influenced by physiological and non-physiological factors independent of motoneuron activity which complicates the interpretation of the interference EMG signal (Farina et al., 2004). Factors affecting the EMG signal are notably the volume conductor between the electrodes and the muscle, muscle geometry, muscle crosstalk, and phase cancellation (Farina et al., 2014). The ability to observe the activity of individual motoneurons makes it possible to overcome these limitations by assessing the neural drive, which corresponds to the sum of the action potentials discharged by the motoneurons innervating the muscle (Fig. 25). In addition, access to the neural drive opens a new window on the motor input commands of motoneurons, notably via the approach used in this thesis, detailed in “VALIDATION OF THE METRICS USED TO INFER MOTONEURON INPUTS”.

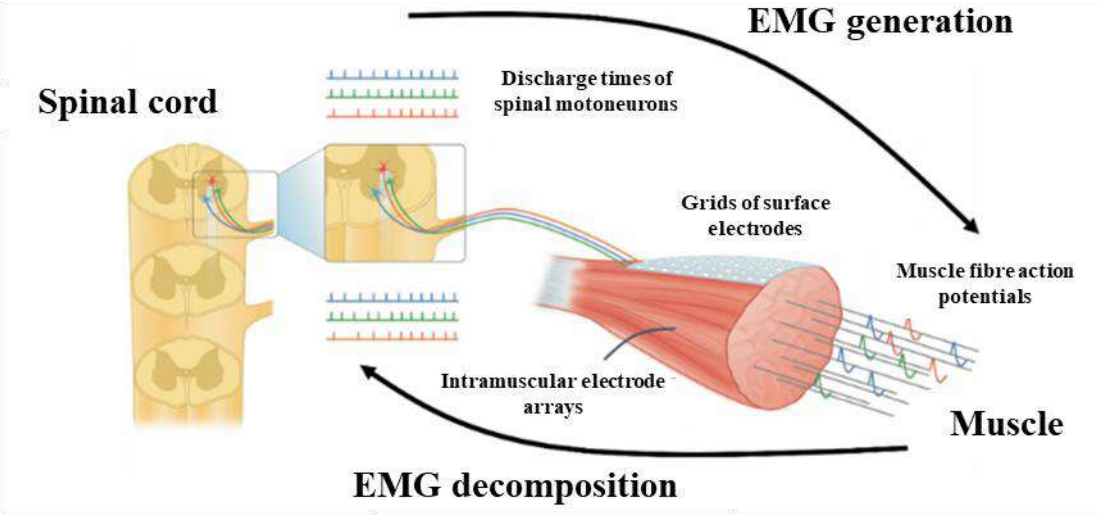

Figure 25. Overview of the EMG decomposition. *The nervous system generates force by activating motor units and modulating their discharge rates. During isometric contractions, the train of motor unit action potentials can be modelled as the convolution of the series of discharge times and the motor unit action potentials. The EMG signals are the sum of the trains of action potentials from the active motor units within the recorded muscle volume. The EMG decomposition with blind source separation consists of inverting the generative model of EMG signals by estimating the series of discharge times for active motor units. For this, blind-source separation algorithms can be applied on EMG signals recorded with grids of surface electrodes. Adapted from Avrillon et al. 2024*

2. EMG decomposition

Following the description of the motor unit (Liddell & Sherrington, 1925), experimentalists developed tools to record their extracellular electrical potentials, with the aim of understanding how the nervous system generates and controls muscle force. From concentric needles to fine wires, from large surface electrodes to dense grids of small surface electrodes (Farina et al., 2016). This last approach was the recording method used in this thesis. Together with algorithms that automatically separate the overlapping activity (i.e., the interference signal) of motor units (Farina & Holobar, 2016; Negro, 2016), it allows the non-invasive recording of tens of motoneurons activity per muscle, as described below.

The process of separating the overlapping activity of motor units into individual motor unit activity relies on the application of a source separation algorithm. In our case, we used the fast Independent Component Analysis (fastICA) algorithm, theoretically described (Farina & Holobar, 2016), validated (Negro, 2016) and implemented in the Muedit software (Avrillon et al., 2024). The main principle behind the source separation algorithm is that each motor unit has a spatio-temporal action potential waveform that differ from all other active motor units within

the recorded muscle volume. Intuitively, it means that each motor unit looks differently on the grid, and the task is thus to identify the particular look of a motor unit to identify when it activates. In technical terms, it consists of optimising a separation vector for each motor unit to separate its series of discharge times from all other active motor units (Farina & Holobar, 2016). As a consequence of this principle, motor units innervating a similar number of muscle fibres and positioned close to each other within the recorded muscle volume are likely not distinguishable. However, increasing the number and spatial distribution of recording electrodes increases the likelihood that each motor unit have a unique motor unit action potential profile (Caillet et al., 2023). The reliable identification of the entire series of discharge times for each motor unit requires stationary recording conditions to keep the separation vector consistent. This explains why, so far, EMG signals should be recorded during isometric contractions. Otherwise, a change in position/orientation of the active muscle fibres relative to the grid electrodes during the recordings can impact temporal and spatial action potential profiles – and thus not align with the main principle behind the decomposition (Avrillon et al., 2024).

The pre-processing of EMG signals first required visual inspection of all the signals to remove the channels with artifacts or low signal to noise ratio, as they may alter the separation vectors. The filtered EMG signals are then extended and whitened before applying the source separation algorithm. Intuitively, the extension step is there to simplify the task of the source separation algorithm by creating short time window of EMG samples that captures the motor unit action potential (MUAP) waveform. So instead of identifying a motor unit only by its spatial profile across electrodes, the algorithm identifies it using its full spatio-temporal profile. Alternatively, it's like converting the time component of the MUAP into a space component; with the extension factor (i.e., time lags) of 16 used in this thesis, the 64 channels of each grid become 16*64=1024 signals. Mathematically, it corresponds to solve an instantaneous linear mixture instead of a convolutive mixture (Negro, 2016). After extension, the signals are whitened through a linear transformation that removes correlations between channels and normalises their variance. This step helps the source separation algorithm that relies on detecting statistical independence between sources.

After pre-processing of the EMG signals, the step to follow consists of iteratively optimising separation vectors for each motor unit to identify a matrix that transforms the whitened EMG signals into the motor unit spike trains (Fig. 26). The separation vector corresponds to a set of weights, $w = [w_1, w_2, w_3, \ldots, w_N]$, applied to all extended-EMG channels (N) to isolate one motor unit. Intuitively, it reflects that motor unit appears on all channels but with different amplitudes.

When fastICA multiplies this vector with the EMG data, it computes a weighted sum of the signals. The weights are determined with a fixed-point algorithm that iteratively optimises the separation vector using a cost function - the skew cost function in this thesis - with aim to maximise the sparsity of the estimated motor unit spike train. The rationale behind maximising the sparsity is that the sum of two or more spike trains is less sparse than a single motor unit spike train. The fixed-point algorithm terminates once the separation vectors are sufficiently invariant between successive iterations, with respect to a pre-set upper bound, or reach 150 iterations. Then, the discharge times are estimated with a peak-detection function and a K-means classification that separate the high peaks (spikes) from the low peaks (noise) (Avrillon et al., 2024). Of note, separation vectors were initialised using the values of the EMG signals at the time instants where the value of the sum of squared EMG signals was maximised.

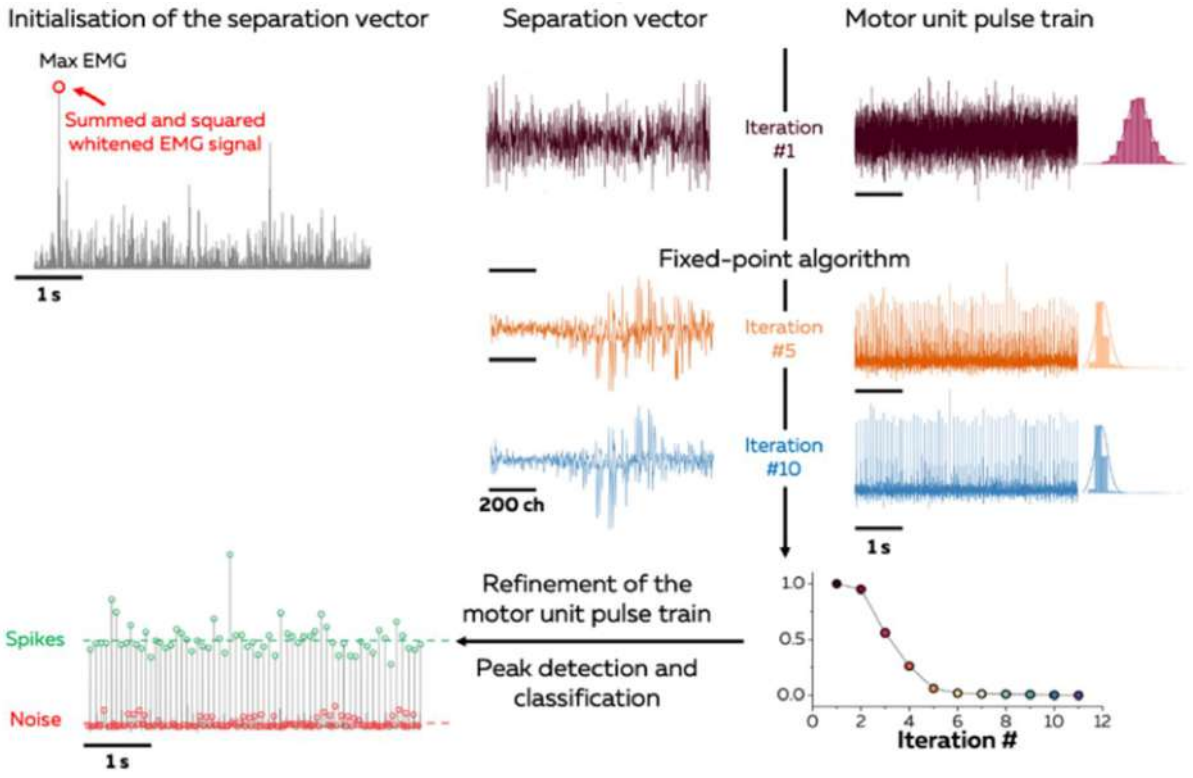

Figure 26. Optimisation of motor unit separation vectors. *A fixed-point algorithm iteratively optimises separation vectors for each motor unit. The projection of EMG signals onto these separation vectors generates motor unit pulse trains, from which the series of discharge times are identified. The separation is initialised using the values of the EMG signals at the time instants where the value of the sum of squared EMG signals is maximised (Max EMG). In this example, the fixed-point algorithm terminated after 11 iterations once the separation vector varied below an imposed upper limit between successive iterations. The evolution of the separation vector, the motor unit pulse train and the distribution of its values are displayed on the right. At the end of the fixed-point algorithm, the discharge times are estimated with a peak-detection function and a K-means classification that separate the high peaks (spikes) from the low peaks (noise). Adapted from Avrillon et al. (2024)*

3. Manual editing of motor unit spike trains

The results provided by the decomposition algorithm need to be assessed for accuracy (Holobar et al., 2014). The silhouette value measures the normalised distance between the spikes and the noise and can be used to assess the reliability of the motor unit spike trains, with a silhouette value higher than 0.9 chosen as threshold for inclusion (Negro, 2016). The manual editing, realised on Muedit, consists of (i) removing spikes causing erroneous discharge rates (outliers), (ii) adding discharge times clearly separated from the noise, (iii) recalculating the separation vector, (iv) reapplying the separation vector on the entire EMG signals, and (v) repeating this procedure until the selection of all the discharge times appears to have been achieved (Fig. 27) (Avrillon et al., 2024). The reliability of this process has been shown to be excellent between operators (Hug et al., 2021). Importantly, as there is a 1 : 1 ratio between action potentials on the neuronal and muscle cell membranes (i.e., the motor unit action potential), this approach informs about the firing behaviour of motoneurons (Farina et al., 2016).

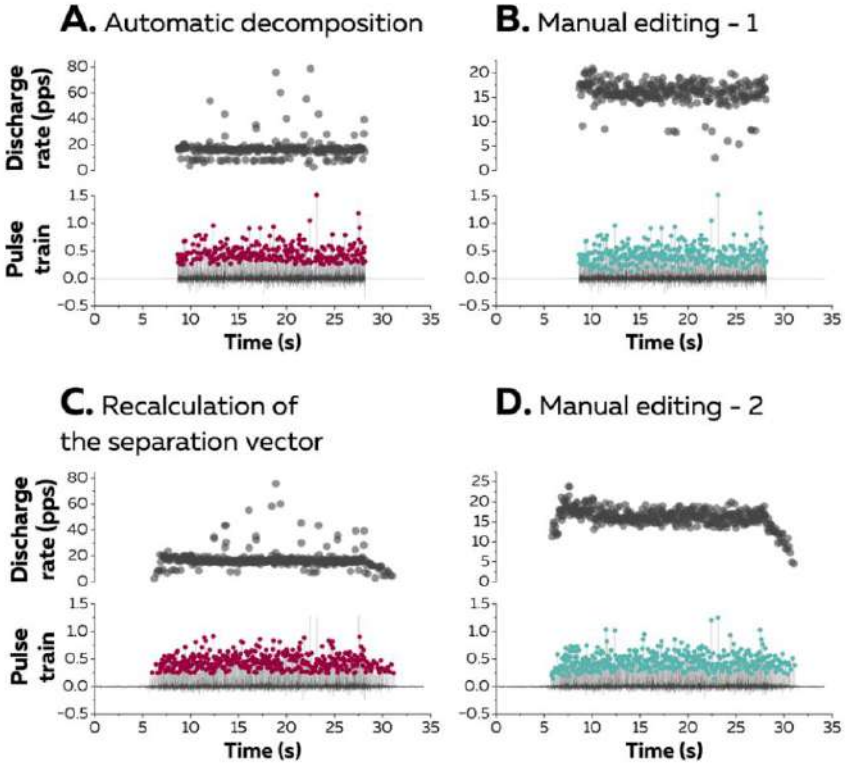

Figure 27. Manual editing of motor unit spike trains. *In this example, the automatic decomposition has been performed on the central segment of the signal, that is, during the plateau of force. (A) After the automatic decomposition, falsely identified discharge times cause erroneous discharge rates while missed discharge times cause drops in discharge rates. (B) One can manually remove or add these discharge times if they are clearly identifiable. (C) After this manual editing, the separation vector is recalculated, and the motor unit pulse train is updated and extended to the limits of the signal. (D) The automatic detection of discharge times is manually corrected another time, and this iterative process stops once the full series of discharge times is identified. From Avrillon et al. (2024)*

4. Validation of spike trains obtained from surface EMG decomposition and manual editing

The crucial problem in EMG decomposition is its accuracy. While any algorithm can provide realistic spike trains, the precise quantification of errors in such estimates remains partially elusive (Marateb et al., 2011). This topic has been largely debated (De Luca et al., 2006, 2015; Farina, Merletti, et al., 2014; Farina & Enoka, 2011). Here, we present what can be considered the three main types of validation.

The first type of validation is via simulation. EMG signals are simulated by generating series of discharge times of motor units via an anatomical model entailing a cylindrical muscle volume with parallel fibres, in which subcutaneous and skin layers separate the muscle from the surface electrodes (Avrillon et al., 2024). Then, EMG signals are decomposed and manually edited to obtain motor unit spike trains. These spike trains are then compared to the ground truth (i.e., the simulated discharge times). Specifically, a rate of agreement is calculated as the ratio between correctly identified discharge times and the sum of correctly identified discharge times, missed discharge times, and falsely identified discharge times. This yields a mean agreement of 95% for surface EMG signals (Avrillon et al., 2024).

A second type of validation assesses the consistency between discharge times identified from surface EMG signals and those obtained through intramuscular EMG signals (Fig. 28), which are considered the reference method (Negro, 2016). The rate of agreement, tested in the first dorsal interosseous muscle, ranges from 98% at 10 %MVT to 91% at 90 %MVT (Negro, 2016).

In addition, the accuracy of EMG decomposition can be assessed for each individual motor unit in each signal analysed. For that, an index of accuracy can be calculated by comparing how much the identified discharge times differ from noise. Specifically, in this thesis, we used the silhouette value, which measures the normalised distance between the spikes and the noise and is used to assess the reliability of the motor unit pulse trains (Negro, 2016). As recommended, we only consider motor units that exhibit a silhouette value higher than 0.9 (Avrillon et al., 2024). These types of index have been shown to correlate significantly with both the sensitivity of the identified MU discharges and their false alarm rates (Holobar et al., 2014), thus constituting the third important type of validity criterion.

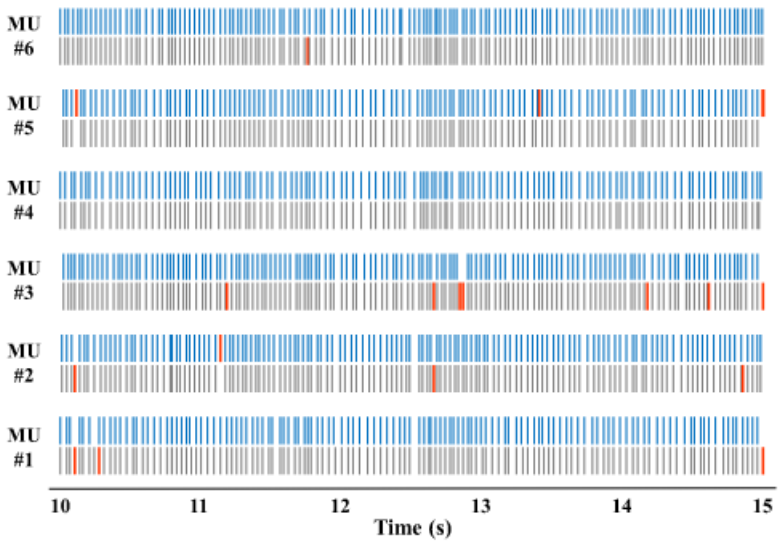

Figure 28. Validation of the decomposition results by comparing decomposition from surface EMG signals to intramuscular EMG signals. *Spike trains obtained by surface EMG decomposition (blue spikes) and intramuscular EMG decomposition (grey spikes) in the first dorsal interosseous at 90 %MVT for six motor units for a representative interval of 5 s duration. Mismatched are shown in red. In this example, the range of agreement calculated for the entire recording of durations 30 s was 91.0 ± 2.2%. Adapted from Negro et al. (2016).*

5. Tracking motor units across contractions

All the studies of this thesis include comparison of motoneuron firing rate-related metrics across different conditions, and thus across different contractions. As a consequence, the EMG decomposition could not directly associate the spike trains of one motor unit in a contraction to the corresponding spike trains of this same motor unit in other contractions. The process of associating the different spike trains to the same motor unit is called the tracking of motor units. To achieve this, the separation vector (also called the motor unit filter) identified in one contraction was applied to the extended and whitened EMG signals of the other contraction (Francic & Holobar, 2021). The resulting spike trains were then compared with those initially obtained and a motor unit was considered tracked if at least 30% of the discharge times was shared (Francic & Holobar, 2021). The details of which contractions were used for the tracking procedure varies depending on the studies. Accordingly, details are in the 'Materials and Methods' section of each study in this thesis. Notably, tracking motor units across contractions can yield a reduced number of motor units for analysis, either due to failure of the tracking procedure or because motor units decomposed across contractions differ, such that only the shared pool is conserved for further analyses.

◥ FIRING RATE-RELATED METRICS

1. Motoneurons recruitment threshold and rate coding

In this thesis, instantaneous firing rates (in pulses per second; pps) were filtered to obtain smooth continuous estimates of firing rate. Specifically, we used support vector regression to create continuous estimates, which minimise fitting errors (Beauchamp et al., 2022). Subsequent analyses are based on these continuous estimates (Fig. 29).

Recruitment threshold of each motoneuron was defined as the torque at its first firing. The firing rate at recruitment was taken as the first value, and the peak firing rate was taken as the maximal value. Firing-rate modulation was calculated as the difference between peak firing rate and firing rate at recruitment.

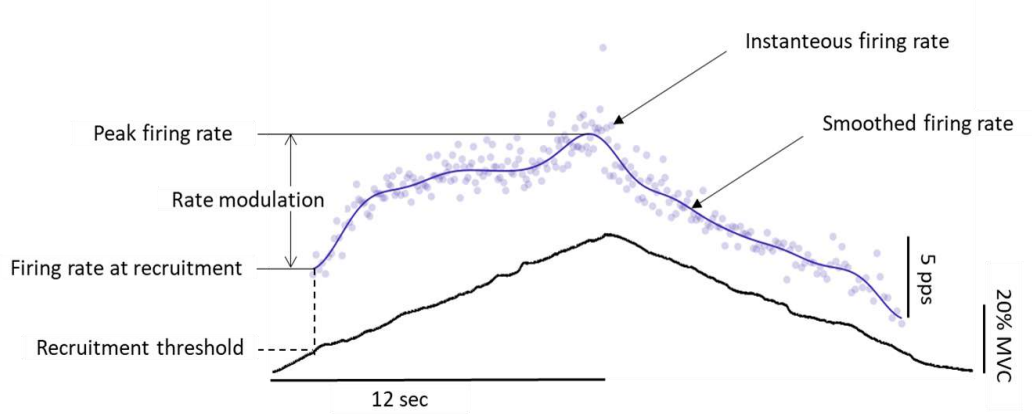

Figure 29. Calculation of recruitment and rate coding metrics. *Instantaneous firing rates of a single motoneuron and the corresponding smoothed estimate (purple trace) are shown during a triangular plantarflexion torque task (black trace). The recruitment threshold of each motoneuron was defined as the torque at the first discharge. Firing rate at recruitment was defined as the initial firing rate, whereas the peak firing rate corresponded to the maximal observed value. Firing rate modulation was calculated as the difference between peak firing rate and firing rate at recruitment.*

2. Historical perspective on estimating synaptic inputs and PICs

As already mentioned in the literature review, mammalian motoneurons have historically been thought of as simple summation devices, linearly adding and subtracting excitatory and inhibitory synaptic inputs to produce graded firing (Granit et al., 1966). However, from the 1970s, it has been demonstrated that similar to other invertebrate/vertebrate neurons (Llinás, 1988), mammalian motoneurons can exhibit nonlinear properties, such as amplification and

prolongation of synaptic input (Hounsgaard et al., 1988; Schwindt & Crill, 1980). The prolongation effect mediated by PICs has been the first to be explored in humans with a series of works that led to the paired motor unit approach (Crone et al., 1988; Eken & Kiehn, 1989; Gorassini et al., 2002; Gorassini et al., 1998; Kiehn & Harris-Warrick, 1992) which has experienced a revival with the rise of non-invasive recording of large population of motoneurons with high density EMG and decomposition (Khurram et al., 2022; Mesquita et al., 2024).

The estimation of PIC-related prolongation in human motoneurons is conceptually straightforward. It involves determining whether a difference exists in net synaptic input between the recruitment and derecruitment phases of a motoneuron, which would indicate the presence of self-sustained firing. To address this, the paired motor unit approach relies on the firing rate of a lower-threshold motor unit as a proxy for the common synaptic input. This requires to assume that both units receive the same synaptic input or at least linearly related synaptic input (common drive) (Farina et al., 2014) and that the control unit responds relatively linearly to the common synaptic input (Bennett et al., 2001). Accordingly, and as will be detailed in the section "4. The paired motor unit approach in practice", a key criterion for applying the paired motor unit approach is that the firing rates of the pairs are highly correlated, in order to ensure that they share a common synaptic input. Conceptually, it might be difficult to understand how the second assumption could hold if the control unit has also a PIC-related depolarised current. However, this simply means that there is an added depolarisation produced by a PICs, and the synaptic current can still produce changes in firing rate. Also, importantly, PICs are activated near recruitment, contributes to the initial acceleration and are not further activated during increases in synaptic input (i.e., already fully activated); thus, it does not interfere with linear rate modulation. Within these conditions, a difference in the firing rate of the control motoneuron between the recruitment and the derecruitment of the test unit would guaranty that responses of the motoneuron could be attributed to intrinsic properties only (i.e., not to a change of synaptic input). This difference of firing rates is called ΔF (in pps) (Fig. 30).

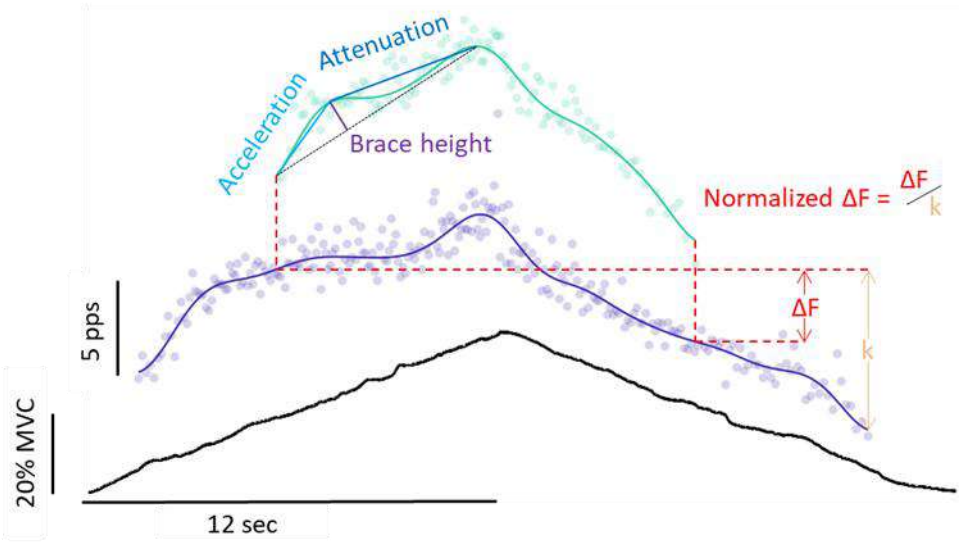

Figure 30. Analyses from motoneuron firing rate. *The geometric approach was used to calculate brace height, acceleration, and attenuation, which were used to estimate the level of neuromodulation, PICs amplification effect on the firing, and the pattern of inhibition, respectively. Persistent inward currents (PICs) prolongation effect on firing were estimated using the paired motoneuron analysis (ΔF). In this example, the test motoneuron's smoothed firing rate is shown in green, while the control units' smoothed firing rates are shown in purple. Normalised ΔF is calculated by dividing ΔF by the difference in the control motoneuron at test motoneuron recruitment and the firing rate at control motoneuron derecruitment.*

Thus, the approach is close to the one used to characterise these properties in animal models, where controlling synaptic input is realised through intracellular current injection (Hounsgaard et al., 1988; Schwindt & Crill, 1980). Comparison of these approaches constituted the first validation of the approach. Estimate of the effect of sustaining motor-unit firing (from change in control unit rate) was quantitatively very similar to that obtained with intracellular recording in vitro in the same population of motoneurons. The consistency of the results from intracellular recording and motor-unit recordings provided a validation of paired-motor-unit method (Bennett et al., 2001). First assessments provided ΔF values around 3.6 Hz for an initial recruitment of 9.8 Hz (Gorassini et al., 2002). This was interpreted as a possible 40% reduction in the estimated synaptic input needed to maintain firing of a motor unit compared with the estimated amount needed to recruit the unit initially. Therefore, it suggested that PICs provide a substantial source of depolarisation in human motoneurons.

Later, it has been suggested that other intrinsic properties, notably via spike frequency adaptation (i.e., the tendency of firing rate to decrease with time), could lead to positive ΔF values, even in the absence of a PIC contribution (Revill & Fuglevand, 2011). However, the use of

biophysical models of motoneurons revealed that although ΔF values are not linearly related to PIC levels and can be affected by other factors, ΔF values > 1 Hz require a significant level of PIC generated by dendritic channels, and increases in PIC above this minimum level should lead to higher ΔF values. Thus, it was thought that although other factors can contribute, variations in discharge hysteresis and ΔF values primarily reflect the contribution of dendritic PICs to motoneuron activation. As will be detailed below, current best knowledge suggests that ΔF is the result of the combined influence of neuromodulatory inputs and of the pattern of inhibition (Beauchamp et al., 2023; Chardon et al., 2024). As a consequence of its dependence on inhibitory inputs, ΔF is thus not a good estimate of neuromodulatory inputs. Nevertheless, it reflects the prolongation effect of PICs on firing rate during in vivo assessment, that would not occur without metabotropic neuromodulatory inputs.

Beyond its prolongation effect, neuromodulatory inputs, through PICs, also induce an amplification of the synaptic inputs and thus non-linearities in motoneuron discharge. Specifically, PIC amplification causes a sharp initial rise of the discharge followed by a saturation, during a linear increase in force production. Thus, the discharge profile during a linear ascending phase of force yielded potential quantifiable properties that can be used to estimate neuromodulatory inputs. Based on this idea, Beauchamp et al. (2023) proposed to quantify the non-linearity in the discharge profile with a « geometric approach » (Fig. 30). As detailed in the next section, this method defines three main metrics: brace height, acceleration slope and attenuation slope. Intuitively, brace height corresponds to the maximal deviation in discharge rate from linear increase (i.e., the theoretical net synaptic input); acceleration correspond to the initial slope of the discharge rate; and attenuation slope corresponds to the slope after saturation.

Importantly, and as will be detailed in the section “VALIDATION OF THE METRICS USED TO INFER MOTONEURON INPUTS”, modeling studies (Beauchamp et al., 2023; Chardon et al., 2024) have shown that:

- *brace height* is specifically sensitive to the level of neuromodulation, which is likely proportional to monoamine release and enhances the effective strength of PIC channels;
- *attenuation slope* is specifically sensitive to the pattern of inhibition, that is how synaptic inhibition covary with synaptic excitation, such that a steeper attenuation slope reflects a stronger push-pull inhibitory pattern, meaning inhibition decreases as excitation increases; and

- *acceleration slope*, reflecting the amplification effect of PICs on firing rate (Avrillon et al., 2024; Revill & Fuglevand, 2017), is the result of the combined influence of neuromodulatory inputs and of the pattern of inhibition. Acceleration slope is thus the counterpart of ΔF, which reflects the prolongation effect of PICs on firing rate and is also influenced by both neuromodulatory inputs and the pattern of inhibition.

Thus, the contribution of inhibitory and neuromodulatory inputs to the motoneuron behaviour; as well as the amplification and prolongation effect of PICs (i.e., PIC-mediated amplification and prolongation) can be inferred from specific features of the firing rate (Beauchamp, et al., 2023; Chardon et al., 2024).

3. The geometric approach in practice

The geometric approach assesses how much the motoneuron firing rate deviates from a linear relationship with time output during the ramp-up phase of the contractions. More precisely, the relationship with time was used in Studies 2 and 3 while torque relationship with %MVT or N.m was used in Study 1. The rationale behind all these variables is that they correlate with the net synaptic input received by the motoneuron pool. For example, the net synaptic input likely increases during the ascending phase of the contractions, which is represented by the concomitant increases in torque (Beauchamp et al., 2023) or time (Chardon et al., 2024). While the torque is conceptually better, we chose to present the time in Studies 2 and 3 because it facilitates comparison across populations and conditions. Notably, results in this thesis were consistent across these different options.

Continuing the illustration with time, the smoothed firing rate of each motoneuron was plotted against the time generated during a contraction. The largest perpendicular distance between this firing rate and a hypothetical linear increase from recruitment to peak firing rate was quantified, and this distance was defined as brace height. To ensure that brace height reflects only the relative deviation from a linear pattern and to eliminate any bias from differences in peak firing rates across groups, brace height was normalised to the height of a right triangle, where the hypotenuse runs from the point of recruitment to the peak firing rate. We excluded firing trains of motoneurons if they showed a negative slope during the acceleration phase or had a negative brace height before normalisation. This method splits the firing rate into acceleration and attenuation phases, which could unintentionally create an artificial attenuation phase if the true attenuation phase had not been reached during the ascending phase of the triangular contraction.

To avoid this, motoneuron firing trains were excluded if the duration between recruitment and peak firing rate was shorter than 3 s. Exhaustive visual assessment of the geometric approach to motoneuron firing rates (Fig. 31) made us reconsider this criterion along the thesis, and a 4 s threshold was used in the Study 3. In addition to brace height, we calculated the slopes of both the initial acceleration phase and the subsequent attenuation phase of the motoneuron firing rate (Fig. 30).

Notably, as the geometric approach required sufficient time activation, it cannot be used in the higher threshold motoneurons of a given contraction intensity. Conversely, the paired motor unit approach requires the use of lower threshold motoneurons and it thus not usable for low threshold motoneurons.

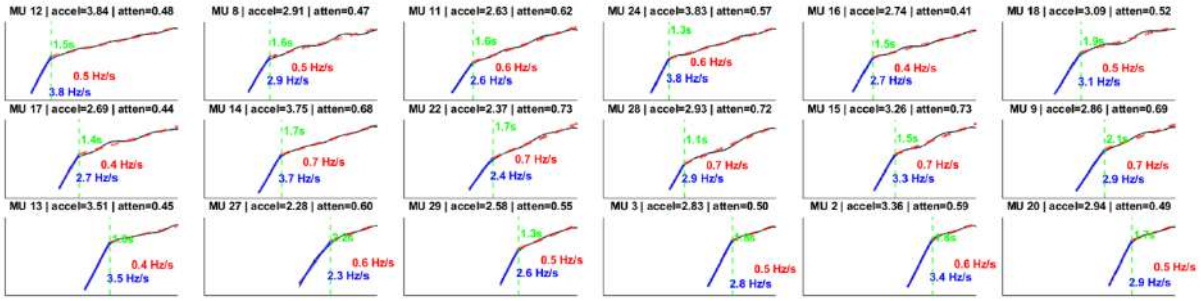

Figure 31. Visualisation of the acceleration and attenuation slopes. *An exhaustive visual assessment of the geometric approach applied to motoneuron firing rates was performed, showing for each motor unit (MU) the acceleration (blue) and attenuation (red) slopes, as well as the onset of the attenuation phase (green).*

Previous studies in stroke have described what has been presented as a particular feature of rate coding: negative rate modulation, defined as a decrease in firing rate following the initial increase despite continued increases in torque or EMG amplitude (Beauchamp et al., 2023; Mottram et al., 2009). Because this pattern can challenge the geometric approach, we implemented a bilinear fit to separate the initial increase from the subsequent saturation in Study 3. An exhaustive visual assessment of this approach was performed, as illustrated in Figure 32.

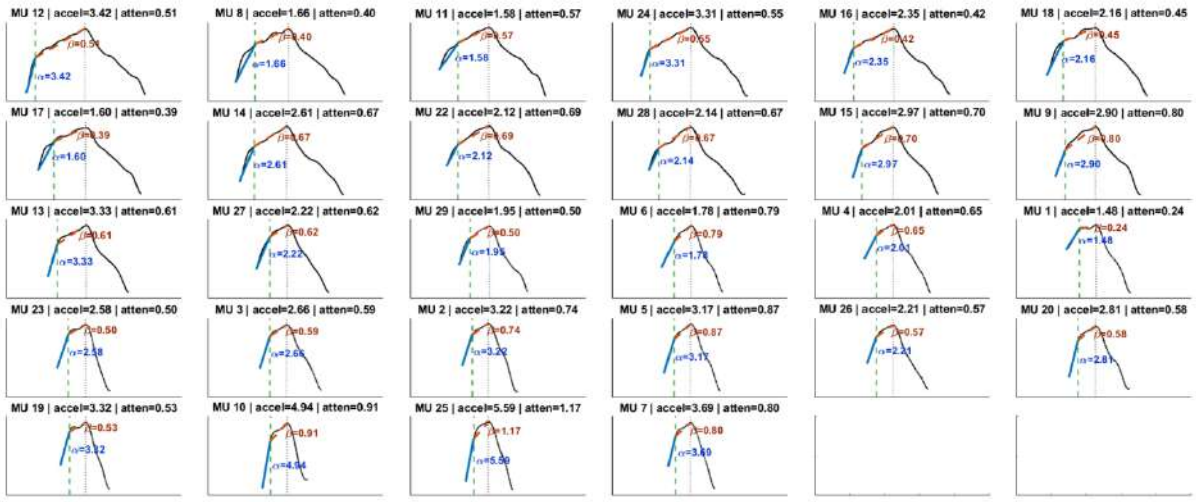

Figure 32. Visualisation of the bilinear approach. *An exhaustive visual assessment of the bilinear approach applied to motoneuron firing rates was performed, showing for each motor unit (MU) the acceleration (blue) and attenuation (red) slopes.*

4. The paired motor unit approach in practice

Non-linearities in motoneuron firing during the descending phase of triangular contractions were quantified using the paired motoneuron analysis (Gorassini et al., 2002). For this analysis, motoneurons with a lower recruitment threshold (control units) were paired with motoneurons with a higher recruitment threshold (test units). The difference in the firing rate of the control motoneuron between the time at recruitment and the time at derecruitment of the test unit was calculated and referred to as ΔF. In agreement with previous work, the criteria for including a pair of motoneurons were as follows: 1) the test motoneuron should fire for at least 2 seconds, 2) the test motoneuron should be recruited at least 1 second after the control motoneuron to ensure full activation of PIC, 3) the test motoneuron should be derecruited at least 1.5 seconds before the control motoneuron to avoid overestimation of ΔF, and 4) a coefficient of determination (r^2) > 0.7 should be observed between the smoothed firing rates of the test and control motoneuron (Hassan et al., 2020). ΔF values are presented as "unit-wise" averages for all suitable test-control motoneuron pairs, thus reducing the number of ΔF values to one value per test unit. *ΔF* reflects the prolongation effect of PICs on firing rate and is the result of the combined influence of neuromodulatory inputs and of the pattern of inhibition (Beauchamp et al., 2023; Chardon et al., 2024). Because ΔF depends on the firing rates of the control unit, which differ between the two populations studied here, we complemented the analysis by normalising ΔF to the maximal value that could have occurred based on the modulation of the control motoneuron. Specifically, ΔF was divided by the difference in the control motoneuron firing rate at test

motoneuron recruitment and at control motoneuron derecruitment (i.e., “k”, Fig. 30) (Škarabot et al., 2025). An exhaustive visual assessment of this approach was performed, as illustrated in Figure 33.

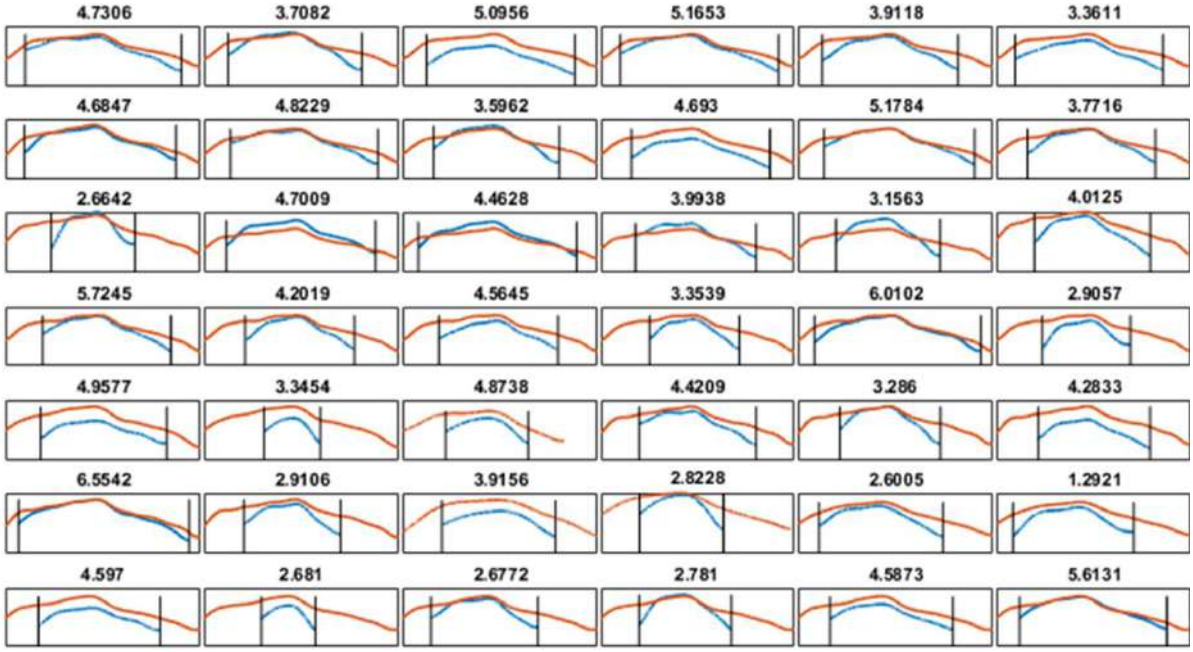

Figure 33. Visualisation of the paired motor unit approach. *An exhaustive visual assessment of the paired motor unit approach was performed, showing for each pair the two firing rates, as well as the ΔF calculation and its resulting value. Firing rates of test motor units are shown in blue, whereas firing rates of control motor units are shown in red. Corresponding ΔF values are displayed above the firing-rate plots.*

5. MUAP

MUAP amplitude was used as a proxy for motor unit size. In detail, MUAPs were extracted using spike-triggered averaging of high-density surface EMG signals. Single differential EMG signals were computed along the electrode columns and used for subsequent analysis. Spike-triggered averaging was performed using all the firing times identified by decomposition as triggers. MUAPs were extracted using a 170-sample window centered on each firing time (~12 ms), and the resulting averaged waveforms were detrended (Fig. 34). For each motor unit, peak-to-peak amplitude was calculated for each available single differential channel as the difference between the maximum and minimum values of the averaged MUAP waveform. The MUAP amplitude for a given motor unit was defined as the maximum peak-to-peak value observed across all channels. This procedure was applied to all identified motor units, and MUAP amplitude values were subsequently grouped according to the corresponding muscle.

Figure 34. Recording of motor unit action potentials. *Motor unit action potentials (MUAPs) were extracted using spike-triggered averaging of high-density surface EMG signals. Each trace represents the average MUAP over a 12 ms window centred on each discharge. This example illustrates MUAPs from two soleus motor units recorded within the same EMG grid.*

◥ VALIDATION OF THE METRICS USED TO INFER MOTONEURON INPUTS

1. Introduction to conductance models of motoneurons

In the literature review, we introduced the Goldman equation, which expresses the dependency of the membrane potential on ionic permeability and ion concentrations. This notably allowed determination of the resting membrane potential. However, this equation is limited for describing time-dependent changes in membrane potential or for quantifying the magnitude of individual ionic currents. This information can be obtained using a simple mathematical model derived from electric circuit theory. The model, called an equivalent circuit, represents the key electrical properties of the neuron using resistors, batteries, and capacitors. Equivalent circuits provide both biophysical insight and a quantitative description of how ionic currents generate changes in membrane potential and ultimately electrical signals (i.e., sequences of action potentials) in neurons. This type of model was used to validate the metrics employed to infer motoneuron inputs and is therefore presented below. First, the original Hodgkin–Huxley model is introduced for pedagogical purposes. The following section will present the main adaptations of this model, along with the rationale and results of the simulations used to validate metric interpretation (Beauchamp et al., 2023; Chardon et al., 2024).

In terms of electrical properties, the lipid bilayer confers capacitance to the membrane, defined as the ability of an electrical nonconductor to separate charges across it. The separation of charges on the inner and outer surfaces of the cell membrane gives rise to the transmembrane potential difference, given by:

$$V = Q/C$$

Equation (4)

where Q is the net excess positive or negative charge on each side of the capacitor and C is the capacitance.

However, the membrane behaves as a leaky capacitor because it is studded with ion channels that can conduct charge. Otherwise, the lipid bilayer itself has effectively zero conductance or infinite resistance. Importantly, unlike a resistor, which responds to a step current with an instantaneous voltage change, the membrane potential evolves over time due to its capacitance.

To change the charge across the capacitor, there must be current across the capacitor (I_c). Since current is the flow of charge per unit time ($I_c = \Delta Q/\Delta t$), the change in voltage across a capacitor depends on both the magnitude and duration of the current:

$$\Delta V = I_c \,.\, \Delta t / C$$

Equation (5)

In neurons, the current across the capacitor corresponds to the flux of ions moving through membane channels according to their selectivity. Accordingly, taking account of the two mains ions Na^+ ($I_{NA}{}^+$) and K+ ($I_K{}^+$), and addind a leak current (I_L) that accounts for baseline membrane permeability to ions, the change of membrane voltage is given by:

$$C \frac{dV}{dt} = -(I_{Na} + I_K + I_L)$$

Equation (6)

So far, the notion of permeability has been used to describe the opening of ion channels. A crucial part of the modeling process is the transition from permeability to conductance, which represents its cellular level modelisation. In the equivalent circuit, a particular ion conductance of the cell membrane in its resting state equals the number of open channels multiplied by the conductance of a single channel. However, for the purpose of linking the membrane voltage (V_m) to ions currents, the important notion is to incorporate the dependance of each ionic current to the electrical and chemical driving forces, which is given by:

$$I_x = g_x \,(E_x - V_m)$$

Equation (7)

Where g is the conductance, E the equilibrium potential and x a particular ion. The conductance is modeled as a resistor governed by Ohm's law (I = g.V), while the difference between the voltage membrane and the equilibrium potential represents the electrochemical driving force, which is modeled as a battery (ions are pushed toward their equilibrium potential). The resulting equivalent circuit is shown in Figure 35.

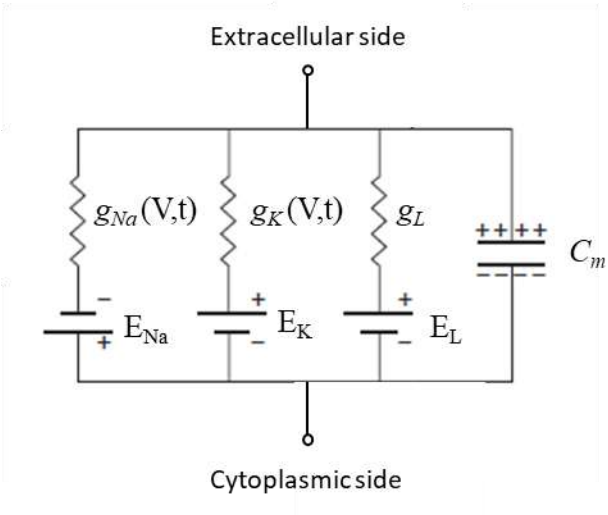

Figure 35. A simple equivalent circuit of a neuron. *The basic components of Hodgkin–Huxley-type models, which represent the biophysical characteristics of the cell membrane, include the lipid bilayer, represented as a capacitance (C_m). Voltage-gated and leak ion channels are represented by conductances (g). The electrochemical gradients driving the flow of ions are represented by batteries (E).*

What have been ignored so far is that channels underlying action potentials are voltage gated, implying that conductance is both voltage- and time-dependent. Combining these elements, the voltage-current relationship becomes:

$$C\,\frac{dV}{dt} = -(\,g_k(V,t)(E_k - V_m) + \,g_{Na}(V,t)(E_{Na} - V_m) + \,g_L(E_L - V_m))$$

Equation (8)

In detail, the ionic conductances are defined by three differential equations that will not be detailed here. However, the relevance of these equations will be illustrated using the sodium conductance, given by:

$$g_{Na}(V,t) = \,\bar{g}_{Na}m^3h$$

Equation (9)

Where $\bar{g}_{Na}$ is the maximal conductance of the sodium channels, m the activation gate variable and h the inactivation gate variable.

Originally, Hodgkin and Huxley empirically fitted their experimental measurements to derive equations describing Na^+ and K^+ conductances as functions of voltage and time. Despite their empirical nature, these formulations provided critical insight into the biophysical basis of voltage gating. Specifically, they suggested the existence of an ion channel gate composed of three

activation subunits, all of which must be open for channel activation (reflected by m^3), and a separate inactivation mechanism represented by h. Remarkably, these predictions were confirmed more than 50 years later through X-ray crystallography studies of voltage-gated channels. In sodium channels, this revealed a structure consistent with the model: three activation-related subunits and a fourth subunit associated with inactivation, corresponding to three functional states: resting, activated, and inactivated. Each represents a distinct channel conformation (Fig. 36).

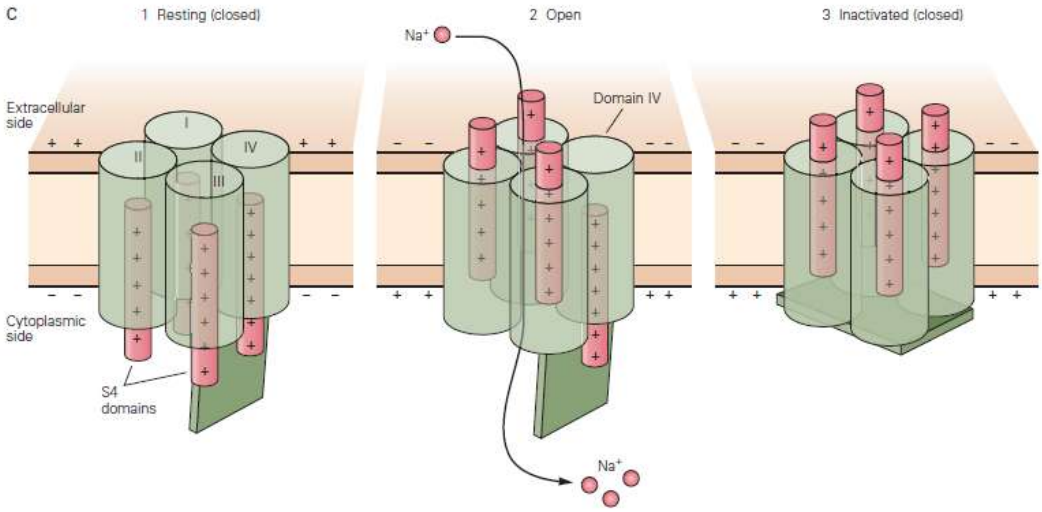

Figure 36. Different conformations of sodium channels. *Diagrams depict the redistribution of gating charge and positions of the activation and inactivation gates when the channel is at rest, open, and inactivated. The red cylinders represent the S4 regions containing the positive gating charges. Depolarisation of the cell membrane from the resting state causes the gating charge to move outward. Outward movement of the S4 regions of domains I, II, and III is associated with activation, whereas slower movement of the S4 region of domain IV is associated with inactivation. The movement of the S4 region of domain IV allows an intracellular loop between domains III and IV (depicted as a green rectangle) to bind to a docking site at the inside of the pore, allosterically stabilising an inactivated closed state. From Kandel et al. (2021)*

2. Input commands induces “signatures” in motoneuron firing patterns

The model presented above is limited in its ability to account for the diversity of motoneuron behaviours. Accordingly, a more complex model was implemented for the following studies. Specifically, the model detailed below was developed to reproduce the range of input–output behaviours recorded in GM motoneurons in decerebrate cats, with additional adaptations to better match firing rate profiles observed during moderate voluntary contractions in humans (Beauchamp et al., 2023; Chardon et al., 2024; Powers & Heckman, 2017).

Like the Hodgkin–Huxley equivalent circuit, this model includes resistor–battery elements in series to represent the dependence of ionic currents on conductance and reversal potential. For convenience, these elements are represented using the "bow-tie" symbol (Fig. 37). The model includes Na^+, K^+, and leak conductances, as well as additional conductances accounting for afterhyperpolarisation (I_{mAHP}) and hyperpolarisation-activated mixed-cation current (I_{HCN}), and resistors that link the soma and dendrite compartments.

Importantly, the model also includes calcium conductance mediating the slowly-activating PIC (CaPIC) into each of the dendritic compartments, given by:

$$I_{CaL} = g_{CaL} m_{CaL} (V - E_{CaL})$$

Equation (10)

Where I_{CaL} is the current for the L-type calcium channel, g_{CaL} is the conductance of the L-type calcium channel, m_{CaL} is the activation gate, V is the compartment voltage, and E_{CaL} is the reversal potential for the L-type calcium channel.

The model is implemented as a motoneuron pool, consisting of 20 motoneurons with a range of intrinsic properties humans (Beauchamp et al., 2023; Chardon et al., 2024; Powers & Heckman, 2017). As detailed below, these properties enable the model to reproduce characteristic features of human motoneuron behaviour, including orderly recruitment and nonlinear rate modulation (Powers & Heckman, 2017).

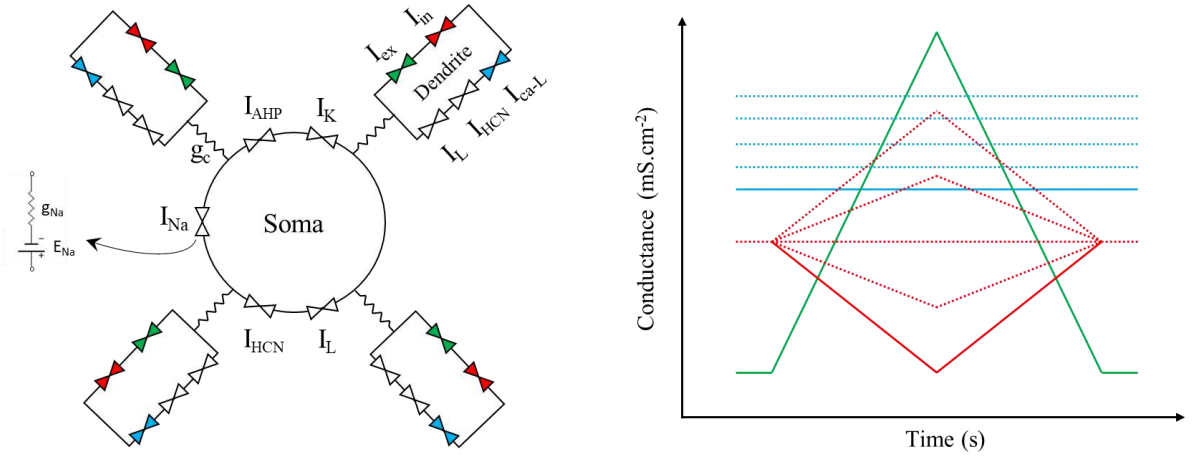

Figure 37. Conductance-based motoneuron model and simulation possibilities. *The model includes a soma compartment connected to four dendritic compartments via resistors. Resistor–battery elements are represented using a "bow-tie" symbol and notably include calcium conductances mediating persistent inward currents (PICs). Simulations can be run using this model by varying excitatory (green), inhibitory (red), and PIC (blue) conductances as a function of time.*

With this model, simulations can be performed by varying known inputs to evaluate the resulting firing behaviour, thereby linking specific inputs to outputs. Figure 38 illustrates the simple case of varying the excitatory input by changing the excitatory conductance in dendrites. Specifically, a change in excitatory conductance induces corresponding changes in both dendritic compartments (Fig. 38, middle panel, blue and red curves) and the soma (Fig. 38, middle panel, black curve). The firing rate of a given motoneuron is then obtained by computing the inverse of the interspike interval at the soma. A continuous firing rate is subsequently derived by applying a smoothing filter (1-s Hanning filter in Fig. 38). As can be seen in Figure 38 (bottom panel), the excitatory conductance is not linear but noisy, which aim to reproduce that common inputs to motoneuron pools are not perfectly shared but contain noise.

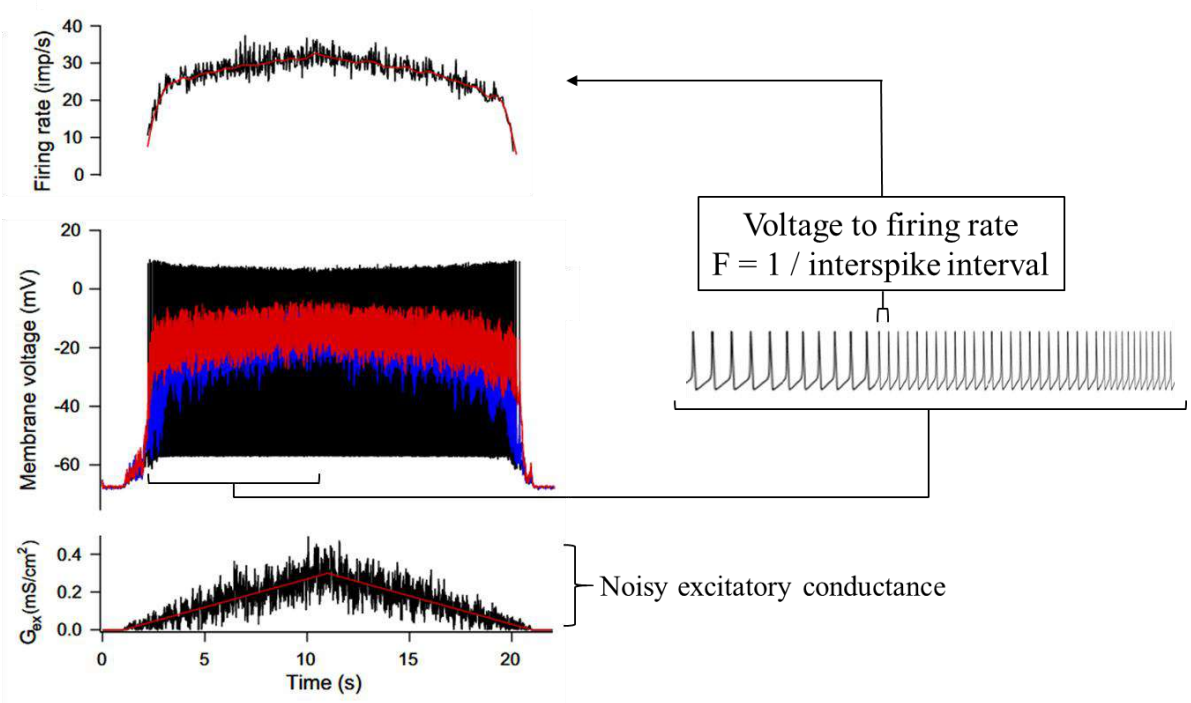

Figure 38. Simulations: from conductance to firing rates. *From top to bottom, a noisy conductance command (black; mean level indicated by a red trace) is applied to the model, which modulates the membrane voltage of dendritic compartments (only two compartments are shown, in blue and red) and of the soma (black). Changes in somatic conductance are converted into raw (black) and smoothed (red) instantaneous firing rates by taking the inverse of interspike intervals. Adapted from Powers & Heckman (2017).*

Studies by Powers & Heckman (2017) and Beauchamp et al. (2023) used this model to examine firing rates across different levels of neuromodulatory drive and patterns of inhibition. Neuromodulatory inputs were adjusted by multiplying the max conductance of the L-type calcium

channels by a multiplier (0.8, 0.9, 1.0, 1.1, 1.2), thereby modulating the magnitude of PICs. The max conductance is defined as:

$$g_{CaL} = \bar{g}_{CaL} R_{mod}$$

Equation (11)

Where R_{mod} is the gain factor that scales the maximum conductance $\bar{g}_{CaL}$, thus completing the equation 10.

The pattern of inhibition was parameterised as a function of excitatory input through dendritic inhibitory conductance. Specifically, inhibition was adjusted to represent either proportional inhibition (positively scaling with excitation) or push–pull inhibition (negatively scaling with excitation). The relationship between inhibitory (I_{in}) and excitatory input (I_{ex}) is given by:

$$I_{in} = G_{in} I_{ex} + b_{in}$$

Equation (12)

Where the excitatory input Iex is multiplied by a gain G_{in} and biased by b_{in} as defined by:

$$b_{in} = G_{in} R_{mod} - 1.25 {R_{mod}}^2 - 1$$

Equation (13)

The inhibitory gain, G_{in}, is varied from –0.7 to 0.7 in increments of 0.1, thereby spanning control schemes from push–pull to proportional inhibition. Notably, these equations explicitly couple inhibition to neuromodulation via the bias term b_{in}.

Results of varying levels of neuromodulatory drive and patterns of inhibition is shown in the Figure 39. Push-pull inhibition leads to firing rate profiles that rise and fall more smoothly with changes in excitatory input, whereas balanced inhibition leads to more pronounced firing rate saturation. Increasing the neuromodulatory level produces higher firing rates, but increases rate saturation, particularly for proportional inhibition. It also produces more hysteresis, leading to discharge that outlasts the excitatory command, particularly for proportional inhibition.

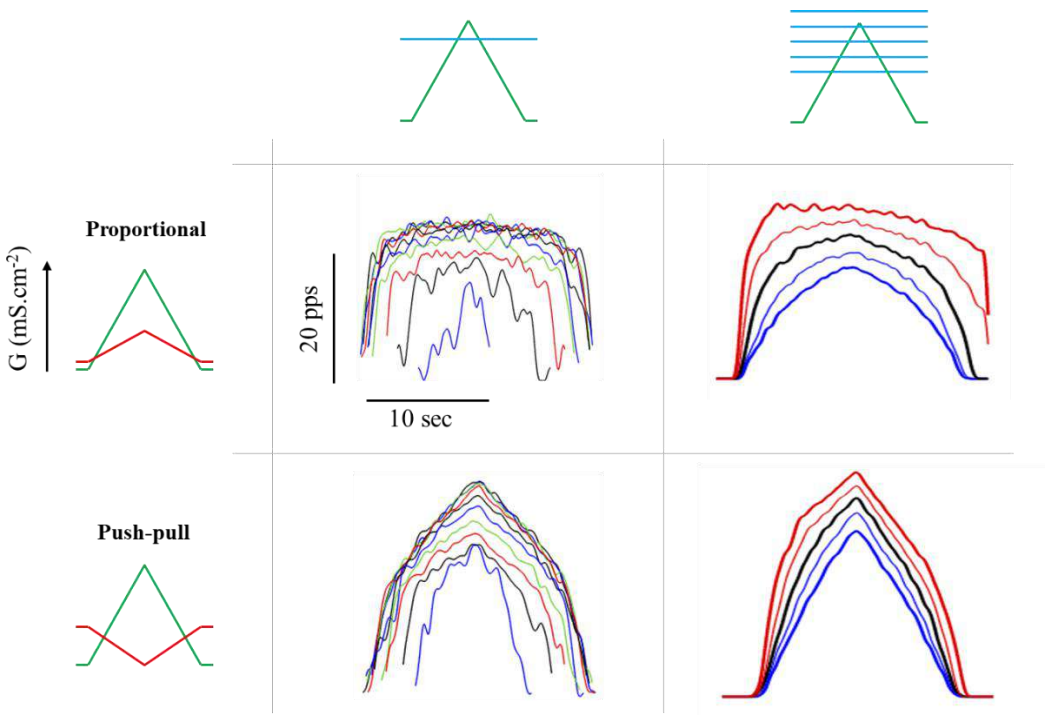

Figure 39. Time course of firing rates depending on the inhibitory pattern and the level of neuromodulatory input. *Model responses to combinations of either proportional or push–pull patterns of inhibition with different levels of neuromodulation are shown either as samples of 10 motoneuron firing rates (thin lines); or as average firing rate responses (thick lines) for the five levels of neuromodulation tested (sky blue lines). Adapted from Powers and Heckman (2017).*

While these results highlight the nonlinear affects specifically related to inhibitory pattern and neuromodulatory drive, the study by Powers & Heckman (2017) did not provide firing-related quantitative metrics directly relatable to synaptic input commands. This gap was addressed by Beauchamp et al. (2023), who linked synaptic input organisation to measurable features of motoneuron firing. Specifically, four main metrics presented above (brace height, attenuation, acceleration, and ΔF) were tested for their ability to detect changes in neuromodulatory and inhibitory inputs through linear regressions. The main results as shown in Figure 40. Theses results clearly reaveled that:

- *brace height* is specifically sensitive to the level of neuromodulation (not associated with the inhibitory pattern);
- *attenuation slope* is specifically sensitive to the pattern of inhibition (not associated with the level of neuromodulation); and
- *acceleration slope* and Δ*F* are the result of the combined influence of neuromodulatory inputs and of the pattern of inhibition.

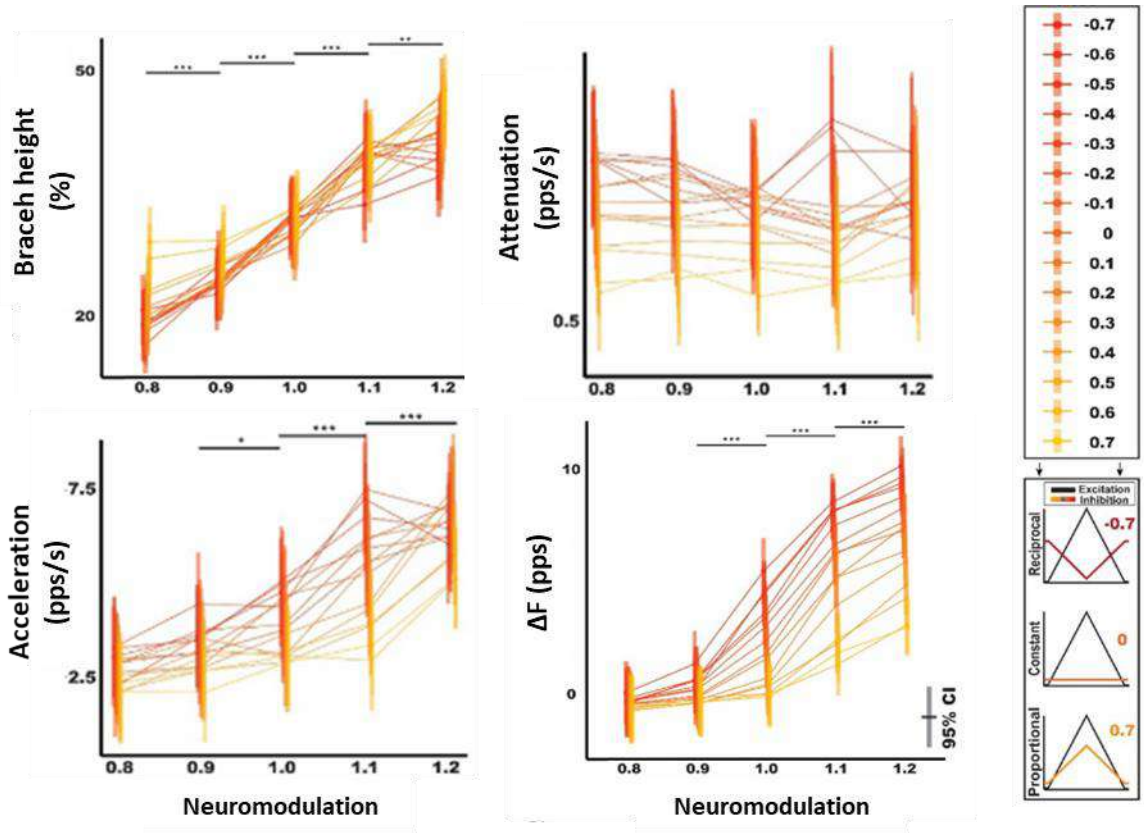

Figure 40. The effects of neuromodulation and inhibitory pattern on ΔF, brace height, acceleration slope, and attenuation slope. *Estimated values are shown on the specified scales with neuromodulation levels across the x-axis and vertical bars indicating mean and 95% confidence intervals (CI). The indicated neuromodulation values represent a multiplier applied to the max conductance of the L-type calcium channel used to simulate the PICs. Horizonal lines connect means for each level of inhibitory profile and are coloured with reciprocal inhibitory patterns in red and proportional inhibitory patterns in yellow. The numerical values and colour mapping indicated in the legend represent the excitation–inhibition coupling, with the pattern of inhibitory input varied in a reciprocal (−, red) or proportional (+, yellow) fashion. These values range from −0.7 to 0.7 and indicate the proportion of inhibition to excitation (i.e. 0.7: peak inhibition conductance ~70% of excitation). pps: pulse-per-second; s: second. Adapted from Beauchamp et al. (2023)*

These findings indicate that motoneuron firing patterns contain exploitable signatures of synaptic input organisation. However, an important limitation remains: these approaches rely on forward simulations with known inputs, whereas in human experiments, inputs are unknown, raising the issue of inverse inference (i.e., inferring inputs from observed outputs). Chardon et al. (2024) addressed this limitation by developing a reverse engineering framework. Their objective was to determine whether firing patterns contain sufficient information to uniquely identify input combinations. A major concern was that the motoneuron input–output relationship may be non-unique, with multiple input configurations producing similar outputs. However, their results demonstrated that firing patterns substantially constrain the solution space,

achieving 75–90% variance explained in predicted inputs. Importantly, nonlinearities induced by neuromodulation generated distinctive features in firing patterns, facilitating input identification.

In this approach, a target motoneuron pool output was imposed as a triangular profile (linear increase followed by decrease). This output corresponded to the cumulative spike train of the 20 motoneurons, approximating a similar force profile (Fig. 41, left), and was held constant across simulations. Thus, unlike previous studies that varied inputs to observe outputs, this approach fixed the output and examined the input combinations required to reproduce it. An important part of the study was to identify the time-varying conductance inputs (Fig. 41, right) necessary to match the target output under different fixed conditions (Fig. 41, middle). Results show that increasing neuromodulation enhances nonlinear behaviour and reduces the level of excitation required to achieve the same output. Conversely, higher excitation is required to counteract inhibition when it scales proportionally with excitation, compared to push–pull inhibition. Notably, the relationship between excitatory conductance and time is nonlinear even when producing a linear output.

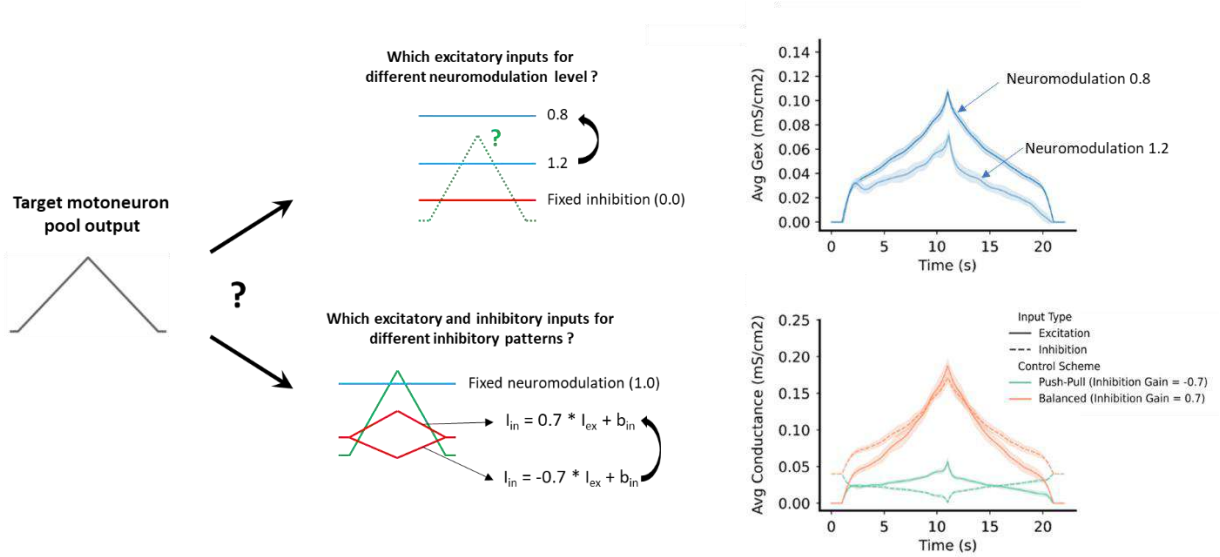

Figure 41. Reverse engineering framework. *The main goal of the approach was to test whether the three inputs can be predicted from motoneuron firing rates. On the upper right is shown the average and standard deviation of the excitatory input to the motoneuron pool required to produce the target output, with neuromodulation values of 0.8 and 1.2. On the lower right is shown the average and standard deviation of excitation (solid) and inhibition (dotted) for the two extremes of inhibitory patterns (push–pull in green and proportional in orange). Adapted from Chardon et al. (2024).*

As in Beauchamp et al. (2023), regression analyses were performed to determine which firing features best predict input organisation. Mutual information scores for each metric (Fig. 42)

reflects how well each one predicts the input organisation on its own. The results were fully consistent with previous findings, supporting the use of brace height to infer neuromodulatory level, and the attenuation slope to infer inhibitory patterns.

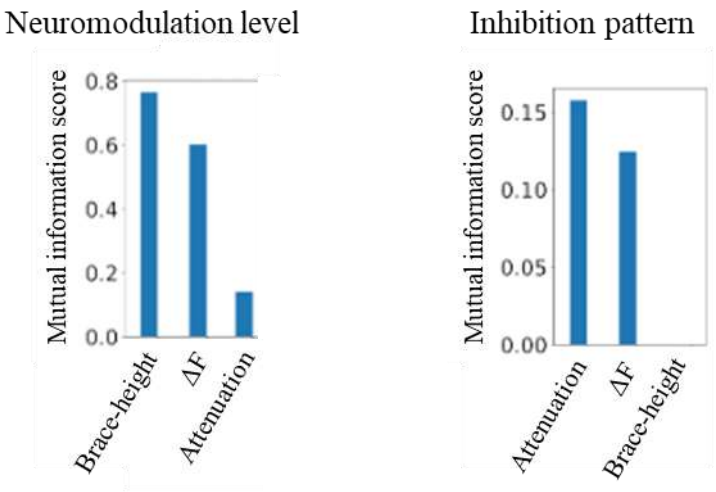

Figure 42. Predictive power of metrics for synaptic inputs in reverse engineering paradigm. *Mutual information scores quantify the predictive capacity of each feature. Brace height was specifically predictive of neuromodulation level, whereas attenuation was specifically predictive of the inhibitory pattern. In contrast, ΔF showed non-specific predictive power, being associated with both neuromodulation level and inhibitory pattern.*

3. Reliability of the metrics

A condition required for appropriate quantification of firing pattern features is a linear increase and decrease of net synaptic input to motoneurons. While this condition cannot be verified, as torque is considered a grossly indirect measure of net synaptic input, it is important that the triangular torque tasks performed by participants do not deviate from a linear pattern. Figure 43 shows the mean torque trace for control, SCI, and stroke individuals. To test whether differences exist between populations, we quantified the distance between the experimental torque trace and the torque target using the root mean square error, testing ascending and descending phases separately (Fig. 43). There was no interaction between group and phase (ascending or descending) ($p = 0.5224$), nor any difference between ascending and descending phases ($p = 0.1636$). In contrast, there was a significant group effect ($p = 0.0019$). Specifically, root mean square error was higher in stroke than in control individuals by 1.48 (95% CI: [0.51–2.45], $d = 1.3$, $p = 0.0013$), while there was no other difference between groups ($p > 0.1540$). Overall, errors in torque matching were small, but stroke individuals, on average, exhibited lower-quality matching than control individuals. Notably, the major deviations from the torque target were

not due to large oscillations in the produced torque but rather to smooth deviations, thus rarely deviating from linearity.

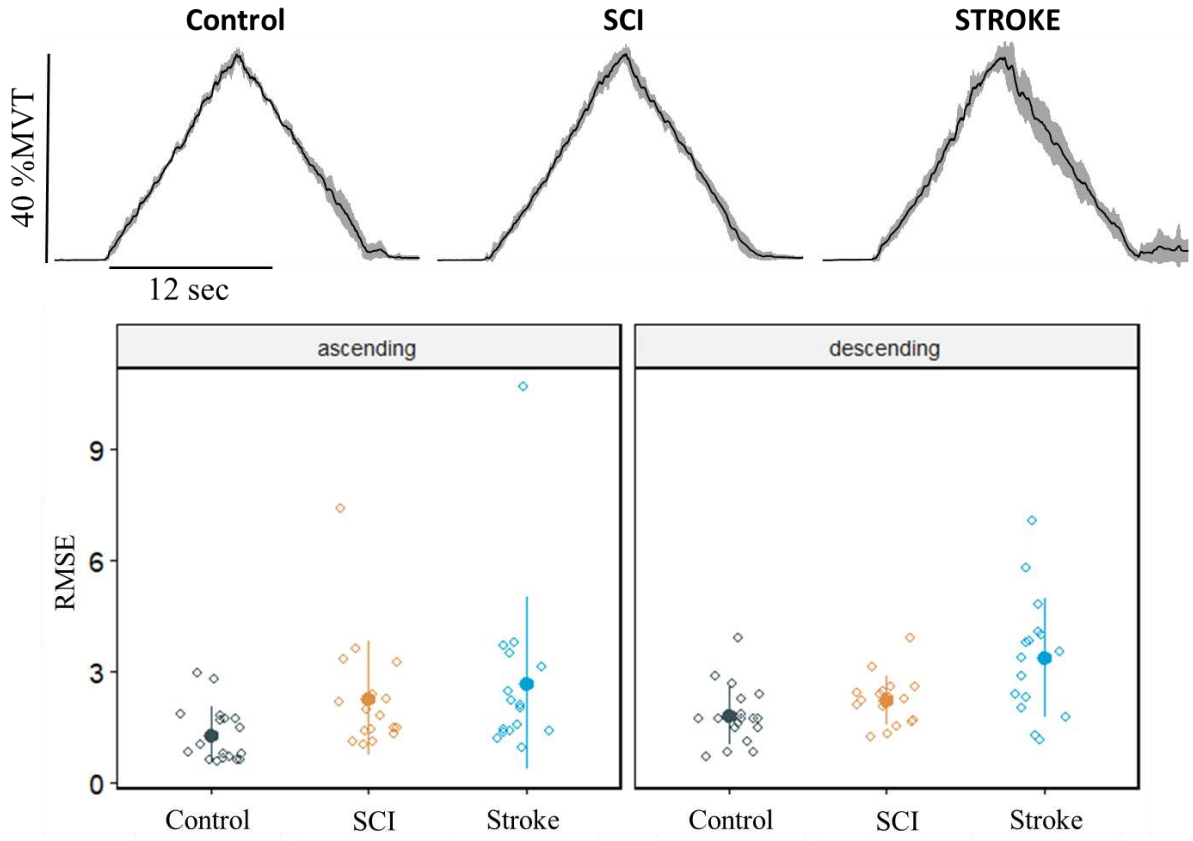

Figure 43. Assessment of torque task performance. *The upper panel shows the mean torque trace for control, SCI, and stroke participants, with variability illustrated by the shaded area (standard deviation). The lower panel shows the deviation between the experimental torque trace and the target torque, quantified using the root mean square error (RMSE), for both ascending and descending phases. Across phases, RMSE was higher in stroke compared with control participants by 1.48 (95% CI [0.51–2.45], d = 1.3, p = 0.0013).*

In Study 2, twenty-seven participants performed the triangular contraction twice, at 40 %MVT, to assess the reliability of the motoneuron firing rate metrics. The reliability was quantified using a multilevel (mixed-effects) modelling approach to appropriately account for the hierarchical structure of the data (motoneurons nested within contractions, nested within participants). For each metric and muscle, a linear mixed model of the form lmer(metric ~ 1 + (1 | id) + (1 | id:trial)) was fitted. This specification partitions the total variance into three components: between-subject variance (σ^2_{id}), between-contraction variance within subjects (σ^2contraction), and residual variance at the motoneuron level ($\sigma^2_{residual}$). This framework allows estimation of reliability at the level of participant-specific averages while properly incorporating the unequal

number of motoneuron contributing to each contraction. The level of participant-specific averages is the one appropriate as the statistical inference is made at this level (i.e., not at the level of the motoneuron nor by averaging motoneurons within muscles before analysis).

The intraclass correlation coefficient (ICC) was derived from these variance components to reflect the reliability of the average of two contractions (k = 2), corresponding to an agreement-type ICC. Specifically, the ICC was computed as:

$$ICC = \frac{{\sigma^2}_{id}}{{\sigma^2}_{id} + \frac{{\sigma^2}_{contraction}}{k} + \frac{{\sigma^2}_{residual}}{k.\bar{n}_{MN}}}$$

Equation (14)

Where $\bar{n}_{MN}$ represents the average number of motoneurons per contraction. This formulation accounts for both within-subject variability across contractions and the precision associated with averaging multiple motoneurons, thereby providing an estimate of reliability at the participant level that is consistent with the mixed-model analyses.

The standard error of measurement (SEM) was calculated as the square root of the within-subject variance, combining both contraction-level and motoneuron-level variability:

$$SEM = \sqrt{{\sigma^2}_{contraction} + \frac{{\sigma^2}_{residual}}{\bar{n}_{MN}}}$$

Equation (15)

The smallest detectable change (SDC), representing the minimal change required to exceed measurement error with 95% confidence, was then derived as:

$$SDC = 1.96 \times \sqrt{2} \times SEM$$

Equation (16)

Together, these metrics provide complementary information on reliability, absolute measurement error, and sensitivity to change, all grounded in a variance decomposition that reflects the multilevel structure of the data. The results are shown in table 2 for GM and SOL separately. Overall, repeatability is good across metrics. However, brace height in the GM and acceleration slope in the SOL display very low repeatability.

Table 2. Reliability of motoneuron-related metrics

Muscle	Metrics	ICC	SEM	SDC
GM	RT	0.88	2.9	8.0
	acceleration	0.75	0.4	1.2
	attenuation	0.60	0.1	0.4
	brace height	0.02	11.2	30.9
	ΔF	0.90	0.5	1.2
	peak FR	0.98	0.7	1.8
SOL	RT	0.60	3.5	9.6
	acceleration	0.26	0.5	1.3
	attenuation	0.46	0.1	0.2
	brace height	0.64	6.7	18.4
	ΔF	0.84	0.6	1.6
	peak FR	0.94	0.6	1.7

ICC, intraclass correlation coefficient; SEM, standard error of measurement; SDC, smallest detectable change; GM, gastrocnemius medialis; SOL, soleus; RT, recruitment threshold; peak FR, peak firing rate.

Agreement between contractions was further explored using Bland–Altman analyses, adapted to also assess the effect of motoneuron number on agreement. For each metric and muscle, values were first averaged at the contraction level using all available motoneurons, and then the difference between the two contractions (trial 2 − trial 1) was computed for each participant. Unlike classical Bland–Altman plots, the x-axis was defined as the average number of motoneurons contributing to each estimate (computed separately for each metric as the mean of the motoneuron counts across the two contractions). This approach allows direct evaluation of whether measurement error is influenced by the number of motoneurons sampled.

For each metric, the mean difference (bias) and the limits of agreement (mean ± 1.96 × SD of the differences) were displayed, providing a visual assessment of systematic bias and absolute agreement (Figure 44 for GM and Figure 45 for SOL). In addition, a linear trend (with standard error) was fitted to examine potential relationships between the magnitude of disagreement and the number of motoneurons. This visualisation enables identification of heteroscedasticity (e.g., larger variability at low motoneuron counts) and potential bias related to sampling density, thereby complementing ICC-based reliability estimates by revealing how precision and agreement depend on the underlying number of observations.

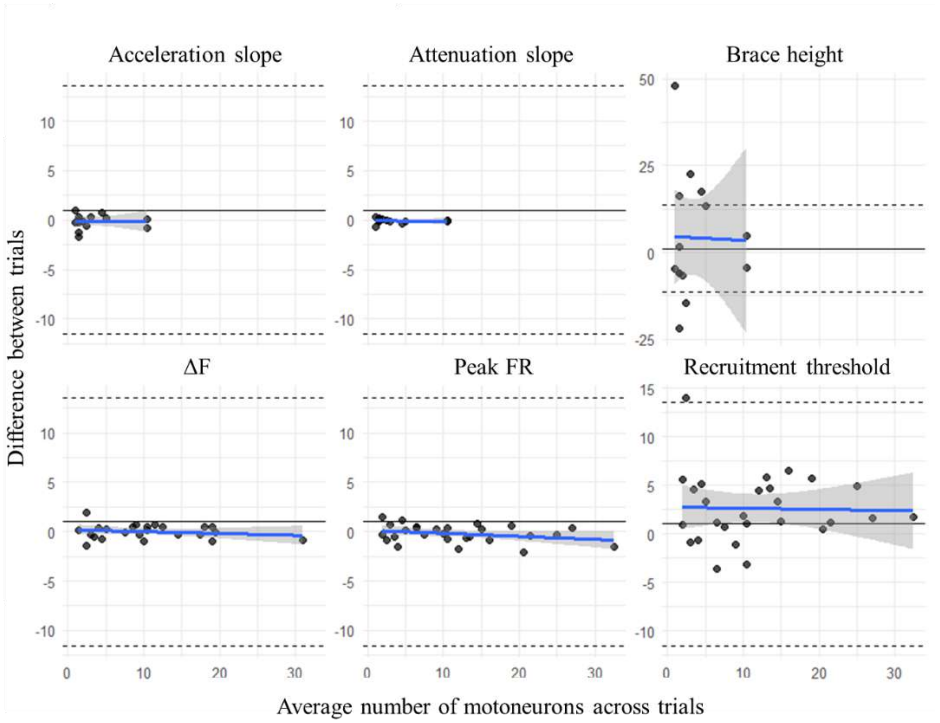

Figure 44. Bland–Altman plots for the GM. *Bland–Altman plots were used to assess the reliability between the two trials as a function of the number of motoneurons included in the analyses. Each dot corresponds to the difference in the corresponding metric between trials for each participant. The resulting linear regression is shown in blue, with its standard error.*

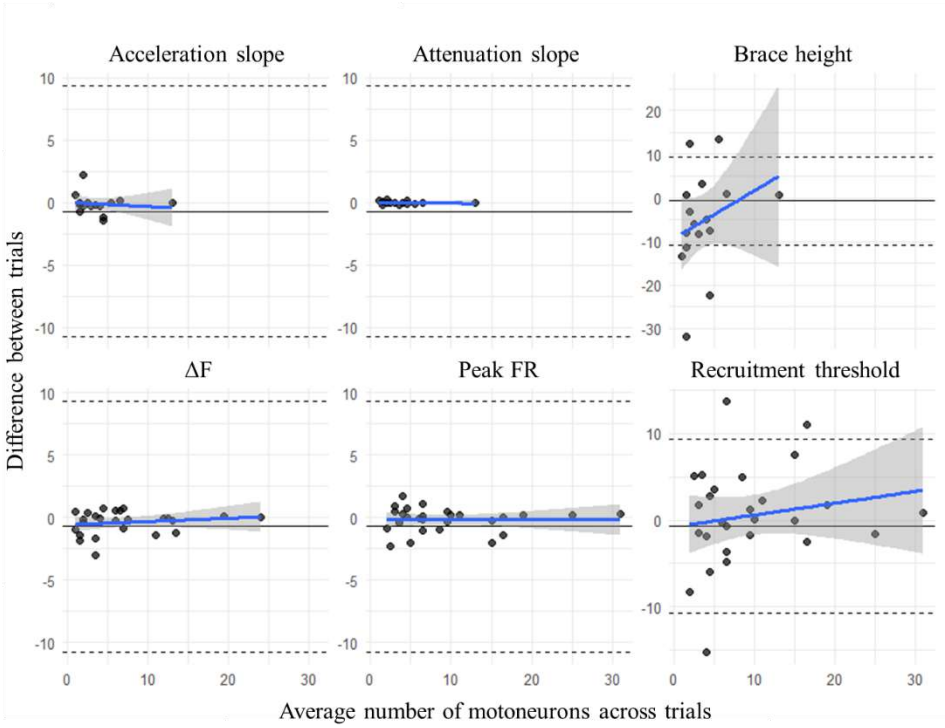

Figure 45. Bland–Altman plots for the SOL. *Bland–Altman plots were used to assess the reliability between the two trials as a function of the number of motoneurons included in the analyses. Each dot corresponds to the difference in the corresponding metric between trials for each participant. The resulting linear regression is shown in blue, with its standard error.*

This analysis revealed very good agreement for most metrics, independent of the number of motoneurons analysed. However, a few exceptions to this trend were observed. Specifically, the recruitment threshold shows some variability across trials, which suggests that decomposition of surface EMG signals may identify different samples of motor units across trials. Furthermore, this analysis confirms the large variability across trials for brace height. It is likely that this increased variability is due to the calculation of brace height, which involves a normalisation procedure (division by the height of the right triangle). Indeed, this step makes brace height sensitive to small changes in the denominator. To illustrate, consider the extreme case where the denominator is close to zero, which would lead to very large values for brace height. Thus, while this normalisation procedure likely confers specific sensitivity to the neuromodulatory level (Beauchamp et al., 2023; Chardon et al., 2024), it comes at a cost of low reliability.

To refine the consequence of the low reliability of brace height, classical Bland-Altman plots for brace height were conducted (Fig. 46). Specifically, individual differences between trials are coloured by group, which allows assessment of wether errors are associated with group-specific patterns, which does not appear to be the case. Overall, it thus appears that errors in brace height measurement are not specific to subpopulations and do not depend on the number of motoneurons used for the analysis. These results support the assumption of random measurement error (Falissard & Gillibert, 2023). Consequently, the low reliability of brace height would not lead to biased inference of group differences but rather only to reduced statistical power to detect true effects. Overall, this makes brace height a less sensitive metric than the others.

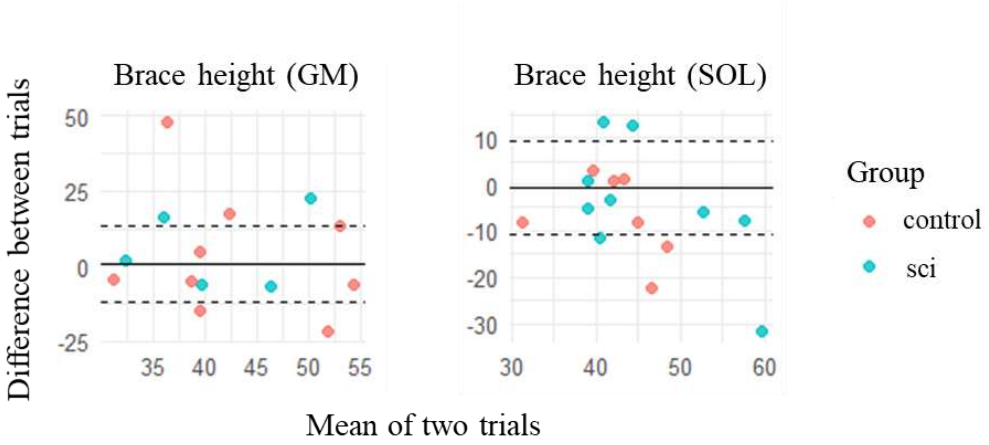

Figure 46. Bland-Altman plots for brace height. *Individual differences between the two trials are plotted against the mean brace height across trials, for both gastrocnemius medialis (GM), and soleus (SOL).*

◥ STUDY 1: MODULATION OF PERSISTENT INWARD CURRENTS IN MOTONEURONS WITH JOINT ANGLE DEPENDS ON MUSCLE LENGTH

KEY POINTS

- A central and unresolved question is how motoneurons are controlled to produce muscle contractions adapted to changes in muscle length, which directly affect the muscle's force-generating capacity.
- Current understanding of this question is largely centred on the control of motoneurons through ionotropic inputs. In this study, we focus on another key contributor to motoneuron depolarisation: persistent inward currents.
- Our findings reveal that the prolongation of motoneurons' discharge induced by persistent inward currents is modulated by muscle length via the regulation of inhibitory inputs.
- These results support that persistent inward currents may serve as an additional mechanism, mediated through inhibition, to adjust motoneuron activity to account for changes in force-generating capacity associated with changes in muscle length.

ABSTRACT

During voluntary movement, activity of motoneurons is modulated to account for changes in muscle force-generating capacity induced by variations in muscle length. To date, research has primarily focused on the modulation of ionotropic inputs, while the role of another key contributor to motoneuron activity, persistent inward currents (PICs), has been largely overlooked. In this human study involving young male participants (n=19), high-density surface electromyography signals were recorded from the gastrocnemius medialis and soleus muscles at different ankle positions, and subsequently decomposed into motor unit spiking activity. Metrics extracted from these spiking activities were used to estimate the respective contributions of PICs, neuromodulation, and inhibition to motoneurons activity. To differentiate the impact of muscle length from muscle tension, we compared voluntary contractions performed at both similar relative torque levels and similar absolute torque levels across different ankle positions. Our results revealed that PIC-induced prolongation of motor unit discharges was reduced at longer muscle lengths, accompanied by increased inhibition. This effect was consistent across both relative and absolute torque conditions, supporting the hypothesis that muscle length is the primary driver of PICs modulation with changes in position. These findings suggest that PICs may

serve as an additional mechanism - likely related to inhibitory inputs - to regulate motoneuron activity, ensuring adaptation to changes in muscle length.

1. INTRODUCTION

Voluntary movement relies on dynamic muscle contractions, during which muscle length changes. The neural mechanisms by which motoneuron activity adapts to account for these changes in muscle length - and consequently in force-generating capacity - remain poorly understood. Most previous studies have focused on the modulation of excitatory and inhibitory ionotropic inputs to motoneurons (Pierrot-Deseilligny & Burke, 2012). However, the role of another important contributor to motoneuron activity, persistent inward currents (PICs), has been largely overlooked.

PICs are depolarising currents mediated by sodium and L-type calcium channels on the membrane of motoneurons. These currents amplify and prolong the effects of synaptic inputs on motoneuron activity (Heckman et al., 2009a). PICs are activated by metabotropic neuromodulatory inputs resulting from the release of monoamines (serotonin 5-HT and norepinephrine) on the motoneuron synapse. PICs are also modulated by inhibitory inputs, with a dampening effect of these inputs on PICs demonstrated in both animal (Bui et al., 2008; Hultborn et al., 2003; Hyngstrom et al., 2007; Kuo et al., 2003) and human studies (Gomes et al., 2024; Mesquita et al., 2022; Orssatto et al., 2022; Pearcey et al., 2022; Revill & Fuglevand, 2017). As longer muscle length enhances inhibitory inputs to motoneurons (Colard et al., 2024), it is likely that the contribution of PICs to motoneuron activity decreases as muscle length increases. This may serve as a mechanism for regulating motoneuron activity, adapting it to the muscle's force-generating capacity. This may also reflect an effective mechanism for locally adjusting PICs by countering the diffuse projection of descending monoaminergic drive (Heckman et al., 2008).

Hyngstrom *et al.* (2007) demonstrated in the decerebrate cat that PICs are modulated by changes in joint angles. Specifically, they found that lengthening the dorsiflexor muscles increases reciprocal inhibition to the plantar flexor muscles, thereby reducing PICs in the plantar flexors as they shorten. Divergent observations have been reported in humans, where PICs of the motoneurons innervating the tibialis anterior and gastrocnemius medialis are greater when these muscles are in a shortened position compared to a lengthened position (Beauchamp et al., 2023). Differences between these findings could be attributed to (i) Ib afferent-mediated inhibition, which increases at longer muscle lengths, and which are likely more involved during

voluntary contractions than in paralysed animal models (Khan & Burne, 2009; Stephens et al., 1975); and (ii) key descending systems that modulate inhibition from sensory inputs, which are absent in the decerebrate cat model (Hyngstrom et al., 2007).

This study aimed to better understand the modulation of PICs with joint angle by examining the role of muscle tension and the respective role of inhibition and neuromodulation, during voluntary contractions in humans. The paired-motor unit method (M. Gorassini et al., 2002) and the geometric method (Beauchamp et al., 2023) were used to estimate PICs (metrics: ΔF and acceleration slope of the initial firing), neuromodulation by monoamines (metric: brace height constructed based on the non-linearities in the ascending firing phase) and the pattern of inhibition, i.e., the level of synaptic inhibition in respect of synaptic excitation (metric: attenuation slope of the ascending firing phase). Participants performed plantar flexions at different ankle positions with similar absolute torque and with similar relative torque across ankle positions. By isolating the influence of muscle tension - comparing the same absolute and relative torque at different joint positions - we were able to assess the potential contribution of muscle tension on PICs. We hypothesised that estimates of PICs would decrease as the length of the plantar flexors increases. A similar modulation when absolute and relative torque are kept constant across ankle positions would suggest that changes in muscle length, rather than changes in muscle tension, drive the modulation of PICs with ankle position. We further expected that this decrease would be primarily attributable to the modulation of the pattern of inhibition rather than neuromodulatory inputs.

2. METHODS

Participants and ethical approval

Twenty-four males volunteered for the study, and nineteen (age 24.3 ± 3.9 years, 1.82 ± 5.6 m, 75.0 ± 10.4 kg) were included in the final analyses after successful decomposition of motor units (MUs), while the other five were excluded due to the lack of decomposed MUs (typically between 0 and 2 per contraction). Participants were required to have had no lower limb injuries in the preceding 6 months and were instructed to refrain from caffeine consumption or lower limb training for 24 hours prior to the evaluation. The study protocol was approved by the local ethics committee (CERNI, Nantes Université, IRB: IORG0011023) and written informed consent was obtained prior to testing. Notably, we chose to recruit only males because of our difficulty in decomposing MUs in females in pilot experiments. Subcutaneous fat is likely a contributor to the lower MU yield in females (Jenz et al., 2023).

Experimental protocol

After the warm-up and MVT assessments, participants performed isometric submaximal contractions at the three ankle positions described above, i.e. 20° of plantar flexion, 0°, and 20° of dorsiflexion (Fig. 47). For clarity, these positions will be referred to as 20°, 0°, and -20°, respectively. Additionally, the positions will be described based on the length of the agonist muscle during contraction: the short muscle length position at 20°, the intermediate muscle length position at 0°, and the long muscle length position at -20°. From the short to the long muscle length position, the plantarflexion torque-generating capacity increases, which requires less muscle activation to produce the same absolute torque (Hoffman et al., 2012). To account for the relationship between maximal torque and joint angle (Fig. 47A), we compared similar relative torque across positions to match muscle activation and effort (Relative torque contractions). Furthermore, to distinguish between the effects of muscle length and tension on PICs, participants also performed contractions at similar absolute torques across positions (Absolute torque contractions). For the Relative torque contractions, participants performed trapezoidal contractions at 20% of MVC and triangular contractions at 40% of MVC at each position. As MVC torque increases with increasing muscle length (mean ± sd; short: 114.6 ± 22.4 N.m, intermediate: 175.1 ± 32.5 N.m, long: 201.1 ± 33.4 N.m), the torque of submaximal contractions increases with increasing muscle length. For the Absolute torque contractions, the torque was constant across muscle lengths. It was set to match the torque used at the short muscle length

position during the Relative torque contractions (Fig. 47B). Given that contraction duration affects the discharge rate through MU spike frequency attenuation, which can then affect our estimates of PICs, all contractions had the same duration of 24 seconds (Powers & Heckman, 2015; Škarabot et al., 2023). The two intensities (20% and 40%) were selected to examine whether the position-related modulation of PICs depends on drive intensity. For this comparison, the same rate of torque increase was used to limit the effect of spike-threshold accommodation (Revill & Fuglevand, 2011), leading to different torque patterns across intensities (Fig.47B).

After a familiarisation period, participants completed two contractions for each condition in a randomised order. At least 1 min of rest separated each contraction to minimise fatigue. For each muscle, each position and each condition, only the contraction yielding the highest number of identified MUs was analysed. To compare MU activity across positions and contraction intensities, we tracked MUs for each condition separately (Relative and Absolute torque).

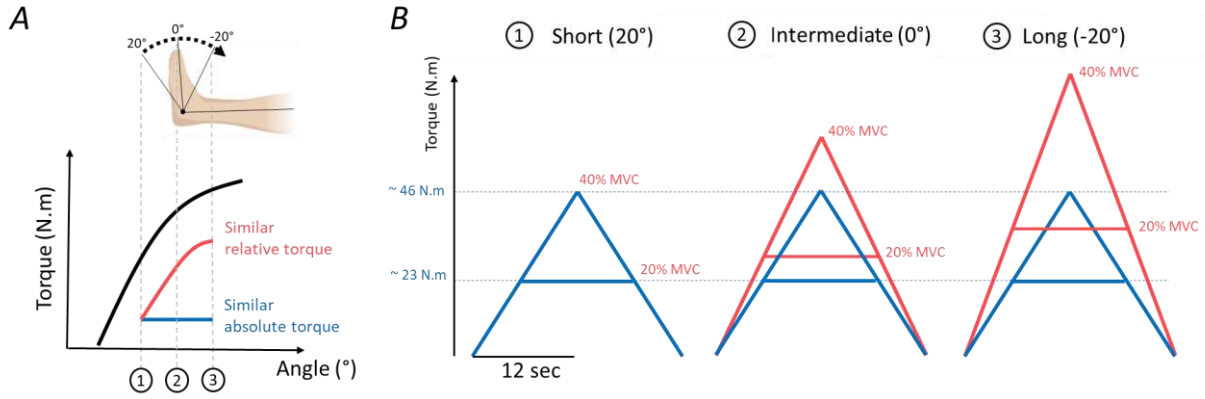

Figure 47. Contraction protocol*. A, participants performed isometric submaximal plantarflexions at three different ankle positions, corresponding to different plantar flexor lengths: 20° (short muscle length position), 0° (intermediate muscle length position), and -20° (long muscle length position). The intensity of the plantarflexions followed either the same absolute torque (in blue), or the same relative torque (in red) across all positions (percentage of maximal voluntary contraction, MVC) across positions. B, the submaximal plantarflexions were performed as either trapezoidal or triangular contractions at 20% and 40% of the MVC at each position (in red) or at the absolute torque (in blue) corresponding to 20% and 40% of the MVC in the short muscle length position. The mean absolute torques were 23 N·m and 46 N·m, respectively.*

Statistical analyses

To assess changes in MU discharge characteristics across joint positions, we applied a linear mixed-effects model to each MU discharge metric (i.e., maximal discharge rate, recruitment

threshold, ΔF, brace height, acceleration, and attenuation), incorporating data from individual MUs. The models included position (short, intermediate, and long), contraction intensity (lower and higher), and their interaction as fixed effects. For random effects, we added a random intercept for each participant and a random slope to account for the variability in the position effect between participants. Additionally, we included a random intercept for each MU [e.g., ΔF ~ position + intensity + position*intensity + (position | id_participant) + (1 | id_participant : id_MU)]. Separate models were fitted for the GM and SOL muscles and conditions (Relative or Absolute torque contractions). In cases where the model failed to converge (which was more common for the SOL due to fewer successfully decomposed and tracked MUs), we simplified the random structure by removing the random intercept for each MU. This adjustment preserved the key random structure that accounts for the effect of position across participants. All analyses were performed using R (v.4.4.0; R Core Team 2021, R Foundation for Statistical Computing, Vienna, Austria), with the lmerTest package (Kuznetsova et al., 2017) to fit the models. For each model, we checked that the assumptions of homoscedasticity, normality, and independence of residuals were met through graphical evaluation. When significant effects were detected, we applied Tukey post-hoc correction for pairwise comparisons. Additionally, we calculated estimated marginal mean differences and standardised differences, along with 95% confidence intervals, using the emmeans package. The alpha level for all statistical tests was set at 5%.

3. RESULTS

Motor unit decomposition and tracking

The decomposition of EMG signals yielded 5734 MUs spike trains, of which 4000 were successfully tracked across at least two contractions and included in the analyses. For the contractions performed at relative torque, 1880 MU spike trains were included in the analysis, with an average of 22.3 ± 11.2 tracked MUs per participant for the GM and 6.7 ± 5.3 tracked MUs per participant for the SOL. On average, MUs were tracked across 3.5 ± 1.4 contractions out of six (3 positions x 2 intensities). For the contractions performed at absolute torque, 2120 MU spike trains were included, with an average of 25.2 ± 9.9 tracked MUs per participant for the GM and 7.7 ± 5.9 tracked MUs per participant for the SOL. On average, MUs were tracked across 3.6 ± 1.4 contractions out of six. An example of the firing rates of tracked MUs is depicted in Figure 48.

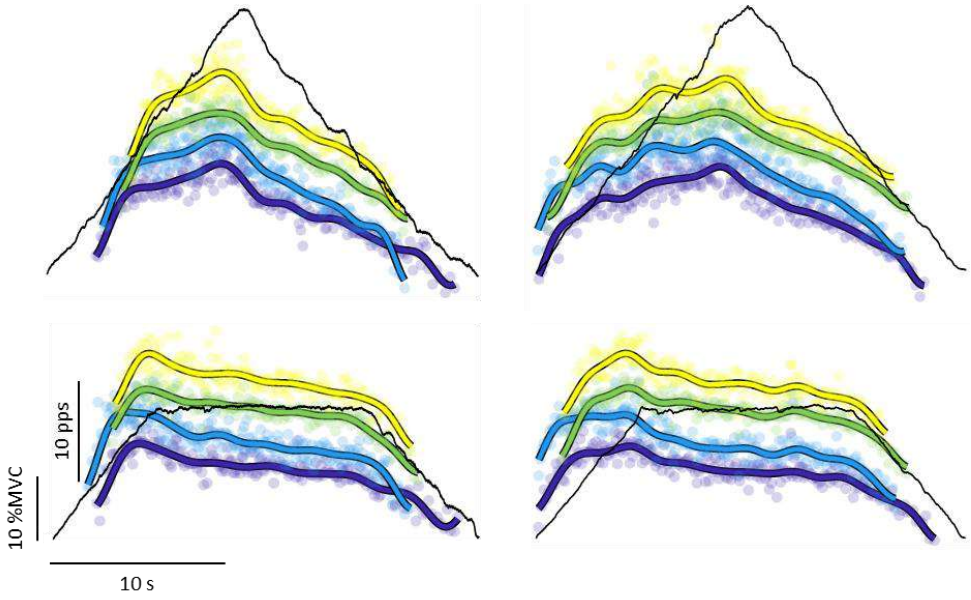

Figure 48. Example of motor unit (MU) firing rates across positions and intensities. *Four tracked MUs of the gastrocnemius medialis (GM) from a representative participant are shown, with each MU represented by a different colour. The figure displays firing rates across two positions (short position on the left, long position on the right) and two intensity levels (peak at 40% MVC on top, plateau at 20% MVC on the bottom). For clarity, firing rates are artificially spaced along the vertical axis.*

Effect of muscle length on ΔF

For the Relative torque contractions, a significant position-by-intensity effect on ΔF was observed for both the GM ($p = 0.0041$) and the SOL ($p = 0.0088$), with lower ΔF values observed

as the muscles operated at longer lengths (Fig. 49). Specifically, for the GM, ΔF decreased from the intermediate to the long muscle length position at both intensities, and from the short to the long muscle length position at the higher intensity only (all $p < 0.0367$). For the SOL, ΔF decreased from the short to the long muscle length position at both intensities, from intermediate to long at the lower intensity, and from the short to the intermediate position at the higher intensity (all $p < 0.0350$). For the Absolute torque contractions, a significant position effect was identified for the GM ($p = 0.0009$), with lower ΔF values at the long muscle length position compared to the short muscle length position, regardless of intensity (all $p < 0.0172$). Although the results for the SOL were not statistically significant, they followed a similar trend with lower ΔF values at the longer muscle lengths (Fig. 49). Overall, the results from both protocols consistently showed lower ΔF values at longer muscle lengths compared to shorter ones. Detailed statistical results are available in the supplemental material (Annexe 1).

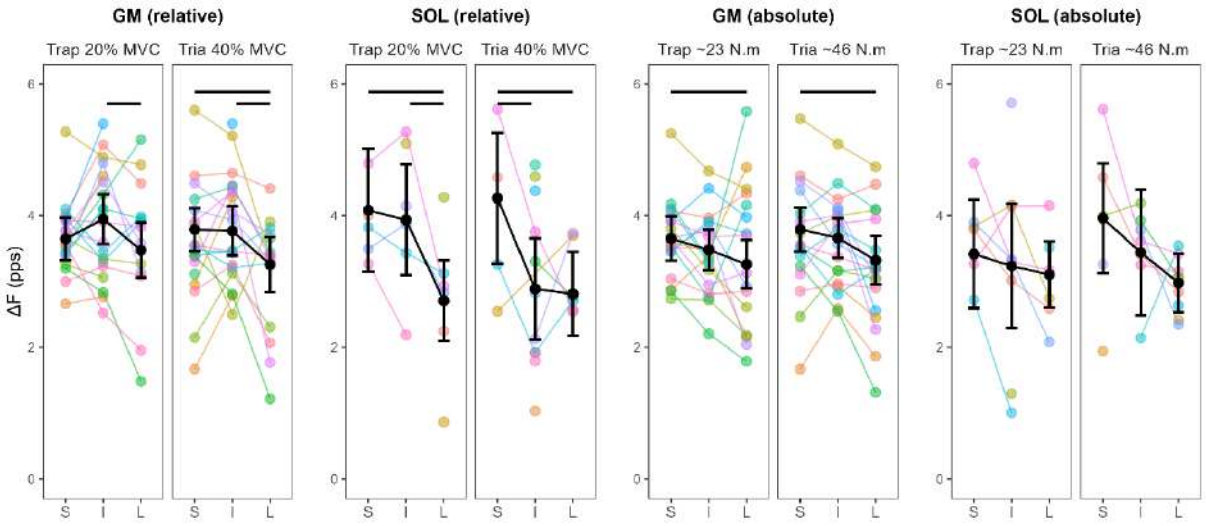

Figure 49. Estimates of persistent inward currents for motor units between positions. *Estimates of persistent inward currents (ΔF) were obtained from the gastrocnemius medialis (GM) and soleus (SOL) muscles at three different muscle lengths: short (S), Intermediate (I), and long (L). ΔF values were compared across positions at either the same relative torque or the same absolute torque, using lower-intensity trapezoidal contractions (Trap) and higher-intensity triangular contractions (Tria). Coloured dots represent participant averages, while black dots and bars show the estimated marginal means predicted by linear mixed-effects models. Horizontal black lines indicate significant differences between muscle lengths ($p < 0.05$).*

Effect of muscle length on acceleration, brace height, and attenuation

For acceleration, a significant position-by-intensity interaction was observed for the GM in both the Relative and Absolute torque contractions (both $p < 0.0001$) (Fig. 50). However, significant differences between positions were only observed at the higher intensity for the Absolute torque contractions, with acceleration being higher at the short muscle length compared to the intermediate and the long muscle length positions (all $p < 0.0116$). No significant position-by-intensity or position effect was observed for the SOL. These results showed a less pronounced effect of position on acceleration than on ΔF.

For brace height, a significant position-by-intensity interaction was observed for the GM in both the Relative and Absolute torque contractions (both $p < 0.0151$) (Fig. 50), with higher brace height values at longer muscle length. Specifically, during the Relative torque contractions, brace height was lower at short muscle length compared to intermediate muscle length position at the lower intensity ($p = 0.0474$), and from the short to the long ($p = 0.0003$). It was also lower at short and intermediate muscle lengths compared to the long muscle length position ($p = 0.0010$) at the higher intensity. During the Absolute torque contractions, brace height was only modulated at the highest intensity, with a greater value at intermediate muscle length compared to the short muscle length position ($p = 0.0239$). For the SOL, while a significant position-by-intensity interaction was observed for the Absolute torque contractions, no significant post hoc differences were identified, and no clear trend was evident (Fig. 50). Overall, brace height, which reflects the contribution of neuromodulatory inputs to MU discharge rates was higher at longer muscle lengths in the GM, but remained unchanged in the SOL. This contrasts with the observed reductions in ΔF and small-to-no reduction of acceleration at longer muscle lengths, suggesting that changes in neuromodulatory inputs are unlikely to drive the observed muscle-length modulation of ΔF.

For attenuation, a significant position-by-intensity interaction was observed for the GM in both the Relative and Absolute torque contractions (both $p < 0.0001$) (Fig. 50). Specifically, attenuation was lower at longer muscle lengths, but this effect was observed only at the higher intensity. In the Relative torque contractions, differences were observed between all three positions (all $p < 0.0174$), whereas in the Absolute torque protocol, attenuation was lower at both intermediate and long muscle lengths compared to short length (all $p < 0.0007$). For the SOL, no significant position-by-intensity interaction was observed ($p = 0.6401$). Although a significant position effect was identified for the Relative torque contractions ($p = 0.0081$), post-hoc tests

did not reveal significant differences between positions. Overall, attenuation, which is positively associated with a push-pull pattern of inhibition, exhibited a similar behaviour to ΔF, suggesting that inhibition may contribute to the muscle-length-dependent modulation of ΔF.

Acceleration, brace height, and attenuation have been shown to have a weak association with the recruitment threshold of MUs (Beauchamp et al., 2023). Given the substantial variations in recruitment threshold across positions, as illustrated in Fig. 51, we performed additional analyses to assess whether recruitment threshold acted as a confounding factor for these metrics in the GM, where most results supporting our interpretation originated. The same statistical analyses were performed on a reduced dataset, excluding MUs with the greatest differences in recruitment threshold across position until the mean variation in recruitment threshold between short and long muscle positions reached zero, ultimately retaining approximately 25% of the MUs. Detailed statistical results are available in the supplementary material (Annexe 1). Overall, this secondary analysis reinforces the limited influence of muscle position on acceleration while confirming the observed increase in brace height and decrease in attenuation at longer muscle lengths.

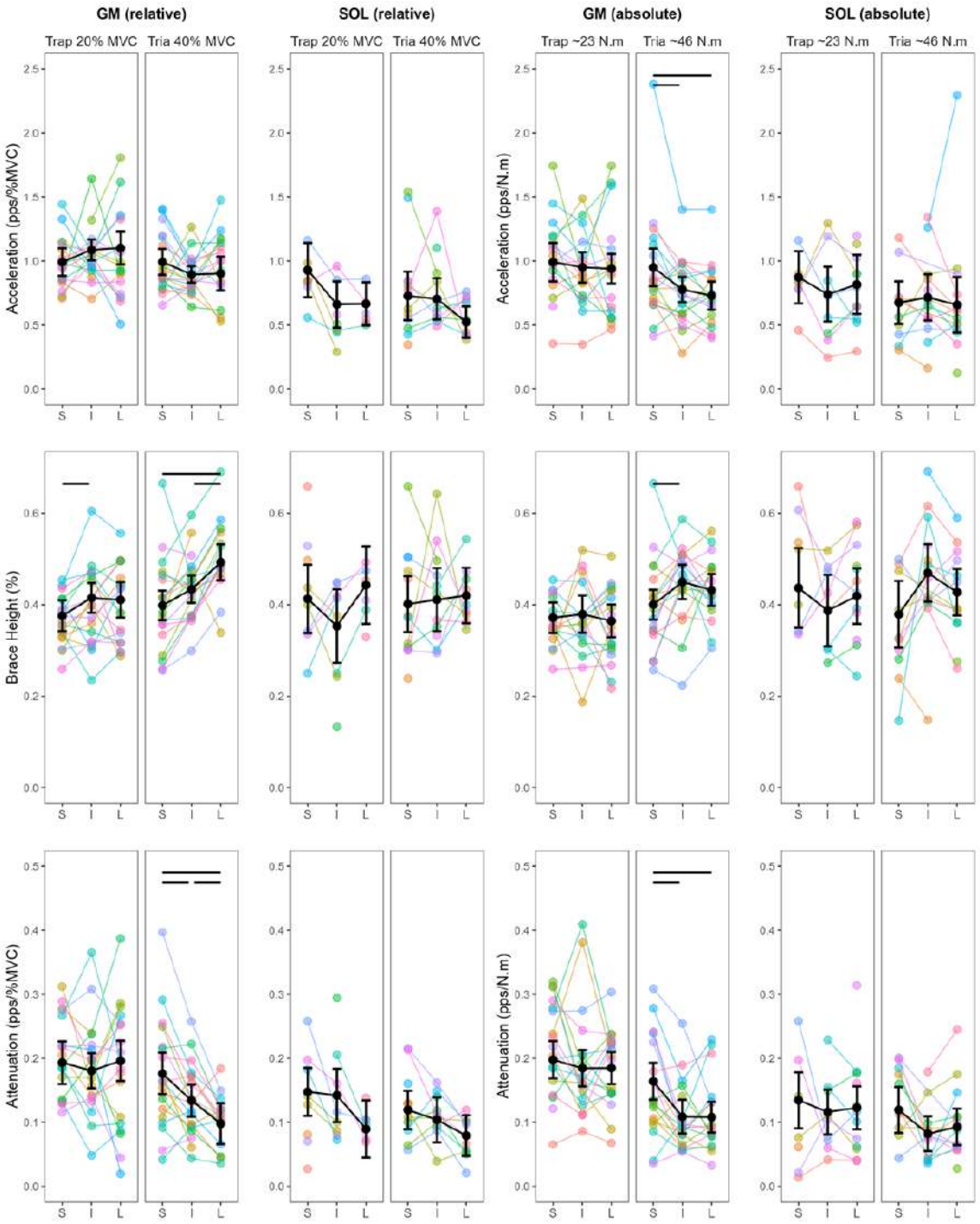

Figure 50. Parameters from the geometric approach for motor units across positions. *Brace height (top row), acceleration (middle row) and attenuation (bottom row) were obtained from the gastrocnemius medialis (GM) and soleus (SOL) motor units at three different muscle lengths: short (S), intermediate (I), and long (L). These metrics were compared across positions at either the same relative torque or the same absolute torque, using lower-intensity trapezoidal contractions (Trap) and higher-intensity triangular contractions (Tria). Coloured dots represent participant averages, while black dots and bars show the estimated marginal means predicted by linear mixed-effects models. Horizontal black lines indicate significant differences between muscle lengths ($p < 0.05$).*

Effect of muscle length on motor unit recruitment threshold and maximal discharge rate

When considering the recruitment threshold, a significant position-by-intensity interaction was observed for both the GM and SOL for both Absolute and Relative Torque contractions (both $p < 0.0001$) (Fig. 51). A distinct pattern emerged for both muscles at the higher intensity: longer lengths were associated with a lower recruitment threshold for GM MUs and a higher recruitment threshold for SOL MUs. Specifically, for the GM during the Relative torque contractions, differences were observed across all three positions (all $p < 0.0184$), while during the Absolute torque protocol, differences were noted between the long muscle length position and the two other positions (all $p < 0.0001$). For the SOL, differences were observed in both protocols between the short and other positions. This differential changes in recruitment threshold between GM and SOL was less pronounced at lower intensity. For the GM, a decrease was also observed from the long to the other positions in the Relative torque contractions, but only from intermediate to long muscle length position in the Absolute torque contractions, while a significant increase was noted between the short and intermediate muscle length positions. For the SOL, no significant differences were observed at lower intensity. Overall, these findings indicate that the distribution of neural drive during the initiation of the contraction across GM and SOL MUs varies with ankle angle.

For maximal discharge rate, a significant position-by-intensity interaction was observed for both the GM and SOL in both Absolute and Relative torque contractions (all $p < 0.0001$) (Fig. 51). During the Absolute torque contractions, maximal discharge rates were lower at longer muscle lengths compared to shorter ones. Specifically, for the GM at lower intensity, differences were observed between all three positions (all $p < 0.0040$). At higher intensity, a decrease was observed from short to intermediate and long muscle length positions (all $p < 0.0001$). For the SOL, a decrease was observed from short to intermediate and long muscle length positions at lower intensity (all $p < 0.0142$), but no significant differences were found at higher intensity. The lower maximal discharge rates observed during the Absolute torque contractions at longer muscle lengths are consistent with the expected increase in muscle force-generating capacity at those lengths. In contrast, the results from the Relative torque contractions were less systematic. For the GM, maximal discharge rates increased from short and intermediate to long muscle length positions at lower intensity (all $p < 0.0095$), but decreased from short to intermediate and long muscle length positions at higher intensity (all $p < 0.0038$). For SOL, maximal discharge rate decreased from short to intermediate and long muscle length positions at higher intensity (all $p < 0.0025$) but did not vary significantly at lower intensity.

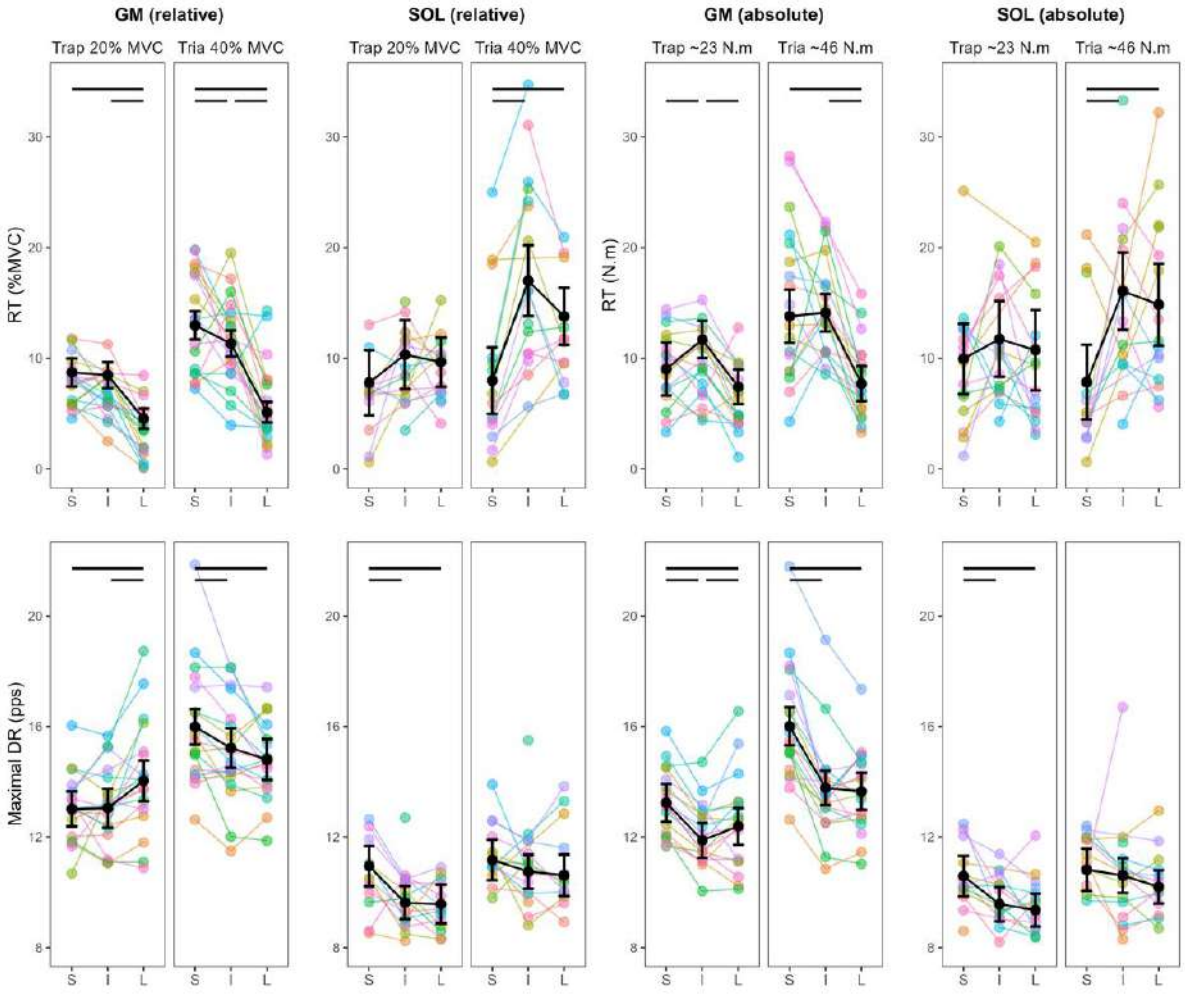

Figure 51. Recruitment threshold and maximal discharge rates for motor units tracked between positions. *Recruitment threshold (RT, top row) and maximal discharge rates (maximal DR, bottom row) were obtained from the gastrocnemius medialis (GM) and soleus (SOL) muscles at three different ankle positions: short (S), intermediate (I), and long (L), corresponding to different lengths of the plantar flexors. These parameters were compared across positions at either the same relative torque or the same absolute torque, using lower-intensity trapezoidal contractions (Trap) and higher-intensity triangular contractions (Tria). Coloured dots represent participant averages, while black dots and bars show the estimated marginal means predicted by linear mixed-effects models. Horizontal black lines indicate significant differences between muscle lengths ($p < 0.05$).*

4. DISCUSSION

In this study involving young males, we investigated the contribution of PICs to the firing patterns of two plantar flexor muscles during submaximal contractions performed at different ankle positions, and therefore, at different muscle lengths. The prolongation effect of PICs, assessed through ΔF, was lower at longer muscle lengths. This was observed at both similar relative and absolute torque levels, supporting the hypothesis that muscle length, rather than muscle tension, primarily drives the modulation of PICs estimates. A more pronounced proportional pattern of inhibition, assessed through the attenuation slope, was observed, suggesting that inhibitory inputs, rather than neuromodulatory inputs, play a key role in modulating PICs prolongation effect as joint position changes. Overall, the study provides evidence that PICs prolongation effect is modulated by muscle length likely through inhibitory inputs.

PICs prolongation effect, not amplification, are lower at long compared to short muscle length during voluntary isometric contraction

The prolongation and amplification effects of PICs were estimated across different ankle positions, using paired MU analysis (Gorassini et al., 2002) and a geometric approach (Beauchamp et al., 2023), respectively. We found a reduced prolongation effect at longer muscle length, which confirms previous recent work (Beauchamp et al., 2023). However, PICs amplification of discharge rate did not differ between ankle positions. It is possible that the amplification and prolongation effects of PICs are, at least in part, dissociable. One potential explanation for this dissociation could involve time-varying inhibition. For example, it has been proposed that during the ascending phase of a contraction, inhibition related to contraction intensity, likely originating from peripheral receptors (via interposed interneurons) and Renshaw cells, can contribute to the saturation of motoneuron firing (Revill & Fuglevand, 2017). Additionally, the possibility of a dissociation between PICs amplification and prolongation effects might be attributed to the different types of ion channels generating PICs. The two primary types of channels responsible for PICs are voltage-gated sodium channels and L-type voltage-gated calcium channels, which differ significantly in their properties. Sodium-related PICs are more readily deactivated compared to calcium-related PICs (Heckman et al., 2009a). Therefore, a possible explanation for differential modulations of PICs amplification and prolongation is that changes in muscle length primarily affect calcium-mediated PICs.

Modulation of PICs by ankle angle reflects muscle length rather than muscle tension

To determine the role of muscle length and muscle tension in the modulation of PIC estimates, we compared ΔF at the same absolute torque across positions. Interestingly, when assessed at the same ankle angle, ΔF values were similar between the Absolute and Relative torque contractions, both showing lower values at longer lengths. The overall lack of differences between the Relative and Absolute torque protocols suggests that muscle-force-related inhibition, particularly from Ib-afferents, is unlikely to be a major contributor to the observed differences in ΔF across ankle angles. Conversely, the consistently lower ΔF values observed at more dorsiflexed ankle angles strongly suggests a muscle length-driven mechanism.

Our findings differ from similar work in decerebrate cats, which observed the opposite modulation of PICs with muscle length (Hyngstrom et al., 2007). In that study, the influence of Ib afferents was excluded because they do not respond to passive changes in muscle length, which could have explained the opposite modulation. However, our results suggest that PICs modulation is not driven by force production, making it unlikely that Ib afferents explain this discrepancy. A more plausible explanation for these divergent observations is the strong influence of descending systems, such as the corticospinal tract, on the Ia inhibitory system (Hyngstrom et al., 2007), which was partially absent in the decerebrate cat model. This indirectly underlies the potential role of descending systems in modulating PICs in response to changes in muscle length. This interpretation is further supported by the modulation of estimates of PICs observed in humans during involuntary contractions (i.e., using vibration–stimulation protocols) (Trajano et al., 2014) that is similar to the modulation found in decerebrate cats.

Modulation of PICs by ankle angle may reflects inhibitory inputs rather than neuromodulatory inputs

PICs activation depends on monoamine neuromodulators, such as serotonin and noradrenaline (Heckman et al., 2009a). Therefore, one possible explanation for the lower PICs estimates at longer muscle lengths is a reduced release of serotonin and/or noradrenaline onto motoneurons. However, we observed that brace height, a metric that predicts changes in neuromodulation (Beauchamp et al., 2023; Chardon et al., 2024), remained unchanged in the SOL and was even higher at long muscle lengths in the GM. The fact that brace height exhibited no modulation or the opposite pattern compared to ΔF suggests that neuromodulatory inputs are unlikely to explain the observed changes in ΔF across muscle lengths. A more likely explanation for the lower ΔF at long muscle lengths is the influence of synaptic inhibition on motoneurons which may

overcome the potentially higher neuromodulatory drive at longer lengths, thereby shaping the modulation of PICs.

PICs also depend on the balance between inhibitory and excitatory inputs (i.e., the pattern of inhibition), that we assessed in this study with the analysis of the attenuation slope of MU discharge (Beauchamp et al., 2023; Chardon et al., 2024). An increase in the relative amount of inhibition, compared to excitatory input, is typically associated with a reduction in PICs (Binder et al., 2020; Heckman et al., 2009a). We observed a general decrease in the attenuation slope when muscles were lengthened, suggesting a shift towards a more pronounced inhibitory input relative to excitation (i.e., a more proportional or less push-pull pattern). This shift likely contributed to the observed reduction in PICs estimates. Even though the underlying sources of the relative increase in inhibition cannot be determined from our results, we suggest that reciprocal inhibition (Hyngstrom et al., 2007) and recurrent inhibition (Bui et al., 2008) - which have been shown to dampen PICs - may play a role. Alternatively, the relative increase in inhibition may result from a reduced baseline level of inhibition at shorter muscle lengths (Beauchamp et al., 2023).

The metrics derived from the geometric approach have been proposed to reflect the types of inputs received by motoneurons (i.e., excitation, inhibition and neuromodulation). However, experimental findings challenge the interpretation of these metrics. For example, although the attenuation slope has been proposed as an indicator of inhibition, no difference was observed between voluntary co-contraction and agonist-only contraction (Gomes et al., 2024), despite these conditions are supposed to involve different patterns of inhibition. These limitations highlight the need for future studies to confirm whether the observed modulation of PICs by ankle angle reflects changes in inhibitory inputs, rather than neuromodulatory influences.

Role of inhibitory control of PICs according to muscle length

At longer muscle lengths in the triceps surae, less neural drive is needed to produce the same force, which aligns with the decrease in maximal discharge rates of MUs observed at long muscle length for the same absolute torque. Thus, the reduction in estimates of PICs with increasing muscle length suggests that PICs may serve as an additional mechanism, probably mediated through inhibition, to adjust motoneuron recruitment and firing rates based on the muscle's force generating capacity. Overall, these findings support the idea that the flexibility of inhibitory pathways extends to the flexible control of dendritic PICs. Since PICs are believed to act

as gain controllers (Johnson & Heckman, 2014; Wei et al., 2014), the role of inhibitory systems becomes even more critical in matching the demands of motor tasks. Consequently, any dysfunction in the inhibitory system could lead to severe motor dysfunctions, as PICs would remain poorly controlled. Failure of motor control mechanisms, such as recurrent or reciprocal inhibition, could worsen a misdirected motor command by failing to properly adjust PICs and, therefore, the intrinsic excitability of motoneurons. This could be particularly relevant in conditions where descending inputs are disrupted (e.g., spinal cord injury, stroke-induced hemiparesis), leading to muscle-length-related deficits such as spasticity or involuntary antagonist muscle contractions (Gracies, 2005b).

Methodological considerations

Some methodological issues need consideration. First, even though the decomposed MU population represents only a subset of the entire motor pool (Farina & Holobar, 2016), we tracked MUs across positions, preventing bias in MUs sampling between conditions. Second, the estimates of PICs magnitude were based on MUs recruited during low-intensity isometric contractions and cannot therefore be directly extrapolated to higher-threshold MUs or to dynamic contractions. Finally, the results need to be confirmed in females.

Conclusion

This study provides strong evidence that the reduction in PICs-induced prolongation of MU discharge rate in a lengthened triceps surae position is driven primarily by changes in muscle length rather than changes in muscle tension and by inhibitory inputs, rather than by muscle tension or metabotropic neuromodulation. This highlights inhibition as a potential mechanism for adjusting motoneuron recruitment and gain based on the force-generating capacity of muscles and the demands of motor tasks. As a result, a failure to properly regulate inhibitory mechanisms could be particularly harmful, potentially contributing to the muscle length-related impairment observed in conditions such as stroke or spinal cord injury.

◥ STUDY 2: DISRUPTED INHIBITORY-EXCITATORY BALANCE UNDERLIES SPINAL MOTONEURON DYSFUNCTION IN INCOMPLETE SPINAL CORD INJURY

KEY POINTS

- Incomplete spinal cord injury disrupts voluntary movement, in part by impairing motoneuron rate coding, yet the synaptic mechanisms underlying this dysfunction remain poorly understood in humans.
- By analysing large motoneunon populations from triceps surae muscles, we estimated the relative contributions of excitatory, inhibitory, and neuromodulatory inputs to motoneuron rate coding after chronic incomplete spinal cord injury.
- We provide evidence that individuals with spinal cord injury show no alteration in estimated neuromodulatory inputs, but a disrupted inhibitory–excitatory balance shifted towards greater inhibition.
- Experimental conditions designed to modulate inhibition altered motoneuron firing in controls but not in individuals with incomplete spinal cord injury
- Together, these results indicate that increased inhibition during voluntary contraction likely contributes to impaired rate coding and muscle weakness after spinal cord injury in humans.

ABSTRACT

Incomplete spinal cord injury disrupts voluntary movement, in part through motoneuron dysfunction, yet the mechanisms underlying this dysfunction remain poorly understood. Using a non-invasive approach to decode the spiking activity of large populations of spinal motoneurons, we quantified the relative contributions of excitatory, inhibitory, and neuromodulatory inputs to motoneuron rate coding after chronic incomplete spinal cord injury. Eighteen participants with incomplete spinal cord injury and 18 age- and sex-matched control participants performed submaximal isometric plantar flexion tasks while high-density surface electromyography was recorded from the soleus and gastrocnemius medialis muscles. Motoneuron firing behaviour was analysed to estimate the neuromodulatory drive and the inhibitory-excitatory balance. Participants with incomplete spinal cord injury exhibited lower rate coding than controls. Estimates of neuromodulatory drive did not differ between groups, whereas individuals with spinal cord injury showed a shift in the inhibitory-excitatory balance toward greater inhibition compared with controls. Furthermore, increasing inhibitory input through muscle length changes and antagonist tendon vibration modulated motoneuron firing in controls, but not in individuals with incomplete spinal cord injury. Together, these findings suggest that impaired

rate coding after incomplete spinal cord injury arises from an altered inhibitory-excitatory balance rather than reduced neuromodulatory drive. Taking advantage of methodological advances to decode spinal motoneurons activity during voluntary contraction, this study identified excessive inhibitory input to spinal motoneurons as a key neural mechanism contributing to muscle weakness and impaired motor function in individuals with incomplete spinal cord injury.

1. INTRODUCTION

Incomplete spinal cord injury (SCI) leads to profound alterations in the neural control of movement. Disruption of supraspinal inputs to spinal motoneurons and interneurons at and below the level of the lesion results in muscle weakness and impaired motor function (McDonald & Sadowsky, 2002). Although changes in motoneuron firing characteristics have been described (Thomas et al., 2014), the underlying mechanisms remain poorly understood. In particular, little is known about how SCI alters the relative contributions of excitatory, neuromodulatory, and inhibitory synaptic inputs to motoneuron output.

Muscle force is regulated by modulating the number of active motoneurons (recruitment) and the firing rate of already active motoneurons (rate coding). In individuals with incomplete SCI, a reduction in rate coding has been reported in several muscles (Debenham et al., 2024; Kizyte et al., 2025; Thomas et al., 2014; Wiegner et al., 1993). The mechanisms underlying these alterations remain unclear. Beyond the essential role of excitatory inputs, neuromodulatory inputs contribute to motoneuron rate coding by increasing intrinsic motoneuron excitability through the activation of persistent inward currents (PICs). These currents provide an additional intrinsic depolarising drive that amplifies and prolongs the effects of synaptic excitation in motoneurons (Hultborn et al., 2003; Y. Li & Bennett, 2003; Schwindt & Crill, 1980). Although spinal cord injury can disrupt descending monoaminergic drive, animal studies have demonstrated compensatory mechanisms, such as constitutively active 5-HT_2 receptors, that preserve PICs despite reduced monoaminergic drive (D'Amico et al., 2014; Murray et al., 2010). Whether PICs are preserved in humans with incomplete SCI remains unknown.

Inhibitory inputs, notably those mediated by Ia interneurons and Renshaw cells, also play an important role in shaping motoneuron output by interacting with both excitatory inputs and PICs (Hyngstrom et al., 2007; Kuo et al., 2003; Powers & Heckman, 2017). Importantly, increases in the net input to motoneurons can arise through distinct patterns of inhibition. One such pattern is the push-pull pattern, in which a decrease in synaptic inhibition occurs in parallel

with increased synaptic excitation, thereby supporting higher rate coding and amplifying the effects of PICs (Johnson et al., 2012; Powers & Heckman, 2017; Škarabot et al., 2025). However, after SCI, inhibitory control is altered (Crone, 2003; Knikou & Mummidisetty, 2011), with a notable increase in recurrent inhibition (Shefner et al., 1992). This change may disrupt the normal push-pull interaction between excitation and inhibition and ultimately contribute to firing rate saturation, a phenomenon observed following SCI (Thomas et al., 2014).

Two experimental paradigms are particularly relevant for investigating inhibitory control of motoneuron output. First, changes in muscle length modulate motoneuron excitability through length-dependent inhibitory mechanisms, such as recurrent inhibition (Colard et al., 2025). Specifically, at longer muscle lengths, an increased inhibitory influence is associated with a reduced PIC-mediated prolongation of motoneuron firing rate (Beauchamp et al., 2025; Goreau et al., 2025; Valenčič et al., 2026). Second, vibration applied to the tendons of the antagonist muscles modulates motoneuron output and PIC prolongation effect, via enhanced Ia-mediated reciprocal inhibition (Mesquita et al., 2022; Pearcey et al., 2022). Together, these experimental conditions highlight the flexible and context-dependent regulation of motoneuron output and PIC effects on firing, and therefore provide relevant frameworks for examining inhibitory control of motoneuron output in individuals with incomplete SCI.

In this human study, we aimed to determine how synaptic inputs shape motoneuron rate coding in individuals with incomplete SCI. To this end, we identified large populations of motoneurons (up to 36 per muscle per contraction) by decomposing high-density EMG signals collected during submaximal isometric contractions. We first compared the contribution of inhibitory and neuromodulatory inputs to motoneuron firing rates in plantar flexor muscles between individuals with chronic incomplete SCI and healthy controls, using a framework that links specific motoneuron firing features, such as nonlinear firing acceleration and prolonged firing, to underlying synaptic inputs (Beauchamp et al., 2023; Chardon et al., 2024). We then experimentally manipulated inhibitory inputs through changes in muscle length and antagonist tendon vibration to gain further insights into the role of inhibitory inputs in shaping motoneuron behaviour.

2. METHODS

Participants and ethical approval

Eighteen individuals with incomplete SCI (mean ± SD: 55 ± 19 years, 175 ± 8 cm, 77 ± 15 kg, two women, Table 3) and 18 control participants (50 ± 20 years, 178 ± 8 cm, 74 ± 14 kg, two women) participated in the study. All participants provided written informed consent, and the experimental procedures were approved by the local ethics committee (CERNI, Nantes Université, IRB: IORG0011023). Participants with SCI had sustained their injury at least five months before enrollment and were classified using the International Standards for Neurological Classification of Spinal Cord Injury (ISNCSCI) as having a C2-L1 lesion. Based on the American Spinal Cord Injury Impairment Scale (AIS), one participant was classified as AIS C, and the remaining 17 as AIS D. Eleven participants had a non-traumatic aetiology. Twelve participants with SCI were taking anti-spastic medication (baclofen and/or pregabalin and/or gabapentin), and five were taking serotonergic medication (duloxetine or paroxetine or mirtazapine) at the time of enrollment. Spasticity was assessed using the modified Tardieu scale. Participants with incomplete SCI were required to have had no orthopedic or neurosurgical intervention within the previous three months and no intramuscular injections of botulinum toxin in the plantar flexors during the same period. Control participants were required to have had no lower limb injuries in the previous six months. All participants were instructed not to consume caffeine the day of the evaluation. For individuals with incomplete SCI, the tested leg was the one with the lower maximal voluntary plantar flexion torque, unless this torque was below 15 N.m. In those cases, the limb with greater capacity was selected. As a result, in the incomplete SCI group, 8 of 18 participants were tested on their dominant leg (defined as the leg used to kick a ball), compared with 9 of 18 in the control group.

The maximal voluntary torque (MVT) of the plantar flexors in the incomplete SCI group was 42.9 ± 33.4 N.m when the muscle was placed at a short length and 62.3 ± 38.0 N.m at an intermediate length (Fig. 52A). In the control group, MVTs were 104.1 ± 33.7 N.m and 145.5 ± 49.6 N.m in the short and intermediate lengths, respectively.

Table 3. Characteristics of individuals with incomplete spinal cord injury.

Participant	age	sexe	Assess-ment on the domin-nent side	AIS	SCI level	Years post SCI	Ae-tiology	SCI ins-tallation time-frame	Identi-fied me-dullary syn-drome	Antispas-tic medi-cation	Serotoner-gic medica-tion	Torque at 0° (N.m)	MTS knee flexed	MTS straight knee
1	35	M	yes	D	T3	0.5	NT	A	no	GAB	DUL	18	3	3
2	42	M	no	C	C4	7	NT	C	no	BAC	none	46	0	0
3	19	M	yes	D	C7	4	T	A	BS	BAC	none	10	2	3
4	75	M	no	D	T1	0.6	NT	A	no	none	none	96	2	1
5	57	M	yes	D	T12	8	NT	C	no	GAB	none	56	2	2
6	72	F	no	D	C3	6	NT	SA	no	PGAB	none	36	2	2
7	40	M	no	D	C4	5	NT	SA	no	PGAB	none	74	3	3
8	81	M	no	D	C3	5	NT	C	BS	none	none	16	2	2
9	61	M	no	D	C4	11	T	A	BS	BAC, PGAB	DUL	44	2	2
10	73	M	yes	D	C8	2	NT	C	no	PGAB	none	90	2	2
11	54	M	yes	D	C3	4	NT	C	BS	GAB	DUL	162	2	2
12	64	M	no	D	C8	20	NT	A	ventral	none	PAR	76	1	2
13	51	M	yes	D	C2	34	T	A	BS	BAC, GAB	none	85	0	2
14	71	M	no	D	C4	2.4	T	A	no	none	MIR	81	2	2
15	49	F	yes	D	C7	29	T	A	BS	PGAB	none	46	1	2
16	54	M	no	D	C6	1	NT	C	no	none	none	81	3	3
17	18	M	yes	D	C7	0.5	T	A	BS	GAB	none	85	2	2
18	75	M	no	D	L1	9	T	A	ventral	none	yes	11	0	0

AIS, American Spinal Injuty Association Impairment Scale; M, male; F, female, T, traumatic, NT, non-traumatic; A, acute; C, chronic, SA, subacute; BS, Brown-Séquard; MTS, Modified Tardieu Scale; GAB, gabapentin; BAC, baclofen; PGAB, pregabalin; DUL, duloxetine; PAR, paroxetine; MIR, mirtazapine.

Experimental protocol

After the warm-up and MVT assessments, participants performed several isometric submaximal triangular contractions, each consisting of 12-second ascending and descending phases. To compare motoneuron behaviour between groups while accounting for large differences in MVT, participants performed a contraction at both a similar relative torque (40% of their MVT) and a similar absolute torque (30 N.m), all performed in the neutral ankle position (0°). To assess how motoneuron behaviour adapts to muscle length, participants also performed a contraction at a shorter muscle length (20° of plantarflexion), at 40% of their MVT in this position (Fig 52B). For clarity, these positions are described based on the length of the plantar flexor muscles: the short muscle length position at 20° of plantarflexion and the intermediate muscle length position at 0°. These two joint positions have been shown to induce measurable differences in

fascicle length of gastrocnemius medialis (GM) and soleus (SOL) (Colard et al., 2025; Kuzyk et al., 2018).

To assess how reciprocal inhibition affects motoneuron behaviour, vibration was applied to the tendons of the antagonist muscles during contractions in both positions (for the contractions at 40% of their MVT). High-frequency vibration (115 Hz; Vibrasens, Technoconcept, Saint-Maurice, France) was applied to the distal tibialis anterior (TA) tendon during plantarflexion contractions by manually pressing the vibrator to the tendon with a force of 15 ± 2 N. Vibration started 10 s before the onset of the triangular contraction and continued until after the torque returned to baseline, ensuring that the entire contraction was covered.

After a familiarisation period for the first condition, participants completed one contraction per condition in randomised order, resulting in a total of five submaximal contractions. At least one minute of rest was provided between contractions to minimise fatigue and the warm-up effect of PICs (Bennett et al., 1998).

Electromyography

To obtain information on muscle activation (Fig 52C), we reproduced a bipolar configuration by averaging two groups of 25 channels located at the extremities of each grid and then computing the difference between these averages, yielding a single value per grid. The values from the two grids were subsequently averaged to obtain a single value per muscle. The EMG amplitude was analysed as a normalised root mean square over a 300 ms window, by normalising RMS values to the RMS value of the same electrode during the maximal voluntary contraction (EMGmax).

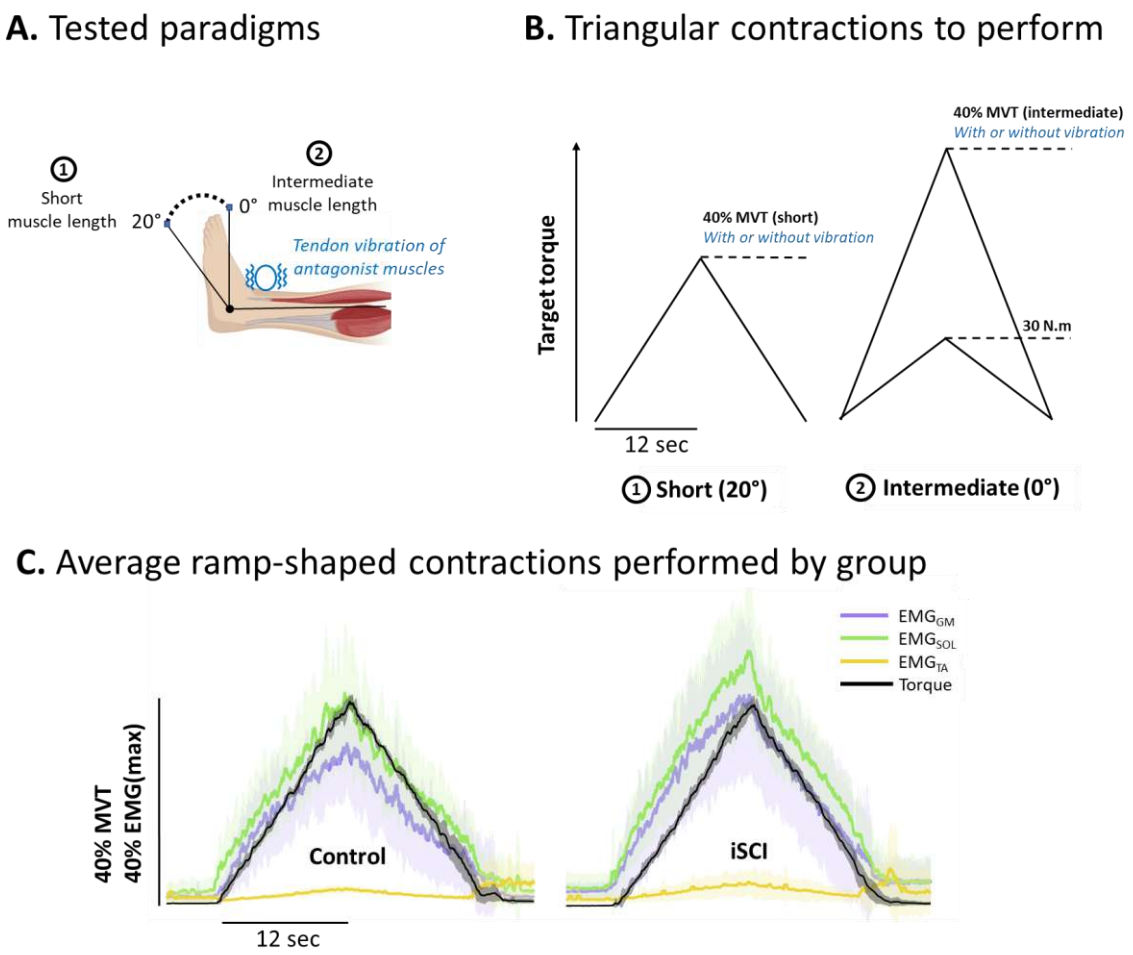

Figure 52. Experimental setup. *A, participants performed isometric submaximal plantarflexions at two ankle positions, corresponding to different plantar flexor lengths: 20° (short muscle length position) and 0° (intermediate muscle length position). Tendon vibrations was applied to the antagonist muscles (i.e., dorsiflexor muscles) during contractions to induce reciprocal inhibition. B, the submaximal plantarflexions were performed to 40% of the maximal voluntary contraction torque (MVT) at each position. In addition, a plantarflexion to 30 N.m was performed to compare groups on the same absolute torque. C, mean (thick line) and standard differences (clear outline) of torque and normalised EMG amplitude of gastrocnemius medialis (GM), soleus (SOL) and tibialis anterior (TA), in the control and the incomplete spical cord injury (iSCI group), during the contraction up to 40% MVT in intermediate position.*

Statistical analyses

To assess differences in motoneuron firing characteristics between groups during contractions at 40% MVT and 30 N.m performed at an intermediate muscle length, we applied a linear mixed-effects model to each motoneuron firing metric (i.e., recruitment threshold, firing rate at recruitment, peak firing rate, firing rate modulation, ΔF, normalised ΔF, brace height, acceleration, attenuation and MUAP amplitude). The models included the group (incomplete SCI, control), muscle (gastrocnemius medialis, soleus) and their interactions as fixed effects. The full random-effects structure consisted of a random intercept for each participant and random slopes

to account for between participants variability in the fixed effects [e.g., lmer(metric ~ group*muscle + (group*muscle|id_participant))]. For each model, the random-effects structure was selected by minimising the bayesian information criterion across all plausible random-slope structures. The random slope for the primary effect of interest (group) was always retained, as it represents the key source of between-participant variability for the tested condition.

To test the effects of position and vibration, separate models were fitted including the effect of interest (position: short, intermediate; or vibration: on, off), together with muscle (gastrocnemius medialis, soleus), group (incomplete SCI, control), and their interactions as fixed effects. The random-effects structure was selected using the same procedure; however, in these models the retained random slope corresponded to the effect of interest (position or vibration), rather than group.

To compare TA coactivation between groups, we compared TA EMG amplitude during the similar relative torque contraction at the intermediate muscle length (shown in Fig. 52C) using a t-test. We considered the EMG normalised to the maximal value obtained during the maximal dorsiflexion contraction.

All analyses were performed in R (v.4.4.0; R Core Team 2021, R Foundation for Statistical Computing, Vienna, Austria). Statistical significance was assessed using the lmerTest package in R (Kuznetsova et al., 2017), which uses Satterthwaite's type III method to approximate degrees of freedom and generate p-values for mixed effects models. Model assumptions of homoscedasticity, normality, and independence of residuals were verified graphically. When significant effects were detected, Sidak post-hoc corrections were applied. Estimated marginal mean differences with 95% confidence intervals and standardised effect sizes (Cohen's d) were calculated using the emmeans package. The alpha level for all statistical tests was set at 0.05.

3. RESULTS

Motoneuron yield and TA coactivation

In the incomplete SCI group, an average of 9.3 ± 7.5 motoneurons for the GM and 10.3 ± 8.1 motoneurons for the SOL were identified per contraction and participant. In the control group, an average of 13.5 ± 7.8 motoneurons for the GM and 8.2 ± 6.1 motoneurons for the SOL were identified per contraction and participant. TA coactivation during triangular contractions did not differ between groups when assessed using normalised EMG (control vs. incomplete SCI: 2.80 ± 4.07 vs. 3.13 ± 1.68 % of EMGmax, p = 0.7965).

Differences between groups at intermediate muscle length (0°)

Recruitment threshold, rate coding and motor unit action potential amplitude

An example of smoothed motoneuron firing rate from a single contraction in one control and one incomplete SCI participant (#10) is shown in Figure 53.

There were no significant between-group differences in recruitment threshold (p = 0.2406 for the 40% MVT contractions, and p = 0.2517 for the 30 N.m contractions), nor any interaction between group and muscle (p = 0.5848 for the 40% MVT contractions, and p = 0.2428 for the 30 N.m contractions) (Fig. 53). For the 40% MVT contractions, there was a significant interaction between group and muscle for both firing rate at recruitment (p = 0.0431) and peak firing rate (p = 0.0091). Specifically, firing rate at recruitment was lower in the incomplete SCI group than in the control group by 1.87 pps in the GM (95% CI: [1.01–2.72], d = 1.43, p = 0.0001) and by 0.88 pps in the SOL (95% CI: [0.23–1.54], d = 0.68, p = 0.0096). Peak firing rate was also lower in the incomplete SCI group by 4.52 pps in the GM (95% CI: [2.88–6.16], d = 3.27, p < 0.0001) and by 2.49 pps in the SOL (95% CI: [1.49–3.49], d = 1.8, p < 0.0001). There was no significant interaction between group and muscle for firing rate modulation (p = 0.0674) but there was a main effect of group, with lower modulation values in the incomplete SCI group (d = 1.43, p < 0.0001). Overall, similar results were observed for the 30 N.m contractions, with all firing-rate metrics lower in the incomplete SCI group compared to the control group. Specifically, there were significant main effects of group for firing rate at recruitment (d = 0.97, p = 0.0106), peak firing rate (d = 1.82, p = 0.0016), and firing rate modulation (d = 0.66, p = 0. 0147), with no interaction between group and muscle (all p > 0.4827).

When considering the MUAP amplitude during the 30 N.m contractions, there was no significant between-group differences (p = 0.7115), nor any interaction between group and muscle (p = 0.0792). For the 40% MVT contractions, there was a significant interaction between group and muscle (p = 0.0424), with lower MUAP amplitude in the incomplete SCI group in the GM by 8.2 mV (95% CI: [1.05–15.38], d = 0.74, p < 0.0259) but not in the SOL (p = 0.9584).

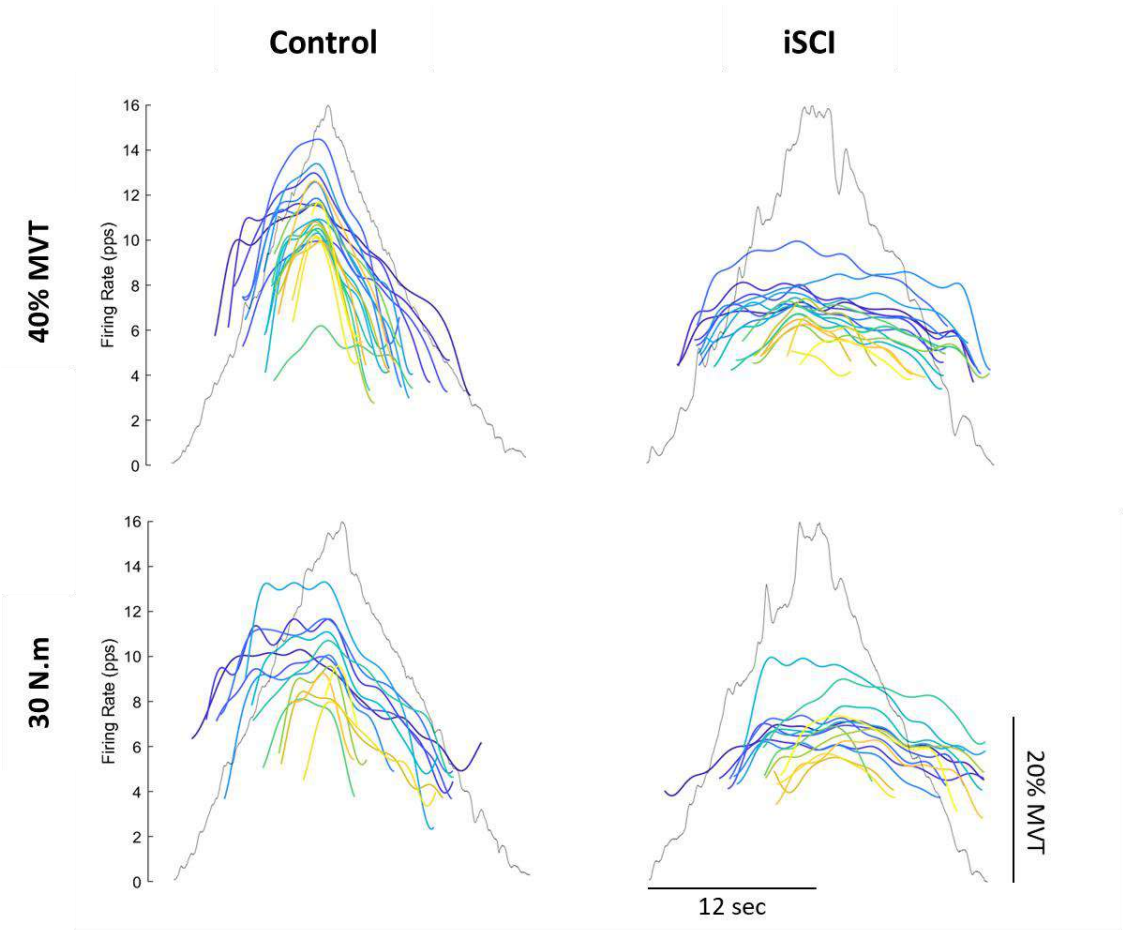

Figure 53. Typical motoneuron firing rates in control (CTL) and incomplete SCI (iSCI) participants. *Plantarflexion torque (grey trace) and smoothed firing rates of 20 identified motoneurons (coloured traces) are shown for a control participant (left) and an individual with incomplete SCI (#10, right). Within each plot, smoothed firing rates are shown with darker colours (purple) for lower threshold neurons and lighter colours (yellow) for higher threshold neurons.*

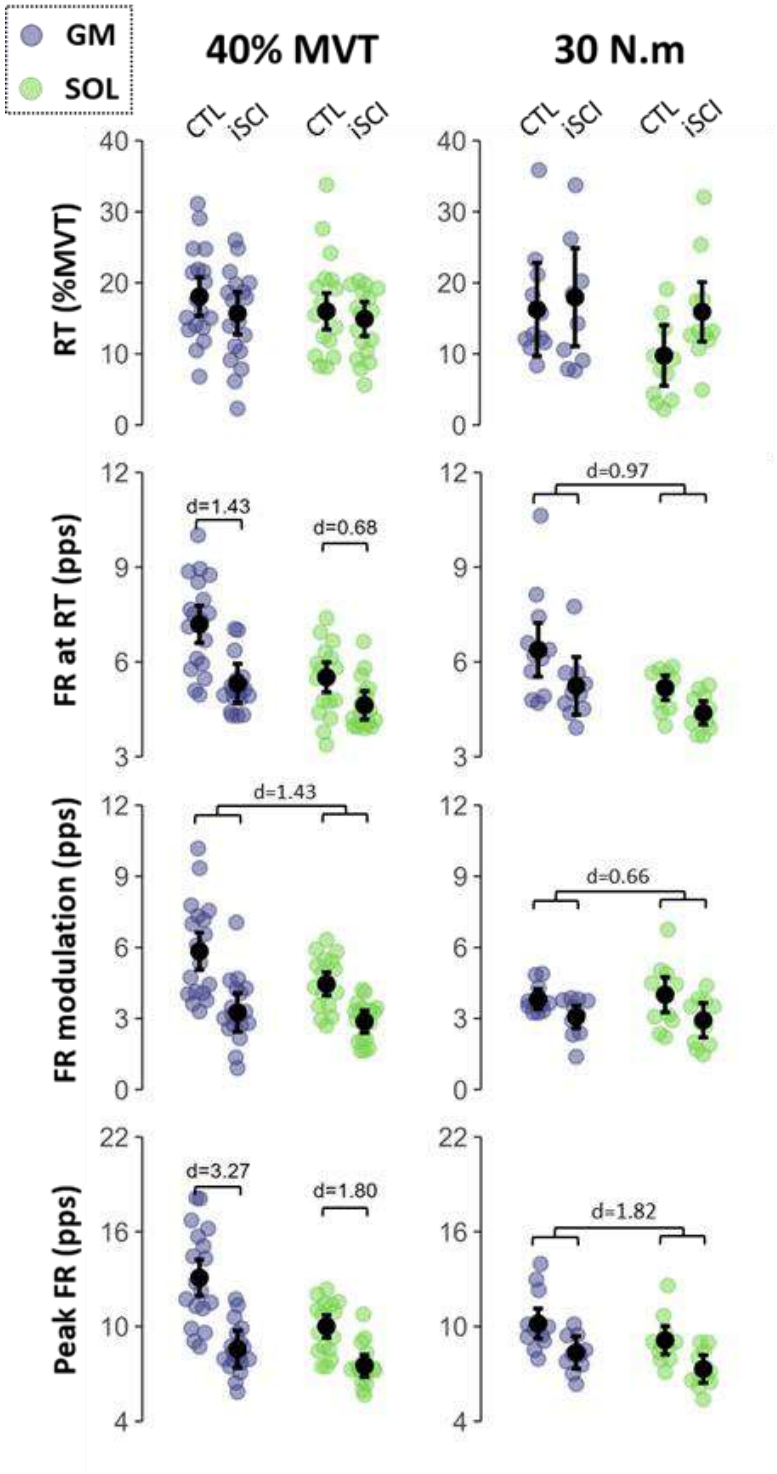

Figure 54. Motoneuron recruitment thresholds and rate coding. *The incomplete SCI (iSCI) and control (CTL) groups are compared at either the same relative torque (40% MVT) or the same absolute torque (30 N.m). Recruitment threshold (RT), firing rate at recruitment (DR RT), firing rate modulation (FR modulation), and peak firing rate (max DR), were obtained from the gastrocnemius medialis (GM, purple) and soleus (SOL, green). Coloured dots represent participant averages, while black dots and bars indicate the estimated marginal means with 95% confidence intervals predicted by linear mixed-effects models. Cohen's d is reported for significant differences.*

Estimates of synaptic inputs to motoneurons

Brace height did not differ between groups ($p = 0.3311$ for the 40% MVT contractions and $p = 0.2399$ for the 30 N·m contractions), nor was there any interaction between group and muscle ($p = 0.5974$ and $p = 0.3818$, respectively), suggesting no group differences in estimated neuromodulatory input (Fig. 54). Conversely, attenuation slope showed no significant interaction between group and muscle ($p = 0.3982$), but a significant main effect of group for the 40% MVT contractions, with lower attenuation slopes in the incomplete SCI group ($d = 0.91$, $p < 0.0001$). This finding indicates a less pronounced push-pull inhibitory pattern in the incomplete SCI group compared with controls. There were no significant differences including the group factor for the 30 N.m contractions (muscle-group interaction: $p = 0.2728$; group effect: $p = 0.2275$). When considering acceleration, there was a significant interaction between group and muscle for the 40% MVT contractions ($p = 0.0111$). Specifically, acceleration was lower in the incomplete SCI group by 1.19 $pps.s^{-1}$ in the GM (95% CI: [0.82–1.55], $d = 1.66$, $p < 0.0001$) and by 0.69 $pps.s^{-1}$ in the SOL (95% CI: [0.43–0.96], $d = 0.97$, $p < 0.0001$). Similar results were observed for the 30 N.m contractions, with no muscle-group interaction ($p = 0.9160$) but a significant main effect of group, with lower acceleration in the incomplete SCI group ($d = 0.58$, $p = 0.0023$). Because attenuation slope differed between groups whereas brace height did not, the reduced acceleration found here likely reflects greater inhibitory input rather than altered neuromodulation.

When considering ΔF, there was a significant main effect of group for both the 40% MVT contractions ($p = 0.0018$) and the 30 N.m contractions ($p = 0.0050$), with no significant interaction between group and muscle ($p = 0. 5350$ for the 40% MVT contractions, and $p = 0.7365$ for the 30 N.m contractions). Specifically, ΔF was lower in the incomplete SCI group (40% MVT contraction: $d = 1.2$, $p = 0.0017$; 30 N.m contraction: $d = 0.96$, $p = 0.0048$). When considering normalised ΔF, there was no significant group effect for the 40% MVT contractions ($p = 0.5504$) nor significant interaction between group and muscle ($p = 7940$). However, for the 30 N.m contractions, a significant interaction between group and muscle was observed ($p = 0.0151$), with normalised ΔF being 28.8 percentage points lower in the GM of the incomplete SCI group (95% CI: [14.1–43.6], $d = 1.2$, $p = 0.0011$), while no group difference was found in the SOL ($p = 0.8010$).

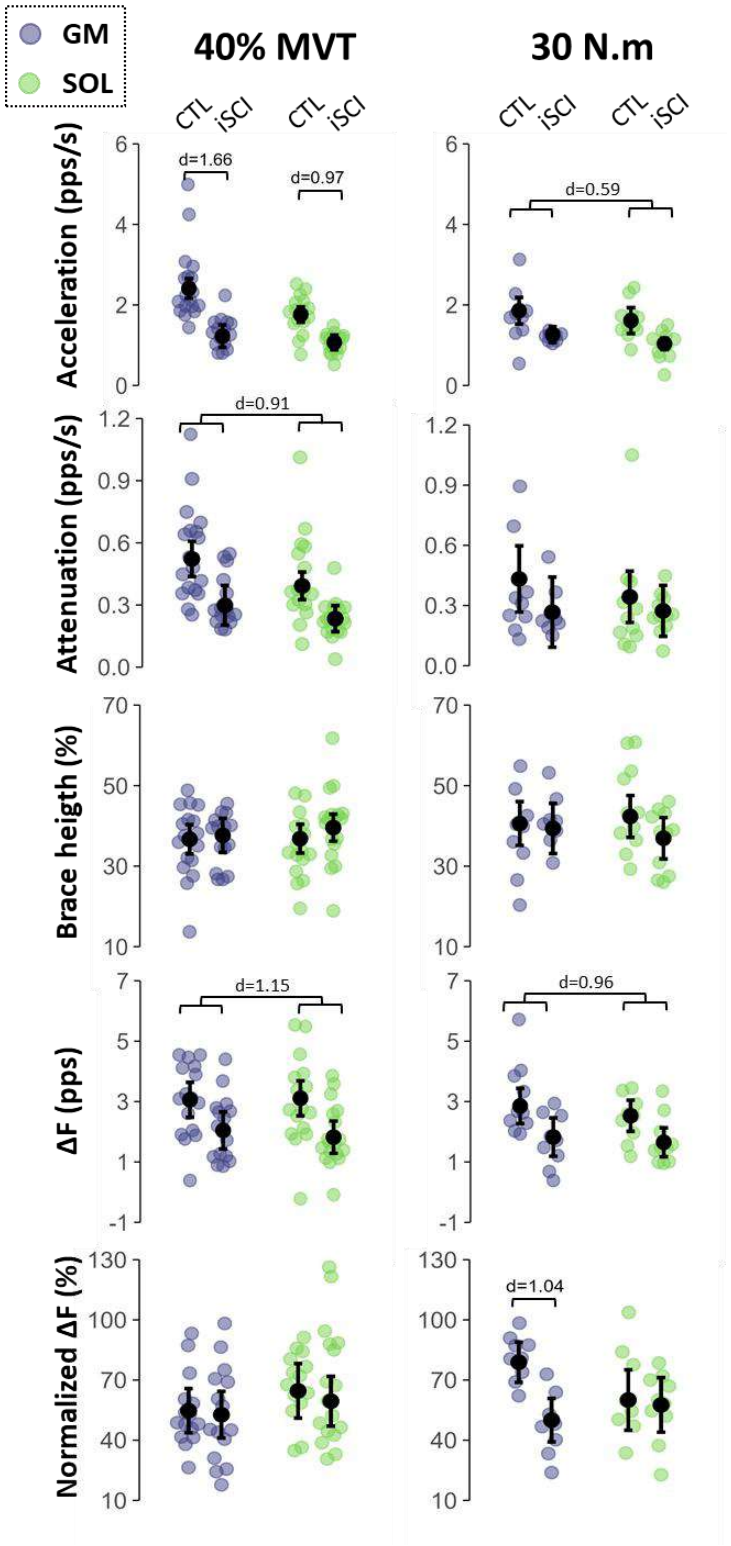

Figure 54. Estimates of synaptic inputs to motoneurons. *The incomplete SCI (iSCI) and control (CTL) groups are compared at either the same relative torque (40% MVT) or the same absolute torque (30 N.m). The acceleration slope, attenuation slope, brace height, ΔF, and normalised ΔF were obtained from the gastrocnemius medialis (GM, purple) and soleus (SOL, green). Coloured dots represent participant averages, while black dots and bars indicate the estimated marginal means with 95% confidence intervals predicted by linear mixed-effects models. Cohen's d is reported for significant results.*

Modulation of motoneuron behaviour in response to change in muscle length and vibration

Modulation of motoneuron firing rates was compared between the incomplete SCI and control groups for the 40% MVT contractions under two conditions: change in muscle length and the application of vibration to the tendons of the antagonist muscles. For the muscle-length condition, we compared the short and intermediate positions. For the vibration condition, we compared contractions with and without vibration at the short muscle length, as no modulation of firing rate was observed at the intermediate position with vibration in either group.

An example of smoothed motoneuron firing rate from one control and one participant with incomplete SCI (#10) at short muscle length, intermediate muscle length, and during tendon vibration is shown in Figure 55.

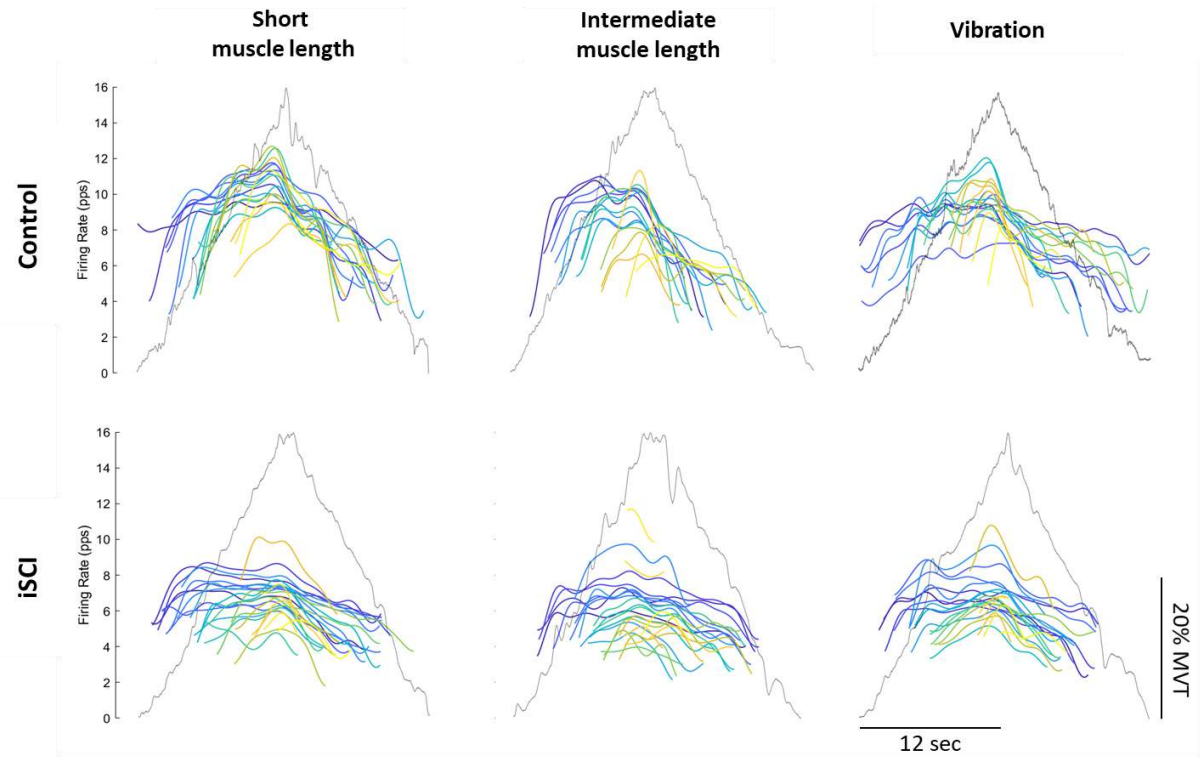

Figure 55. Typical effects of muscle length and vibration on motoneuron firing rates in control (CTL) and incomplete SCI (iSCI). *Plantarflexion torques (grey trace) and smoothed firing rates of decomposed soleus motoneurons (coloured traces) for a control participant (upper panel) and an incomplete SCI participant (#10, lower panel). Contractions were performed at short muscle length (left), intermediate muscle length (middle), and with the application of vibration to the tendons of the antagonist muscles (right). For both participants, smoothed firing rates are shown with darker colours (purple) at lower thresholds and lighter colours (yellow) at higher thresholds.*

Recruitment threshold and rate coding

For the following results, the effects of interest are those involving interactions between group and condition (muscle length or vibration), including both group-condition interactions and group-condition-muscle interactions.

For the muscle length condition, there were no significant interactions involving group for recruitment threshold (all $p > 0.0558$) or firing rate at recruitment (all $p > 0.0611$) (Fig. 56). When considering peak firing rate, there was an interaction between group and muscle length ($p = 0.0132$), with no significant interaction between group, muscle length, and muscle ($p = 0.1500$). Specifically, the control group showed a higher peak firing rate at short compared to intermediate muscle length, regardless of the muscle ($d = 0.73$, $p = 0.0001$), whereas no difference between muscle lengths was observed in the incomplete SCI group ($p = 0.5150$). When considering firing rate modulation, there was a significant interaction between group, muscle length and muscle ($p = 0.0144$). In the control group, firing rate modulation was higher in the GM at short compared with intermediate muscle length by 0.85 pps (95% CI: [0.35–1.34], $d = 0.59$, $p = 0.0017$), whereas no difference was observed in the SOL ($p = 0.7812$). In the incomplete SCI group, firing rate modulation did not differ across muscle lengths, regardless of the muscle (all $p > 0.3726$).

For the vibration condition, there were no significant interactions involving the group factor for recruitment threshold (all $p > 0.1719$). There was an interaction between group and vibration for firing rate at recruitment ($p = 0.0292$) and for peak firing rate ($p = 0.0029$), with no significant interaction between group, vibration, and muscle (all $p > 0.5268$). In controls, vibration reduced firing rate at recruitment ($d = 0.41$, $p = 0.0358$) and peak firing rate ($d = 0.56$, $p = 0.0021$), whereas no significant effects were observed in the incomplete SCI group. There were no significant interactions involving the group factor for rate modulation (all $p > 0.2824$).

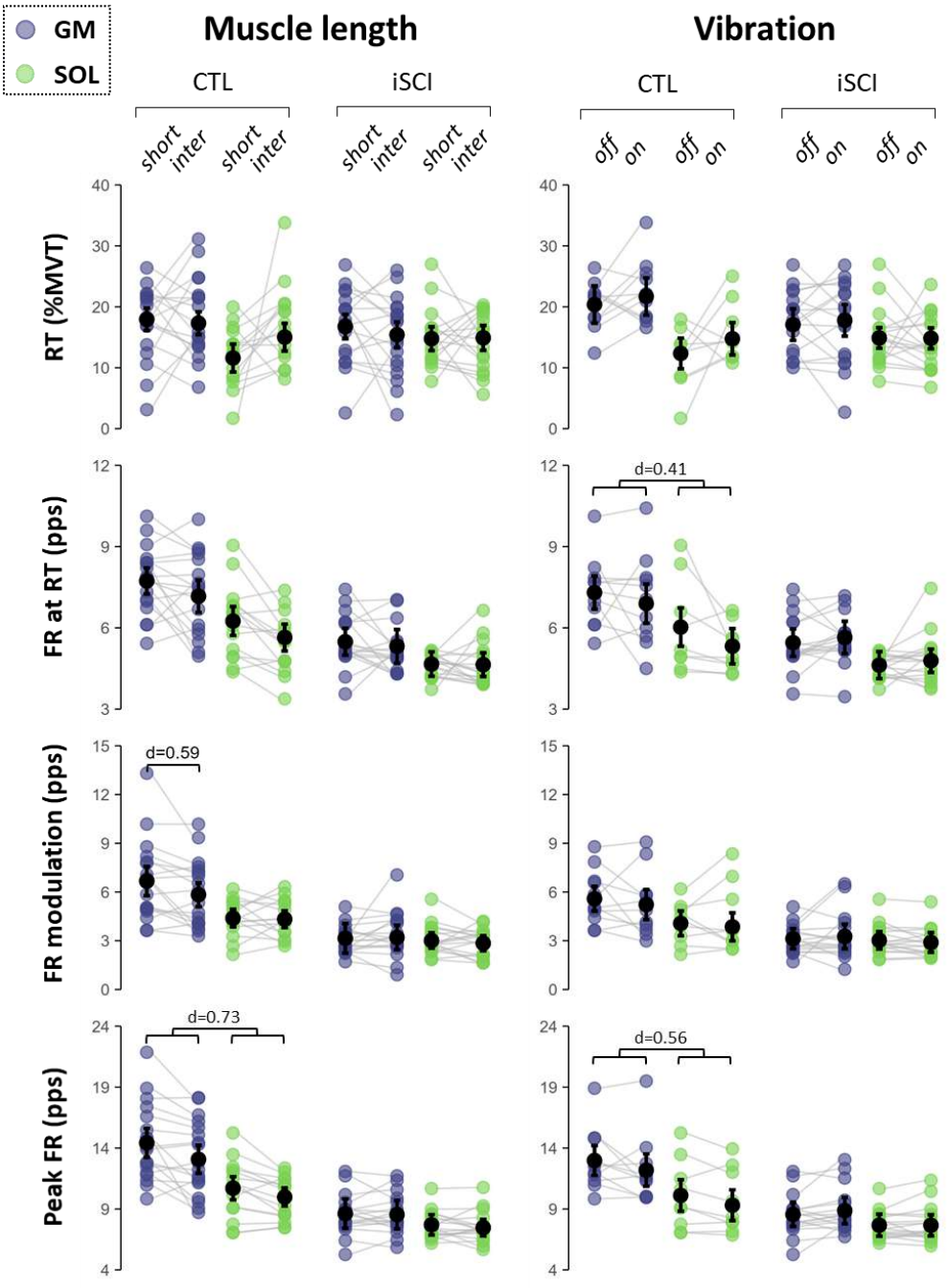

Figure 56. Effect of muscle length and vibration in motoneuron recruitment threshold and rate coding. *The modulation of motoneuron rate coding and recruitment threshold between the incomplete SCI (iSCI) and control (CTL) groups are compared in response to changes in muscle length at the same relative torque (40% MVT), and the application of tendon vibration to antagonist muscles, at short muscle length (20° of plantarflexion). Recruitment threshold (RT), firing rate at recruitment (DR RT), firing rate modulation (FR modulation), and peak firing rate (peak FR), were obtained from the gastrocnemius medialis (GM, purple) and soleus (SOL, green). Coloured dots represent participant averages, while black dots and bars indicate the estimated marginal means with 95% confidence intervals predicted by linear mixed-effects models. Cohen's d is reported for significant results ($p < 0.05$).*

Estimates of synaptic inputs to motoneurons

For the muscle length condition, there was a significant interaction between group, muscle length, and muscle for brace height ($p = 0.0345$), although post hoc tests revealing no significant differences (all $p > 0.1342$). There was no interaction between group and muscle length, nor between group, muscle length, and muscle for acceleration ($p > 0.1820$), or attenuation ($p > 0.1693$) (Fig. 57). When considering ΔF, there was an interaction between group, muscle and muscle length ($p = 0.0097$). Specifically, there were no significant changes in the incomplete SCI group (all $p > 0.2965$), whereas the control group showed higher ΔF at short muscle length in the GM by 0.33 pps (95% CI: [0.019–0.64], $d = 0.36$, $p = 0.0388$) and lower ΔF at short muscle length in the SOL by 0.51 pps (95% CI: [0.026–1.0], $d = 0.56$, $p = 0.0400$). By contrast, when considering normalised ΔF, there was no significant interaction was found between group and muscle length ($p = 0.8854$), nor between group, muscle length, and muscle ($p = 0.0938$).

For the vibration condition, there was no interaction between group and vibration, nor between group, vibration, and muscle for brace height (all $p > 0.0584$), acceleration (all $p > 0.1322$), or attenuation (all $p > 0.2775$). When considering ΔF, there was an interaction between group, muscle and vibration ($p = 0.0004$). Specifically, there were no significant difference in the incomplete SCI group (all $p > 0.1881$), whereas the control group showed higher ΔF without than with vibration in the GM by 0.79 pps (95% CI: [0.062–1.53], $d = 0.86$, $p = 0.0005$), with no difference in the SOL ($p = 0.8545$). By contrast, when considering normalised ΔF, there was no significant interaction was found between group and vibration ($p = 0. 5309$), nor between group, vibration, and muscle ($p = 0.6477$).

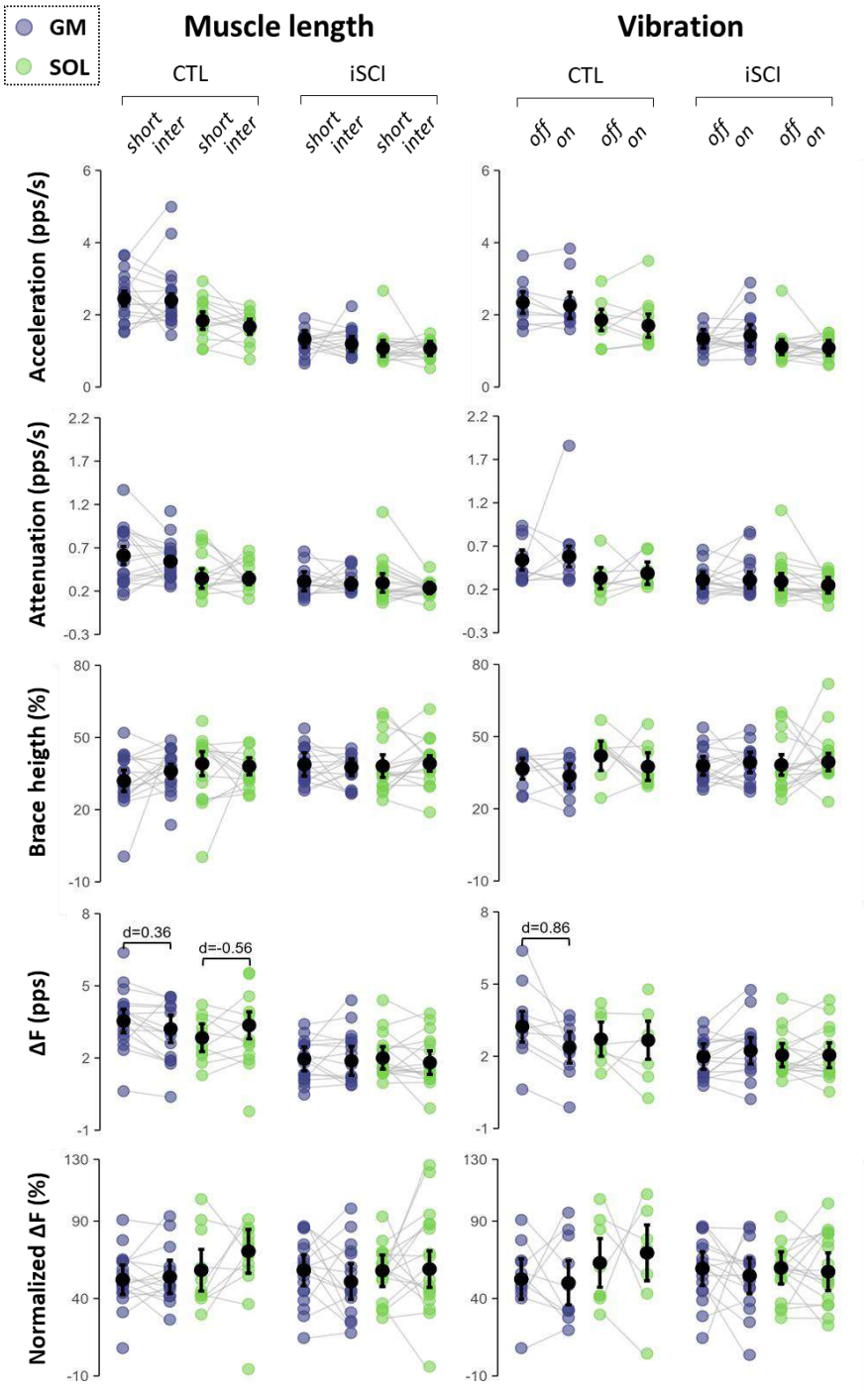

Figure 57. Effect of muscle length and vibration in estimates of synaptic inputs to motoneurons. *The modulation of motoneuron estimates of synaptic inputs to motoneurons between the incomplete SCI (iSCI) and control (CTL) groups are compared in response to changes in muscle length at the same relative torque (40% MVT), and the application of tendon vibration to antagonist muscles, at short muscle length (20° of plantarflexion). The acceleration slope, attenuation slope, brace height, ΔF, and normalised ΔF were obtained from the gastrocnemius medialis (GM, purple) and soleus (SOL, green). Coloured dots represent participant averages, while black dots and bars indicate the estimated marginal means with 95% confidence intervals predicted by linear mixed-effects models. Cohen's d is reported for significant results ($p < 0.05$).*

Results from supplementary analyses

First, because plantarflexion torque-generating capacity increases from short to intermediate muscle lengths, we included an additional contraction at an intermediate joint position (0°), matched to 40% MVT obtained at the short muscle length (20°), as presented in the supplemental materials (Annexe 2). This condition yielded results consistent with those of the relative torque-matched contractions (see supplemental material). Second, a subset of participants with sufficient ankle range of motion (SCI: n = 9; control: n = 10) performed contractions at a long muscle length (10° dorsiflexion). In the control group, this supplemental condition strengthened the previously described muscle length–dependent effects, with the longer muscle length inducing even greater changes than the intermediate length, compared with the short length. This was accompanied by a significant reduction in ΔF in the SOL and a reduction in acceleration in GM with increasing muscle length. Importantly, no significant modulation of rate coding or synaptic input metrics was observed in the incomplete SCI group with this supplemental condition. Finally, analyses restricted to the motoneurons successfully tracked across conditions yielded converging results (see supplemental material).

4. DISCUSSION

Based on non-invasive recordings of motoneurons innervating the GM and SOL muscles, this study demonstrates lower rate coding during voluntary contraction in individuals with incomplete SCI. Compared with control participants, these individuals exhibited lower firing rates at recruitment, lower firing rate modulation, and lower peak firing rates. This lower rate coding was associated with a shift in the inhibition-excitation balance toward greater inhibition, with no evidence of altered neuromodulatory input. In contrast to healthy participants, the rate coding of SCI individuals did not adapt to experimental conditions designed to modulate inhibitory input, including changes in muscle length and the application of vibration. Together, these findings suggest that motor impairment during voluntary contraction after incomplete SCI is associated with reduced rate coding caused by excessive inhibitory inputs.

Evidence of lower rate coding after incomplete SCI

We observed markedly reduced rate coding in individuals with incomplete SCI across two lower limb muscles, as reflected by lower firing rates at recruitment, reduced firing rate modulation, and lower peak firing rates. These deficits were consistently observed at both relative (40% MVT) and absolute (30 N.m) contraction levels, making it unlikely that they are attributable to differences in maximal force-generating capacity between groups. Specifically, contractions performed at the same absolute torque corresponded to an average relative torque of ~20% MVT in the control group but ~48% MVT in the SCI group, indicating that individuals with SCI exhibited reduced rate coding despite operating at substantially higher relative intensities. Although these findings contrast with some previous reports showing no change in rate coding after SCI in the triceps brachii (Wiegner et al., 1993), they are consistent with prior observations of lower motoneuron firing rates in the first dorsal interosseous, biceps brachii, and tibialis anterior muscles (Debenham et al., 2024; Kizyte et al., 2025; Thomas et al., 2014). These discrepancies across studies suggest that the present findings may not generalise to all muscles after SCI. However, despite substantial heterogeneity in aetiology, motor capacity, and medication use, individuals with incomplete SCI showed consistent differences compared with the control group, supporting the generalisability of our conclusion.

Inhibition-excitation balance contributes to the lower rate coding after incomplete SCI

To understand the mechanisms underlying the lower rate coding in individuals with SCI, we applied a recently developed geometric analysis of motoneuron firing patterns (Beauchamp et

al., 2023; Chardon et al., 2024) together with the classical paired motor units analysis (Gorassini et al., 2002), to assess the contribution of synaptic inputs. As described in the Methods section, these approaches enable the estimation of the level of neuromodulation (i.e., the level of PICs in motoneurons) using brace height, as well as PIC effects to motoneuron firing. Specifically, PICs lead to an initial amplification effect on firing, quantified by the acceleration slope, and a prolongation effect, quantified by ΔF (see Methods). Importantly, brace height reflects neuromodulation because it is independent of the level of inhibition, unlike the two other metrics. This distinction reflects the ability of inhibitory inputs to dampen the effects of neuromodulation on firing. Our result that brace height did not differ between groups suggests preserved neuromodulatory inputs in individuals with SCI. In contrast, both the acceleration slope and ΔF were consistently lower in the incomplete SCI group, irrespective of contraction intensity or muscle. Taken together, these findings suggest that PIC amplification and prolongation effects on motoneuron firing are reduced following incomplete SCI, despite preserved neuromodulatory input. Importantly, comparisons of PIC effects across motoneuron populations with different modulation of firing rate are inherently challenging, as ΔF depends on firing rate modulation of control motoneurons, which was lower in the incomplete SCI group. To address this limitation, ΔF values were normalised to the maximal ΔF values achievable relative to control unit modulation (Škarabot et al., 2025). After normalisation, group differences were no longer significantly different, except for the GM in the absolute comparison condition. A possible interpretation is that although PIC effects are lower in absolute terms after incomplete SCI, their relative contribution to motoneuron firing is preserved, supporting PICs as a continuing source of depolarising current after incomplete SCI. Of note, the normalisation procedure applied to ΔF likely makes it a more neuromodulation-specific indicator by removing the influence of inhibition on firing, similar to brace height (Beauchamp et al., 2023; Oya et al., 2009).

The geometric analysis of motoneuron firing patterns also allows us to estimate the balance between inhibitory and excitatory inputs (referred to as the pattern of inhibition) through the attenuation slope (Beauchamp et al., 2023; Chardon et al., 2024). Attenuation slopes were lower in the incomplete SCI group for both GM and SOL at 40% MVT, suggesting an altered inhibitory pattern, characterised by a greater inhibitory influence. The pattern of inhibition can range from a strong positive covariation between excitation and inhibition (proportional pattern) to a strong negative covariation (push-pull pattern). The push-pull pattern has been proposed as a mechanism by which the central nervous system increases the input-output gain of motoneurons by raising background inhibition followed by disinhibition to increase force production

(Johnson et al., 2012). This pattern is supported by spinal circuits, such as the organisation of Ia afferents and Ia inhibitory interneurons (Johnson et al., 2012), and aligns with firing patterns observed in healthy humans (Chardon et al., 2024). A push-pull pattern is required to attain high firing rates during high-force contractions (Škarabot et al., 2025) and is more pronounced in trained than in untrained individuals (Škarabot et al., 2026). The lower attenuation slope observed in the incomplete SCI group is consistent with the behaviour predicted by simulations assuming a more proportional inhibitory-excitatory pattern (Chardon et al., 2024). Accordingly, a reduced capacity to regulate inhibition during increasing force production likely contributes to altered motoneuron rate coding. Furthermore, the absence of firing rate modulation in response to experimental manipulations of inhibitory input, achieved through changes in muscle length or the application of vibration, suggests that individuals with incomplete SCI may already operate under elevated inhibition during voluntary contractions, consistent with a more proportional inhibitory-excitatory pattern. One possible mechanism underlying this elevated inhibition is impaired regulation of recurrent inhibition, resulting in increased inhibition concomitant with increasing excitation. In healthy individuals, descending control modulates the activity of Renshaw cells during voluntary contraction. However, this control is often disrupted after upper motor neuron lesions (Katz & Pierrot-Deseilligny, 1982), as a result of decreased supraspinal inhibitory control (Jankowska, 1992). This interpretation is further supported by previous evidence of enhanced recurrent inhibition following incomplete SCI (Shefner et al., 1992).

Lack of motoneuron behaviour adaptation to experimental manipulation of inhibitory inputs

We examined the adaptation of motoneurons by experimentally manipulating inhibitory inputs, through changes in muscle length via joint position and by applying vibration to the tendons of the antagonist muscles during submaximal voluntary contractions. Specifically, increased muscle length was used to notably elicit recurrent inhibition (Colard et al., 2025), whereas antagonist tendon vibration was used to generate reciprocal inhibition through Ia inhibitory interneurons (Burke et al., 1976). As expected, the control group exhibited reduced firing rates at longer muscle lengths and during tendon vibration, accompanied by a reduction in the PIC prolongation effect, especially in the GM. These results largely align with previous work on the effects of muscle length (Beauchamp et al., 2025; Goreau et al., 2025; Valenčič et al., 2026) and antagonist tendon vibration (Mesquita et al., 2022; Pearcey et al., 2022) and are likely explained by

the dampening effect of synaptic inhibition on motoneuron PICs (Bui et al., 2008; Kuo et al., 2003)

In contrast to the control group, the incomplete SCI group showed no change in rate coding in response to changes in muscle length or vibration. One possible explanation for this lack of modulation is that the tested paradigms did not further increase the level of inhibitory inputs in SCI participants, likely because inhibitory interneurons operate near their maximal activity even at very low contraction intensities during voluntary contraction. This is consistent with the high level of inhibition associated with the more proportional inhibitory–excitatory pattern, as described above. Alternatively, the experimental paradigms employed may not have sufficiently activated inhibitory interneurons to further enhance inhibitory inputs. Indeed, reciprocal inhibition is replaced by facilitation after SCI (Crone, 2003; Knikou & Mummidisetty, 2011), and the modulation of recurrent inhibition with muscle length is likely dependent on descending control (Colard et al., 2025), which is altered after SCI (Katz & Pierrot-Deseilligny, 1982; Shefner et al., 1992). Other potential mechanisms that could have limited an increase in inhibitory inputs include the loss of monoaminergic inputs that regulate Ia inhibitory interneurons (Hammar & Jankowska, 2003; Jankowska et al., 2000), as well as a downregulation of KCC2, which increases inhibitory input strength and is reduced after SCI (Boulenguez et al., 2010). Regardless of the underlying mechanisms, these findings highlight the limited capacity of individuals with SCI to adapt the motor command via inhibitory inputs.

Of note, our findings of increased inhibition during voluntary contraction stand in clear contrast to the mechanisms underlying muscle spasms at rest after SCI, which are characterised by reduced synaptic inhibition and increased PICs (Gorassini, 2004; Mahrous et al., 2024). An impaired capacity to regulate inhibition according to task demands (e.g., maintaining muscle relaxation or increasing muscle contraction) may explain this discrepancy and is consistent with our findings of a limited capacity in individuals with SCI to adapt the motor command via inhibitory inputs.

Reduced rate coding is compensated by the recruitment of a greater number of motor units after incomplete SCI

Despite exhibiting lower rate coding than control participants, individuals with incomplete SCI were able to produce the same absolute torque (30 N.m). The lower firing rate observed in the incomplete SCI group must therefore have been compensated by the recruitment of larger motor

units and/or a greater number of motor units. Due to limitations of EMG decomposition in reliably assessing recruitment, we cannot directly determine the compensatory strategies employed. Assuming similar spatial sampling of motor units and comparable volume conductor effects across populations, we used MUAP amplitude as a proxy for motor unit size. We found no between-group differences at 30 N.m, suggesting that individuals with incomplete SCI compensated for their lower rate coding primarily through the recruitment of additional motor units, which is further supported the observation of higher EMG amplitudes in the SCI group (Fig. 52C). This interpretation is consistent with studies showing that motoneurons are recruited up to higher force levels in individuals with SCI than in controls (Thomas et al., 1997; Zijdewind & Thomas, 2003). Importantly, this interpretation is based on indirect measures and unverifiable assumptions; and further work is needed to confirm a greater reliance on recruitment in individuals with incomplete SCI.

Implications for motor impairments related to incomplete SCI

Our results showing that individuals with incomplete SCI operate under elevated inhibitory inputs during voluntary contraction may help explain paresis. Indeed, compensating for this inhibition would require a disproportionate increase in excitatory input to further raise motoneuron output. Given that excitatory descending inputs are already compromised after SCI, this compensatory capacity is likely limited. Consequently, excitatory drive may reach saturation at relatively low force levels, thereby constraining maximal torque production through reduced voluntary activation (H. E. Kim et al., 2015).

In addition, unlike the control group, the incomplete SCI group showed no change in rate coding in response to changes in muscle length. This adaptive pattern in healthy individuals may represent a mechanism that adjusts neural drive to the diminished muscle force-generating capacity at shorter lengths (Goreau et al., 2025). Conversely, the failure to adapt rate coding after incomplete SCI may lead to muscle length-dependent paresis. While this phenomenon has not been directly quantified after SCI, it is consistent with the concept of spastic paresis syndrome, common to central nervous system disorders (Baude et al., 2019; J.-M. Gracies, 2005b), and observed, for example, after stroke (Vinti et al., 2015). In line with this, incomplete SCI is associated with reduced central activation (i.e., paresis), which is more pronounced during shortening contractions (H. E. Kim et al., 2015).

Finally, compensation for reduced rate coding through the recruitment of a greater number of motor units after incomplete SCI implies increased use of high-threshold motor units, including fast fatigable units. This likely contributes to the increased fatigability observed after incomplete SCI (Thomas & Del Valle, 2001).

Conclusion

This study provides the first evidence in humans that voluntary motor deficits after incomplete SCI may be associated with a disrupted balance between inhibitory and excitatory synaptic inputs to motoneurons. During voluntary contractions, individuals with SCI show a limited capacity to modulate inhibitory inputs, resulting in reduced spinal motoneuron rate coding. These findings support excessive inhibition as a key neural mechanism contributing to muscle weakness and impaired motor function after incomplete SCI. Clarifying the mechanisms responsible for this excessive inhibition represents a critical next step, as it constitutes a promising therapeutic target for restoring force-generating capacity after incomplete SCI.

◥ STUDY 3: REDUCED MOTONEURON RATE CODING AFTER STROKE IS ASSOCIATED WITH INCREASED INHIBITORY INPUTS DESPITE INCREASED NEUROMODULATORY INPUTS

KEY POINTS

- Stroke induces muscle weakness, in part by impairing motoneuron rate coding, yet the synaptic mechanisms underlying this dysfunction remain poorly understood in humans.
- By analysing large motoneunon populations from triceps surae muscles, we estimated the relative contributions of excitatory, inhibitory, and neuromodulatory inputs to motoneuron rate coding in chronic stroke.
- We provide evidence that individuals with chronic stroke show a disrupted inhibitory–excitatory balance shifted towards greater inhibition but higher level of estimated neuromodulatory input.
- Experimental conditions designed to modulate inhibition altered motoneuron firing in controls but not in individuals with chronic stroke.
- Together, these results indicate that increased inhibition during voluntary contraction likely contributes to impaired rate coding and muscle weakness in chronic stroke despite a potential upregulation of neuromodulatory inputs as a compensation attempt.

ABSTRACT

Stroke disrupts voluntary movement, in part through motoneuron dysfunction, yet the mechanisms underlying this dysfunction remain poorly understood. Using a non-invasive approach to decode the spiking activity of large populations of spinal motoneurons, we quantified the relative contributions of excitatory, inhibitory, and neuromodulatory inputs to motoneuron rate coding after chronic stroke. Eighteen participants with chronic stroke and 18 age- and sex-matched control participants performed submaximal isometric plantar flexion tasks while high-density surface electromyography was recorded from the soleus and gastrocnemius medialis muscles. Motoneuron firing behaviour was analysed to estimate the inhibitory-excitatory balance and the neuromodulatory level. Participants with chronic stroke exhibited lower rate coding compared with controls. Estimates of synaptic inputs to motoneurons revealed a shift in the inhibition-excitation balance toward greater inhibition and a higher level of neuromodulatory input in the stroke group compared to the control group. Furthermore, increasing inhibitory input through muscle length changes and antagonist tendon vibration modulated motoneuron firing in controls, but not in individuals with chronic stroke. Together, these findings suggest that motor impairment during voluntary contraction in chronic stroke is associated with reduced motoneuron rate coding caused by excessive and poorly adaptable inhibitory inputs, despite increased

neuromodulatory inputs that may correspond to a reorganisation limiting the reduction in rate coding capacity.

1. INTRODUCTION

Stroke induces persistent deficits in voluntary movements, including muscle weakness and impaired force control (Xu et al., 2017). These deficits likely reflect not only damage to descending pathways but also disorganization of the neural commands at the spinal cord level. Because motoneurons are the final level at which neural motor command is integrated into motor output (Heckman & Enoka, 2012), understanding post-stroke motor impairment therefore requires examining how stroke reshapes the synaptic inputs integrated by the motoneuron pool.

In chronic stroke individuals, the normal behaviour of spinal motoneurons is disrupted. Motoneurons are recruited at lower levels of absolute force and possibly with a compressed recruitment range (Gemperline et al., 1995; Hu et al., 2015). Once recruited, motoneuron discharge often fails to scale with increasing force, resulting in lower firing rates, reduced rates of modulation, and sometimes even negative rate modulation (Beauchamp et al., 2023; Chou et al., 2013; Gemperline et al., 1995; Hu et al., 2015; Mottram et al., 2014). The mechanisms producing this altered motoneuron output remain unclear but likely involve changes in the structure of synaptic inputs reaching the motoneuron pool.

Motoneuron rate coding depends on excitatory inputs, which provide the primary source of depolarising current, but also on inhibitory and neuromodulatory inputs, which modify the input–output relationship between excitation and firing rate. Inhibitory inputs can induce changes in the motoneuron input–output relationship through distinct patterns of inhibition. One such pattern is the push–pull organisation, in which a decrease in synaptic inhibition occurs in parallel with increased synaptic excitation, thereby supporting higher rate coding (Johnson et al., 2012; Powers & Heckman, 2017; Škarabot et al., 2025). Neuromodulatory inputs, primarily arising from monoaminergic projections from brainstem nuclei onto motoneurons, contribute to motoneuron rate coding by increasing intrinsic motoneuron excitability through activation of PICs. These currents amplify and prolong the effects of synaptic excitation in motoneurons (Hultborn et al., 2003; Y. Li & Bennett, 2003; Schwindt & Crill, 1980).

Accordingly, mechanisms of altered rate coding could be underpinned by reorganisation of motoneuron synaptic inputs. Regarding neuromodulatory inputs, upregulation of the reticulospinal tract may increase the descending monoaminergic drive onto motoneurons, thus partially

compensating for reduced motoneuron excitability. Regarding inhibitory inputs, reorganisation of descending projections leads to an upregulation of the corticoreticulospinal tract (Jang & Cho, 2022; Zaaimi et al., 2012), which may induce reduced excitatory drive (Baker, 2011), along with upregulation of inhibitory inputs (Mazzocchio, 1997; Pompeiano, 1988). Supporting these hypotheses, a more higher neuromodulatory level and a more proportional pattern of inhibition (i.e., concurrent increase of excitatory and inhibitory inputs) have been estimated in the paretic biceps brachii compared to the contralateral side (Beauchamp et al., 2023). However, the synaptic input organisation of motoneurons during voluntary contraction remains poorly known, especially in lower limb muscles. It is also unknown whether inhibitory inputs remain adaptable in chronic stroke, although such adaptations occur physiologically, notably during changes in muscle length and antagonist vibration (Beauchamp et al., 2025; Goreau et al., 2025; Mesquita et al., 2022; Pearcey et al., 2022; Valenčič et al., 2026).

In this human study, we aimed to determine how synaptic inputs shape motoneuron rate coding in individuals after stroke. To this end, we identified large populations of motoneurons by decomposing high-density EMG signals collected during plantar flexor submaximal isometric contractions. We compared the contribution of inhibitory and neuromodulatory inputs to plantar flexor motoneuron firing in individuals with chronic stroke compared with healthy controls. We used a framework that relates specific motoneuron discharge features to underlying synaptic inputs (Beauchamp et al., 2023; Chardon et al., 2024). To further probe the role of inhibitory inputs in shaping motoneuron firing, we manipulated muscle length and applied antagonist tendon vibration, two interventions known to modulate inhibitory input in healthy individuals (Beauchamp et al., 2025; Goreau et al., 2025; Mesquita et al., 2022; Pearcey et al., 2022; Valenčič et al., 2026). Thus, beyond characterising motoneuron firing behaviour, this study provides insights into how the synaptic inputs to motoneurons are reorganised after stroke.

2. METHODS

Participants and ethical approval

Eighteen individuals with post stroke weakness in plantar flexion, corresponding to a MRC score between 2/5 and 4/5 (mean ± SD: 52 ± 7 years, 171 ± 9 cm, 73 ± 12 kg, three women, Table 4) and 18 control participants (50 ± 20 years, 178 ± 8 cm, 74 ± 14 kg, two women) participated in the study. All participants provided written informed consent, and the experimental procedures were approved by the local ethics committee (CERNI, Nantes Université,

IRB: IORG0011023). Participants with stroke had sustained their injury at least five months before enrollment. Twelve participants had an ischaemic aetiology. Four participants with stroke were taking anti-spastic medication (diazepam or dantrolene or alprazolam or gabapentin), and five were taking serotonergic medication (sertraline or escitalopram) at the time of enrollment. Spasticity was assessed using the modified Tardieu scale. Participants with stroke were required to have had no orthopedic or neurosurgical intervention within the previous three months and no intramuscular injections of botulinum toxin in the plantar flexors during the same period. Control participants were required to have had no lower limb injuries in the previous six months. All participants were instructed not to consume caffeine the day of the evaluation. For individuals with stroke, the tested leg was the one with the lower maximal voluntary plantar flexion torque. As a result, in the stroke group, 9 of 18 participants were tested on their dominant leg (defined as the leg used to kick a ball), compared with 9 of 18 in the control group.

The maximal voluntary torque (MVT) of the plantar flexors in the stroke group was 43.4 ± 28.3 N.m when the muscle was placed at a short length and 67.8 ± 43.6 N.m at an intermediate length (Fig. 58A). In the control group, MVTs were 104.1 ± 33.7 N.m and 145.5 ± 49.6 N.m in the short and intermediate lengths, respectively.

Table 4. Characteristics of individuals with chronic stroke

Participant	age	sex	Side assessment	delay	Aetiology	Location	antispastic medication	serotoninergic medication	Torque at 0° (N.m)	MTS knee flexed	MTS straight knee
1	61	M	ND	25	I	MCA	none	SER	29	2	2
2	41	M	D	2	H	ACA	none	none	34	2	2
3	49	M	ND	1.5	H	ACA	none	none	87	2	2
4	64	M	D	2	H	IC	none	none	21	2	2
5	65	F	D	9	I	MCA	none	none	49	2	2
6	36	M	ND	0.75	H	MCA	none	SER	107	2	3
7	73	M	D	10	I	MCA	none	none	39	1	1
8	53	M	ND	0.4	I	MCA	none	none	128	2	2
9	62	M	ND	2	H	ACA	none	none	169	0	2
10	32	M	ND	3	I	MCA	DIA	SER	94	4	4
11	61	M	ND	14	H	IC	none	SER	25	2	2
12	74	M	D	14	I	MCA	none	none	33	2	2
13	64	M	D	2	I	MCA	none	none	24	2	3
14	50	F	D	0.5	I	MCA	DAN	none	23	2	2
15	19	M	D	9	I	MCA	none	none	117	4	4
16	21	M	ND	1	I	MCA	none	none	83	3	3
17	57	F	ND	2	I	MCA	ALP	ESC	77	2	2
18	65	M	D	1	I	ACA	GAB	none	82	2	2

M, male; F, female, D, dominant; non dominant; MCA, middle cerebral artery; ACA, anterior cerebral artery; IC, internal capsule; H, haemorrhagic; I, ischaemic; DIA, diazepam; DAN, dantrolen; ALP, alpazolam; GAB, gabapentin; SER, sertraline; ESC, escitalopram; MTS, Modified Tardieu Scale.

Experimental protocol

After the warm-up and MVT assessments, participants performed several isometric submaximal triangular contractions, each consisting of 12-second ascending and descending phases. To compare motoneuron behaviour between groups while accounting for large differences in MVT, participants performed a contraction at both a similar relative torque (40% of their MVT) and a similar absolute torque (30 N.m), all performed in the neutral ankle position (0°).

To assess how motoneuron behaviour adapts to muscle length, participants also performed a contraction at a shorter muscle length (20° of plantarflexion), at 40% of their MVT in this position (Fig 58B). For clarity, these positions are described based on the length of the plantar flexor muscles: the short muscle length position at 20° of plantarflexion and the intermediate muscle length position at 0°. These two joint positions have been shown to induce measurable differences in fascicle length of gastrocnemius medialis (GM) and soleus (SOL) (Colard et al., 2025; Kuzyk et al., 2018). From the short to the intermediate position, plantarflexion torque-generating capacity increases, requiring less muscle activation to produce the same absolute

torque (Hoffman et al., 2012). To account for the relationship between maximal torque and joint angle (Fig. 58A), we compared contractions at similar relative torque across positions to match effort (Relative torque contractions). Furthermore, to separate the effects of muscle length and muscle tension, participants also performed contractions at similar absolute torques across positions (Absolute torque contractions). For the Relative torque contractions, participants performed contractions up to 40% MVT at each position. Because MVT increases with muscle length, the torque of submaximal target contractions also increased with muscle length. For the Absolute torque contractions, torque was constant across positions and was set to match the torque used at the short muscle length during the Relative torque contractions (Fig. 58B). Notably, when participants were able to reach 10° dorsiflexion, they performed an additional contraction at this position using the same torque as at the short muscle length.

To assess how reciprocal inhibition affects motoneuron behaviour, vibration was applied to the tendons of the antagonist muscles during contractions in both positions (for the contractions at 40% of their MVT). High-frequency vibration (115 Hz; Vibrasens, Technoconcept, Saint-Maurice, France) was applied to the distal tibialis anterior (TA) tendon during plantarflexion contractions by manually pressing the vibrator to the tendon with a force of 15 ± 2 N. Vibration started 10 s before the onset of the triangular contraction and continued until after the torque returned to baseline, ensuring that the entire contraction was covered.

After a familiarisation period for the first condition, participants completed one contraction per condition in randomised order, resulting in a total of five submaximal contractions. At least one minute of rest was provided between contractions to minimise fatigue and the warm-up effect of PICs (Bennett et al., 1998).

Electromyography

To obtain information on muscle activation (Fig 58C), we reproduced a bipolar configuration by averaging two groups of 25 channels located at the extremities of each grid and then computing the difference between these averages, yielding a single value per grid. The values from the two grids were subsequently averaged to obtain a single value per muscle. The EMG amplitude was analysed as a normalised root mean square over a 300 ms window, by normalising RMS values to the RMS value of the same electrode during the maximal voluntary contraction (EMGmax).

Statistical analyses

To assess differences in motoneuron firing characteristics between groups during contractions at 40% MVT and 30 N.m performed at an intermediate muscle length, we applied a linear mixed-effects model to each motoneuron firing metric (i.e., recruitment threshold, firing rate at recruitment, peak firing rate, firing rate modulation, ΔF, normalised ΔF, brace height, acceleration, attenuation and MUAP amplitude). The models included the group (stroke, control), muscle (gastrocnemius medialis, soleus) and their interactions as fixed effects. The full random-effects structure consisted of a random intercept for each participant and random slopes to account for between participants variability in the fixed effects [e.g., lmer(metric ~ group*muscle + (group*muscle|id_participant))]. For each model, the random-effects structure was selected by minimising the bayesian information criterion across all plausible random-slope structures. The random slope for the primary effect of interest (group) was always retained, as it represents the key source of between-participant variability for the tested condition.

To test the effects of position and vibration, separate models were fitted including the effect of interest (position: short, intermediate; or vibration: on, off), together with muscle (gastrocnemius medialis, soleus), group (incomplete SCI, control), and their interactions as fixed effects. The random-effects structure was selected using the same procedure; however, in these models the retained random slope corresponded to the effect of interest (position or vibration), rather than group.

To compare TA coactivation between groups, we compared TA EMG amplitude during the similar relative torque contraction at the intermediate muscle length (shown in Fig. 58C) using a t-test. We considered the EMG normalised to the maximal value obtained during the maximal dorsiflexion contraction.

All analyses were performed in R (v.4.4.0; R Core Team 2021, R Foundation for Statistical Computing, Vienna, Austria). Statistical significance was assessed using the lmerTest package in R (Kuznetsova et al., 2017), which uses Satterthwaite's type III method to approximate degrees of freedom and generate p-values for mixed effects models. Model assumptions of homoscedasticity, normality, and independence of residuals were verified graphically. When significant effects were detected, Sidak post-hoc corrections were applied. Estimated marginal mean differences with 95% confidence intervals and standardised effect sizes (Cohen's d) were calculated using the emmeans package. The alpha level for all statistical tests was set at 0.05.

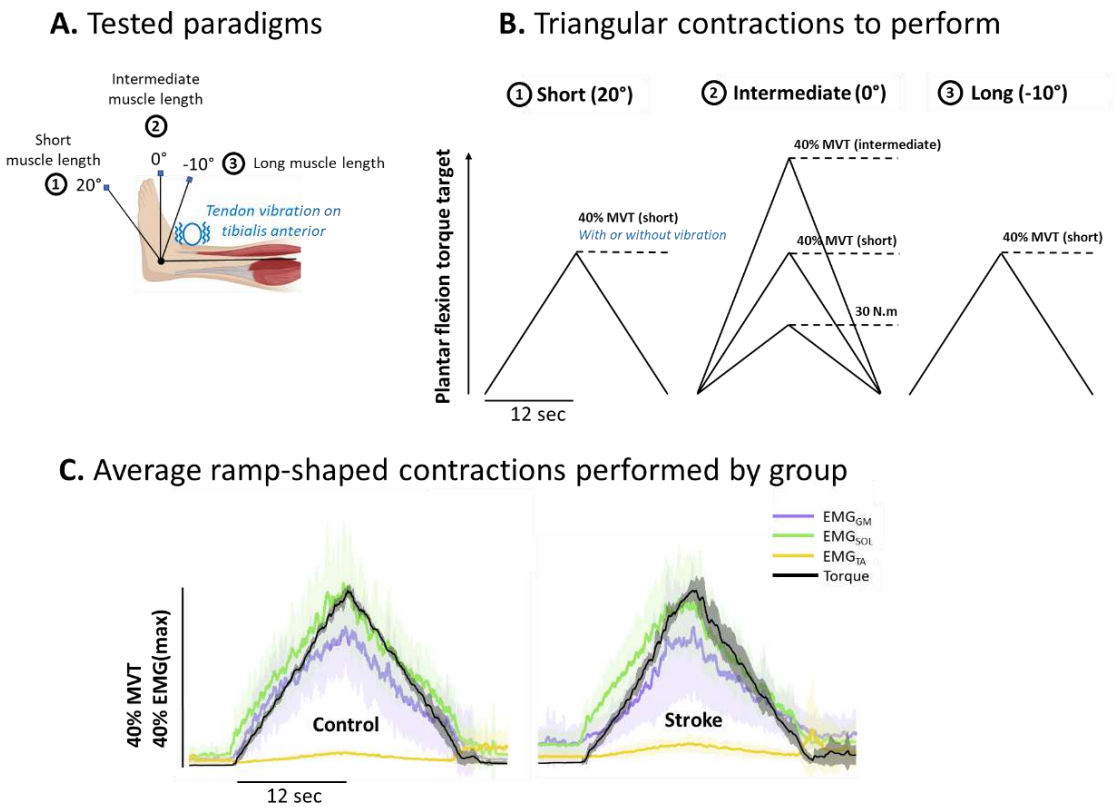

Figure 58. Experimental setup. *A, participants performed isometric submaximal plantarflexions at three ankle positions, corresponding to different plantar flexor lengths: 20° (short muscle length position), 0° (intermediate muscle length position) and 10° of dorsiflexion (-10°, long muscle length position). Tendon vibrations was applied to the antagonist muscles (i.e., dorsiflexor muscles) during contractions to induce reciprocal inhibition, at the short position. B, the submaximal plantarflexions were performed to 40% of the maximal voluntary contraction torque (MVT) at each position or at the same absolute torque in each position, corresponding to 40% of the MVT in the short muscle length position. In addition, a plantarflexion to 30 N.m was performed to compare groups on the same absolute torque. C, mean (thick line) and standard deviations (clear outline) of torque and normalised EMG amplitude of gastrocnemius medialis (GM), soleus (SOL) and tibialis anterior (TA), in the control and the stroke groups, during the contraction up to 40% MVT in intermediate position.*

3. RESULTS

Motoneuron yield and TA coactivation

In the stroke group, an average of 6.4 ± 6.0 motoneurons for the GM and 7.3 ± 5.7 motoneurons for the SOL were identified per contraction and participant. In the control group, an average of 13.5 ± 7.8 motoneurons for the GM and 8.2 ± 6.1 motoneurons for the SOL were identified per contraction and participant. TA coactivation during triangular contractions did not differ between groups when assessed using normalised EMG amplitude (control vs. stroke: 2.80 ± 4.07 % vs. 3.42 ± 1.68 % of EMGmax, p = 0.6336).

Differences between groups at intermediate muscle length (0°)

Recruitment threshold, rate coding and motor unit action potential amplitude

An example of a smoothed motoneuron firing rate from a single contraction in one control and one stroke participant (#10) is shown in Figure 59. For the 40% MVT contractions, there was no significant between-group difference in recruitment threshold (p = 0.8651), nor interaction between group and muscle (p = 0.2023). There was a significant interaction between group and muscle for both firing rate at recruitment (p = 0.0154) and peak firing rate (p = 0.0080). Specifically, in the GM, the stroke group exhibited lower firing rate at recruitment (-1.45 pps, 95% CI: [0.31–2.60], d = 1.05, p = 0.0147) and lower peak firing rate (-3.93 pps, 95% CI: [1.91–5.96], d = 2.77, p = 0.0004) than the control group (Fig. 60). No significant group differences were observed in firing rate at recruitment or peak firing rate in the SOL (all p > 0.1615). For firing rate modulation, there was no significant interaction between group and muscle (p = 0.0828) but a main effect of group was observed, with lower firing rate modulation in the stroke group (d = 1.20, p < 0.0001). When considering the 30 N.m contractions, no significant group differences were observed in motoneuron recruitment threshold or firing rate characteristics (all p > 0.1325).

For the 40% MVT contractions, there was no significant interaction between group and muscle (p = 0.0648), but a main effect of group was observed for MUAP amplitude, with lower values in the stroke group (d = 0.68, p = 0.0041) than in the control group. When considering the 30 N.m contractions, no significant between-group differences were observed (p = 0.2782), nor was there interaction between group and muscle (p = 0.2765).

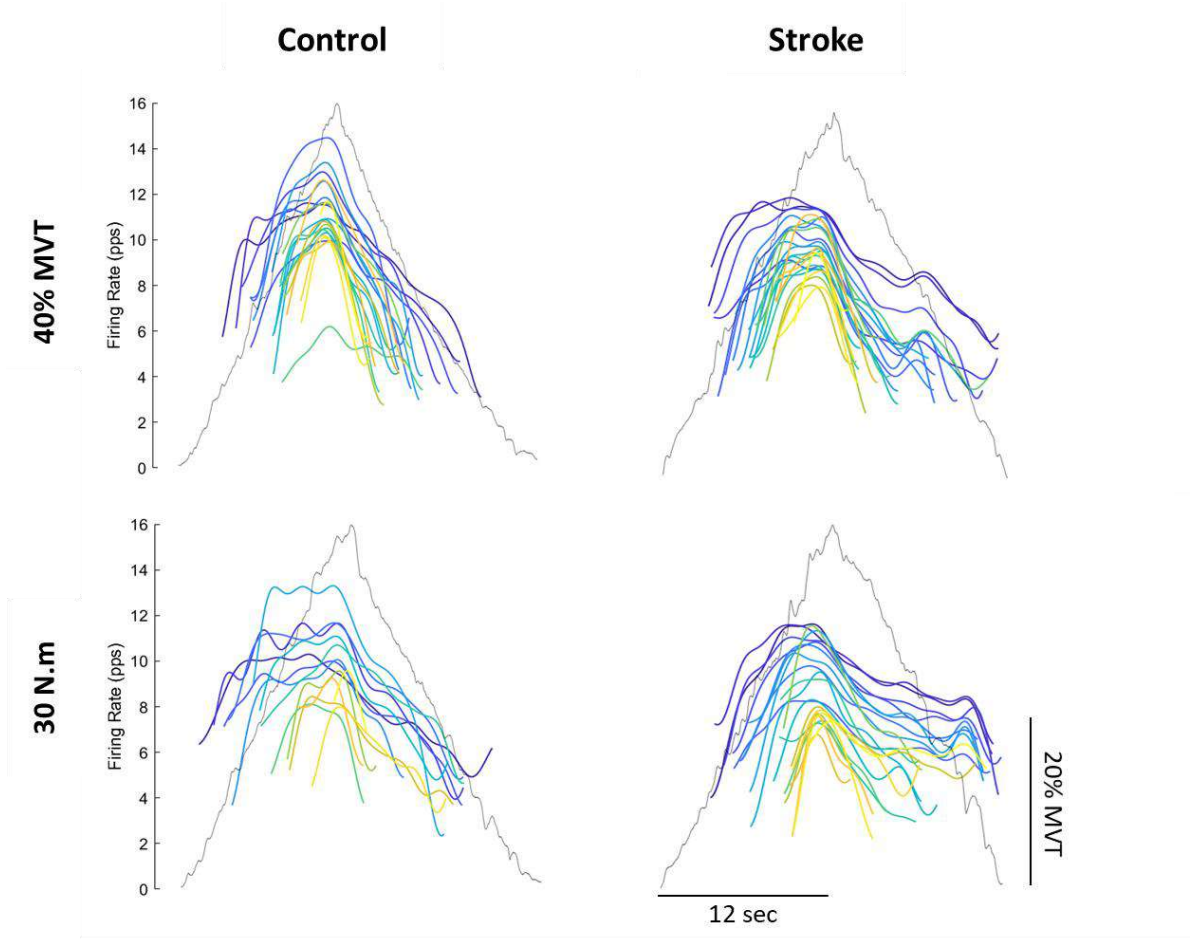

Figure 59. Typical motoneuron firing rates in control and stroke participants. *Plantarflexion torque (grey trace) and smoothed firing rates of 20 identified motoneurons (coloured traces) are shown for a control participant (left) and an individual with stroke (#10, right). Within each plot, smoothed firing rates are shown with darker colours (purple) for lower threshold neurons and lighter colours (yellow) for higher threshold neurons.*

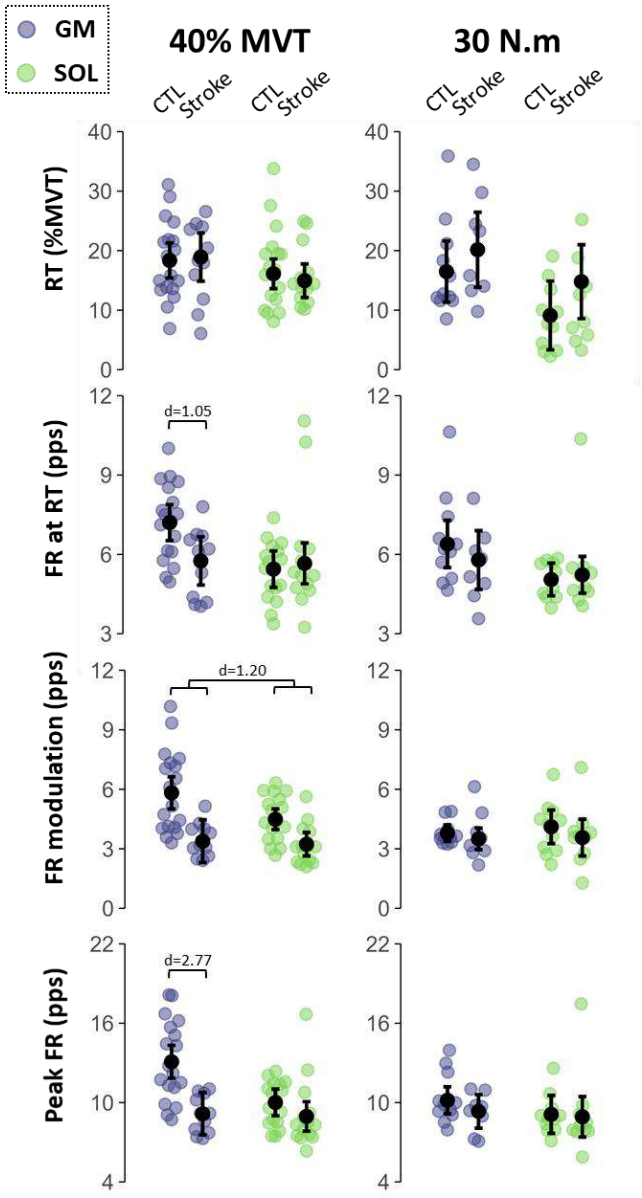

Figure 60. Motoneuron recruitment thresholds and rate coding. *The stroke and control (CTL) groups are compared at either the same relative torque (40% MVT) or the same absolute torque (30 N.m). Recruitment threshold (RT), firing rate at recruitment (DR RT), firing rate modulation (FR modulation), and peak firing rate (max DR), were obtained from the gastrocnemius medialis (GM, purple) and soleus (SOL, green). Coloured dots represent participant averages, while black dots and bars indicate the estimated marginal means with 95% confidence intervals predicted by linear mixed-effects models. Cohen's d is reported for significant differences.*

Estimates of synaptic inputs to motoneurons

For the 40% MVT contractions, there was no significant interaction between group and muscle for any metric (all $p > 0.2583$). There were significant main effects of group, with lower values in the stroke group compared to the control group for acceleration ($d = 0.71$, $p = 0.0083$) and

attenuation from both geometric (d = 0.99, p = 0.0007) and bilinear (d = 1.39, p = 0.0074) approaches. For brace height, there was significant main effect of group, with higher values in the stroke group compared to the control group (d = 0.68, p = 0.0054). Conversely, there were no significant group differences for ΔF (all p > 0.2462) and normalised ΔF (all p > 0.2756). No main effect or interaction was found for any of these metrics when considering the 30 N.m contractions (all p > 0.0712).

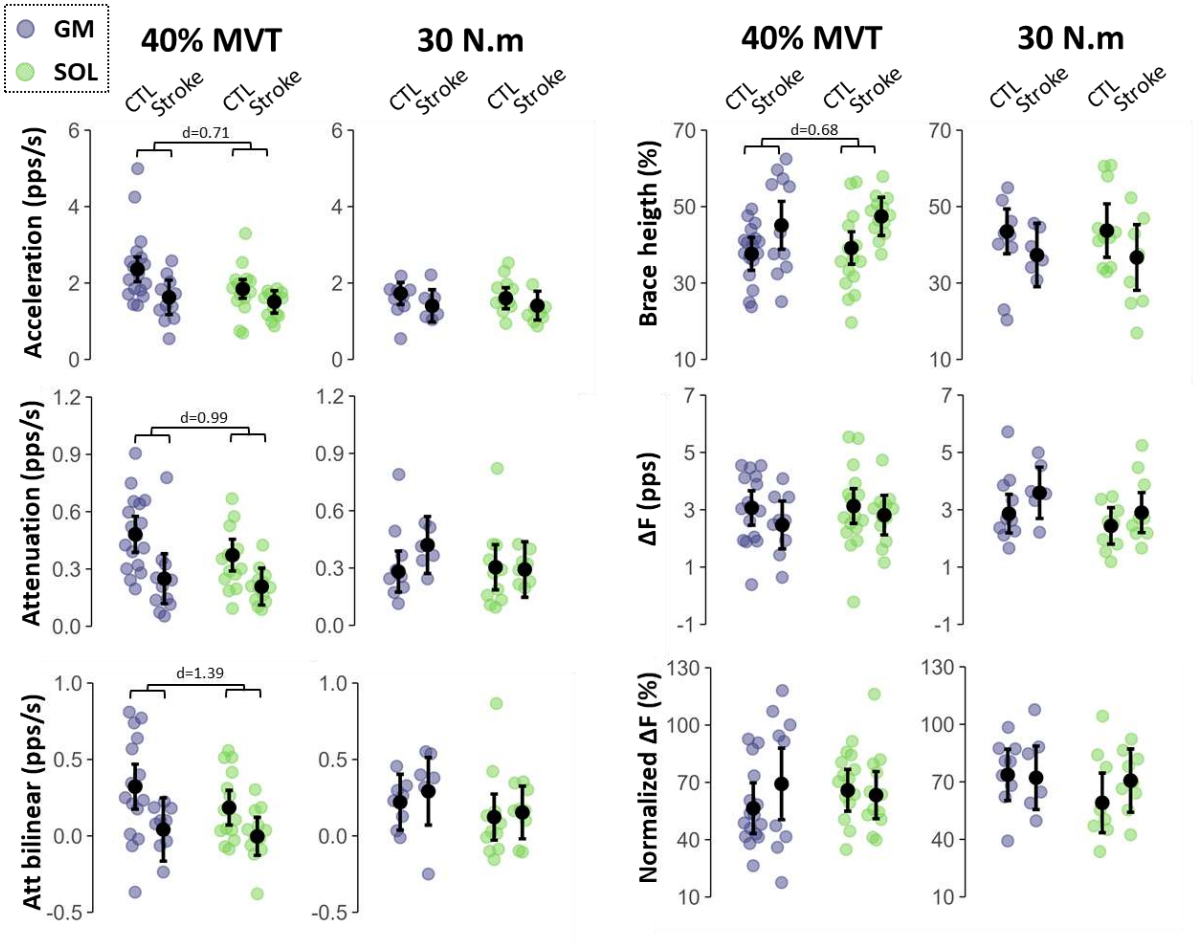

Figure 61. Estimates of synaptic inputs to motoneurons*. The stroke and control (CTL) groups are compared at either the same relative torque (40% MVT) or the same absolute torque (30 N.m). The acceleration slope, attenuation slope calculated from the geometric and bilinear (att bilinear) approaches, brace height, ΔF, and normalised ΔF were obtained from the gastrocnemius medialis (GM, purple) and soleus (SOL, green). Coloured dots represent participant averages, while black dots and bars indicate the estimated marginal means with 95% confidence intervals predicted by linear mixed-effects models. Cohen's d is reported for significant results.*

Modulation of motoneuron behaviour in response to change in muscle length and vibration

Recruitment threshold and rate coding

For the following results, the effects of interest are those involving interactions between group and condition (muscle length or vibration), including both group-condition interactions and group-condition-muscle interactions.

When considering the muscle length condition at similar relative torque between positions, there was an interaction between group, muscle and muscle length for the recruitment threshold ($p = 0.0377$), with a recruitment threshold 3.9 %MVC (95% CI: [1.6–6.1], $d = 0.43$, $p = 0.0009$) higher in intermediate than at short muscle length for the SOL in the control group (Fig. 62). There were no significant interactions involving group for firing rate at recruitment (all $p > 0.4587$), firing rate modulation (all $p > 0.0840$), or peak firing rate ($p > 0.0517$).

When considering the muscle length condition at similar absolute torque between positions, there was an interaction between group, muscle and muscle length for the recruitment threshold ($p = 0.0016$), with a recruitment occuring 1.4 s earlier (95% CI: [0.3–2.4], $d = 0.48$, $p = 0.7556$) at short compared with long muscle length for the GM in the control group; and 1.6 s later (95% CI: [0.4–2.7], $d = 0.55$, $p = 0.0057$) at short compared with long muscle length for the SOL in the control group. There were no significant interactions involving group for firing rate at recruitment (all $p > 0.2805$). For firing rate modulation, there was a significant interaction between muscle length, group and muscle ($p = 0.0420$). Specifically, for the GM, there were higher values at short than at intermediate (+1.01 pps; 95% CI: [0.22–1.81], $d = 0.64$, $p = 0.0103$) and long muscle length (+2.42 pps; 95% CI: [1.22–3.63], $d = 1.52$, $p = 0.0001$), and higher values at intermediate than at long muscle length (+1.41 pps; 95% CI: [0.38–2.43], $d = 0.88$, $p = 0.0064$), in the control group. There was also higher rate modulation at short compared to intermediate muscle length in the stroke group (+1.22 pps; 95% CI: [0.05–2.38], $d = 0.76$, $p = 0.0393$). When considering peak firing rate, there was a significant interaction between muscle length and group ($p = 0.0091$), with values higher at short than at intermediate ($d = 1.04$; $p = 0.0001$) and long muscle length ($d = 1.66$; $p < 0.0001$), and higher at intermediate than at long muscle length, in the control group ($d = 0.62$; $p = 0.0043$). Thus, rate coding substantially decreased at longer muscle length in the control group, whereas the stroke group displayed only limited modulation.

When considering the vibration, there were no significant interactions involving group for recruitment threshold (all $p > 0.6571$), firing rate at recruitment (all $p > 0.3868$), firing rate modulation (all $p > 0.5313$), or peak firing rate ($p > 0.2240$).

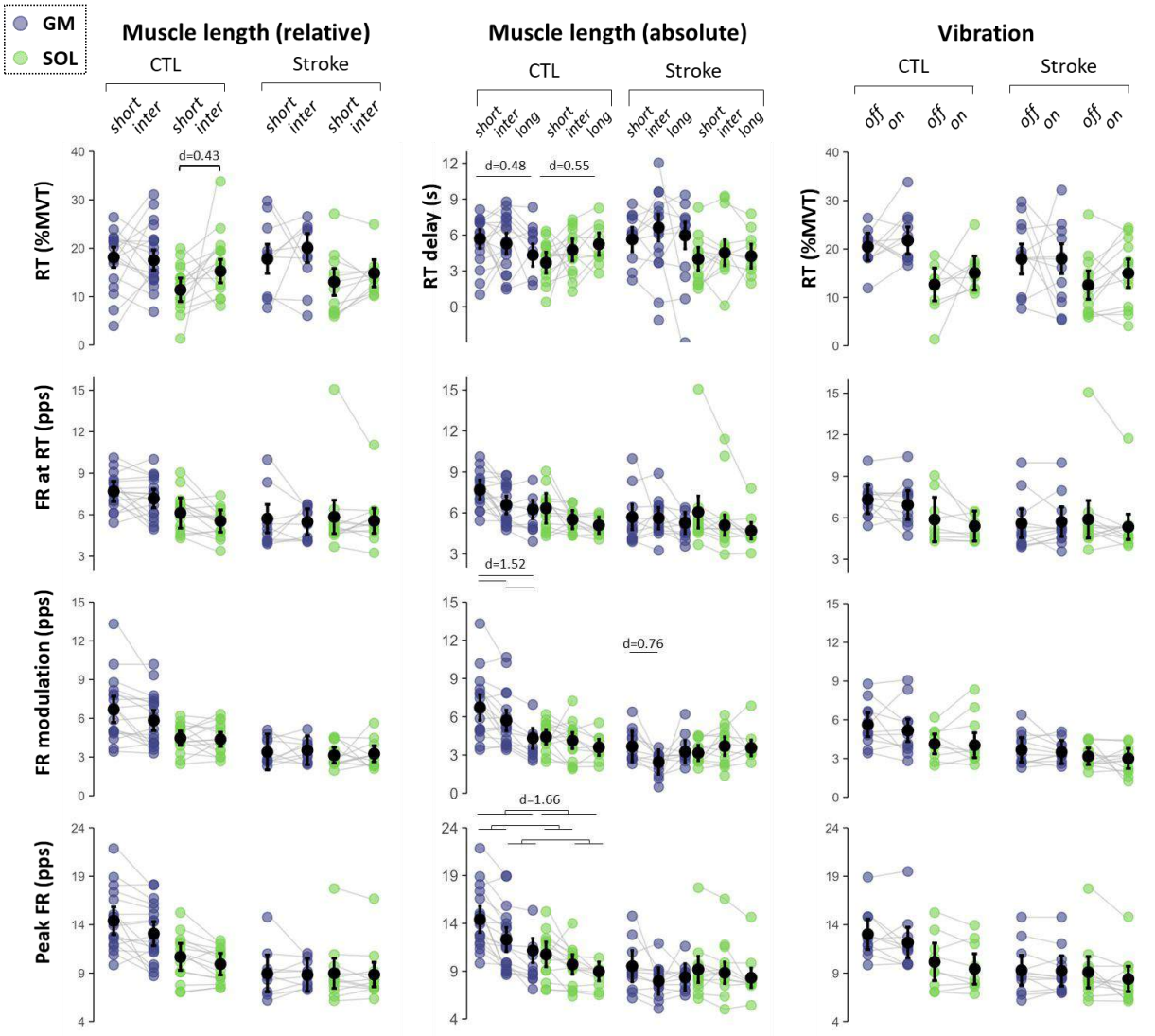

Figure 62. Effect of muscle length and vibration in motoneuron recruitment threshold and rate coding. *The modulation of motoneuron rate coding and recruitment threshold between the stroke and control (CTL) groups are compared in response to changes in muscle length at the same relative torque (40% MVT), and the application of tendon vibration to antagonist muscles, at short muscle length (20° of plantarflexion). Recruitment threshold (RT), firing rate at recruitment (DR RT), firing rate modulation (FR modulation), and peak firing rate (peak FR), were obtained from the gastrocnemius medialis (GM, purple) and soleus (SOL, green). Coloured dots represent participant averages, while black dots and bars indicate the estimated marginal means with 95% confidence intervals predicted by linear mixed-effects models. Cohen's d is reported for significant results ($p < 0.05$).*

Estimates of synaptic inputs to motoneurons

When considering the muscle length condition at similar relative torque between positions, there was no interaction between group and muscle length, nor between group, muscle length, and muscle for acceleration (all $p > 0.8192$), attenuation (all $p > 0.2066$), brace height (all $p > 0.3009$), or normalised ΔF (all $p > 0.3301$) (Fig. 63). There was an interaction between group, muscle length, and muscle for ΔF ($p = 0.0415$). Specifically, there were no significant changes in the stroke group (all $p > 0.8500$), whereas the control group showed a higher ΔF at short muscle length in the GM by 0.29 pps (95% CI: [0.023–0.58], $d = 0.26$, $p = 0.0483$) and a lower ΔF at short muscle length in the SOL by 0.42 pps (95% CI: [0.0141–0.8343], $d = 0.37$, $p = 0.0428$).

When considering the muscle length condition at similar absolute torque between positions, there was an interaction between group, muscle length, and muscle for acceleration ($p = 0.0225$), with acceleration decreasing from short to long muscle length by 0.58 pps/s (95% CI: [0.12–1.05], $d = 0.80$, $p = 0.0106$) for the GM in the control group, and decreasing from short to intermediate muscle length by 0.90 pps/s (95% CI: [0.28–1.52], $d = 1.25$, $p = 0.0019$) for the GM in the stroke group. There were no interactions between group and vibration, nor between group, vibration, and muscle for attenuation (all $p > 0.1403$) or brace height (all $p > 0.0709$), When considering ΔF, there was an interaction between group, muscle length, and muscle ($p = 0.0275$). While there was still no significant modulation with muscle length in the stroke group (all $p > 0.5069$), the control group exhibited a consistent pattern of a decreasing ΔF with increasing muscle length. Specifically, ΔF decreased in the GM from short to intermediate muscle length by 0.38 pps (95% CI: [0.12–0.64], $d = 0.36$, $p = 0.0014$) and from short to long muscle length by 0.64 pps (95% CI: [0.28–1.01], $d = 0.60$, $p = 0.0001$). In the SOL, ΔF decreased from short to long muscle length by 0.50 pps (95% CI: [0.06–0.94], $d = 0.47$, $p = 0.0182$) and from intermediate to long by 0.85 pps (95% CI: [0.39–1.31], $d = 0.80$, $p < 0.0001$). A consistent result emerging from the analyses of the different muscle length comparisons is thus that ΔF substantially decreased at longer muscle length in the control group but not in the stroke group. There was also a significant interaction between group and muscle length for normalised ΔF ($p = 0.0072$), with higher values at intermediate than at long muscle length ($d = 0.89$; $p = 0.0164$).

For the vibration condition, there was no interaction between group and vibration, nor between group, vibration, and muscle for acceleration (all $p > 0.5336$), attenuation (all $p > 0.1336$), brace height (all $p > 0.1256$), or normalised ΔF (all $p > 0.3422$). There was an interaction between

group, vibration, and muscle for ΔF ($p = 0.0024$). Specifically, there were no significant changes in the stroke group (all $p > 0.2789$), whereas the control group showed higher ΔF at short muscle length in the GM by 0.90 pps (95% CI: [0.44–1.35], $d = 0.89$, $p = 0.0010$).

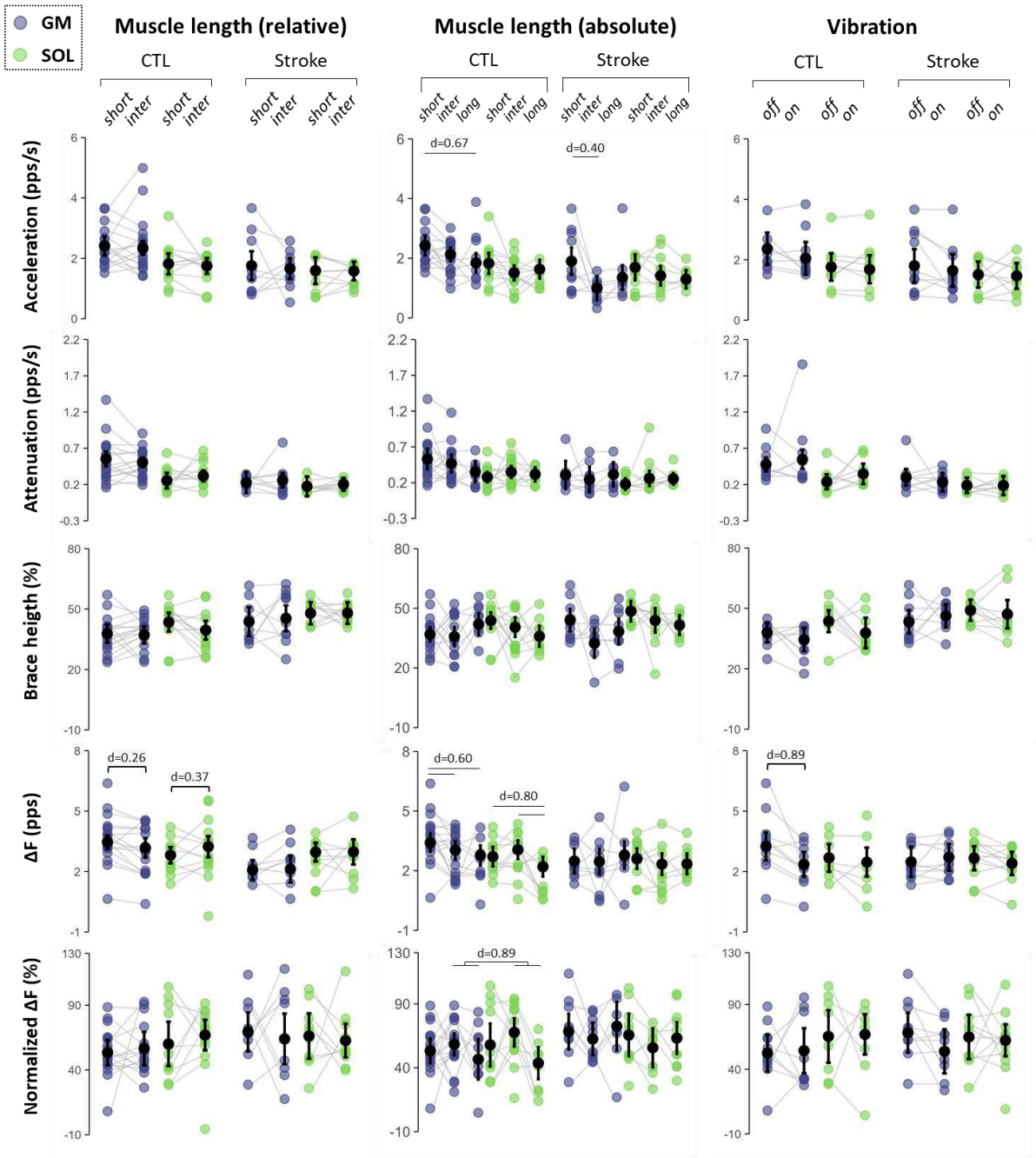

Figure 63. Effect of muscle length and vibration in estimates of synaptic inputs to motoneurons. *The modulation of motoneuron estimates of synaptic inputs to motoneurons between the stroke and control (CTL) groups are compared in response to changes in muscle length at the same relative torque (40% MVT), and the application of tendon vibration to antagonist muscles, at short muscle length (20° of plantarflexion). The acceleration slope, attenuation slope, brace height, ΔF, and normalised ΔF were obtained from the gastrocnemius medialis (GM, purple) and soleus (SOL, green). Coloured dots represent participant averages, while black dots and bars indicate the estimated marginal means with 95% confidence intervals predicted by linear mixed-effects models. Cohen's d is reported for significant results ($p < 0.05$).*

4. DISCUSSION

Based on non-invasive recordings of motoneurons innervating the GM and SOL muscles, this study demonstrates lower rate coding during voluntary contraction in individuals with chronic stroke. Estimates of synaptic inputs to motoneurons revealed a higher level of neuromodulatory input and a shift in the inhibition-excitation balance toward greater inhibition in the stroke group compared to the control group. Changing muscle length and applying vibration to the tendon of the antagonist muscle, which modulates inhibitory inputs, induced adaptations in rate coding and PIC-related prolongation of firing in healthy participants, but almost none in individuals with chronic stroke. Together, these findings suggest that motor impairment during voluntary contraction in chronic stroke is associated with reduced motoneuron rate coding caused by excessive and poorly adaptable inhibitory inputs, despite increased neuromodulatory inputs.

Motoneuron behaviour in chronic stroke

We observed reduced motoneuron rate coding in individuals with chronic stroke when contractions were matched for relative torque (40% MVC). This was evidenced by lower firing rate modulation in GM and SOL, and by lower firing rate at recruitment and peak firing rate in GM only, compared with control individuals. These results align with previous studies (Beauchamp, Hassan, et al., 2023; Chou et al., 2013; Gemperline et al., 1995; Hu et al., 2015; X. Li et al., 2015; Mottram et al., 2014), further supporting the notion of impaired rate coding after stroke and extending it to the GM and SOL muscles.

However, these deficits were no longer observed when contractions were performed at the same absolute torque level (30 N.m), as no between-group differences were found in this condition. This indicates that, at least for relatively low absolute torque values, individuals with stroke can achieve the same absolute torque without differences in motoneuron rate coding compared with healthy individuals. Importantly, 30 N·m corresponded to ~20% MVT in the control group but ~44% MVT in the stroke group. Therefore, for a similar absolute torque output, individuals with stroke operated at a much higher fraction of their maximal capacity. As illustrated in Figure 64, this supports the presence of an altered relationship between mean motoneuron firing rates and relative contraction intensity after stroke (i.e., the rate coding), characterised by a flatter slope. Such a profile would limit the capacity to further increase discharge rate as force demands increase, contributing to impaired muscle activation (i.e., paresis) and reduced force-generating capacity.

At 30 N.m, MUAP amplitude, used as a proxy for motor unit size, did not differ between groups. Conversely, MUAP amplitude was greater in the control group than in the stroke group during the 40% MVT contractions. This result is consistent with a lower contribution of larger, higher-threshold motor units in chronic stroke individuals at this relative contraction intensity. Together with the reduced rate coding observed in the same condition, this suggests that chronic stroke individuals may be limited in their capacity to engage larger motor units as force demands rise, along with their limited ability to increase discharge rate. Importantly, this interpretation is based on indirect measures and unverifiable assumptions of similar spatial sampling of motor units and comparable volume conductor effects across populations, and further work is needed to confirm the recruitment strategies in chronic stroke.

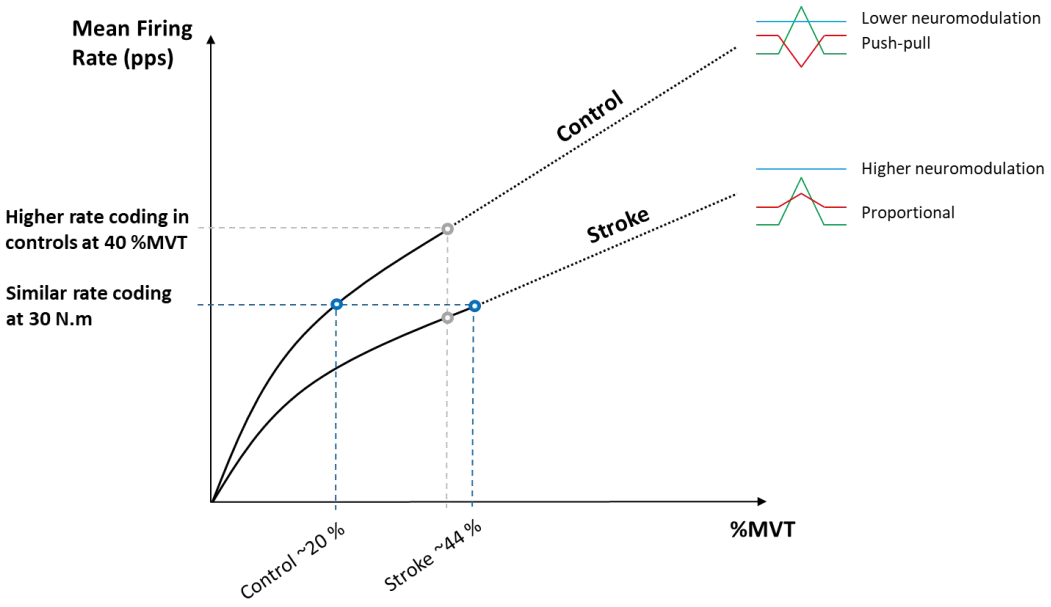

Figure 64. Schematic representation of rate coding and associated synaptic input organisation, in stroke and control individuals. *Greater firing rates were observed in controls compared with stroke individuals at 40 %MVT contractions, whereas similar firing rates were observed at 30 N.m. These results can be interpreted within a common framework by considering a flatter slope of the relationship between mean firing rate within the pool and contraction intensity after stroke. This altered relationship occurred with estimates consistent with greater neuromodulatory input (blue) and a more proportional pattern of inhibition, in which inhibition (red) increases with excitation (green) while decreasing in controls. The dotted black lines represent the extrapolated relationship at untested contraction intensities, suggesting the lower maximal firing rate achievable after stroke.*

An interesting finding was that rate coding decreased more substantially with increasing muscle length in control individuals than in chronic stroke individuals. This suggests that, after stroke, neural drive may be less effectively adjusted to the mechanical force-generating capacity of muscles, which varies with muscle length (Hoffman et al., 2012). As a result, paresis may be

aggravated at short muscle length, where the muscle is mechanically less advantaged and greater neural compensation may be required. This hypothesis has previously been proposed from the EMG amplitude (Gracies, 2005b; Vinti et al., 2015). The present results provide support for this hypothesis at the level of motoneuron output (i.e., neural drive), indicating that the effect is not explained by the limitations of EMG amplitude when muscle length changes (e.g., change in volume conductor or spatial sampling).

Synaptic inputs to motoneurons in chronic stroke

The observations of altered motoneuron output after stroke raise the question of which synaptic mechanisms underlie these changes. Earlier attempts to estimate the level of neuromodulation during voluntary contractions were based on the paired-motor unit method and revealed, as in the present study, that ΔF does not differ between stroke and control individuals (Mottram et al., 2009). However, it has been suggested that ΔF does not solely represent the level of neuromodulation but also reflects the pattern of inhibition acting on motoneuron pool (Beauchamp et al., 2023; Chardon et al., 2024). In this study, we therefore interpreted the synaptic inputs to motoneurons using a framework that links specific firing features to the level of neuromodulatory input and the inhibitory pattern (i.e., covariation of inhibition with respect to excitation) (Beauchamp et al., 2023; Chardon et al., 2024).

Using this framework, chronic stroke individuals exhibited discharge patterns consistent with a shift in the synaptic inputs toward greater inhibition, together with a greater level of neuromodulatory inputs (Figure 64). These results indicate that although stroke increases the level of neuromodulation, the increased inhibition dominates the motor command and leads to reduced rate coding as well as reduced PIC-mediated amplification (diminished acceleration slope) and PIC-mediated prolongation (diminished ΔF) of motoneuron discharge.

Using the same approach, Beauchamp et al. (2023) compared the biceps brachii between the non-paretic and paretic limbs, during both voluntary contractions and involuntary contractions arising from multi-joint synergy recruitment (i.e., activation of the biceps brachii during shoulder abduction, referred to as “flexion synergy”). They reported a progressive increase in both inhibition and neuromodulation estimates, from voluntary contractions in the non-paretic limb to voluntary contractions in the paretic limb, and further to flexion synergy contractions in the paretic limb. Taken with this previous work, our findings support a paradoxical organisation of synaptic inputs to motoneurons after stroke, characterised by increased neuromodulatory input

alongside enhanced inhibitory input. Notably, this altered input pattern appears to be amplified during stroke-specific flexion synergy contractions, suggesting upregulation of alternative descending pathways, such as the reticulospinal tract (Beauchamp et al., 2023). Interestingly, similar analyses in individuals with spinal cord injury revealed lower rate coding without evidence of increased neuromodulatory input (Goreau et al., 2026), highlighting that the paradoxical synaptic pattern observed here may be, at least in part, specific to stroke. It should be noted, however, that the approach used in this study to infer synaptic inputs to motoneurons in chronic stroke relies on the assumption that motoneuron properties do not alter the relationship between the derived metrics and their physiological interpretation. To date, there is no evidence for a specific change in biophysical motoneuron properties after stroke.

Manipulation of synaptic inputs to motoneurons

To further explore the role of inhibition after stroke, we attempted to modulate inhibitory inputs to motoneurons by changing muscle length and applying vibration. In control participants, increasing muscle length reduced rate coding, with lower firing rate modulation and peak firing rate, and was also associated with a decrease in ΔF, consistent with previous findings (Beauchamp et al., 2025; Goreau et al., 2025; Valenčič et al., 2026). In contrast, chronic stroke individuals showed only limited modulation of firing rate with muscle length and no significant modulation of ΔF. Similarly, antagonist tendon vibration modulated ΔF in control participants, as previously found (Mesquita et al., 2022), but not in chronic stroke participants, while motoneuron firing rate metrics remained unchanged in both groups. Together, these findings indicate that the synaptic inputs to motoneurons, especially inhibitory inputs, are less adaptable after stroke. One possible explanation is that the tested paradigms did not further increase the level of inhibitory inputs in stroke participants, likely because inhibitory interneurons operate near their maximal activity even at very low contraction intensities during voluntary contraction. This is consistent with the high level of inhibition associated with the more proportional inhibitory–excitatory pattern described above. Alternatively, the experimental paradigms employed may not have sufficiently activated inhibitory interneurons to further enhance inhibitory inputs. Indeed, vibration-induced reciprocal inhibition may be replaced by facilitation after stroke (Crone, 2003), and recurrent inhibition, likely a main contributor to inhibitory inputs with change of muscle length in control (Colard et al., 2025), is also altered after stroke (Burke et al., 2013; Katz & Pierrot-Deseilligny, 1982). More generally, spinal inhibition on motoneurons is highly dependent on descending inputs, which are altered after stroke (Jankowska, 1992).

Regardless of the underlying mechanisms, these findings highlight the limited capacity of individuals with stroke to adapt the motor command via inhibitory inputs.

After stroke, reorganisation of descending motor pathways leads to upregulation of the cortico-reticulospinal tract (Jang & Cho, 2022; Zaaimi et al., 2012). This reorganisation likely underpins several motor impairments, such as the flexion synergy (Ellis et al., 2009), and may help to explain the reconfiguration of synaptic inputs to motoneuron observed in the present study. In particular, reticulospinal pathways may increase monoaminergic drive to motoneurons (J. Beauchamp et al., 2022; McPherson, Ellis, et al., 2018), while also upregulating inhibitory spinal interneurons, including Renshaw cells (Mazzocchio, 1997; Pompeiano, 1988). This dual influence may contribute to the paradoxical combination of increased neuromodulatory inputs and increase inhibitory inputs suggested by our data.

Conclusion

This study demonstrates that chronic stroke is not merely associated with reduced motoneuron output, but with a pathologically maladaptive and less adaptable synaptic command to the motoneuron pool. Individuals with chronic stroke exhibit reduced rate coding together with firing patterns indicative of stronger inhibitory inputs, despite evidence of increased neuromodulatory inputs. This paradoxical and poorly adaptable input-output organisation may impair the scaling of neural drive with force demands, contributing to paresis.

◥ SUPPLEMENTARY ANALYSES

Supplementary analyses were conducted by integrating data from the three groups of individuals, namely post-stroke, post-SCI, and control participants, from studies 2 and 3. In addition to the previously reported data, additional clinical assessments were incorporated, including MVT, antagonist coactivation during maximal voluntary contraction, and spasticity measures. The first aim of these supplementary analyses was to explore the relationships between motoneuron behaviour metrics, their associations with estimates of paresis (MVT, activation), and their ability to discriminate between groups. The second aim was to examine the relationship between muscle-level clinical measures (coactivation, spasticity, MVT) and estimates of motoneuron synaptic inputs.

1. Method

Additional metrics

In addition to the metrics already presented, the supplementary analyses include the following variables: activation, coactivation, spasticity_EMG, and spasticity_torque.

Activation, an indirect assesment of paresis, corresponds to the maximal EMG amplitude recorded during maximal voluntary contraction, expressed in mV. In detail, from the high-density EMG recording, a bipolar configuration was reconstructed by averaging two groups of 25 channels located at the extremities of each grid and computing the difference between these averages, yielding a single value per grid. The values from the two grids were subsequently averaged to obtain a single value per muscle. The maximal EMG amplitude (activation) was defined as the peak of the root mean square signal computed over a 300 ms window. Thus, one activation value was obtained for both GM and SOL.

Coactivation corresponds to the maximal value of GM and SOL during maximal dorsiflexion voluntary contraction. Specifically, EMG was processed as described above, and the maximal EMG values of GM and SOL during maximal dorsiflexion were normalised to their respective maximal activation values obtained during maximal plantarflexion.

Spasticity was assessed in participants from the pathological groups only. Participants were seated on an isokinetic dynamometer with the knee near full extension, as previously described. Passive ankle movements were performed from 40° of plantarflexion to the maximal

dorsiflexion range of motion. Movements were executed at 60°/s and 120°/s, with two trials per velocity. Analyses were restricted to 90% of the range of motion to avoid end-range artefacts. The area under the curve of GM and SOL EMG and plantarflexion torque was computed. The AUC values from the two trials at each velocity were averaged. Spasticity was quantified as the ratio of values at 120°/s relative to 60°/s, yielding spasticity_EMG (%) for each muscle and a single spasticity_torque (%). This approach isolates the velocity-dependent component of the stretch response, which is crucial for characterising spasticity (Bar-On et al., 2013; Chen et al., 2020; Turpin et al., 2017). Furthermore, the comparison between 60°/s and 120°/s corresponds to velocities sensitive to spasticity (Kim et al., 2005).

Analyses

Principal Component Analysis (PCA) was used as an exploratory technique to reduce dimensionality and identify latent structures within the data, while summarising relationships between variables. Missing data were first standardised and imputed using a PCA-based approach implemented in the missMDA package, which preserves the covariance structure of the dataset. All variables were standardised prior to analysis to account for differences in measurement units and variance magnitude. PCA was then performed using the FactoMineR package on the imputed datasets. Contributions of each variable to the principal components were quantified to identify those driving the main axes of variation. For interpretation, variables pointing in the same direction are positively correlated, variables pointing in opposite directions are negatively correlated, and orthogonal variables are considered independent.

Furthermore, PCA at the individual level was performed, with individuals projected into the principal component space and coloured according to group membership. Group separation in this space indicates discrimination between groups, whereas overlap reflects weak differentiation.

Specifically, both types of PCA were conducted (i) on essential motoneuron-related metrics, together with activation, coactivation, and MVT, including all the three groups; and (ii) on key estimates of synaptic inputs (brace height and attenuation), together with clinical metrics (MVT, activation, coactivation, spasticity_EMG, spasticity_torque), in SCI and stroke individuals.

2. Relationships between variables and group structure

PCA of variables revealed a first principal component accounting for 45% of the variance. Most variables contributed to this component, except coactivation, normalised ΔF, and notably brace height, which alone accounted for more than 35% of the second component (Fig. 65 A & C). The first component seems to primarily reflect the capacity to activate muscles, and it was highly discriminant between control and pathological groups (Fig. 65B). In contrast, the second component, largely driven by brace height, provided strong discrimination between SCI and stroke groups, which were not clearly separated along the first component. Overall, this finding is consistent with Studies 2 and 3, highlighting relatively preserved rate coding in stroke compared with SCI, and a marked increase in brace height in stroke participants.

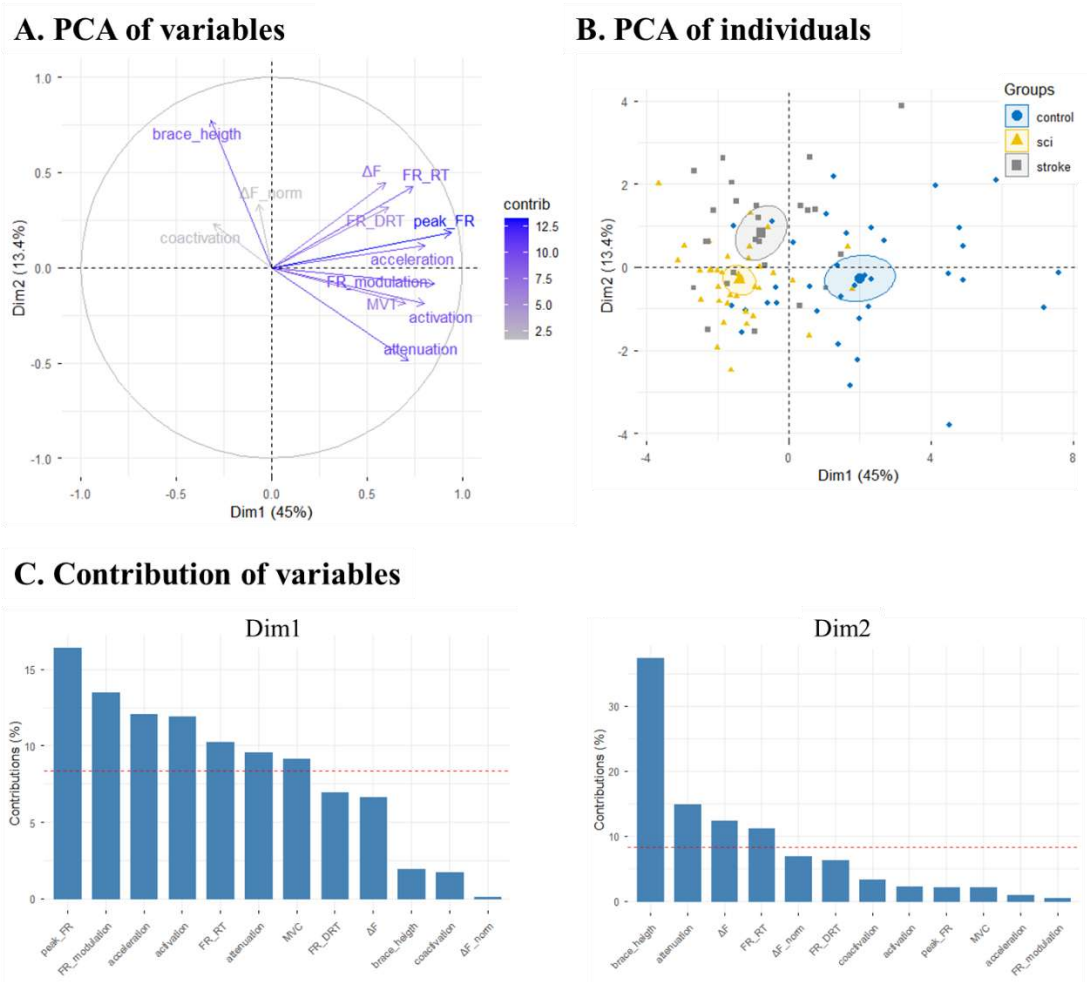

Figure 65. Relationships between variables and group structure. *Principal component analyses (PCA) were conducted at both the variable level (A) and the individual level (one point per muscle per individual) (B). Variable contributions to the first (Dim1) and second (Dim2) principal components are shown in (C). ΔF_norm, normalised ΔF; FR_RT, firing rate at recruitment; FR_DRT, firing rate at derecruitment; peak_FR, peak firing rate; FR_modulation, firing rate modulation; MVT, maximal voluntary contraction torque.*

3. Relationships between clinical measures and estimates of synaptic inputs

PCA of variables revealed two principal components explaining similar proportions of variance (28.8% and 25.6%). The distribution of variables indicates that the first dimension is primarily driven by clinical measures, with MVT showing the strongest contribution, whereas the second dimension reflects the structure of synaptic input, characterised by a negative correlation between brace height and attenuation (Fig. 66). This separation suggests that estimates of synaptic input are largely independent of clinical measures, indicating the absence of a simple linear relationship between neuromodulatory input, inhibitory patterns, and clinical features. The negative correlation between brace height and attenuation further suggests that high neuromodulatory input is globally associated with a more proportional inhibitory pattern. These adaptations suggest concurrent increases in neuromodulation and inhibition, which appear more pronounced in stroke individuals.

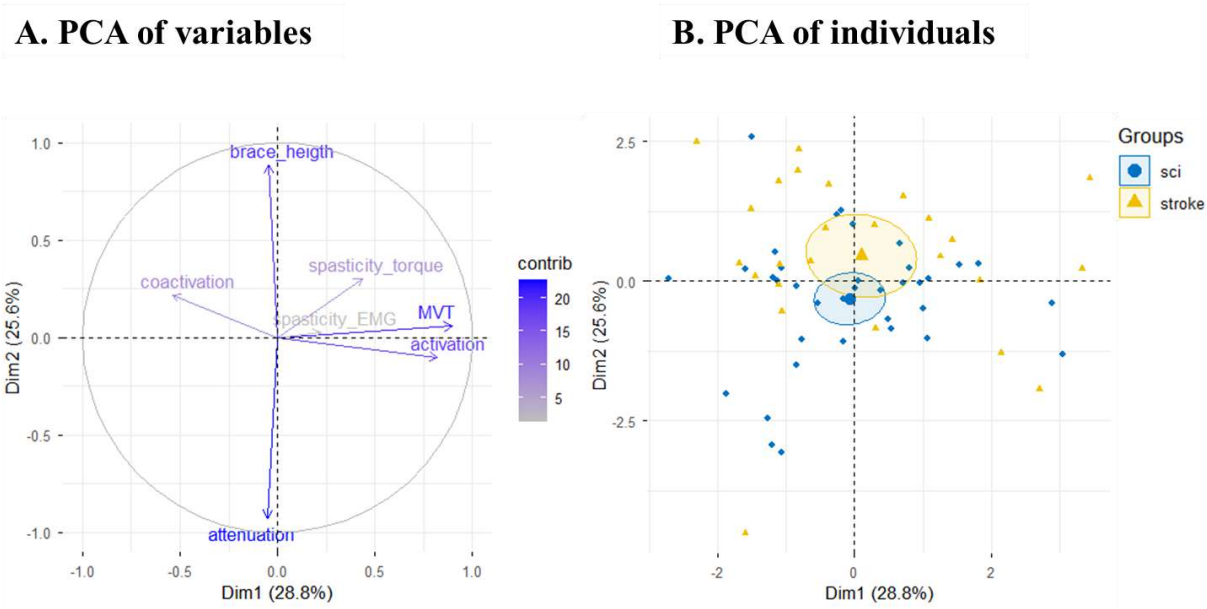

Figure 66. Relationships between clinical measures and estimates of synaptic inputs. *Principal component analyses (PCA) were conducted at both the variable level (A) and the individual level (one point per muscle per individual) (B).*

OVERALL DISCUSSION

The overarching aim of this thesis was to better characterise the organisation of synaptic inputs after stroke and SCI, and to determine how these inputs adapt to changes in joint position and vibration in both healthy and pathological conditions. All studies followed a common experimental framework, in which participants performed isometric plantarflexion tasks while high-density EMG signals were recorded and decomposed into individual motoneuron firing patterns. The organisation of synaptic inputs was then inferred from firing pattern signatures.

Overall, this work demonstrates that: (i) in healthy individuals, PIC-mediated prolongation decreases with increasing muscle length, likely due to increase in inhibitory inputs; and (ii) both SCI and stroke are associated with reduced motoneuron rate coding, underpinned by increased inhibitory inputs. After stroke, this increased inhibition was accompanied by an upregulation of neuromodulatory inputs. These findings will be discussed in light of the methods used to estimate motoneuron synaptic inputs. We will also consider how these results integrate within the broader field, highlighting current limitations and future challenges. Finally, potential clinical implications will be presented.

◥ ESTIMATING SYNAPTIC INPUTS VIA MOTONEURON FIRING PATTERNS

1. EMG decomposition

The experimental work conducted in this thesis was performed in humans, which substantially constrains the approaches available to investigate central nervous system function. In practice, only indirect measurements can be obtained due to ethical limitations. This stands in contrast to the expanding experimental possibilities in animal models. For instance, optogenetics enables the selective activation of specific neuronal populations during *in vivo* experiments, thereby greatly enhancing mechanistic understanding (e.g., Levine et al., 2014). Obtaining meaningful neuroscience insights from human data is therefore inherently challenging. One valuable avenue lies in accessing motoneuron activity. Due to the one-to-one relationship between motoneurons and muscle fibre action potentials, information about neural activity can be inferred from muscle recordings. Motoneuron recording has a long history (Farina et al., 2016), and recent decades have seen major advances driven by improvements in decomposition

algorithms (Farina & Holobar, 2016; Negro, 2016) and EMG hardware. It is now possible to record a substantial portion of the motoneuron pool (Avrillon et al., 2024).

In the present work (Studies 2 and 3), we obtained on average the following number of motor units for the GM: 13.5 ± 7.8 (control), 9.3 ± 7.5 (SCI), and 6.4 ± 6.0 (stroke). For the SOL, the corresponding values were 8.2 ± 6.1, 10.3 ± 8.1, and 7.3 ± 5.7. These results demonstrate that high-density surface EMG decomposition is feasible in populations with central nervous system injuries, which was rarely achieved at the outset of this thesis (2022). Moreover, the number of identified motoneurons did not differ markedly between control and pathological groups. However, the number of decomposed motor units remains far below the total population, which consists of hundreds of units in plantar flexor muscles (Heckman & Enoka, 2012). In addition, variability in the number of identified units is high, although this is not specific to pathological conditions. Surface EMG decomposition is physiologically limited by the attenuation of signal amplitude with depth, which restricts detection primarily to superficial motor units. This limitation could be addressed using intramuscular EMG recordings. Another limitation is that decomposition is biased toward larger, higher-threshold motor units. Consequently, it is difficult to track the same units across a wide range of contraction intensities. This constraint led us to limit contraction intensity to 40% MVT, or slightly higher in participants with low MVT during the 30 N.m task. Alternatively, multiple contractions at different intensities could be combined to reconstruct the full range of rate coding (Avrillon et al., 2024), which would be particularly valuable for characterising paresis. The reasons underlying inter-individual variability in decomposition performance remain an active area of research. Factors such as volume conductor properties (e.g., subcutaneous fat thickness) likely play a role (Oliveira et al., 2022). In practice, especially in clinical environments, additional factors such as electrical interference (e.g., from nearby MRI systems…) can also affect signal quality.

In addition, decomposition requires manual editing, which introduces a degree of subjectivity. Although this process has been shown to be highly reliable across operators (Hug et al., 2021) during plateau contractions, this reliability does not necessarily extend to the initial and final discharge phases, which may be less reliably edited yet are critical for subsequent analyses. Of note, a common concern in EMG recordings is crosstalk, where signals originate from muscles other than the target muscle. This is unlikely with high-density EMG decomposition, as signal attenuation through tissue limits detection to relatively superficial and localised motor units. Overall, future improvements could focus on enhancing automation in signal editing, refining decomposition algorithms (Grison et al., 2025), and advancing recording technologies (Caillet

et al., 2023). Nevertheless, the present work leverages state-of-the-art methods and provides a larger sample of motoneurons than previous studies investigating motoneuron behaviour following SCI and stroke in lower limb muscles.

2. Synaptic input signatures in the firing patterns

Since the work of Powers & Heckman (2017), it has become clear that different types of synaptic inputs exert distinct and specific effects on motoneuron firing rate profiles. Prior to this thesis, estimation of synaptic inputs was largely limited to the paired motor unit approach. More recently, studies by Beauchamp et al., (2023) and Chardon et al. (2024) introduced new quantitative features of firing behaviour (i.e., the geometric approach) and demonstrated associations between these features and the underlying structure of synaptic inputs. In combination with EMG decomposition, these advances enable non-invasive estimation of synaptic input organisation. This approach was applied in the present thesis, providing deeper insight into synaptic organisation following SCI and stroke. However, several limitations must be acknowledged.

The primary limitation is that this approach relies on statistical associations between firing features and synaptic inputs, which are not perfect. The variance in synaptic inputs explained by these features is incomplete, limiting the certainty with which specific features can be attributed to specific input types. To overcome this limit, one promising direction is the application of reverse-engineering approaches to human experimental data, with the goal of reconstructing the time-varying conductances of synaptic inputs underlying observed firing patterns (Chardon et al., 2024). However, this approach faces substantial challenges. First, the computational burden is considerable due to the vast solution space of possible input combinations. To give an idea of the scale, Chardon et al. (2024) required a supercomputer to perform their simulations; equivalent computations on a standard computer (16 cores) would take approximately 15 years. Future progress may reduce this burden by constraining the solution space to physiologically plausible inputs and by improving access to supercomputers. Being less optimistic, we can highlight that current models already impose strong assumptions, such as fixed neuromodulatory input levels for the entire duration of contractions and fixed relationships between excitatory and inhibitory inputs.

A second fundamental limitation is the absence of ground truth in humans. The exact levels of excitatory, inhibitory, and neuromodulatory inputs to motoneurons are unknown, making it impossible to directly validate inferred input structures. Nevertheless, this framework remains

valuable for hypothesis-driven research and for strengthening the interpretation of experimental findings. A distinctive aspect of this thesis was the application of these methods in individuals with stroke and SCI. An initial concern was whether participants would be able to perform the required torque tasks. In practice, most patients were able to perform the tasks with capacities comparable to controls, although additional trials were often needed, and fatigue sometimes prevented completion of the full protocol. Overall, this aspect of the study was successful.

Applying these methods in pathological populations also raises the question of whether the relationships between firing features and synaptic inputs remain valid. The motoneuron pool model used to support these inferences is based on data from decerebrate cats, with adaptations to approximate human firing behaviour (Beauchamp et al., 2023; Chardon et al., 2024; Powers & Heckman, 2017). It is therefore not a model specifically derived from healthy human motoneurons. What matters for our work is the assumption that motoneurons in stroke and SCI receive similar types of synaptic inputs (in terms of levels of common inputs) and retain similar intrinsic properties, which are essential parameters of the model used for validation (Beauchamp et al., 2023; Chardon et al., 2024; Powers & Heckman, 2017). While this cannot currently be verified directly, several observations support this assumption. For example, as in healthy individuals, firing rates remain highly correlated, suggesting a similar structure of common inputs. Moreover, stroke and SCI do not typically directly affect motoneurons (except at the lesion site in SCI), making major alterations in intrinsic properties unlikely, although this remains to be further explored.

We began this section by highlighting the discrepancy between investigation possibilities in animal models and humans. It is therefore important to emphasise that several of our findings are not consistent with previous animal-based studies. For example, our results on PIC modulation with joint position contrast with those reported in decerebrate cat models (Hyngstrom et al., 2007), and the increased inhibition observed after SCI differs from findings obtained during spasms at the cellular level (Mahrous et al., 2024). Rather than opposing these approaches, these differences likely reflect distinct experimental conditions and research questions, making them ultimately complementary.

◥ MODULATION OF SYNAPTIC INPUTS WITH MUSCLE LENGTH IN HEALTHY INDIVIDUALS

Estimating synaptic inputs from motoneuron firing rates has attracted sustained interest in recent years. One key finding of this growing body of research is that it provides evidence that monoaminergic neuromodulation is an effective mechanism in humans. Specifically, the use of serotonin receptor antagonists leads to a decrease in ΔF, thereby supporting a crucial role of 5-HT in regulating motor activity through PICs (Goodlich et al., 2023, 2024). In addition, whole-body relaxation has been shown to reduce ΔF in human motoneurons (Mesquita et al., 2022), whereas remote handgrip contractions increase ΔF in lower-limb muscles (Orssatto et al., 2022). Because these effects globally modulate ΔF, they likely involve changes in monoaminergic input to motoneurons. Another substantial body of evidence highlights that sensory-mediated inputs also influence motoneuron firing behaviour by altering PIC-mediated effects on motoneuron behaviour. For instance, vibration of the antagonist tendon or its electrical stimulation decreases ΔF (Orssatto et al., 2022; Pearcey et al., 2022).

In this context, Study 1 aimed to determine whether PIC modulation contributes to adapting activation to mechanical demands, and through which synaptic inputs. We found that PIC-mediated prolongation (ΔF) decreases with increasing muscle length, suggesting that it may serve as a mechanism to adapt activation to mechanical force-generating capacity. This result was similar in Studies 2 and 3, which included older participants (50 ± 20 years compared to 24.3 ± 3.9 years in Study 1), indicating a consistent effect across ages.

As ΔF depends on both neuromodulatory and inhibitory inputs, it does not provide a direct estimate of either. However, it reflects the specific firing-prolongation pattern, which itself informs motoneuron output and has direct implications for force production. The functional consequences of firing prolongation remain debated. For example, force plateaus following a decrease in force, reflecting sustained activation of higher-threshold motoneurons via PICs, are associated with increased force variability, suggesting that this “involuntary” sustained activation may be difficult for the central nervous system to compensate, thereby impairing motor performance (Beauchamp et al., 2025). Conversely, PIC-induced nonlinearities may compensate for intrinsic muscle nonlinearities, forming an integral component of the motoneuron–muscle predictive controller (Chardon et al., 2026). More generally, it remains unclear whether these nonlinearities are merely consequences of neuromodulatory gain adaptation or whether they carry functional value per se. It is noteworthy that reverse-engineering simulations in

Chardon et al. (2024) revealed the necessity of non-linear excitatory inputs at high levels of neuromodulation, implying additional complexity for the central nervous system in controlling motor output.

During the thesis, two additional studies tested the effect of muscle length (Beauchamp et al., 2025; Valenčič et al., 2026) and reported similar findings, strengthening confidence in this result. A specific contribution of our study was to test joint position effects at both the same absolute and relative torque levels across positions. Because results were consistent across conditions, this modulation appears independent of contraction intensity, suggesting that Ib-related inhibition is unlikely to be the primary mechanism. This result is particularly important because it rules out one of the main confounding factors explaining discrepancies between human and decerebrate cat findings regarding PIC modulation (Hyngstrom et al., 2007). It therefore points toward the decerebrate state, associated with altered descending control of inhibitory interneurons, as the main source of discrepancy. This also raised the question of how such modulation behaves in stroke and SCI, where descending control is impaired, which we addressed in Studies 2 and 3 and discussed in the next section.

Longer muscle length led to decreased ΔF, accompanied by a slight increase in brace height and a reduction in attenuation slope, clearly indicating a role for inhibitory inputs in this modulation. This raises the question of which inhibitory pathways are involved. As recurrent inhibition increases at longer muscle lengths in humans (Colard et al., 2025), and no other postsynaptic inhibitory mechanism seems to fully account for this modulation pattern, we proposed that recurrent inhibition may be a primary contributor to the modulation of PIC-mediated prolongation with muscle length. More generally, recurrent inhibition appears to be a key regulator of PICs. Both computational and animal studies indicate that Renshaw cells exert their inhibitory influence on highly effective regions of the motoneuron to regulate PIC contributions to motoneurons discharge (Bui et al., 2008; Hultborn et al., 2003).

In line with this, our master's research project, published during the first year of this thesis, also invoked recurrent inhibition to explain our findings. This study primarily compared ΔF across resistance-trained, endurance-trained, and inactive individuals, revealing no significant differences (Goreau et al., 2024). The second aim was to map ΔF values across lower-limb muscles. We assessed five muscles, and correlation analyses showed that not all muscles were correlated, whereas agonist muscles exhibited stronger correlations, which we attributed to a shared local inhibitory input, namely recurrent inhibition. This raises the question: could recurrent inhibition

underlie the variability of ΔF across muscles? While the classical functional explanation suggests that higher ΔF would be advantageous in proximal, posture-oriented muscles, this does not align with experimental observations. Conversely, the apparent increase in ΔF with muscle distality is consistent with the reported decrease in recurrent inhibition along the proximal–distal axis (Dernoncourt et al., 2026.; Edgley et al., 2021). The extent to which recurrent inhibition shapes the contribution of PICs to motoneuron firing, however, remains to be determined.

◥ CHANGES OF SYNAPTIC INPUTS AFTER SCI AND STROKE

Most of the knowledge regarding post-synaptic inhibitory inputs to motoneurons after stroke and SCI comes from the H-conditioned paradigm. The main findings are that, after both stroke and SCI, reciprocal Ia inhibition decreases (Crone, 2003), and recurrent inhibition increases (Katz & Pierrot-Deseilligny, 1982; Shefner et al., 1992). Overall, the H-reflex at rest is increased, and the phenotype is generally interpreted as a disinhibited state, although presynaptic and other pathways may also contribute to this global state. Thus, evidence tends to support reduced inhibition overall, with the exception of recurrent inhibition, which does not consistently show differences (Burke et al., 2013). One drawback of the H-reflex is that it attempts to isolate specific mechanisms while assessing them in a non-functional state. One attempt to overcome this limitation was the study by Gorassini at al. (2004), which recorded motor units and applied paired motor unit analysis during spasms in SCI, revealing substantial ΔF values. On one hand, this study clearly supports a contribution of PICs to spasms. On the other hand, the opposite result would have been unexpected, as PICs are voltage-gated channels and are expected to activate once motoneurons are depolarised. Thus, while PICs may sustain prolonged spasms, this does not necessarily demonstrate that they constitute the primary driving mechanism. However, these findings in humans are generally corroborated by animal models. For example, recent studies point toward increased PICs and reduced inhibition as mechanisms underlying spasms (Mahrous et al., 2024).

As argued earlier, one fundamental difference between these approaches and the one used here is that synaptic inputs are assessed during actual voluntary contractions, thereby limiting extrapolation across states. While signs of overactivity after stroke and SCI affect quality of life, the main clinical feature remains impaired voluntary movement, which represents a key target for improvement. This state-dependence of evaluation is critical in interpreting our results, which differ markedly from those obtained at rest or during involuntary contractions. Indeed,

our results indicate increased inhibition with respect to excitation after both stroke and SCI, whereas changes in neuromodulation were observed only after stroke, with evidence suggesting an upregulation. To further support this approach, it should be noted that H-reflex stimulation imposes non-physiological recruitment patterns (e.g., high synchronisation). In addition, several studies demonstrate state-dependent differences in spinal control. For example, H-reflex excitability is higher at rest after SCI compared to controls but increases to a much lesser extent during voluntary contraction (Chen & Perez, 2022; Vastano & Perez, 2020).

It is interesting to note that, despite similar impairments in rate coding, our approach distinguishes different synaptic input organisations in stroke and SCI (Figure 67). This supports the interpretation that these estimates are not driven by reduced firing rate capacity. The differences between populations suggest distinct underlying mechanisms in terms of the pathways mediating synaptic input organisation. A common mechanism in both SCI and stroke may be altered descending control of spinal inhibition (Jankowska, 1992). Further details remain speculative, but recurrent inhibition may play a central role in the altered inhibitory pattern. The negative feedback provided by recurrent inhibition offers a parsimonious explanation for the proportional inhibition pattern. As excitatory input increases, motoneuron firing rates increase and, in the absence of proper regulation of Renshaw cells, lead to increased inhibitory input, resulting in a concurrent rise in excitatory and inhibitory inputs. An important line of evidence suggests that upregulation of the corticoreticulospinal tract is a key feature after stroke (Jang & Cho, 2022; McPherson, Chen, et al., 2018; Zaaimi et al., 2012). This may explain both the increased neuromodulatory input, as the reticulospinal tract conveys monoaminergic projections to motoneurons, and the proportional inhibition pattern, as it also regulates spinal inhibitory interneurons and reduces motoneuron EPSP amplitude compared to the corticospinal tract (Baker, 2011).

Regarding SCI, the absence of increased neuromodulatory or PIC levels in our results contrasts with findings from animal models of spasms (Li & Bennett, 2003; Mahrous et al., 2024). Beyond the difference in assessment state (involuntary vs voluntary contractions), this discrepancy may also arise from differences in lesion type. In animal models, lesions are typically complete, which may induce distinct adaptations, such as increased activation of constitutively active 5-HT2 receptors that maintain PICs despite reduced monoaminergic input (D'Amico et al., 2014; Murray et al., 2010). More generally, lesion size and location likely contribute to variability in motor outcomes. A particularly relevant feature in stroke is the preservation of ipsilesional corticofugal pathways, which predicts recovery (Miyai et al., 1997; Pantano et al., 1995) and may

constrain motor commands to alternative pathways, notably the reticulospinal tract (Baines et al., 2026). This may contribute to the altered synaptic input organisation observed in this thesis. Finally, another factor that may contribute to variability is that participants were taking medications, including serotonergic and antispastic drugs. However, the sample size and heterogeneity of treatments did not allow us to assess this factor.

◥ CHANGES OF FIRING BEHAVIOUR AFTER SCI AND STROKE

1. Firing rate

Previous studies have aimed to characterise rate coding after SCI (Thomas et al. (2014); for review) and stroke (Beauchamp et al., 2023; Chou et al., 2013; Gemperline et al., 1995; Hu et al., 2015; X. Li et al., 2015; Mottram et al., 2014). In general, these studies consistently report lower firing rates in these pathological populations, consistent with our results. Some muscles may be different in this regard, as clear differences were not always observed, for instance in the triceps brachii (Wiegner et al., 1993). However, contradictory findings require further investigation using improved methods before exploring potential muscle-specific adaptive mechanisms.

An interesting finding is that, within a given muscle after SCI, some motor units exhibit increased firing rates, suggesting intra-muscle variability, which may be related to axonal sprouting (Thomas et al., 2014). In addition to using approaches that allow recording a greater number of motoneurons and including lower-limb muscles, Studies 2 and 3 were designed to compare populations at the same absolute force level. This approach notably allowed us to determine whether different populations rely on distinct motoneuron outputs to produce the same force, which is relevant as many daily-life activities require absolute rather than relative force (e.g., pressing a car pedal). However, the main reason we used the same absolute force comparison is that it allowed us to address the potential dependence of synaptic input structure on the absolute force produced.

Interestingly, SCI individuals exhibited lower rate coding than controls at the same absolute force, suggesting an adaptive strategy to generate force. Estimating motor unit size revealed no differences between groups, indicating that reduced rate coding may be compensated by recruiting more motor units. The fact that this occurs after SCI but not after stroke is consistent with the lower rate coding capacity observed in SCI. Contractions at 30 N.m also expand the

range of relative contraction intensities tested. A key perspective would be to assess rate coding across the full range up to maximal voluntary contraction. Our results across intensities provide a first approximation of the full range of rate coding across populations and summarise several findings. Accordingly, Figure 67 schematically represents rate coding, highlighting a progressive decrease from control (neutral length) to control (long length), stroke, and SCI. This decrease is associated with increased inhibition, partly offset by higher neuromodulation in stroke, which may limit its impact (Fig. 67).

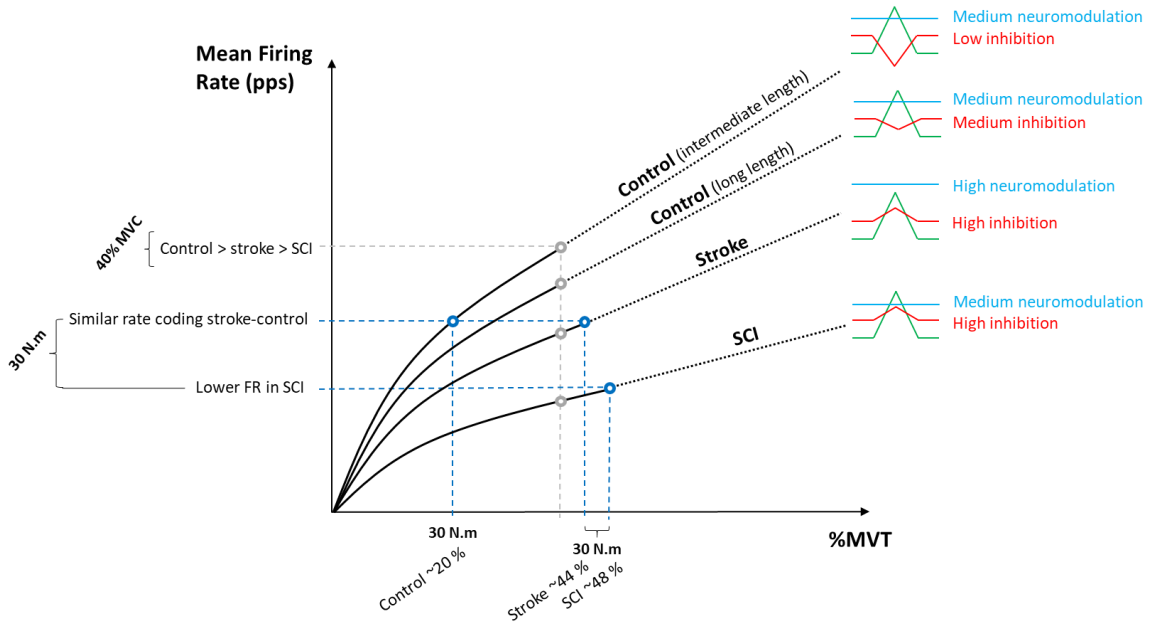

Figure 67. Schematic representation of rate coding and associated synaptic input organisation in control (at intermediate and long muscle lengths), stroke, and SCI individuals. *At 40% MVT, the order from lowest to highest firing rates was: SCI, stroke, control at long muscle length, and control at intermediate muscle length. At 30 N·m, similar firing rates were observed between stroke and control, with lower firing rates in SCI. These results can be interpreted within a common framework by considering the slope of the relationship between mean firing rate within the motoneuron pool and contraction intensity. The dotted black lines represent the extrapolated relationships at untested contraction intensities. These relationships are associated with specific organisations of synaptic input. From control at intermediate muscle length to SCI, the decrease in rate coding is accompanied by increasing inhibition (red) relative to excitation (green). Rate coding appears more preserved after stroke than after SCI, likely due to an upregulation of the neuromodulatory level (sky blue).*

The modulation of firing behaviour with joint position was observed in controls but not in pathological individuals. As discussed in the literature review, force production capacity is altered in a muscle-length-dependent manner. This results from antagonist co-contraction,

exacerbated by antagonist stretch (Vinti et al., 2013), which limits joint torque, as well as changes in muscle properties (Gracies, 2005a). These features notably lead to the striking impairment of individuals producing a torque opposite to the one aimed at the level of an articulation. Another proposed mechanism is muscle-length-dependent paresis, with greater impairment at short muscle lengths, potentially increasing difficulty due to co-contraction and antagonist stretch. However, this hypothesis has not been adequately tested. Previous attempts (Vinti et al., 2015) relied on EMG amplitude, which is limited when comparing activation across muscle lengths.

Thus, Studies 2 and 3 provide the first evidence supporting this hypothesis at the motoneuron output level (i.e., neural drive). Interestingly, results were consistent across stroke and SCI, suggesting a more general feature of central nervous system injuries. Notably, PIC-mediated firing prolongation failed to increase at short muscle lengths in pathological individuals, suggesting that impaired PIC regulation to mechanical demands may contribute to paresis. As these results are based on submaximal contractions, they should be confirmed using interpolated twitch technique across muscle lengths.

What has been suggested as a particular feature of rate coding in stroke is negative rate modulation, defined as a decrease in firing rate following the initial increase despite continued increases in torque or EMG amplitude (Beauchamp et al., 2023; Mottram et al., 2009). Because this pattern can challenge the geometric approach, we implemented a bilinear fit separating the initial increase and subsequent saturation in Study 3. This did not alter the results, largely because negative rate modulation was not highly prevalent in our sample. Regarding negative rate modulation, Figure 68 illustrates several features. First, negative rate modulation occurs in all populations, although it appears more frequent in stroke, consistent with increased neuromodulation combined with altered inhibition. Second, EMG amplitude during contraction suggests that negative rate modulation is unlikely to result solely from altered muscle coordination, although some variability may contribute. In this regard, one could argue that providing EMG feedback would better preserve linearity between force and neural drive, but this would restrict analysis to a single muscle and make the task more difficult. Finally, negative rate modulation can also varies across and within muscles, and the determinants of this variability remain largely unknown.

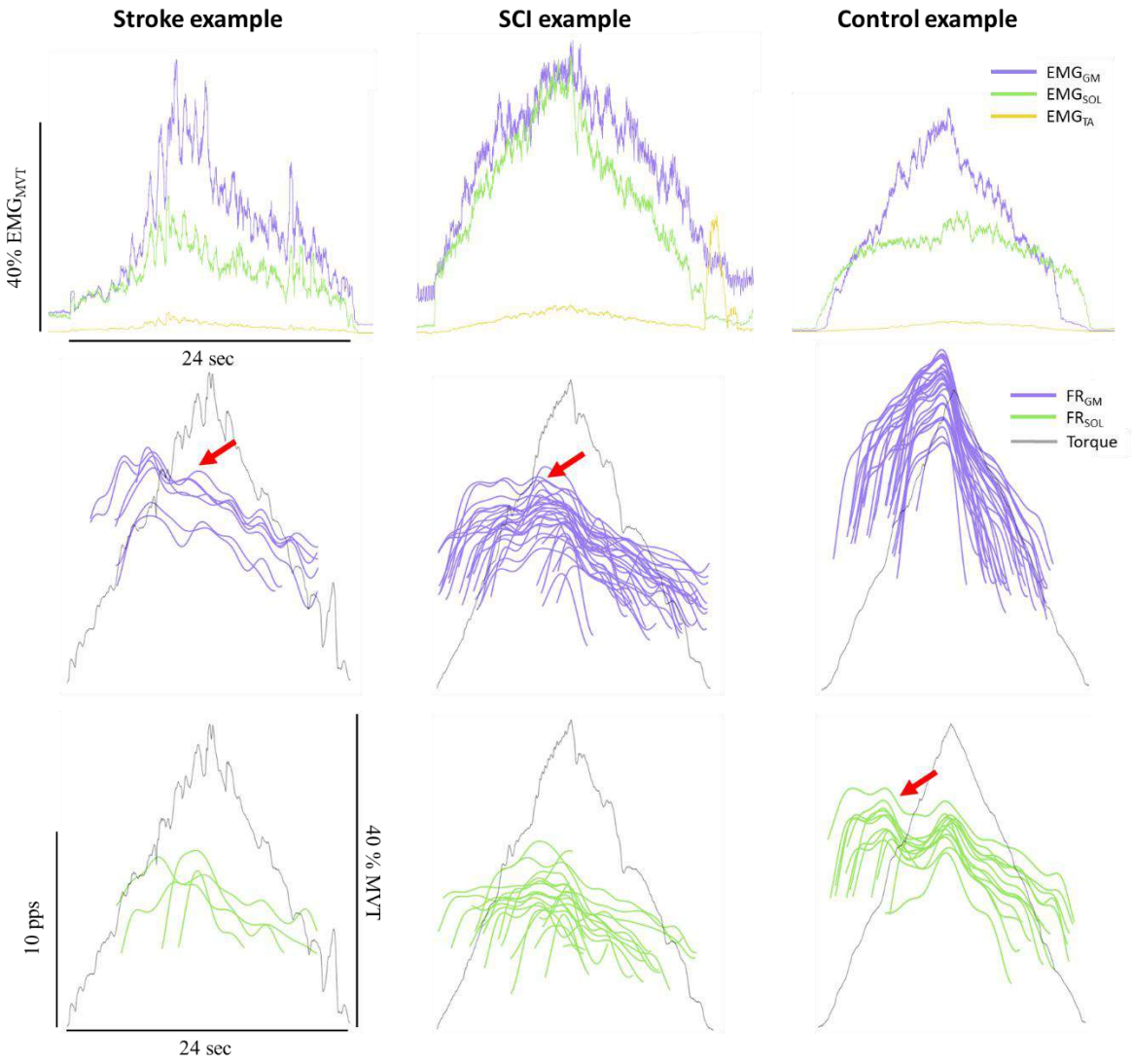

Figure 68. Negative rate modulation occurs in all populations. *For each population, a participant displaying negative rate modulation is shown. The top panel shows EMG amplitude for the gastrocnemius medialis (GM), soleus (SOL), and tibialis anterior (TA). The middle and lower panels show the corresponding firing rates for the GM (purple) and SOL (green), respectively. Red arrows indicate the occurrence of negative rate modulation.*

2. Recruitment threshold

Besides rate coding, force is determined by the recruitment of additional motor units. In stroke, it is often argued that motor unit recruitment thresholds are reduced and the range of recruitment thresholds is compressed. These claims originate from studies assessing absolute recruitment torque, which report lower mean recruitment torque and reduced recruitment of the highest-threshold motor units (Gemperline et al., 1995). However, when analysis is based on absolute recruitment torque, a reduction in maximal torque, due to factors other than recruitment

threshold, can be sufficient to produce these results. This is likely the case, for example, because of reduced rate coding or muscle atrophy. Regarding SCI, it is often argued that motor unit recruitment plays a greater role in force production, because units are recruited up to higher relative forces than normal (Thomas et al., 2014). But here again, reduced rate coding alone may explain this observation. Indeed, if there is no capacity to increase force through firing rate, then the gap between the highest recruited motor units and maximal voluntary torque is reduced. Our attempt in this thesis to gain more insight regarding recruitment thresholds was to estimate motor unit size through their MUAP amplitude. As higher-threshold motor units are larger, MUAP amplitude provides an indirect estimate. Control individuals displayed higher MUAP amplitudes at 40% MVT than SCI, and even more so compared to stroke. This means that, to produce 40% MVT, SCI and stroke individuals do not recruit their highest-threshold motor units despite lower firing rates, suggesting that they may have a limited ability to recruit these units. Overall, knowledge regarding changes in recruitment strategies remains limited. In our opinion, the two key questions are whether the synaptic input required to recruit the same motor unit is altered, and whether the remaining synaptic input is sufficient to recruit the full motor unit pool. However, new approaches are required to address these questions in humans.

◥ CLINICAL IMPLICATION

A result we did not discuss so far is that control and post-stroke or post-SCI individuals displayed very similar synaptic input organisation at the same absolute torque (the 30 N·m contraction). In other words, healthy individuals exhibit adaptations in synaptic input organisation with increasing contraction intensity. In particular, and consistent with other studies (Škarabot et al., 2025), they shift toward a more pronounced push–pull pattern as intensity increases. It is thus possible that this adaptive capacity is lost after SCI and stroke. The notion of repertoire, for example used to describe the loss of independence in flexor synergy patterns after stroke, could be extended to a reduced repertoire of synaptic input organisation and might be a fruitful way of approaching these impairments.

This notion is consistent with the paradoxical coexistence of overactivity at rest and paresis during voluntary contraction. Indeed, without the ability to adapt synaptic inputs, the motor system may be constrained to a fixed operating state, one that permits some facilitation of motor output but is associated with excessive involuntary activity. This loss of flexibility is supported by studies showing hyperexcitability at rest but hypoactivity during voluntary contraction

(Chen & Perez, 2022; Vastano & Perez, 2020). The general pattern of progressive reorganisation from paresis to overactivity over time post-injury suggests that the central nervous system adopts the best fixed state while balancing multiple constraints: favoring stability over dexterity through increased co-contraction (Nielsen et al., 2020), favoring abnormal synergies over complete paresis (Ellis et al., 2009), and possibly favoring a proportional inhibition pattern, which enhances precision at the expense of strength.

Identifying the neural circuits underlying these abnormalities is critical to guide treatment strategies. These changes could be constrained by anatomical limitations, for example if the reticulospinal tract represents the primary remaining pathway for voluntary activation, with limited capacity for selective control and strong neuromodulatory drive. In such cases, attempts to restore synaptic inputs purely through plasticity may have limited effectiveness. Rehabilitation practitioners should therefore consider anatomical constraints when designing interventions and managing expectations, as patients may already operate near the optimal solution allowed by their remaining neural pathways. Whether these changes are driven by structural constraints or reorganisation, the reduced repertoire of synaptic input organisation highlights the limitations of therapies targeting a presupposed pathological fixed levels of excitation, inhibition, or neuromodulation. Indeed, any static level may be maladaptive depending on task demands. Thus, while pharmacological treatments are effective for specific signs (e.g., Baclofen for spasms), they remain limited in addressing the fundamental loss of adaptability.

In contrast, more appropriate therapeutic strategies would aim to restore dynamic sensorimotor integration, enabling flexible adaptation to varying task demands and environments (Nielsen et al., 2020). However, such approaches are constrained by the limits of neural plasticity. When these limits are reached, compensatory strategies become necessary. One promising avenue is to leverage residual motoneuron activity, decoded via EMG decomposition, to control external devices such as exoskeletons (Grison et al., 2025). However, the results of this thesis complement the well-supported view that movement is not limited to muscle contraction but also involves interaction with the environment and adaptation to nonlinear muscle–tendon properties, which notably require integration of sensory inputs, with their associated associated challenges.

◥ PERSPECTIVES

In this thesis, the approach used to estimate motoneuron synaptic inputs was to calculate specific features in the motoneuron firing pattern that are known to be linearly associated with synaptic input parameters. For example, a reduced attenuation slope is indicative of a positive relation between excitatory and inhibitory conductances (i.e., a proportional inhibitory pattern). Thus, by observing a reduction in attenuation slope after SCI and stroke, we could infer that these injuries lead to a more proportional pattern of inhibition than in control individuals. On one hand, this inference procedure is simple and justified because of the linear relationship between the extracted features and specific input characteristics. On the other hand, it is limited to comparisons of relative differences across populations. For example, we can state that SCI and stroke individuals likely exhibit a more proportional pattern of inhibition than control individuals, but we cannot estimate the precise value nor quantify the uncertainty of this inference. How can these limitations be overcome?

A first solution is to mimic the reverse engineering approach described previously (Chardon et al., 2024) by iteratively adjusting a noisy excitatory conductance to align the cumulative spike trains of simulated motoneurons with those from experimental data. As only some iterations produce firing patterns similar to the observed ones (in terms of quantified features), the space of synaptic inputs that lead to these results defines the set of possible underlying synaptic input organisations. In addition, this approach can reveal input configurations that fail to reproduce the observed data, making them unlikely candidates. This approach was used to assess the effect of contraction intensity and revealed that only a shift towards a strong push–pull inhibitory pattern is consistent with the increase in firing rates observed at high intensity (Škarabot et al., 2025).

A theoretically more robust approach would be to directly use experimental data to predict synaptic inputs. In this regard, the fitted regressions used in Chardon et al. (2024) could be used to predict synaptic inputs (e.g., the level of neuromodulation). However, such a frequentist approach treats synaptic parameters as fixed but unknown values and provides a single best estimate, with uncertainty expressed only in terms of variability of the observed features (such as prediction intervals). This is inappropriate because different synaptic input organisations can lead to the same firing output, making the exact inputs indistinguishable from the observed firing. This issue, where an exact solution may not exist or may not be unique, is commonly

referred to as an inverse or ill-posed problem and arises in many domains (O'Sullivan, 1986). One way to capture the correct uncertainty structure is a Bayesian approach, which treats synaptic input parameters as random variables and explicitly models uncertainty about them, capturing the fact that multiple synaptic configurations may explain the same firing behaviour. More specifically, a promising approach to address this inverse problem is simulation-based inference (Cranmer et al., 2020). The general principle is to run the model with many different synaptic inputs to motoneurons, generate the corresponding simulated firing patterns, and use these simulations to learn the probabilistic relationship between inputs and outputs. In this way, a neural network can approximate the distribution of synaptic inputs most compatible with the observed data, thereby enabling inference directly from experimental observations. Such an approach has been used recently in human motoneurons, enabling non-invasive estimation of recurrent inhibition during voluntary contraction (Dernoncourt et al., 2026).

One recurring theme emerging from the results of this thesis is the role of recurrent inhibition in shaping motoneuron synaptic inputs, raising the following questions: Is recurrent inhibition the primary contributor to the modulation of PIC-mediated prolongation with muscle length? Does it underlie the variability of PIC-mediated prolongation across muscles? Does altered recurrent inhibition explain changes in inhibitory patterns in central nervous system injuries? To address these questions, it would be theoretically possible to combine the highly biophysically realistic motoneuron model described in this thesis (Powers & Heckman, 2017), which integrates PIC conductances, with recurrent spinal pathways as implemented in Dernoncourt et al., (2026). From this model, these hypotheses could be tested using simulation-based inference, where a trained neural network would learn the contribution of recurrent inhibition to the synaptic inputs and then be applied to experimental data. Such an approach would allow inference of both the types of inputs (excitatory, inhibitory, neuromodulatory) and the specific pathways that mediate them.

Our work also has clinical implications. As revealed by the supplementary analyses, the same clinical sign (paresis, quantified through firing rate) may arise from different motoneuron synaptic input organisations that do not correlate with impairments, such as antagonist coactivation or spasticity. As a consequence, if a therapeutic intervention aims to address the specific motoneuron input deficits underlying abnormal motoneuron behaviour, it is necessary to assess synaptic input organisation, which cannot be inferred from clinical signs alone. In addition, the differences between our results obtained during voluntary contraction and those reported during rest or involuntary contraction suggest that synaptic inputs should be assessed under

functionally relevant conditions. The fundamental adaptability of synaptic input commands also requires caution when using pharmacological treatments that may alter synaptic inputs in a relatively fixed manner. In this regard, further studies are required to assess the effects of pharmacological treatments on synaptic inputs depending on both dose and motor task. It is possible that current treatments effective for involuntary signs (e.g., Baclofen for spasms) may be detrimental with respect to paresis, and that this has not been detected due to insufficient assessment of voluntary motor impairments. We can even question whether early use of GABAergic medication may aggravate the reduced adaptability of inhibitory inputs observed at the chronic stage**.**

Our finding of muscle-length-dependent alterations in rate coding (and thus in paresis) should be complemented by evaluating their functional consequences. In particular, determining whether these alterations result in functional weakness and persist during dynamic tasks such as walking would help establish their functional relevance. Finally, the current best assessment of paresis is the interpolated twitch technique (Allen et al., 1995; Klein et al., 2010b). This method provides an estimate of voluntary activation but is uncomfortable or even painful. Conversely, developing non-invasive methods to determine motoneuron behaviour at high contraction intensities in a clinical setting would allow a direct and painless characterisation, leading to better evaluation of interventions and improved therapeutic strategies.

◥ CONCLUSION

The global objective of this thesis was to better define the organisation of synaptic inputs to motoneurons during voluntary contraction after stroke and SCI, and to determine how these inputs adapt to changes in inhibitory input in both health and disease. Our results revealed a shift in the inhibitory–excitatory balance towards greater inhibition after both SCI and stroke, compared with controls. However, estimates of neuromodulatory input were higher after stroke than in controls, whereas no difference was observed between SCI and control individuals. Our results also showed that firing rates and PIC-induced prolongation of motoneuron firing were reduced at longer muscle lengths and during antagonist tendon vibration in healthy individuals, but not in SCI and stroke individuals. In healthy individuals, these results were associated with increased inhibitory input and may represent an adaptation to variations in the muscle's force-generating capacity with changes in muscle length. Conversely, in chronic stroke and SCI, this may reflect muscle-length paresis and, more broadly, a reduced capacity to adapt inhibitory

input to mechanical constraints. These changes in synaptic input after stroke and SCI were associated with reduced rate-coding capacity, suggesting a reduced maximal capacity to increase motoneuron firing rates after stroke and SCI, ultimately contributing to muscle weakness.

BIBLIOGRAPHY

Adams, H. P., Bendixen, B. H., Kappelle, L. J., Biller, J., Love, B. B., Gordon, D. L., & Marsh, E. E. (1993). Classification of subtype of acute ischemic stroke. Definitions for use in a multicenter clinical trial. TOAST. Trial of Org 10172 in Acute Stroke Treatment. *Stroke*, *24*(1), 35-41. https://doi.org/10.1161/01.str.24.1.35

Adams, M. M., & Hicks, A. L. (2005). Spasticity after spinal cord injury. *Spinal Cord*, *43*(10), 577-586. https://doi.org/10.1038/sj.sc.3101757

Adams, R. A., Shipp, S., & Friston, K. J. (2013). Predictions not commands : Active inference in the motor system. *Brain Structure and Function*, *218*(3), 611-643. https://doi.org/10.1007/s00429-012-0475-5

Allen, G. M., Gandevia, S. C., & McKenzie, D. K. (1995). Reliability of measurements of muscle strength and voluntary activation using twitch interpolation. *Muscle & Nerve*, *18*(6), 593-600. https://doi.org/10.1002/mus.880180605

Aston-Jones, G., Chen, S., Zhu, Y., & Oshinsky, M. L. (2001). A neural circuit for circadian regulation of arousal. *Nature Neuroscience*, *4*(7), 732-738. https://doi.org/10.1038/89522

Avrillon, S., Hug, F., Baker, S. N., Gibbs, C., & Farina, D. (2024). Tutorial on MUedit : An open-source software for identifying and analysing the discharge timing of motor units from electromyographic signals. *Journal of Electromyography and Kinesiology*, *77*, 102886. https://doi.org/10.1016/j.jelekin.2024.102886

Avrillon, S., Hug, F., Enoka, R. M., Caillet, A. H., & Farina, D. (2024). The identification of extensive samples of motor units in human muscles reveals diverse effects of neuromodulatory inputs on the rate coding. *eLife*, *13*, RP97085. https://doi.org/10.7554/eLife.97085.3

Aymard, C. (2000). Presynaptic inhibition and homosynaptic depression : A comparison between lower and upper limbs in normal human subjects and patients with hemiplegia. *Brain*, *123*(8), 1688-1702. https://doi.org/10.1093/brain/123.8.1688

Azim, E., Jiang, J., Alstermark, B., & Jessell, T. M. (2014). Skilled reaching relies on a V2a propriospinal internal copy circuit. *Nature*, *508*(7496), 357-363. https://doi.org/10.1038/nature13021

Baines, A., Glover, I. S., Baker, A. M. E., Krakauer, J. W., & Baker, S. N. (s. d.). *Extent of damage to descending output from cortex rather than to specific corΘcal regions drives the emergence of flexor synergy in non-human primates*.

Baker, S. N. (2011). The primate reticulospinal tract, hand function and functional recovery. *The Journal of Physiology*, *589*(23), 5603-5612. https://doi.org/10.1113/jphysiol.2011.215160

Baker, S. N., & Perez, M. A. (2017). Reticulospinal Contributions to Gross Hand Function after Human Spinal Cord Injury. *The Journal of Neuroscience*, *37*(40), 9778-9784. https://doi.org/10.1523/JNEUROSCI.3368-16.2017

Bareyre, F. M., Kerschensteiner, M., Raineteau, O., Mettenleiter, T. C., Weinmann, O., & Schwab, M. E. (2004). The injured spinal cord spontaneously forms a new intraspinal circuit in adult rats. *Nature Neuroscience*, *7*(3), 269-277. https://doi.org/10.1038/nn1195

Bar-On, L., Aertbeliën, E., Wambacq, H., Severijns, D., Lambrecht, K., Dan, B., Huenaerts, C., Bruyninckx, H., Janssens, L., Van Gestel, L., Jaspers, E., Molenaers, G., & Desloovere, K. (2013). A clinical measurement to quantify spasticity in children with cerebral palsy by integration of multidimensional signals. *Gait & Posture*, *38*(1), 141-147. https://doi.org/10.1016/j.gaitpost.2012.11.003

Baude, M., Nielsen, J. B., & Gracies, J.-M. (2019). The neurophysiology of deforming spastic paresis : A revised taxonomy. *Annals of Physical and Rehabilitation Medicine*, *62*(6), 426-430. https://doi.org/10.1016/j.rehab.2018.10.004

Beauchamp, J. A., Hassan, A. S., McPherson, L. M., Negro, F., Pearcey, G. E. P., Cummings, M., Heckman, C., & Dewald, J. P. A. (2023). *Motor unit firing rate modulation is more impaired during flexion synergy-driven contractions of the biceps brachii in chronic stroke* [Preprint]. Neurology. https://doi.org/10.1101/2023.11.22.23298905

Beauchamp, J. A., Khurram, O. U., Dewald, J. P. A., Heckman, C., & Pearcey, G. E. P. (2022). A computational approach for generating continuous estimates of motor unit discharge rates and visualizing population discharge characteristics. *Journal of Neural Engineering*, *19*(1), 016007. https://doi.org/10.1088/1741-2552/ac4594

Beauchamp, J. A., Pearcey, G. E. P., Khurram, O. U., Chardon, M., Wang, Y. C., Powers, R. K., Dewald, J. P. A., & Heckman, C. (2023). A geometric approach to quantifying the neuromodulatory effects of persistent inward currents on individual motor unit discharge patterns. *Journal of Neural Engineering*, *20*(1), 016034. https://doi.org/10.1088/1741-2552/acb1d7

Beauchamp, J. A., Pearcey, G. E. P., Khurram, O. U., Negro, F., Dewald, J. P. A., & Heckman, C. J. (2025). Intrinsic properties of spinal motoneurons degrade ankle torque control in humans. *The Journal of Physiology*, *603*(8), 2443-2463. https://doi.org/10.1113/JP287446

Beauchamp, J., Urday, S., Plaisier, T., Heckman, C., & Dewald, J. (2022). Acute Attenuation of Motor Impairments With a Noradrenergic Pharmacological Agent in Chronic Hemiparetic Stroke. *Archives of Physical Medicine and Rehabilitation*, *103*(12), e117. https://doi.org/10.1016/j.apmr.2022.08.743

Beauchamp, James. A., Pearcey, G. E. P., Khurram, O. U., Negro, F., Dewald, J. P. A., & Heckman, Cj. (2023). *Intrinsic properties of spinal motoneurons degrade ankle torque control in humans* [Preprint]. Physiology. https://doi.org/10.1101/2023.10.23.563670

Bédard, P. J., Tremblay, L. E., Barbeau, H., Filion, M., Maheux, R., Richards, C. L., & DiPaolo, T. (1987). Action of 5-hydroxytryptamine, substance P, thyrotropin-releasing hormone and clonidine on motoneurone excitability. *The Canadian Journal of Neurological Sciences. Le Journal Canadien Des Sciences Neurologiques*, *14*(3 Suppl), 506-509. https://doi.org/10.1017/s0317167100038002

Beer, R. F., Dewald, J. P. A., & Rymer, W. Z. (2000). Deficits in the coordination of multijoint arm movements in patients with hemiparesis : Evidence for disturbed control of limb dynamics. *Experimental Brain Research*, *131*(3), 305-319. https://doi.org/10.1007/s002219900275

Bennett, D. J. (2008). Demystifying Spasticity : Reply to Dietz. *Journal of Neurophysiology*, *99*(2), 1041-1043. https://doi.org/10.1152/jn.01279.2007

Bennett, D. J., Hultborn, H., Fedirchuk, B., & Gorassini, M. (1998). Short-Term Plasticity in Hindlimb Motoneurons of Decerebrate Cats. *Journal of Neurophysiology*, *80*(4), 2038-2045. https://doi.org/10.1152/jn.1998.80.4.2038

Bennett, D. J., Li, Y., Harvey, P. J., & Gorassini, M. (2001). Evidence for Plateau Potentials in Tail Motoneurons of Awake Chronic Spinal Rats With Spasticity. *Journal of Neurophysiology*, *86*(4), 1972-1982. https://doi.org/10.1152/jn.2001.86.4.1972

Berg, R. W., Willumsen, A., & Lindén, H. (2019). When networks walk a fine line : Balance of excitation and inhibition in spinal motor circuits. *Current Opinion in Physiology*, *8*, 76-83. https://doi.org/10.1016/j.cophys.2019.01.006

Besomi, M., Hodges, P. W., Clancy, E. A., Van Dieën, J., Hug, F., Lowery, M., Merletti, R., Søgaard, K., Wrigley, T., Besier, T., Carson, R. G., Disselhorst-Klug, C., Enoka, R. M., Falla, D., Farina, D., Gandevia, S., Holobar, A., Kiernan, M. C., McGill, K., … Tucker, K. (2020). Consensus for experimental design in electromyography (CEDE) project : Amplitude normalization matrix. *Journal of Electromyography and Kinesiology*, *53*, 102438. https://doi.org/10.1016/j.jelekin.2020.102438

Binder, M. D., Powers, R. K., & Heckman, C. J. (2020). Nonlinear Input-Output Functions of Motoneurons. *Physiology*, *35*(1), 31-39. https://doi.org/10.1152/physiol.00026.2019

Bizzi, E., & Cheung, V. C. K. (2013). The neural origin of muscle synergies. *Frontiers in Computational Neuroscience*, *7*, 51. https://doi.org/10.3389/fncom.2013.00051

Blum, K. P., Lamotte D'Incamps, B., Zytnicki, D., & Ting, L. H. (2017). Force encoding in muscle spindles during stretch of passive muscle. *PLOS Computational Biology*, *13*(9), e1005767. https://doi.org/10.1371/journal.pcbi.1005767

Boulenguez, P., Liabeuf, S., Bos, R., Bras, H., Jean-Xavier, C., Brocard, C., Stil, A., Darbon, P., Cattaert, D., Delpire, E., Marsala, M., & Vinay, L. (2010). Down-regulation of the potassium-chloride cotransporter KCC2 contributes to spasticity after spinal cord injury. *Nature Medicine*, *16*(3), 302-307. https://doi.org/10.1038/nm.2107

Bui, T. V., Grande, G., & Rose, P. K. (2008). Relative Location of Inhibitory Synapses and Persistent Inward Currents Determines the Magnitude and Mode of Synaptic Amplification in Motoneurons. *Journal of Neurophysiology*, *99*(2), 583-594. https://doi.org/10.1152/jn.00718.2007

Burke, D., Hagbarth, K. E., Löfstedt, L., & Wallin, B. G. (1976). The responses of human muscle spindle endings to vibration of non-contracting muscles. *The Journal of Physiology*, *261*(3), 673-693. https://doi.org/10.1113/jphysiol.1976.sp011580

Burke, D., Wissel, J., & Donnan, G. A. (2013). Pathophysiology of spasticity in stroke. *Neurology*, *80*(Issue 3, Supplement 2), S20-S26. https://doi.org/10.1212/WNL.0b013e31827624a7

Byblow, W. D., Stinear, C. M., Barber, P. A., Petoe, M. A., & Ackerley, S. J. (2015). Proportional recovery after stroke depends on corticomotor integrity. *Annals of Neurology*, *78*(6), 848-859. https://doi.org/10.1002/ana.24472

Caillet, A. H., Avrillon, S., Kundu, A., Yu, T., Phillips, A. T. M., Modenese, L., & Farina, D. (2023). Larger and Denser : An Optimal Design for Surface Grids of EMG Electrodes to Identify Greater and More Representative Samples of Motor Units. *Eneuro*, *10*(9), ENEURO.0064-23.2023. https://doi.org/10.1523/ENEURO.0064-23.2023

Carmichael, S. T. (2016). The 3 Rs of Stroke Biology : Radial, Relayed, and Regenerative. *Neurotherapeutics*, *13*(2), 348-359. https://doi.org/10.1007/s13311-015-0408-0

Chardon, M., Heckman, C. J., & Rymer, W. Z. (2026). A new perspective on spinal motoneuron persistent currents : Predictive compensation for muscle nonlinearities. *The Journal of Physiology*, JP289912. https://doi.org/10.1113/JP289912

Chardon, M. K., Wang, Y. C., Garcia, M., Besler, E., Beauchamp, J. A., D'Mello, M., Powers, R. K., & Heckman, C. J. (2024). Supercomputer framework for reverse engineering firing patterns of neuron populations to identify their synaptic inputs. *eLife*, *12*, RP90624. https://doi.org/10.7554/eLife.90624

Chen, B., & Perez, M. A. (2022). Altered regulation of Ia afferent input during voluntary contraction in humans with spinal cord injury. *eLife*, *11*, e80089. https://doi.org/10.7554/eLife.80089

Chen, B., Sangari, S., Lorentzen, J., Nielsen, J. B., & Perez, M. A. (2020). Bilateral and asymmetrical contributions of passive and active ankle plantar flexors stiffness to spasticity in humans with spinal cord injury. *Journal of Neurophysiology*, *124*(3), 973-984. https://doi.org/10.1152/jn.00044.2020

Chou, L.-W., Palmer, J. A., Binder-Macleod, S., & Knight, C. A. (2013). Motor unit rate coding is severely impaired during forceful and fast muscular contractions in individuals post stroke. *Journal of Neurophysiology*, *109*(12), 2947-2954. https://doi.org/10.1152/jn.00615.2012

Cleland, B. T., & Madhavan, S. (2021). Ipsilateral motor pathways to the lower limb after stroke : Insights and opportunities. *Journal of Neuroscience Research*, *99*(6), 1565-1578. https://doi.org/10.1002/jnr.24822

Colard, J., Duclay, J., Betus, Y., Cattagni, T., & Jubeau, M. (2024). *Muscle length modulates recurrent inhibition and post-activation depression differently according to contraction type*. https://doi.org/10.1101/2024.12.10.627478

Colard, J., Duclay, J., Betus, Y., Cattagni, T., & Jubeau, M. (2025). Muscle Length Modulates Recurrent Inhibition and Presynaptic Inhibition of Ia Afferents Differently Depending on Type of Contraction. *European Journal of Neuroscience*, *62*(1), e70172. https://doi.org/10.1111/ejn.70172

Collinger, J. L., Wodlinger, B., Downey, J. E., Wang, W., Tyler-Kabara, E. C., Weber, D. J., McMorland, A. J., Velliste, M., Boninger, M. L., & Schwartz, A. B. (2013). High-performance neuroprosthetic control by an individual with tetraplegia. *The Lancet*, *381*(9866), 557-564. https://doi.org/10.1016/S0140-6736(12)61816-9

Courtine, G., Song, B., Roy, R. R., Zhong, H., Herrmann, J. E., Ao, Y., Qi, J., Edgerton, V. R., & Sofroniew, M. V. (2008). Recovery of supraspinal control of stepping via indirect propriospinal relay connections after spinal cord injury. *Nature Medicine*, *14*(1), 69-74. https://doi.org/10.1038/nm1682

Cramer, S. C. (2008). Repairing the human brain after stroke : I. Mechanisms of spontaneous recovery. *Annals of Neurology*, *63*(3), 272-287. https://doi.org/10.1002/ana.21393

Cranmer, K., Brehmer, J., & Louppe, G. (2020). The frontier of simulation-based inference. *Proceedings of the National Academy of Sciences of the United States of America*, *117*(48), 30055-30062. https://doi.org/10.1073/pnas.1912789117

Cremoux, S., Amarantini, D., Tallet, J., Dal Maso, F., & Berton, E. (2016). Increased antagonist muscle activity in cervical SCI patients suggests altered reciprocal inhibition during elbow contractions. *Clinical Neurophysiology*, *127*(1), 629-634. https://doi.org/10.1016/j.clinph.2015.03.016

Crone, C. (2003). Appearance of reciprocal facilitation of ankle extensors from ankle flexors in patients with stroke or spinal cord injury. *Brain*, *126*(2), 495-507. https://doi.org/10.1093/brain/awg036

Crone, C., Hultborn, H., Jespersen, B., & Nielsen, J. (1987). Reciprocal Ia inhibition between ankle flexors and extensors in man. *The Journal of Physiology*, *389*(1), 163-185. https://doi.org/10.1113/jphysiol.1987.sp016652

Crone, C., Hultborn, H., Kiehn, O., Mazieres, L., & Wigström, H. (1988). Maintained changes in motoneuronal excitability by short-lasting synaptic inputs in the decerebrate cat. *The Journal of Physiology*, *405*(1), 321-343. https://doi.org/10.1113/jphysiol.1988.sp017335

D'Amico, J. M., Condliffe, E. G., Martins, K. J. B., Bennett, D. J., & Gorassini, M. A. (2014). Recovery of neuronal and network excitability after spinal cord injury and implications for spasticity. *Frontiers in Integrative Neuroscience*, *8*. https://doi.org/10.3389/fnint.2014.00036

d'Avella, A., & Bizzi, E. (2005). Shared and specific muscle synergies in natural motor behaviors. *Proceedings of the National Academy of Sciences*, *102*(8), 3076-3081. https://doi.org/10.1073/pnas.0500199102

Day, S. J., & Hulliger, M. (2001). Experimental Simulation of Cat Electromyogram : Evidence for Algebraic Summation of Motor-Unit Action-Potential Trains. *Journal of Neurophysiology*, *86*(5), 2144-2158. https://doi.org/10.1152/jn.2001.86.5.2144

De Luca, C. J., Adam, A., Wotiz, R., Gilmore, L. D., & Nawab, S. H. (2006). Decomposition of Surface EMG Signals. *Journal of Neurophysiology*, *96*(3), 1646-1657. https://doi.org/10.1152/jn.00009.2006

De Luca, C. J., Nawab, S. H., & Kline, J. C. (2015). Clarification of methods used to validate surface EMG decomposition algorithms as described by Farina et al. (2014). *Journal of Applied Physiology*, *118*(8), 1084-1084. https://doi.org/10.1152/japplphysiol.00061.2015

Debenham, M. I. B., Franz, C. K., & Berger, M. J. (2024). Neuromuscular consequences of spinal cord injury : New mechanistic insights and clinical considerations. *Muscle & Nerve*, *70*(1), 12-27. https://doi.org/10.1002/mus.28070

Delwaide, P. J., & Oliver, E. (1988). Short-latency autogenic inhibition (IB inhibition) in human spasticity. *Journal of Neurology, Neurosurgery, and Psychiatry*, *51*(12), 1546-1550. https://doi.org/10.1136/jnnp.51.12.1546

Dernoncourt, F., Avrillon, S., Cattagni, T., Farina, D., & Hug, F. (s. d.). *Probabilistic inference of Homonymous and Heteronymous Recurrent Inhibition in Human Muscles from Large-Scale Motor Neuron Recordings*. https://doi.org/10.64898/2025.12.19.694963

DeVivo, M. J. (1997). Causes and costs of spinal cord injury in the United States. *Spinal Cord*, *35*(12), 809-813. https://doi.org/10.1038/sj.sc.3100501

Diedrichsen, J., Hashambhoy, Y., Rane, T., & Shadmehr, R. (2005). Neural correlates of reach errors. *The Journal of Neuroscience: The Official Journal of the Society for Neuroscience*, *25*(43), 9919-9931. https://doi.org/10.1523/JNEUROSCI.1874-05.2005

Dietz, V., & Sinkjaer, T. (2007). Spastic movement disorder : Impaired reflex function and altered muscle mechanics. *The Lancet Neurology*, *6*(8), 725-733. https://doi.org/10.1016/S1474-4422(07)70193-X

Dimitriou, M. (2022). Human muscle spindles are wired to function as controllable signal-processing devices. *eLife*, *11*, e78091. https://doi.org/10.7554/eLife.78091

Donnan, G. A., Fisher, M., Macleod, M., & Davis, S. M. (2008). Stroke. *Lancet*, *371*(9624), 1612-1623. https://doi.org/10.1016/S0140-6736(08)60694-7

Dorsch, S., Ada, L., & Canning, C. G. (2016). Lower Limb Strength Is Significantly Impaired in All Muscle Groups in Ambulatory People With Chronic Stroke : A Cross-Sectional Study. *Archives of Physical Medicine and Rehabilitation*, *97*(4), 522-527. https://doi.org/10.1016/j.apmr.2015.10.106

Duan, Z., Kizyte, A., Forslund, E. B., Gutierrez-Farewik, E. M., Herman, P., & Wang, R. (2026). Adaptation of motor unit synergies in the synergetic ankle plantarflexors in ambulatory persons with incomplete spinal cord injury. *Journal of NeuroEngineering and Rehabilitation*, *23*(1), 42. https://doi.org/10.1186/s12984-026-01874-2

Duchaine, F., Espagnacq, M., Bensmail, D., Regaert, C., Denys, P., & Levy, J. (2024). A novel approach to the epidemiology of people living with spinal cord injuries in France based on an original algorithm from public health insurance data. *Journal of Epidemiology and Population Health*, *72*(5), 202773. https://doi.org/10.1016/j.jeph.2024.202773

Edgley, S. A., Williams, E. R., & Baker, S. N. (2021). Spatial and Temporal Arrangement of Recurrent Inhibition in the Primate Upper Limb. *The Journal of Neuroscience*, *41*(7), 1443-1454. https://doi.org/10.1523/JNEUROSCI.1589-20.2020

Eken, T., & Kiehn, O. (1989). Bistable firing properties of soleus motor units in unrestrained rats. *Acta Physiologica Scandinavica*, *136*(3), 383-394. https://doi.org/10.1111/j.1748-1716.1989.tb08679.x

Ellis, M. D., Drogos, J., Carmona, C., Keller, T., & Dewald, J. P. A. (2012). Neck rotation modulates flexion synergy torques, indicating an ipsilateral reticulospinal source for impairment in stroke. *Journal of Neurophysiology*, *108*(11), 3096-3104. https://doi.org/10.1152/jn.01030.2011

Ellis, M. D., Sukal-Moulton, T., & Dewald, J. P. A. (2009). Progressive shoulder abduction loading is a crucial element of arm rehabilitation in chronic stroke. *Neurorehabilitation and Neural Repair*, *23*(8), 862-869. https://doi.org/10.1177/1545968309332927

EM-SCI Study Group, Van Middendorp, J. J., Hosman, A. J. F., Pouw, M. H., & Van De Meent, H. (2009). ASIA impairment scale conversion in traumatic SCI : Is it related with the ability to walk? A descriptive comparison with functional ambulation outcome measures in 273 patients. *Spinal Cord*, *47*(7), 555-560. https://doi.org/10.1038/sc.2008.162

Esposito, M. S., Capelli, P., & Arber, S. (2014). Brainstem nucleus MdV mediates skilled forelimb motor tasks. *Nature*, *508*(7496), 351-356. https://doi.org/10.1038/nature13023

Faist, M., Mazevet, D., Dietz, V., & Pierrot-Deseilligny, E. (1994). A quantitative assessment of presynaptic inhibition of la afferents in spastics : Differences in hemiplegics and paraplegics. *Brain*, *117*(6), 1449-1455. https://doi.org/10.1093/brain/117.6.1449

Falissard, B., & Gillibert, A. (2023). *Comprendre et utiliser les statistiques en médecine* (4e éd). Elsevier Masson.

Farina, D., & Enoka, R. M. (2011). Surface EMG decomposition requires an appropriate validation. *Journal of Neurophysiology*, *105*(2), 981-982; author reply 983-984. https://doi.org/10.1152/jn.00855.2010

Farina, D., & Holobar, A. (2016). Characterization of Human Motor Units From Surface EMG Decomposition. *Proceedings of the IEEE*, *104*(2), 353-373. https://doi.org/10.1109/JPROC.2015.2498665

Farina, D., Merletti, R., & Enoka, R. M. (2004). The extraction of neural strategies from the surface EMG. *Journal of Applied Physiology*, *96*(4), 1486-1495. https://doi.org/10.1152/japplphysiol.01070.2003

Farina, D., Merletti, R., & Enoka, R. M. (2014). The extraction of neural strategies from the surface EMG : An update. *Journal of Applied Physiology*, *117*(11), 1215-1230. https://doi.org/10.1152/japplphysiol.00162.2014

Farina, D., Negro, F., & Dideriksen, J. L. (2014). The effective neural drive to muscles is the common synaptic input to motor neurons. *The Journal of Physiology*, *592*(16), 3427-3441. https://doi.org/10.1113/jphysiol.2014.273581

Farina, D., Negro, F., Muceli, S., & Enoka, R. M. (2016). *Principles of Motor Unit Physiology Evolve With Advances in Technology*. *31*.

Feigin, V. L., Abate, M. D., Abate, Y. H., Abd ElHafeez, S., Abd-Allah, F., Abdelalim, A., Abdelkader, A., Abdelmasseh, M., Abd-Elsalam, S., Abdi, P., Abdollahi, A., Abdoun, M., Abd-Rabu, R., Abdulah, D. M., Abdullahi, A., Abebe, M., Abeldaño Zuñiga, R. A., Abhilash, E. S., Abiodun, O. O., … Murray, C. J. L. (2024). Global, regional, and national burden of stroke and its risk factors, 1990–2021 : A systematic analysis for the Global Burden of Disease Study 2021. *The Lancet Neurology*, *23*(10), 973-1003. https://doi.org/10.1016/S1474-4422(24)00369-7

Feldman, A. G. (1986). Once more on the equilibrium-point hypothesis (lambda model) for motor control. *Journal of Motor Behavior*, *18*(1), 17-54. https://doi.org/10.1080/00222895.1986.10735369

Feldman, A. G. (2015). *Referent control of action and perception : Challenging conventional theories in behavioral neuroscience*. Springer New York. https://doi.org/10.1007/978-1-4939-2736-4

Filli, L., Engmann, A. K., Zörner, B., Weinmann, O., Moraitis, T., Gullo, M., Kasper, H., Schneider, R., & Schwab, M. E. (2014). Bridging the gap : A reticulo-propriospinal detour bypassing an incomplete spinal cord injury. *The Journal of Neuroscience: The Official Journal of the Society for Neuroscience*, *34*(40), 13399-13410. https://doi.org/10.1523/JNEUROSCI.0701-14.2014

Fisher, K. M., Zaaimi, B., Edgley, S. A., & Baker, S. N. (2021). Extensive Cortical Convergence to Primate Reticulospinal Pathways. *The Journal of Neuroscience*, *41*(5), 1005-1018. https://doi.org/10.1523/JNEUROSCI.1379-20.2020

Fouad, K., Pedersen, V., Schwab, M. E., & Brösamle, C. (2001). Cervical sprouting of corticospinal fibers after thoracic spinal cord injury accompanies shifts in evoked motor responses. *Current Biology*, *11*(22), 1766-1770. https://doi.org/10.1016/S0960-9822(01)00535-8

Francic, A., & Holobar, A. (2021). On the Reuse of Motor Unit Filters in High Density Surface Electromyograms Recorded at Different Contraction Levels. *IEEE Access*, *9*, 115227-115236. https://doi.org/10.1109/ACCESS.2021.3104762

Franklin, T. C., & Granata, K. P. (2007). Role of reflex gain and reflex delay in spinal stability—A dynamic simulation. *Journal of Biomechanics*, *40*(8), 1762-1767. https://doi.org/10.1016/j.jbiomech.2006.08.007

Gemperline, J. J., Allen, S., Walk, D., & Rymer, W. Z. (1995). Characteristics of motor unit discharge in subjects with hemiparesis. *Muscle & Nerve*, *18*(10), 1101-1114. https://doi.org/10.1002/mus.880181006

Georgopoulos, A., Kettner, R., & Schwartz, A. (1988). Primate motor cortex and free arm movements to visual targets in three- dimensional space. II. Coding of the direction of movement by a neuronal population. *The Journal of Neuroscience*, *8*(8), 2928-2937. https://doi.org/10.1523/JNEUROSCI.08-08-02928.1988

Georgopoulos, A. P., & Carpenter, A. F. (2015). Coding of movements in the motor cortex. *Current Opinion in Neurobiology*, *33*, 34-39. https://doi.org/10.1016/j.conb.2015.01.012

Georgopoulos, A. P., Kalaska, J. F., Caminiti, R., & Massey, J. T. (1982). On the relations between the direction of two-dimensional arm movements and cell discharge in primate motor cortex. *The Journal of Neuroscience: The Official Journal of the Society for Neuroscience*, *2*(11), 1527-1537. https://doi.org/10.1523/JNEUROSCI.02-11-01527.1982

Glasser, M. F., Coalson, T. S., Robinson, E. C., Hacker, C. D., Harwell, J., Yacoub, E., Ugurbil, K., Andersson, J., Beckmann, C. F., Jenkinson, M., Smith, S. M., & Van Essen, D. C. (2016). A multi-modal parcellation of human cerebral cortex. *Nature*, *536*(7615), 171-178. https://doi.org/10.1038/nature18933

Glover, I. S., & Baker, S. N. (2022). Both Corticospinal and Reticulospinal Tracts Control Force of Contraction. *The Journal of Neuroscience*, *42*(15), 3150-3164. https://doi.org/10.1523/JNEUROSCI.0627-21.2022

Goldenberg, G. (2013). Apraxia. *WIREs Cognitive Science*, *4*(5), 453-462. https://doi.org/10.1002/wcs.1241

Gomes, M. M., Jenz, S. T., Beauchamp, J. A., Negro, F., Heckman, C. J., & Pearcey, G. E. P. (2024). Voluntary co-contraction of ankle muscles alters motor unit discharge characteristics and reduces estimates of persistent inward currents. *The Journal of Physiology*, *602*(17), 4237-4250. https://doi.org/10.1113/JP286539

Goodlich, B. I., Del Vecchio, A., Horan, S. A., & Kavanagh, J. J. (2023). Blockade of 5-HT $_2$ receptors suppresses motor unit firing and estimates of persistent inward currents during voluntary muscle contraction in humans. *The Journal of Physiology*, *601*(6), 1121-1138. https://doi.org/10.1113/JP284164

Goodlich, B. I., Pearcey, G. E. P., Del Vecchio, A., Horan, S. A., & Kavanagh, J. J. (2024). Antagonism of 5-HT $_2$ receptors attenuates self-sustained firing of human motor units. *The Journal of Physiology*, JP285867. https://doi.org/10.1113/JP285867

Gorassini, M. A. (2004). Role of motoneurons in the generation of muscle spasms after spinal cord injury. *Brain*, *127*(10), 2247-2258. https://doi.org/10.1093/brain/awh243

Gorassini, M. A., Bennett, D. J., & Yang, J. F. (1998). Self-sustained firing of human motor units. *Neuroscience Letters*, *247*(1), 13-16. https://doi.org/10.1016/S0304-3940(98)00277-8

Gorassini, M., Yang, J. F., Siu, M., & Bennett, D. J. (2002). Intrinsic Activation of Human Motoneurons : Possible Contribution to Motor Unit Excitation. *Journal of Neurophysiology*, *87*(4), 1850-1858. https://doi.org/10.1152/jn.00024.2001

Goreau, V., Hug, F., Jannou, A., Dernoncourt, F., Crouzier, M., & Cattagni, T. (2024). Estimates of persistent inward currents in lower limb muscles are not different between inactive, resistance-trained, and endurance-trained young males. *Journal of Neurophysiology*, *131*(2), 166-175. https://doi.org/10.1152/jn.00278.2023

Goreau, V., Hug, F., Simon, L., Le Sant, G., Gross, R., & Cattagni, T. (2026). *Disrupted Inhibitory-Excitatory Balance Underlies Spinal Motoneuron Dysfunction in Incomplete Spinal ord Injury*. Neuroscience. https://doi.org/10.64898/2026.02.14.705880

Goreau, V., Morvan, Q., Hug, F., Le Sant, G., Gross, R., & Cattagni, T. (2025). Modulation of persistent inward currents in alpha motoneurons with joint angle depends on muscle length. *Journal of Neurophysiology*, *134*(2), 493-503. https://doi.org/10.1152/jn.00097.2025

Goulding, M., Bourane, S., Garcia-Campmany, L., Dalet, A., & Koch, S. (2014). Inhibition downunder : An update from the spinal cord. *Current Opinion in Neurobiology*, *26*, 161-166. https://doi.org/10.1016/j.conb.2014.03.006

Gracies, J., Alter, K. E., Biering-Sørensen, B., Dewald, J. P. A., Dressler, D., Esquenazi, A., Franco, J. H., Jech, R., Kaji, R., Jin, L., Lim, E. C. H., Raghavan, P., Rosales, R., Shalash, A. S., Simpson, D. M., Suputtitada, A., Vecchio, M., Wissel, J., & for the Spasticity Study Group of the International Parkinson and Movement Disorders Society. (2024). Spastic Paresis : A Treatable Movement Disorder. *Movement Disorders*, mds.30038. https://doi.org/10.1002/mds.30038

Gracies, J.-M. (2005a). Pathophysiology of spastic paresis. I : Paresis and soft tissue changes. *Muscle & Nerve*, *31*(5), 535-551. https://doi.org/10.1002/mus.20284

Gracies, J.-M. (2005b). Pathophysiology of spastic paresis. II : Emergence of muscle overactivity. *Muscle & Nerve*, *31*(5), 552-571. https://doi.org/10.1002/mus.20285

Granit, R., Kernell, D., & Lamarre, Y. (1966). Algebraical summation in synaptic activation of motoneurones firing within the 'primary range' to injected currents. *The Journal of Physiology*, *187*(2), 379-399. https://doi.org/10.1113/jphysiol.1966.sp008097

Gray, V., Rice, C. L., & Garland, S. J. (2012). Factors That Influence Muscle Weakness Following Stroke and Their Clinical Implications : A Critical Review. *Physiotherapy Canada*, *64*(4), 415-426. https://doi.org/10.3138/ptc.2011-03

Grefkes, C., & Ward, N. S. (2014). Cortical Reorganization After Stroke : How Much and How Functional? *The Neuroscientist*, *20*(1), 56-70. https://doi.org/10.1177/1073858413491147

Grey, M. J., Klinge, K., Crone, C., Lorentzen, J., Biering-Sørensen, F., Ravnborg, M., & Nielsen, J. B. (2008). Post-activation depression of Soleus stretch reflexes in healthy and spastic humans. *Experimental Brain Research*, *185*(2), 189-197. https://doi.org/10.1007/s00221-007-1142-6

Grison, A., Mendez Guerra, I., Clarke, A. K., Muceli, S., Ibáñez, J., & Farina, D. (2025). Unlocking the full potential of high-density surface EMG : Novel non-invasive high-yield motor unit decomposition. *The Journal of Physiology*, *603*(8), 2281-2300. https://doi.org/10.1113/JP287913

Guzik, A., & Bushnell, C. (2017). Stroke Epidemiology and Risk Factor Management. *Continuum*, *23*(1), 15-39. https://doi.org/10.1212/CON.0000000000000416

Hagbarth, K. E., Wallin, G., & Löfstedt, L. (1973). Muscle spindle responses to stretch in normal and spastic subjects. *Scandinavian Journal of Rehabilitation Medicine*, *5*(4), 156-159.

Hammar, I., & Jankowska, E. (2003). Modulatory Effects of α1-, α2-, and β-Receptor Agonists on Feline Spinal Interneurons with Monosynaptic Input from Group I Muscle Afferents. *The Journal of Neuroscience*, *23*(1), 332-338. https://doi.org/10.1523/JNEUROSCI.23-01-00332.2003

Hammerbeck, U., Tyson, S. F., Samraj, P., Hollands, K., Krakauer, J. W., & Rothwell, J. (2021). The Strength of the Corticospinal Tract Not the Reticulospinal Tract Determines Upper-Limb Impairment Level and Capacity for Skill-Acquisition in the Sub-Acute Post-Stroke Period. *Neurorehabilitation and Neural Repair*, *35*(9), 812-822. https://doi.org/10.1177/15459683211028243

Hari, K., Lucas-Osma, A. M., Metz, K., Lin, S., Pardell, N., Roszko, D. A., Black, S., Minarik, A., Singla, R., Stephens, M. J., Pearce, R. A., Fouad, K., Jones, K. E., Gorassini, M. A., Fenrich, K. K., Li, Y., & Bennett, D. J. (2022). GABA facilitates spike propagation through branch points of sensory axons in the spinal cord. *Nature Neuroscience*, *25*(10), 1288-1299. https://doi.org/10.1038/s41593-022-01162-x

Harvey, P. J., Li, X., Li, Y., & Bennett, D. J. (2006). 5-HT_2 Receptor Activation Facilitates a Persistent Sodium Current and Repetitive Firing in Spinal Motoneurons of Rats With and Without Chronic Spinal Cord Injury. *Journal of Neurophysiology*, *96*(3), 1158-1170. https://doi.org/10.1152/jn.01088.2005

Hassan, A., Thompson, C. K., Negro, F., Cummings, M., Powers, R. K., Heckman, C. J., Dewald, J. P. A., & McPherson, L. M. (2020). Impact of parameter selection on estimates of motoneuron excitability using paired motor unit analysis. *Journal of Neural Engineering*, *17*(1), 016063. https://doi.org/10.1088/1741-2552/ab5eda

Heald, J. B., Franklin, D. W., & Wolpert, D. M. (2018). Increasing muscle co-contraction speeds up internal model acquisition during dynamic motor learning. *Scientific Reports*, *8*(1), 16355. https://doi.org/10.1038/s41598-018-34737-5

Heckman, C. J., & Binder, M. D. (1991). Computer simulation of the steady-state input-output function of the cat medial gastrocnemius motoneuron pool. *Journal of Neurophysiology*, *65*(4), 952-967. https://doi.org/10.1152/jn.1991.65.4.952

Heckman, C. J., & Binder, M. D. (1993). Computer simulations of the effects of different synaptic input systems on motor unit recruitment. *Journal of Neurophysiology*, *70*(5), 1827-1840. https://doi.org/10.1152/jn.1993.70.5.1827

Heckman, C. J., & Enoka, R. M. (2012). Motor Unit. In R. Terjung (Éd.), *Comprehensive Physiology* (1re éd., p. 2629-2682). Wiley. https://doi.org/10.1002/cphy.c100087

Heckman, C. J., Hyngstrom, A. S., & Johnson, M. D. (2008). Active properties of motoneurone dendrites : Diffuse descending neuromodulation, focused local inhibition: Active properties of motoneurones. *The Journal of Physiology*, *586*(5), 1225-1231. https://doi.org/10.1113/jphysiol.2007.145078

Heckman, C. J., Lee, R. H., & Brownstone, R. M. (2003). Hyperexcitable dendrites in motoneurons and their neuromodulatory control during motor behavior. *Trends in Neurosciences*, *26*(12), 688-695. https://doi.org/10.1016/j.tins.2003.10.002

Heckman, C. J., Mottram, C., Quinlan, K., Theiss, R., & Schuster, J. (2009a). Motoneuron excitability : The importance of neuromodulatory inputs. *Clinical Neurophysiology*, *120*(12), 2040-2054. https://doi.org/10.1016/j.clinph.2009.08.009

Heckman, C. J., Mottram, C., Quinlan, K., Theiss, R., & Schuster, J. (2009b). Motoneuron excitability : The importance of neuromodulatory inputs. *Clinical Neurophysiology*, *120*(12), 2040-2054. https://doi.org/10.1016/j.clinph.2009.08.009

Henneman, E., & Mendell, L. M. (1981). Functional Organization of Motoneuron Pool and its Inputs. *Comprehensive Physiology*, *1981*(12S2), 423-507. https://doi.org/10.1002/j.2040-4603.1981.tb00849.x

Hiersemenzel, L.-P., Curt, A., & Dietz, V. (s. d.). *From spinal shock to spasticity*.

Hochman, S., Garraway, S. M., Machacek, D. W., & Shay, B. L. (s. d.). *5-HT Receptors and the Neuromodulatory Control of Spinal Cord Function*.

Hoffman, B. W., Lichtwark, G. A., Carroll, T. J., & Cresswell, A. G. (2012). A comparison of two Hill-type skeletal muscle models on the construction of medial gastrocnemius length-tension curves in humans in vivo. *Journal of Applied Physiology*, *113*(1), 90-96. https://doi.org/10.1152/japplphysiol.00070.2012

Hökfelt, T., Arvidsson, U., Cullheim, S., Millhorn, D., Nicholas, A. P., Pieribone, V., Seroogy, K., & Ulfhake, B. (2000). Multiple messengers in descending serotonin neurons : Localization and functional implications. *Journal of Chemical Neuroanatomy*, *18*(1-2), 75-86. https://doi.org/10.1016/S0891-0618(99)00037-X

Holobar, A., Minetto, M. A., & Farina, D. (2014). Accurate identification of motor unit discharge patterns from high-density surface EMG and validation with a novel signal-based performance metric. *Journal of Neural Engineering*, *11*(1), 016008. https://doi.org/10.1088/1741-2560/11/1/016008

Holstege, J. C., & Kuypers, H. G. J. M. (1987). Brainstem projections to spinal motoneurons : An update. *Neuroscience*, *23*(3), 809-821. https://doi.org/10.1016/0306-4522(87)90160-6

Hounsgaard, J., Hultborn, H., Jespersen, B., & Kiehn, O. (1988). Bistability of alpha-motoneurones in the decerebrate cat and in the acute spinal cat after intravenous 5-hydroxytryptophan. *The Journal of Physiology*, *405*(1), 345-367. https://doi.org/10.1113/jphysiol.1988.sp017336

Hsiao, D. J. N., S. F. (2001). Knee muscle isometric strength, voluntary activation and antagonist co-contraction in the first six months after stroke. *Disability and Rehabilitation*, *23*(9), 379-386. https://doi.org/10.1080/0963828001006656

Hu, X., Suresh, N. L., Chardon, M. K., & Rymer, W. Z. (2015). Contributions of motoneuron hyperexcitability to clinical spasticity in hemispheric stroke survivors. *Clinical Neurophysiology*, *126*(8), 1599-1606. https://doi.org/10.1016/j.clinph.2014.11.005

Hug, F., Avrillon, S., Del Vecchio, A., Casolo, A., Ibanez, J., Nuccio, S., Rossato, J., Holobar, A., & Farina, D. (2021). Analysis of motor unit spike trains estimated from high-density surface electromyography is highly reliable across operators. *Journal of*

Electromyography and Kinesiology: Official Journal of the International Society of Electrophysiological Kinesiology, *58*, 102548. https://doi.org/10.1016/j.jelekin.2021.102548

Hug, F., Avrillon, S., Ibáñez, J., & Farina, D. (2023). Common synaptic input, synergies and size principle : Control of spinal motor neurons for movement generation. *The Journal of Physiology*, *601*(1), 11-20. https://doi.org/10.1113/JP283698

Hultborn, H., Denton, M. E., Wienecke, J., & Nielsen, J. B. (2003). Variable amplification of synaptic input to cat spinal motoneurones by dendritic persistent inward current. *The Journal of Physiology*, *552*(3), 945-952. https://doi.org/10.1113/jphysiol.2003.050971

Hyngstrom, A. S., Johnson, M. D., Miller, J. F., & Heckman, C. J. (2007). Intrinsic electrical properties of spinal motoneurons vary with joint angle. *Nature Neuroscience*, *10*(3), 363-369. https://doi.org/10.1038/nn1852

Ibrahim, I. K., Berger, W., Trippel, M., & Dietz, V. (1993). Stretch-induced electromyographic activity and torque in spastic elbow muscles : Differential modulation of reflex activity in passive and active motor tasks. *Brain*, *116*(4), 971-989. https://doi.org/10.1093/brain/116.4.971

Jacobs, B. L., Martín-Cora, F. J., & Fornal, C. A. (2002). Activity of medullary serotonergic neurons in freely moving animals. *Brain Research Reviews*, *40*(1-3), 45-52. https://doi.org/10.1016/S0165-0173(02)00187-X

Jakobsson, F., Grimby, L., & Edström, L. (1992). Motoneuron activity and muscle fibre type composition in hemiparesis. *Scandinavian Journal of Rehabilitation Medicine*, *24*(3), 115-119.

Jang, S. H., & Cho, M. J. (2022). Role of the Contra-Lesional Corticoreticular Tract in Motor Recovery of the Paretic Leg in Stroke : A Mini-Narrative Review. *Frontiers in Human Neuroscience*, *16*, 896367. https://doi.org/10.3389/fnhum.2022.896367

Jang, S. H., & Lee, S. J. (2019). Corticoreticular Tract in the Human Brain : A Mini Review. *Frontiers in Neurology*, *10*, 1188. https://doi.org/10.3389/fneur.2019.01188

Jankowska, E. (1992). Interneuronal relay in spinal pathways from proprioceptors. *Progress in Neurobiology*, *38*(4), 335-378. https://doi.org/10.1016/0301-0082(92)90024-9

Jankowska, E., Hammar, I., Chojnicka, B., & Hedén, C. H. (2000). Effects of monoamines on interneurons in four spinal reflex pathways from group I and/or group II muscle afferents. *European Journal of Neuroscience*, *12*(2), 701-714. https://doi.org/10.1046/j.1460-9568.2000.00955.x

Jayaraman, A., Gregory, C. M., Bowden, M., Stevens, J. E., Shah, P., Behrman, A. L., & Vandenborne, K. (2006). Lower extremity skeletal muscle function in persons with incomplete spinal cord injury. *Spinal Cord*, *44*(11), 680-687. https://doi.org/10.1038/sj.sc.3101892

Jenz, S. T., Beauchamp, J. A., Gomes, M. M., Negro, F., Heckman, C. J., & Pearcey, G. E. P. (2023). Estimates of persistent inward currents in lower limb motoneurons are larger in

females than in males. *Journal of Neurophysiology*, *129*(6), 1322-1333. https://doi.org/10.1152/jn.00043.2023

Jo, H. J., & Perez, M. A. (2020). Corticospinal-motor neuronal plasticity promotes exercise-mediated recovery in humans with spinal cord injury. *Brain*, *143*(5), 1368-1382. https://doi.org/10.1093/brain/awaa052

Johnson, M. D., & Heckman, C. J. (2014). Gain control mechanisms in spinal motoneurons. *Frontiers in Neural Circuits*, *8*. https://doi.org/10.3389/fncir.2014.00081

Johnson, M. D., Hyngstrom, A. S., Manuel, M., & Heckman, C. J. (2012). Push–Pull Control of Motor Output. *The Journal of Neuroscience*, *32*(13), 4592-4599. https://doi.org/10.1523/JNEUROSCI.4709-11.2012

Johnson, M. D., Thompson, C. K., Tysseling, V. M., Powers, R. K., & Heckman, C. J. (2017). Shar. *Journal of Neurophysiology*, *118*(1), 520-531. https://doi.org/10.1152/jn.00018.2017

Jutzeler, C. R., Freund, P., Huber, E., Curt, A., & Kramer, J. L. K. (2015). Neuropathic Pain and Functional Reorganization in the Primary Sensorimotor Cortex After Spinal Cord Injury. *The Journal of Pain*, *16*(12), 1256-1267. https://doi.org/10.1016/j.jpain.2015.08.008

Kandel, E. R., Koester, J. D., Mack, S. H., & Siegelbaum, S. A. (Éds.). (2021). *Principles of neural science* (Sixth edition). McGraw-Hill Education LLC.

Kang, Y., Ding, H., Zhou, H., Wei, Z., Liu, L., Pan, D., & Feng, S. (2017). Epidemiology of worldwide spinal cord injury : A literature review. *Journal of Neurorestoratology*, *Volume 6*, 1-9. https://doi.org/10.2147/JN.S143236

Katoozian, L., Tahan, N., Zoghi, M., & Bakhshayesh, B. (2018). The Onset and Frequency of Spasticity After First Ever Stroke. *Journal of the National Medical Association*, *110*(6), 547-552. https://doi.org/10.1016/j.jnma.2018.01.008

Katz, R., & Pierrot-Deseilligny, E. (1982). RECURRENT INHIBITION OF α—MOTONEURONS IN PATIENTS WITH UPPER MOTOR NEURON LESIONS. *Brain*, *105*(1), 103-124. https://doi.org/10.1093/brain/105.1.103

Keizer, K., & Kuypers, H. G. (1989). Distribution of corticospinal neurons with collaterals to the lower brain stem reticular formation in monkey (Macaca fascicularis). *Experimental Brain Research*, *74*(2), 311-318. https://doi.org/10.1007/BF00248864

Khan, S. I., & Burne, J. A. (2009). Afferents contributing to autogenic inhibition of gastrocnemius following electrical stimulation of its tendon. *Brain Research*, *1282*, 28-37. https://doi.org/10.1016/j.brainres.2009.04.048

Khurram, O. U., Pearcey, G. E. P., Chardon, M. K., Kim, E. H., García, M., & Heckman, C. J. (2022). The Cellular Basis for the Generation of Firing Patterns in Human Motor Units. In M. J. O'Donovan & M. Falgairolle (Éds.), *Vertebrate Motoneurons* (Vol. 28, p. 233-258). Springer International Publishing. https://doi.org/10.1007/978-3-031-07167-6_10

Kiehn, O., & Harris-Warrick, R. M. (1992). 5-HT modulation of hyperpolarization-activated inward current and calcium-dependent outward current in a crustacean motor neuron. *Journal of Neurophysiology*, *68*(2), 496-508. https://doi.org/10.1152/jn.1992.68.2.496

Kim, D. Y., Park, C., Chon, J. S., Ohn, S. H., Park, T. H., & Bang, I. K. (2005). Biomechanical Assessment with Electromyography of Post-Stroke Ankle Plantar Flexor Spasticity. *Yonsei Medical Journal*, *46*(4), 546. https://doi.org/10.3349/ymj.2005.46.4.546

Kim, H. E., Corcos, D. M., & Hornby, T. G. (2015). Increased spinal reflex excitability is associated with enhanced central activation during voluntary lengthening contractions in human spinal cord injury. *Journal of Neurophysiology*, *114*(1), 427-439. https://doi.org/10.1152/jn.01074.2014

Kizyte, A., Zhang, H., Forslund, E. B., Gutierrez-Farewik, E. M., & Wang, R. (2025). Neuromuscular adaptations in soleus and tibialis anterior muscles in persons with spinal cord injury. *Journal of NeuroEngineering and Rehabilitation*, *22*(1), 239. https://doi.org/10.1186/s12984-025-01794-7

Klein, C. S., Brooks, D., Richardson, D., McIlroy, W. E., & Bayley, M. T. (2010a). Voluntary activation failure contributes more to plantar flexor weakness than antagonist coactivation and muscle atrophy in chronic stroke survivors. *Journal of Applied Physiology*, *109*(5), 1337-1346. https://doi.org/10.1152/japplphysiol.00804.2009

Klein, C. S., Brooks, D., Richardson, D., McIlroy, W. E., & Bayley, M. T. (2010b). Voluntary activation failure contributes more to plantar flexor weakness than antagonist coactivation and muscle atrophy in chronic stroke survivors. *Journal of Applied Physiology*, *109*(5), 1337-1346. https://doi.org/10.1152/japplphysiol.00804.2009

Knikou, M. (2005). Effects of hip joint angle changes on intersegmental spinal coupling in human spinal cord injury. *Experimental Brain Research*, *167*(3), 381-393. https://doi.org/10.1007/s00221-005-0046-6

Knikou, M. (2008). The H-reflex as a probe : Pathways and pitfalls. *Journal of Neuroscience Methods*, *171*(1), 1-12. https://doi.org/10.1016/j.jneumeth.2008.02.012

Knikou, M., & Mummidisetty, C. K. (2011). Reduced reciprocal inhibition during assisted stepping in human spinal cord injury. *Experimental Neurology*, *231*(1), 104-112. https://doi.org/10.1016/j.expneurol.2011.05.021

Krakauer, J. W., & Carmichael, S. T. (2017). *Broken Movement : The Neurobiology of Motor Recovery after Stroke*. The MIT Press. https://doi.org/10.7551/mitpress/9310.001.0001

Kuo, J. J., Lee, R. H., Johnson, M. D., Heckman, H. M., & Heckman, C. J. (2003). Active Dendritic Integration of Inhibitory Synaptic Inputs In Vivo. *Journal of Neurophysiology*, *90*(6), 3617-3624. https://doi.org/10.1152/jn.00521.2003

Kuo, J. J., Lee, R. H., Zhang, L., & Heckman, C. J. (2006). Essential role of the persistent sodium current in spike initiation during slowly rising inputs in mouse spinal neurones. *The Journal of Physiology*, *574*(3), 819-834. https://doi.org/10.1113/jphysiol.2006.107094

Kuypers, H. G. J. M. (1964). The Descending Pathways to the Spinal Cord, their Anatomy and Function. In *Progress in Brain Research* (Vol. 11, p. 178-202). Elsevier. https://doi.org/10.1016/S0079-6123(08)64048-0

Kuznetsova, A., Brockhoff, P. B., & Christensen, R. H. B. (2017). **lmerTest** Package : Tests in Linear Mixed Effects Models. *Journal of Statistical Software*, *82*(13). https://doi.org/10.18637/jss.v082.i13

Kuzyk, S. L., Smart, R. R., Simpson, C. L., Fedorov, A., & Jakobi, J. M. (2018). Influence of fascicle length on twitch potentiation of the medial gastrocnemius across three ankle angles. *European Journal of Applied Physiology*, *118*(6), 1199-1207. https://doi.org/10.1007/s00421-018-3849-4

Laliberte, A. M., Goltash, S., Lalonde, N. R., & Bui, T. V. (2019). Propriospinal Neurons : Essential Elements of Locomotor Control in the Intact and Possibly the Injured Spinal Cord. *Frontiers in Cellular Neuroscience*, *13*, 512. https://doi.org/10.3389/fncel.2019.00512

Lamontagne, A., Richards, C. L., & Malouin, F. (2000). Coactivation during gait as an adaptive behavior after stroke. *Journal of Electromyography and Kinesiology*, *10*(6), 407-415. https://doi.org/10.1016/S1050-6411(00)00028-6

Lamy, J.-C., Wargon, I., Mazevet, D., Ghanim, Z., Pradat-Diehl, P., & Katz, R. (2009). Impaired efficacy of spinal presynaptic mechanisms in spastic stroke patients. *Brain*, *132*(3), 734-748. https://doi.org/10.1093/brain/awn310

Landau, W. M. (2004). Spasticity After Stroke : Why Bother? *Stroke*, *35*(8), 1787-1788. https://doi.org/10.1161/01.STR.0000136388.80433.eb

Laporte, Y., & Lloyd, D. P. C. (1952). Nature and Significance of the Reflex Connections Established by Large Afferent Fibers of Muscular Origin. *American Journal of Physiology-Legacy Content*, *169*(3), 609-621. https://doi.org/10.1152/ajplegacy.1952.169.3.609

Le Pera, D., Graven-Nielsen, T., Valeriani, M., Oliviero, A., Di Lazzaro, V., Tonali, P. A., & Arendt-Nielsen, L. (2001). Inhibition of motor system excitability at cortical and spinal level by tonic muscle pain. *Clinical Neurophysiology*, *112*(9), 1633-1641. https://doi.org/10.1016/S1388-2457(01)00631-9

Lee, R. H., & Heckman, C. J. (1999). Paradoxical Effect of QX-314 on Persistent Inward Currents and Bistable Behavior in Spinal Motoneurons In Vivo. *Journal of Neurophysiology*, *82*(5), 2518-2527. https://doi.org/10.1152/jn.1999.82.5.2518

Lee, R. H., & Heckman, C. J. (2000). Adjustable Amplification of Synaptic Input in the Dendrites of Spinal Motoneurons *In Vivo*. *The Journal of Neuroscience*, *20*(17), 6734-6740. https://doi.org/10.1523/JNEUROSCI.20-17-06734.2000

Lemon, R. N. (2008). Descending Pathways in Motor Control. *Annual Review of Neuroscience*, *31*(1), 195-218. https://doi.org/10.1146/annurev.neuro.31.060407.125547

Lemon, R. N., & Griffiths, J. (2005). Comparing the function of the corticospinal system in different species : Organizational differences for motor specialization? *Muscle & Nerve*, *32*(3), 261-279. https://doi.org/10.1002/mus.20333

Leonardi, M., Lee, H., Kostanjsek, N., Fornari, A., Raggi, A., Martinuzzi, A., Yáñez, M., Almborg, A.-H., Fresk, M., Besstrashnova, Y., Shoshmin, A., Castro, S. S., Cordeiro, E. S., Cuenot, M., Haas, C., Maart, S., Maribo, T., Miller, J., Mukaino, M., … Kraus de Camargo, O. (2022). 20 Years of ICF-International Classification of Functioning, Disability and Health : Uses and Applications around the World. *International Journal of Environmental Research and Public Health*, *19*(18), 11321. https://doi.org/10.3390/ijerph191811321

Leroy, F., Lamotte d'Incamps, B., Imhoff-Manuel, R. D., & Zytnicki, D. (2014). Early intrinsic hyperexcitability does not contribute to motoneuron degeneration in amyotrophic lateral sclerosis. *eLife*, *3*, e04046. https://doi.org/10.7554/eLife.04046

Levin, M. F., & Feldman, A. G. (1994). The role of stretch reflex threshold regulation in normal and impaired motor control. *Brain Research*, *657*(1-2), 23-30. https://doi.org/10.1016/0006-8993(94)90949-0

Levin, M. F., Kleim, J. A., & Wolf, S. L. (2009). What Do Motor "Recovery" and "Compensation" Mean in Patients Following Stroke? *Neurorehabilitation and Neural Repair*, *23*(4), 313-319. https://doi.org/10.1177/1545968308328727

Levin, M. F., Selles, R. W., Verheul, M. H., & Meijer, O. G. (2000). Deficits in the coordination of agonist and antagonist muscles in stroke patients : Implications for normal motor control. *Brain Research*, *853*(2), 352-369. https://doi.org/10.1016/s0006-8993(99)02298-2

Levine, A. J., Hinckley, C. A., Hilde, K. L., Driscoll, S. P., Poon, T. H., Montgomery, J. M., & Pfaff, S. L. (2014). Identification of a cellular node for motor control pathways. *Nature Neuroscience*, *17*(4), 586-593. https://doi.org/10.1038/nn.3675

Li, H., Wang, S.-R., Wang, L.-K., Chen, X.-F., Zhao, C.-J., Duan, S., Liu, N., & Wang, D.-S. (2010). Perihematomal Pathological Changes in Neurons and Astrocytes Following Acute Cerebral Hemorrhage. *International Journal of Neuroscience*, *120*(11), 683-690. https://doi.org/10.3109/00207454.2010.513460

Li, X., Holobar, A., Gazzoni, M., Merletti, R., Rymer, W. Z., & Zhou, P. (2015). Examination of Poststroke Alteration in Motor Unit Firing Behavior Using High-Density Surface EMG Decomposition. *IEEE Transactions on Biomedical Engineering*, *62*(5), 1242-1252. https://doi.org/10.1109/TBME.2014.2368514

Li, Y., & Bennett, D. J. (2003). Persistent Sodium and Calcium Currents Cause Plateau Potentials in Motoneurons of Chronic Spinal Rats. *Journal of Neurophysiology*, *90*(2), 857-869. https://doi.org/10.1152/jn.00236.2003

Li, Y., Gorassini, M. A., & Bennett, D. J. (2004). Role of Persistent Sodium and Calcium Currents in Motoneuron Firing and Spasticity in Chronic Spinal Rats. *Journal of Neurophysiology*, *91*(2), 767-783. https://doi.org/10.1152/jn.00788.2003

Liddell, E. G. T., & Sherrington, C. S. (1925). Recruitment and some other features of reflex inhibition. *Proceedings of the Royal Society of London. Series B, Containing Papers of a Biological Character*, *97*(686), 488-518. https://doi.org/10.1098/rspb.1925.0016

Lin, K.-H., Chen, Y.-C., Luh, J.-J., Wang, C.-H., & Chang, Y.-J. (2012). H-Reflex, Muscle Voluntary Activation Level, and Fatigue Index of Flexor Carpi Radialis in Individuals With Incomplete Cervical Cord Injury. *Neurorehabilitation and Neural Repair*, *26*(1), 68-75. https://doi.org/10.1177/1545968311418785

Llinás, R. R. (1988). The Intrinsic Electrophysiological Properties of Mammalian Neurons : Insights into Central Nervous System Function. *Science*, *242*(4886), 1654-1664. https://doi.org/10.1126/science.3059497

Lo, E. H. (2008). A new penumbra : Transitioning from injury into repair after stroke. *Nature Medicine*, *14*(5), 497-500. https://doi.org/10.1038/nm1735

Lorach, H., Galvez, A., Spagnolo, V., Martel, F., Karakas, S., Intering, N., Vat, M., Faivre, O., Harte, C., Komi, S., Ravier, J., Collin, T., Coquoz, L., Sakr, I., Baaklini, E., Hernandez-Charpak, S. D., Dumont, G., Buschman, R., Buse, N., … Courtine, G. (2023). Walking naturally after spinal cord injury using a brain-spine interface. *Nature*, *618*(7963), 126-133. https://doi.org/10.1038/s41586-023-06094-5

Lundell, H., Christensen, M. S., Barthélemy, D., Willerslev-Olsen, M., Biering-Sørensen, F., & Nielsen, J. B. (2011). Cerebral activation is correlated to regional atrophy of the spinal cord and functional motor disability in spinal cord injured individuals. *NeuroImage*, *54*(2), 1254-1261. https://doi.org/10.1016/j.neuroimage.2010.09.009

Macefield, V. G. (2013). Discharge rates and discharge variability of muscle spindle afferents in human chronic spinal cord injury. *Clinical Neurophysiology*, *124*(1), 114-119. https://doi.org/10.1016/j.clinph.2012.05.015

Macht, M. B., & Kuhn, R. A. (1948). The Occurrence of Extensor Spasm in Patients with Complete Transection of the Spinal Cord. *New England Journal of Medicine*, *238*(10), 311-314. https://doi.org/10.1056/NEJM194803042381001

Maganaris, C. N. (2001). Force–length characteristics of *in vivo* human skeletal muscle. *Acta Physiologica Scandinavica*, *172*(4), 279-285. https://doi.org/10.1046/j.1365-201x.2001.00799.x

Mahrous, A., Birch, D., Heckman, C. J., & Tysseling, V. (2024). Muscle Spasms after Spinal Cord Injury Stem from Changes in Motoneuron Excitability and Synaptic Inhibition, Not Synaptic Excitation. *The Journal of Neuroscience*, *44*(1), e1695232023. https://doi.org/10.1523/JNEUROSCI.1695-23.2023

Mangalam, M., & Stergiou, N. (2026). The equilibrium point hypothesis revisited : Why threshold control does not explain human movement. *Experimental Brain Research*, *244*(3), 44. https://doi.org/10.1007/s00221-026-07242-9

Marateb, H. R., McGill, K. C., Holobar, A., Lateva, Z. C., Mansourian, M., & Merletti, R. (2011). Accuracy assessment of CKC high-density surface EMG decomposition in biceps femoris muscle. *Journal of Neural Engineering*, *8*(6), 066002. https://doi.org/10.1088/1741-2560/8/6/066002

Matthews, P. B. C. (1981). Muscle Spindles : Their Messages and Their Fusimotor Supply. *Comprehensive Physiology*, *1981*(12S2), 189-228. https://doi.org/10.1002/j.2040-4603.1981.tb00844.x

May, Z., Fenrich, K. K., Dahlby, J., Batty, N. J., Torres-Espín, A., & Fouad, K. (2017). Following Spinal Cord Injury Transected Reticulospinal Tract Axons Develop New Collateral Inputs to Spinal Interneurons in Parallel with Locomotor Recovery. *Neural Plasticity*, *2017*, 1-15. https://doi.org/10.1155/2017/1932875

Mazzocchio, R. (1997). Involvement of spinal recurrent inhibition in spasticity. Further insight into the regulation of Renshaw cell activity. *Brain*, *120*(6), 991-1003. https://doi.org/10.1093/brain/120.6.991

McDonald, J. W., & Sadowsky, C. (2002). Spinal-cord injury. *The Lancet*, *359*(9304), 417-425. https://doi.org/10.1016/S0140-6736(02)07603-1

McPherson, J. G., Chen, A., Ellis, M. D., Yao, J., Heckman, C. J., & Dewald, J. P. A. (2018). Progressive recruitment of contralesional cortico-reticulospinal pathways drives motor impairment post stroke : Dynamic cortical laterality and arm function post stroke. *The Journal of Physiology*, *596*(7), 1211-1225. https://doi.org/10.1113/JP274968

McPherson, J. G., Ellis, M. D., Harden, R. N., Carmona, C., Drogos, J. M., Heckman, C. J., & Dewald, J. P. A. (2018). Neuromodulatory Inputs to Motoneurons Contribute to the Loss of Independent Joint Control in Chronic Moderate to Severe Hemiparetic Stroke. *Frontiers in Neurology*, *9*, 470. https://doi.org/10.3389/fneur.2018.00470

McPherson, J. G., Ellis, M. D., Heckman, C. J., & Dewald, J. P. A. (2008). Evidence for Increased Activation of Persistent Inward Currents in Individuals With Chronic Hemiparetic Stroke. *Journal of Neurophysiology*, *100*(6), 3236-3243. https://doi.org/10.1152/jn.90563.2008

Merletti, R., & Muceli, S. (2019). Tutorial. Surface EMG detection in space and time : Best practices. *Journal of Electromyography and Kinesiology*, *49*, 102363. https://doi.org/10.1016/j.jelekin.2019.102363

Mesquita, R. N. O., Taylor, J. L., Heckman, C. J., Trajano, G. S., & Blazevich, A. J. (2024). Persistent inward currents in human motoneurons : Emerging evidence and future directions. *Journal of Neurophysiology*, jn.00204.2024. https://doi.org/10.1152/jn.00204.2024

Mesquita, R. N. O., Taylor, J. L., Trajano, G. S., Škarabot, J., Holobar, A., Gonçalves, B. A. M., & Blazevich, A. J. (2022). Effects of reciprocal inhibition and whole-body relaxation on persistent inward currents estimated by two different methods. *The Journal of Physiology*, *600*(11), 2765-2787. https://doi.org/10.1113/JP282765

Michaels, J. A., Dann, B., & Scherberger, H. (2016). Neural Population Dynamics during Reaching Are Better Explained by a Dynamical System than Representational Tuning. *PLOS Computational Biology*, *12*(11), e1005175. https://doi.org/10.1371/journal.pcbi.1005175

Michaels, J. A., Kashefi, M., Zheng, J., Codol, O., Weiler, J., Kersten, R., Lau, J. C., Gribble, P. L., Diedrichsen, J., & Pruszynski, J. A. (2025). Sensory expectations shape neural population dynamics in motor circuits. *Nature*, *648*(8094), 668-677. https://doi.org/10.1038/s41586-025-09690-9

Miller, M., Flansbjer, U.-B., & Lexell, J. (2009). Voluntary Activation of the Knee Extensors in Chronic Poststroke Subjects. *American Journal of Physical Medicine & Rehabilitation*, *88*(4), 286-291. https://doi.org/10.1097/PHM.0b013e318198b569

Miyai, I., Blau, A. D., Reding, M., & Volpe, B. T. (1997). Patients with Stroke Confined to Basal Ganglia Have Diminished Response to Rehabilitation Efforts. *Neurology*, *48*(1), 95-101. https://doi.org/10.1212/WNL.48.1.95

Moolenaar, G.-M., Holloway, J. A., & Trouth, C. O. (1976). Responses of caudal raphe neurons to peripheral somatic stimulation. *Experimental Neurology*, *53*(2), 304-313. https://doi.org/10.1016/0014-4886(76)90073-X

Moore, C. D., Craven, B. C., Thabane, L., Laing, A. C., Frank-Wilson, A. W., Kontulainen, S. A., Papaioannou, A., Adachi, J. D., & Giangregorio, L. M. (s. d.). *Lower-extremity muscle atrophy and fat infiltration after chronic spinal cord injury*.

Morita, H., Shindo, M., Momoi, H., Yanagawa, S., Ikeda, S., & Yanagisawa, N. (2006). Lack of modulation of Ib inhibition during antagonist contraction in spasticity. *Neurology*, *67*(1), 52-56. https://doi.org/10.1212/01.wnl.0000223399.59212.f4

Mottram, C. J., Heckman, C. J., Powers, R. K., Rymer, W. Z., & Suresh, N. L. (2014). Disturbances of motor unit rate modulation are prevalent in muscles of spastic-paretic stroke survivors. *Journal of Neurophysiology*, *111*(10), 2017-2028. https://doi.org/10.1152/jn.00389.2013

Mottram, C. J., Suresh, N. L., Heckman, C. J., Gorassini, M. A., & Rymer, W. Z. (2009). Origins of Abnormal Excitability in Biceps Brachii Motoneurons of Spastic-Paretic Stroke Survivors. *Journal of Neurophysiology*, *102*(4), 2026-2038. https://doi.org/10.1152/jn.00151.2009

Mottram, C. J., Wallace, C. L., Chikando, C. N., & Rymer, W. Z. (2010). Origins of Spontaneous Firing of Motor Units in the Spastic–Paretic Biceps Brachii Muscle of Stroke Survivors. *Journal of Neurophysiology*, *104*(6), 3168-3179. https://doi.org/10.1152/jn.00463.2010

Murray, K. C., Nakae, A., Stephens, M. J., Rank, M., D'Amico, J., Harvey, P. J., Li, X., Harris, R. L. W., Ballou, E. W., Anelli, R., Heckman, C. J., Mashimo, T., Vavrek, R., Sanelli, L., Gorassini, M. A., Bennett, D. J., & Fouad, K. (2010). Recovery of motoneuron and locomotor function after spinal cord injury depends on constitutive activity in 5-HT2C receptors. *Nature Medicine*, *16*(6), 694-700. https://doi.org/10.1038/nm.2160

Musampa, N. K., Mathieu, P. A., & Levin, M. F. (2007). Relationship between stretch reflex thresholds and voluntary arm muscle activation in patients with spasticity. *Experimental Brain Research*, *181*(4), 579-593. https://doi.org/10.1007/s00221-007-0956-6

Naghavi, M., Kyu, H. H., A, B., Aalipour, M. A., Aalruz, H., Ababneh, H. S., Abafita, B. J., Abaraogu, U. O., Abbafati, C., Abbasi, M., Abbaspour, F., Abbastabar, H., Abd Al Magied, A. H. A., Abd ElHafeez, S., Abdalla, A. N., Abdalla, M. A., Abdallah, E. M., Abdeeq, B. A., Abdel Razeq, N. M. I., … Murray, C. J. L. (2025). Global burden of 292 causes of death in 204 countries and territories and 660 subnational locations, 1990–2023 : A systematic analysis for the Global Burden of Disease Study 2023. *The Lancet*, *406*(10513), 1811-1872. https://doi.org/10.1016/S0140-6736(25)01917-8

Negro, F. (2016). Multi-channel intramuscular and surface EMG decomposition by convolutive blind source separation. *J. Neural Eng.*

Ng, S. S. M., & Shepherd, R. B. (2000). Weakness in Patients with Stroke : Implications for Strength Training in Neurorehabilitation. *Physical Therapy Reviews*, *5*(4), 227-238. https://doi.org/10.1179/108331900786166650

Nielsen, J. B., Christensen, M. S., Farmer, S. F., & Lorentzen, J. (2020). Spastic movement disorder : Should we forget hyperexcitable stretch reflexes and start talking about inappropriate prediction of sensory consequences of movement? *Experimental Brain Research*, *238*(7-8), 1627-1636. https://doi.org/10.1007/s00221-020-05792-0

Nielsen, J. B., Petersen, N. T., Crone, C., & Sinkjaer, T. (2005). Stretch Reflex Regulation in Healthy Subjects and Patients with Spasticity. *Neuromodulation: Technology at the Neural Interface*, *8*(1), 49-57. https://doi.org/10.1111/j.1094-7159.2005.05220.x

Nielsen, J., Sinkj�r, T., Toft, E., & Kagamihara, Y. (1994). Segmental reflexes and ankle joint stiffness during co-contraction of antagonistic ankle muscles in man. *Experimental Brain Research*, *102*(2). https://doi.org/10.1007/BF00227521

Niyo, G., Almofeez, L. I., Erwin, A., & Valero-Cuevas, F. J. (2024). A computational study of how an α- to γ-motoneurone collateral can mitigate velocity-dependent stretch reflexes during voluntary movement. *Proceedings of the National Academy of Sciences*, *121*(34), e2321659121. https://doi.org/10.1073/pnas.2321659121

Oliveira, D. S. D., Casolo, A., Balshaw, T. G., Maeo, S., Lanza, M. B., Martin, N. R. W., Maffulli, N., Kinfe, T. M., Eskofier, B. M., Folland, J. P., Farina, D., & Del Vecchio, A. (2022). Neural decoding from surface high-density EMG signals : Influence of anatomy and synchronization on the number of identified motor units. *Journal of Neural Engineering*, *19*(4), 046029. https://doi.org/10.1088/1741-2552/ac823d

Omrani, M., Kaufman, M. T., Hatsopoulos, N. G., & Cheney, P. D. (2017). Perspectives on classical controversies about the motor cortex. *Journal of Neurophysiology*, *118*(3), 1828-1848. https://doi.org/10.1152/jn.00795.2016

Onodera, S., & Hicks, T. P. (2010). Carbocyanine Dye Usage in Demarcating Boundaries of the Aged Human Red Nucleus. *PLoS ONE*, *5*(12), e14430. https://doi.org/10.1371/journal.pone.0014430

Orssatto, L. B. R., Fernandes, G. L., Blazevich, A. J., & Trajano, G. S. (2022). Facilitation–inhibition control of motor neuronal persistent inward currents in young and older adults. *The Journal of Physiology*, JP283708. https://doi.org/10.1113/JP283708

O'Sullivan, F. (1986). A Statistical Perspective on Ill-Posed Inverse Problems. *Statistical Science*, *1*(4). https://doi.org/10.1214/ss/1177013525

Oudega, M., & Perez, M. A. (2012). Corticospinal reorganization after spinal cord injury. *The Journal of Physiology*, *590*(16), 3647-3663. https://doi.org/10.1113/jphysiol.2012.233189

Oya, T., Riek, S., & Cresswell, A. G. (2009). Recruitment and rate coding organisation for soleus motor units across entire range of voluntary isometric plantar flexions :

Recruitment and rate coding strategies for soleus motor units. *The Journal of Physiology*, *587*(19), 4737-4748. https://doi.org/10.1113/jphysiol.2009.175695

Pantano, P., Formisano, R., Ricci, M., Di Piero, V., Sabatini, U., Barbanti, P., Fiorelli, M., Bozzao, L., & Lenzi, G. L. (1995). Prolonged muscular flaccidity after stroke. Morphological and functional brain alterations. *Brain: A Journal of Neurology*, *118 (Pt 5)*, 1329-1338. https://doi.org/10.1093/brain/118.5.1329

Papaioannou, S., & Dimitriou, M. (2021). Goal-dependent tuning of muscle spindle receptors during movement preparation. *Science Advances*, *7*(9), eabe0401. https://doi.org/10.1126/sciadv.abe0401

Pearcey, G. E. P., Khurram, O. U., Beauchamp, J. A., Negro, F., & Heckman, C. J. (2022). *Antagonist tendon vibration dampens estimates of persistent inward currents in motor units of the human lower limb* [Preprint]. Physiology. https://doi.org/10.1101/2022.08.02.502526

Perrier, J., & Cotel, F. (2008). Serotonin differentially modulates the intrinsic properties of spinal motoneurons from the adult turtle. *The Journal of Physiology*, *586*(5), 1233-1238. https://doi.org/10.1113/jphysiol.2007.145706

Perrier, J.-F., & Hounsgaard, J. (2003). 5-HT_2 Receptors Promote Plateau Potentials in Turtle Spinal Motoneurons by Facilitating an L-Type Calcium Current. *Journal of Neurophysiology*, *89*(2), 954-959. https://doi.org/10.1152/jn.00753.2002

Picelli, A., Tamburin, S., Gajofatto, F., Zanette, G., Praitano, M., Saltuari, L., Corradini, C., & Smania, N. (2014). Association between Severe Upper Limb Spasticity and Brain Lesion Location in Stroke Patients. *BioMed Research International*, *2014*, 1-6. https://doi.org/10.1155/2014/162754

Pierrot-Deseilligny, E. (avec Burke, D.). (2012). *The circuitry of the human spinal cord : Spinal and corticospinal mechanisms of movement*. Cambridge University Press.

Pierrot-Deseilligny, E., & Burke, D. J. (2012). *The circuitry of the human spinal cord : Spinal and corticospinal mechanisms of movement*. Cambridge University Press.

Pompeiano, O. (1988). Chapter 7 The role of Renshaw cells in the dynamic control of posture during vestibulospinal reflexes. In *Progress in Brain Research* (Vol. 76, p. 83-95). Elsevier. https://doi.org/10.1016/S0079-6123(08)64494-5

Powers, R. K., & Binder, M. D. (2001). Input-output functions of mammalian motoneurons. In *Reviews of Physiology, Biochemistry and Pharmacology* (Vol. 143, p. 137-263). Springer Berlin Heidelberg. https://doi.org/10.1007/BFb0115594

Powers, R. K., & Heckman, C. J. (2015). Contribution of intrinsic motoneuron properties to discharge hysteresis and its estimation based on paired motor unit recordings : A simulation study. *Journal of Neurophysiology*, *114*(1), 184-198. https://doi.org/10.1152/jn.00019.2015

Powers, R. K., & Heckman, C. J. (2017). Synaptic control of the shape of the motoneuron pool input-output function. *Journal of Neurophysiology*, *117*(3), 1171-1184. https://doi.org/10.1152/jn.00850.2016

Proske, U., & Gandevia, S. C. (2012). The proprioceptive senses : Their roles in signaling body shape, body position and movement, and muscle force. *Physiological Reviews*, *92*(4), 1651-1697. https://doi.org/10.1152/physrev.00048.2011

Prut, Y., & Perlmutter, S. I. (2003). Firing properties of spinal interneurons during voluntary movement. I. State-dependent regularity of firing. *The Journal of Neuroscience: The Official Journal of the Society for Neuroscience*, *23*(29), 9600-9610. https://doi.org/10.1523/JNEUROSCI.23-29-09600.2003

Rehme, A. K., Eickhoff, S. B., Rottschy, C., Fink, G. R., & Grefkes, C. (2012). Activation likelihood estimation meta-analysis of motor-related neural activity after stroke. *NeuroImage*, *59*(3), 2771-2782. https://doi.org/10.1016/j.neuroimage.2011.10.023

Reisman, D. S., McLean, H., Keller, J., Danks, K. A., & Bastian, A. J. (2013). Repeated Split-Belt Treadmill Training Improves Poststroke Step Length Asymmetry. *Neurorehabilitation and Neural Repair*, *27*(5), 460-468. https://doi.org/10.1177/1545968312474118

Renshaw, B. (1941). INFLUENCE OF DISCHARGE OF MOTONEURONS UPON EXCITATION OF NEIGHBORING MOTONEURONS. *Journal of Neurophysiology*, *4*(2), 167-183. https://doi.org/10.1152/jn.1941.4.2.167

Revill, A. L., & Fuglevand, A. J. (2011). Effects of persistent inward currents, accommodation, and adaptation on motor unit behavior : A simulation study. *Journal of Neurophysiology*, *106*(3), 1467-1479. https://doi.org/10.1152/jn.00419.2011

Revill, A. L., & Fuglevand, A. J. (2017). Inhibition linearizes firing rate responses in human motor units : Implications for the role of persistent inward currents: Inhibition linearizes firing rate responses in motor units. *The Journal of Physiology*, *595*(1), 179-191. https://doi.org/10.1113/JP272823

Ronzano, R., Lancelin, C., Bhumbra, G. S., Brownstone, R. M., & Beato, M. (2021). Proximal and distal spinal neurons innervating multiple synergist and antagonist motor pools. *eLife*, *10*, e70858. https://doi.org/10.7554/eLife.70858

Rosenzweig, E. S., Courtine, G., Jindrich, D. L., Brock, J. H., Ferguson, A. R., Strand, S. C., Nout, Y. S., Roy, R. R., Miller, D. M., Beattie, M. S., Havton, L. A., Bresnahan, J. C., Edgerton, V. R., & Tuszynski, M. H. (2010). Extensive spontaneous plasticity of corticospinal projections after primate spinal cord injury. *Nature Neuroscience*, *13*(12), 1505-1510. https://doi.org/10.1038/nn.2691

Rosso, C., & Samson, Y. (2014). The ischemic penumbra : The location rather than the volume of recovery determines outcome. *Current Opinion in Neurology*, *27*(1), 35-41. https://doi.org/10.1097/WCO.0000000000000047

Roux, F., Niare, M., Charni, S., Giussani, C., & Durand, J. (2020). Functional architecture of the motor homunculus detected by electrostimulation. *The Journal of Physiology*, *598*(23), 5487-5504. https://doi.org/10.1113/JP280156

Rupp, R., Biering-Sørensen, F., Burns, S. P., Graves, D. E., Guest, J., Jones, L., Read, M. S., Rodriguez, G. M., Schuld, C., Tansey-MD, K. E., Walden, K., & Kirshblum, S. (2021). International Standards for Neurological Classification of Spinal Cord Injury. *Topics in Spinal Cord Injury Rehabilitation*, *27*(2), 1-22. https://doi.org/10.46292/sci2702-1

Sakai, S. T., Davidson, A. G., & Buford, J. A. (2009). Reticulospinal neurons in the pontomedullary reticular formation of the monkey (Macaca fascicularis). *Neuroscience*, *163*(4), 1158-1170. https://doi.org/10.1016/j.neuroscience.2009.07.036

Sangari, S., & Perez, M. A. (2019). Imbalanced Corticospinal and Reticulospinal Contributions to Spasticity in Humans with Spinal Cord Injury. *The Journal of Neuroscience: The Official Journal of the Society for Neuroscience*, *39*(40), 7872-7881. https://doi.org/10.1523/JNEUROSCI.1106-19.2019

Sangari, S., & Perez, M. A. (2022). Prevalence of spasticity in humans with spinal cord injury with different injury severity. *Journal of Neurophysiology*, *128*(3), 470-479. https://doi.org/10.1152/jn.00126.2022

Schallert, T., Fleming, S. M., Leasure, J. L., Tillerson, J. L., & Bland, S. T. (2000). CNS plasticity and assessment of forelimb sensorimotor outcome in unilateral rat models of stroke, cortical ablation, parkinsonism and spinal cord injury. *Neuropharmacology*, *39*(5), 777-787. https://doi.org/10.1016/S0028-3908(00)00005-8

Schieber, M. H., & Hibbard, L. S. (1993). How Somatotopic Is the Motor Cortex Hand Area? *Science*, *261*(5120), 489-492. https://doi.org/10.1126/science.8332915

Schwindt, P. C., & Crill, W. E. (1980). Properties of a persistent inward current in normal and TEA-injected motoneurons. *Journal of Neurophysiology*, *43*(6), 1700-1724. https://doi.org/10.1152/jn.1980.43.6.1700

Scott, S. H. (2004). Optimal feedback control and the neural basis of volitional motor control. *Nature Reviews. Neuroscience*, *5*(7), 532-546. https://doi.org/10.1038/nrn1427

Scott, S. H., & Kalaska, J. F. (1997). Reaching Movements With Similar Hand Paths But Different Arm Orientations. I. Activity of Individual Cells in Motor Cortex. *Journal of Neurophysiology*, *77*(2), 826-852. https://doi.org/10.1152/jn.1997.77.2.826

Seo, J. P., & Jang, S. H. (2013). Different Characteristics of the Corticospinal Tract According to the Cerebral Origin : DTI Study. *American Journal of Neuroradiology*, *34*(7), 1359-1363. https://doi.org/10.3174/ajnr.A3389

Shadmehr, R., & Krakauer, J. W. (2008). A computational neuroanatomy for motor control. *Experimental Brain Research*, *185*(3), 359-381. https://doi.org/10.1007/s00221-008-1280-5

Shefner, J. M., Berman, S. A., Sarkarati, M., & Young, R. R. (1992). Recurrent inhibition is increased in patients with spinal cord injury. *Neurology*, *42*(11), 2162-2162. https://doi.org/10.1212/WNL.42.11.2162

Skagerberg, G., Björklund, A., Lindvall, O., & Schmidt, R. H. (1982). Origin and termination of the diencephalo-spinal dopamine system in the rat. *Brain Research Bulletin*, *9*(1-6), 237-244. https://doi.org/10.1016/0361-9230(82)90136-8

Škarabot, J., Beauchamp, J. A., & Pearcey, G. E. (2023). *Human motor unit discharge patterns reveal differences in neuromodulatory and inhibitory drive to motoneurons across contraction levels* [Preprint]. Neuroscience. https://doi.org/10.1101/2023.10.16.562612

Škarabot, J., Beauchamp, J. A., & Pearcey, G. E. P. (2025). Human motor unit discharge patterns reveal differences in neuromodulatory and inhibitory drive to motoneurons across contraction levels. *Journal of Neurophysiology*, *134*(5), 1429-1444. https://doi.org/10.1152/jn.00249.2025

Škarabot, J., Thomason, H., Nazaroff, B. M., Connelly, C. D., Valenčič, T., Ho, M. L., Tyagi, K., Beauchamp, J. A., & Pearcey, G. E. P. (2026). The modulation of human motoneuron discharge patterns with contraction force in resistance- and endurance-trained individuals. *Journal of Applied Physiology*, japplphysiol.00835.2025. https://doi.org/10.1152/japplphysiol.00835.2025

Smith, C. C., Paton, J. F. R., Chakrabarty, S., & Ichiyama, R. M. (2017). Descending Systems Direct Development of Key Spinal Motor Circuits. *The Journal of Neuroscience*, *37*(26), 6372-6387. https://doi.org/10.1523/JNEUROSCI.0149-17.2017

Soulard, J., Huber, C., Baillieul, S., Thuriot, A., Renard, F., Aubert Broche, B., Krainik, A., Vuillerme, N., Jaillard, A., & on behalf of the ISIS-HERMES Group. (2020). Motor tract integrity predicts walking recovery : A diffusion MRI study in subacute stroke. *Neurology*, *94*(6). https://doi.org/10.1212/WNL.0000000000008755

Squair, J. W., Skinnider, M. A., & Courtine, G. (2025). Unbiased discovery of neuronal architectures. *Science*, *390*(6773), 566-568. https://doi.org/10.1126/science.adx6741

Steeves, J. D., Lammertse, D., Curt, A., Fawcett, J. W., Tuszynski, M. H., Ditunno, J. F., Ellaway, P. H., Fehlings, M. G., Guest, J. D., Kleitman, N., Bartlett, P. F., Blight, A. R., Dietz, V., Dobkin, B. H., Grossman, R., Short, D., Nakamura, M., Coleman, W. P., Gaviria, M., & Privat, A. (2007). Guidelines for the conduct of clinical trials for spinal cord injury (SCI) as developed by the ICCP panel : Clinical trial outcome measures. *Spinal Cord*, *45*(3), 206-221. https://doi.org/10.1038/sj.sc.3102008

Stephens, J. A., Reinking, R. M., & Stuart, D. G. (1975). Tendon organs of cat medial gastrocnemius : Responses to active and passive forces as a function of muscle length. *Journal of Neurophysiology*, *38*(5), 1217-1231. https://doi.org/10.1152/jn.1975.38.5.1217

Stinear, J. W., & Byblow, W. D. (2004). The contribution of cervical propriospinal premotoneurons in recovering hemiparetic stroke patients. *Journal of Clinical Neurophysiology: Official Publication of the American Electroencephalographic Society*, *21*(6), 426-434. https://doi.org/10.1097/00004691-200411000-00006

Swayne, O. B. C., Rothwell, J. C., Ward, N. S., & Greenwood, R. J. (2008). Stages of Motor Output Reorganization after Hemispheric Stroke Suggested by Longitudinal Studies of Cortical Physiology. *Cerebral Cortex*, *18*(8), 1909-1922. https://doi.org/10.1093/cercor/bhm218

Takeoka, A., Vollenweider, I., Courtine, G., & Arber, S. (2014). Muscle Spindle Feedback Directs Locomotor Recovery and Circuit Reorganization after Spinal Cord Injury. *Cell*, *159*(7), 1626-1639. https://doi.org/10.1016/j.cell.2014.11.019

Thomas, C. K., Bakels, R., Klein, C. S., & Zijdewind, I. (2014). Human spinal cord injury : Motor unit properties and behaviour. *Acta Physiologica*, *210*(1), 5-19. https://doi.org/10.1111/apha.12153

Thomas, C. K., Broton, J. G., & Calancie, B. (1997). Motor unit forces and recruitment patterns after cervical spinal cord injury. *Muscle & Nerve*, *20*(2), 212-220. https://doi.org/10.1002/(SICI)1097-4598(199702)20:2%3C212::AID-MUS12%3E3.0.CO;2-4

Thomas, C. K., & Del Valle, A. (2001). The role of motor unit rate modulation versus recruitment in repeated submaximal voluntary contractions performed by control and spinal cord injured subjects. *Journal of Electromyography and Kinesiology*, *11*(3), 217-229. https://doi.org/10.1016/S1050-6411(00)00055-9

Thomas, C. K., Tucker, M. E., & Bigland-Ritchie, B. (1998). Voluntary Muscle Weakness and Co-Activation After Chronic Cervical Spinal Cord Injury. *Journal of Neurotrauma*, *15*(2), 149-161. https://doi.org/10.1089/neu.1998.15.149

Thomas Carmichael, S., Wei, L., Rovainen, C. M., & Woolsey, T. A. (2001). New Patterns of Intracortical Projections after Focal Cortical Stroke. *Neurobiology of Disease*, *8*(5), 910-922. https://doi.org/10.1006/nbdi.2001.0425

Thrift, A. G., Dewey, H. M., Macdonell, R. A. L., McNeil, J. J., & Donnan, G. A. (2001). Incidence of the Major Stroke Subtypes : Initial Findings From the North East Melbourne Stroke Incidence Study (NEMESIS). *Stroke*, *32*(8), 1732-1738. https://doi.org/10.1161/01.STR.32.8.1732

Todorov, E., & Jordan, M. I. (2002). Optimal feedback control as a theory of motor coordination. *Nature Neuroscience*, *5*(11), 1226-1235. https://doi.org/10.1038/nn963

Tohyama, T., Kinoshita, M., Kobayashi, K., Isa, K., Watanabe, D., Kobayashi, K., Liu, M., & Isa, T. (2017). Contribution of propriospinal neurons to recovery of hand dexterity after corticospinal tract lesions in monkeys. *Proceedings of the National Academy of Sciences of the United States of America*, *114*(3), 604-609. https://doi.org/10.1073/pnas.1610787114

Trajano, G. S., Seitz, L. B., Nosaka, K., & Blazevich, A. J. (2014). Can passive stretch inhibit motoneuron facilitation in the human plantar flexors? *Journal of Applied Physiology*, *117*(12), 1486-1492. https://doi.org/10.1152/japplphysiol.00809.2014

Turpin, N. A., Feldman, A. G., & Levin, M. F. (2017). Stretch-reflex threshold modulation during active elbow movements in post-stroke survivors with spasticity. *Clinical Neurophysiology*, *128*(10), 1891-1897. https://doi.org/10.1016/j.clinph.2017.07.411

Urbin, M. A. (2025). Adaptation in the spinal cord after stroke : Implications for restoring cortical control over the final common pathway. *The Journal of Physiology*, *603*(3), 685-721. https://doi.org/10.1113/JP285563

Urbin, M. A., Royston, D. A., Weber, D. J., Boninger, M. L., & Collinger, J. L. (2019). What is the functional relevance of reorganization in primary motor cortex after spinal cord injury? *Neurobiology of Disease*, *121*, 286-295. https://doi.org/10.1016/j.nbd.2018.09.009

Valenčič, T., Maeo, S., Kluzek, S., Holobar, A., Škarabot, J., & Folland, J. P. (2026). Motor unit discharge properties of the vastii muscles and their modulation with contraction level

depend on the knee-joint angle. *Journal of Applied Physiology*, *140*(1), 322-337. https://doi.org/10.1152/japplphysiol.00951.2024

Vallbo, Å. B. (1970). Discharge Patterns in Human Muscle Spindle Afferents during Isometric Voluntary Contractions. *Acta Physiologica Scandinavica*, *80*(4), 552-566. https://doi.org/10.1111/j.1748-1716.1970.tb04823.x

Vastano, R., & Perez, M. A. (2020). Changes in motoneuron excitability during voluntary muscle activity in humans with spinal cord injury. *Journal of Neurophysiology*, *123*(2), 454-461. https://doi.org/10.1152/jn.00367.2019

Vinti, M., Bayle, N., Hutin, E., Burke, D., & Gracies, J.-M. (2015). Stretch-sensitive paresis and effort perception in hemiparesis. *Journal of Neural Transmission*, *122*(8), 1089-1097. https://doi.org/10.1007/s00702-015-1379-3

Vinti, M., Couillandre, A., Hausselle, J., Bayle, N., Primerano, A., Merlo, A., Hutin, E., & Gracies, J.-M. (2013). Influence of effort intensity and gastrocnemius stretch on co-contraction and torque production in the healthy and paretic ankle. *Clinical Neurophysiology*, *124*(3), 528-535. https://doi.org/10.1016/j.clinph.2012.08.010

Wei, K., Glaser, J. I., Deng, L., Thompson, C. K., Stevenson, I. H., Wang, Q., Hornby, T. G., Heckman, C. J., & Kording, K. P. (2014). Serotonin Affects Movement Gain Control in the Spinal Cord. *Journal of Neuroscience*, *34*(38), 12690-12700. https://doi.org/10.1523/JNEUROSCI.1855-14.2014

Wenger, N., Moraud, E. M., Gandar, J., Musienko, P., Capogrosso, M., Baud, L., Le Goff, C. G., Barraud, Q., Pavlova, N., Dominici, N., Minev, I. R., Asboth, L., Hirsch, A., Duis, S., Kreider, J., Mortera, A., Haverbeck, O., Kraus, S., Schmitz, F., … Courtine, G. (2016). Spatiotemporal neuromodulation therapies engaging muscle synergies improve motor control after spinal cord injury. *Nature Medicine*, *22*(2), 138-145. https://doi.org/10.1038/nm.4025

Wiegner, A. W., Wierzbicka, M. M., Davies, L., & Young, R. R. (1993). Discharge properties of single motor units in patients with spinal cord injuries. *Muscle & Nerve*, *16*(6), 661-671. https://doi.org/10.1002/mus.880160613

Williams, G., Hassett, L., Clark, R., Bryant, A., Olver, J., Morris, M. E., & Ada, L. (2019). Improving Walking Ability in People With Neurologic Conditions : A Theoretical Framework for Biomechanics-Driven Exercise Prescription. *Archives of Physical Medicine and Rehabilitation*, *100*(6), 1184-1190. https://doi.org/10.1016/j.apmr.2019.01.003

Wilson, L. R., Gandevia, S. C., Inglis, J. T., Gracies, J.-M., & Burke, D. (1999). Muscle spindle activity in the affected upper limb after a unilateral stroke. *Brain*, *122*(11), 2079-2088. https://doi.org/10.1093/brain/122.11.2079

Windhorst, U. (1996). ON THE ROLE OF RECURRENT INHIBITORY FEEDBACK IN MOTOR CONTROL. *Progress in Neurobiology*, *49*(6), 517-587. https://doi.org/10.1016/0301-0082(96)00023-8

Wolpert, D. M., & Flanagan, J. R. (2016). Computations underlying sensorimotor learning. *Current Opinion in Neurobiology*, *37*, 7-11. https://doi.org/10.1016/j.conb.2015.12.003

Wolpert, D. M., & Ghahramani, Z. (2000). Computational principles of movement neuroscience. *Nature Neuroscience*, *3 Suppl*, 1212-1217. https://doi.org/10.1038/81497

Wu, M., Hornby, T. G., Hilb, J., & Schmit, B. D. (2005). Extensor spasms triggered by imposed knee extension in chronic human spinal cord injury. *Experimental Brain Research*, *162*(2), 239-249. https://doi.org/10.1007/s00221-004-2173-x

Xu, J., Ejaz, N., Hertler, B., Branscheidt, M., Widmer, M., Faria, A. V., Harran, M. D., Cortes, J. C., Kim, N., Celnik, P. A., Kitago, T., Luft, A. R., Krakauer, J. W., & Diedrichsen, J. (2017). Separable systems for recovery of finger strength and control after stroke. *Journal of Neurophysiology*, *118*(2), 1151-1163. https://doi.org/10.1152/jn.00123.2017

Zaaimi, B., Edgley, S. A., Soteropoulos, D. S., & Baker, S. N. (2012). Changes in descending motor pathway connectivity after corticospinal tract lesion in macaque monkey. *Brain*, *135*(7), 2277-2289. https://doi.org/10.1093/brain/aws115

Zackowski, K. M. (2004). How do strength, sensation, spasticity and joint individuation relate to the reaching deficits of people with chronic hemiparesis? *Brain*, *127*(5), 1035-1046. https://doi.org/10.1093/brain/awh116

Zijdewind, I., & Thomas, C. K. (2003). Motor Unit Firing During and After Voluntary Contractions of Human Thenar Muscles Weakened by Spinal Cord Injury. *Journal of Neurophysiology*, *89*(4), 2065-2071. https://doi.org/10.1152/jn.00492.2002

1. Annexe 1: supplemental material for Study 1

Parameters			F test	p-value	Contrasts for lower intensity (trapeze)	estimate [CI 95%]	d [CI 95%]	p-value	Contrasts for higher intensity (triangle)	estimate [CI 95%]	d [CI 95%]	p-value
ΔF (pps)	Relative	GM	position	**0.0273**	short - intermediate	-0.30 [-0.64, 0.041]	-0.45 [-0.87, -0.027]	0.0919	short - intermediate	0.022 [-0.33, 0.37]	0.032 [-0.40, 0.46]	0.9869
			intensity	0.0968	short - long	0.17 [-0.27, 0.62]	0.26 [-0.29, 0.80]	0.5945	short - long	0.53 [0.085, 0.98]	0.79 [0.24, 1.3]	**0.0180**
			position * intensity	**0.0041**	intermediate - long	0.47 [0.026, 0.92]	0.71 [0.16, 1.3]	**0.0367**	intermediate - long	0.51 [0.065, 0.96]	0.76 [0.21, 1.3]	**0.0231**
		SOL	position	**0.0009**	short - intermediate	0.15 [-1.53, 1.83]	0.19 [-1.5, 1.9]	0.9448	short - intermediate	1.38 [0.090, 2.67]	1.8 [0.39, 3.3]	**0.0350**
			intensity	0.1559	short - long	1.37 [0.22, 2.52]	1.8 [0.55, 3.1]	**0.0219**	short - long	1.45 [0.22, 2.52]	1.9 [0.56, 3.3]	**0.0199**
			position * intensity	**0.0088**	intermediate - long	1.23 [0.12, 2.33]	1.6 [0.39, 2.9]	**0.0285**	intermediate - long	0.075 [-0.97, 1.12]	0.10 [-1.0, 1.2]	0.9810
	Absolute	GM	position	**0.0080**	short - intermediate	0.17 [-0.080, 0.42]	0.33 [-0.071, 0.74]	0.2248	short - intermediate	0.13 [-0.12, 0.38]	0.25 [-0.15, 0.65]	0.4087
			intensity	**0.0019**	short - long	0.39 [0.064, 0.72]	0.76 [0.23, 1.3]	**0.0172**	short - long	0.47 [0.14, 0.78]	0.91 [0.39, 1.4]	**0.0041**
			position * intensity	0.4650	intermediate - long	0.22 [-0.14, 0.58]	0.42 [-0.15, 1.0]	0.3017	intermediate - long	0.34 [-0.0095, 0.69]	0.66 [0.10, 1.2]	0.0575
		SOL	position	0.2453	short - intermediate	0.18 [-1.28, 1.64]	0.36 [-2.0, 2.7]	0.9387	short - intermediate	0.52 [-0.94, 1.98]	1.0 [-1.3, 3.4]	0.6299
			intensity	0.1263	short - long	0.31 [-0.84, 1.47]	0.62 [-1.2, 2.5]	0.7394	short - long	0.98 [-0.13, 2.09]	1.9 [0.11, 3.7]	0.0873
			position * intensity	0.1334	intermediate - long	0.13 [-1.15, 1.41]	0.26 [-1.8, 2.3]	0.9585	intermediate - long	0.46 [-0.80, 1.72]	0.91 [-1.1, 2.9]	0.6048
acceleration (pps/%MVC)	Relative	GM	position	0.9785	short - intermediate	-0.095 [-0.24, 0.053]	-0.29 [-0.67, 0.086]	0.2773	short - intermediate	0.098 [-0.031, 0.23]	0.30 [-0.026, 0.63]	0.1593
			intensity	**<.0001**	short - long	-0.11 [-0.27, 0.046]	-0.34 [-0.73, 0.059]	0.2073	short - long	0.091 [-0.062, 0.24]	0.28 [-0.11, 0.66]	0.3159
			position * intensity	**0.0005**	intermediate - long	-0.015 [-0.18, 0.15]	-0.047 [-0.47, 0.38]	0.9726	intermediate - long	-0.0076 [-0.17, 0.15]	0.023 [-0.43, 0.38]	0.9922
		SOL	position	0.1210	short - intermediate	0.27 [-0.043, 0.58]	1.1 [0.038, 2.2]	0.0996	short - intermediate	0.023 [-0.25, 0.30]	0.098 [-0.86, 1.1]	0.9733
			intensity	**0.0288**	short - long	0.26 [-0.071, 0.60]	1.1 [-0.065, 2.3]	0.1432	short - long	0.20 [-0.079, 0.49]	0.87 [-0.13, 1.9]	0.1796
			position * intensity	0.0678	intermediate - long	-0.0041 [-0.31, 0.30]	-0.018 [-1.1, 1.0]	0.9994	intermediate - long	0.18 [-0.076, 0.44]	0.77 [-0.13, 1.7]	0.1932
acceleration (pps/N.m)	Absolute	GM	position	**0.0229**	short - intermediate	0.041 [-0.12, 0.20]	0.11 [-0.25, 0.47]	0.8193	short - intermediate	0.17 [0.036, 0.31]	0.46 [0.16, 0.76]	**0.0116**
			intensity	**<.0001**	short - long	0.052 [-0.094, 0.20]	0.14 [-0.18, 0.46]	0.6683	short - long	0.22 [0.088, 0.35]	0.58 [0.29, 0.87]	**0.0010**
			position * intensity	**0.0254**	intermediate - long	0.011 [-0.15, 0.17]	0.029 [-0.31, 0.37]	0.9842	intermediate - long	0.047 [-0.080, 0.17]	0.12 [-0.15, 0.40]	0.6322
		SOL	position	0.8834	short - intermediate	0.13 [-0.20, 0.46]	0.49 [-0.52, 1.5]	0.5911	short - intermediate	-0.042 [-0.31, 0.23]	-0.15 [-0.96, 0.65]	0.9129
			intensity	**0.0099**	short - long	0.056 [-0.29, 0.40]	0.21 [-0.84, 1.3]	0.9155	short - long	0.017 [-0.28, 0.32]	0.061 [-0.85, 0.97]	0.9886
			position * intensity	0.3426	intermediate - long	-0.077 [-0.36,0.20]	-0.28 [-1.1, 0.58]	0.7842	intermediate - long	0.058 [-0.17, 0.29]	0.21 [-0.48, 0.91]	0.7919
brace height (%)	Relative	GM	position	**0.0096**	short - intermediate	-0.039 [-0.078, -0.00038]	-0.44 [-0.81, -0.078]	**0.0474**	short - intermediate	-0.036 [-0.069, -0.0021]	-0.41 [-0.72, -0.090]	0.0360
			intensity	**<.0001**	short - long	-0.035 [-0.086, 0.017]	-0.39 [-0.88, 0.090]	0.2328	short - long	-0.094 [-0.15,-0.044]	-1.1 [-1.6, -0.59]	**0.0003**
			position * intensity	**<.0001**	intermediate - long	0.0043 [-0.034, 0.042]	0.050 [-0.31, 0.41]	0.9584	intermediate - long	-0.059 [-0.094, -0.023]	-0.67 [-1.0, -0.33]	**0.0010**
		SOL	position	0.2589	short - intermediate	0.059 [-0.074, 0.19]	0.49 [-0.42, 1.4]	0.5173	short - intermediate	-0.0096 [-0.13, 0.11]	-0.080 [-0.87, 0.71]	0.9731
			intensity	0.7339	short - long	-0.030 [-0.16, 0.10]	-0.25 [-1.2, 0.67]	0.8445	short - long	-0.019 [-0.12, 0.10]	-0.16 [-0.82, 0.51]	0.8741
			position * intensity	0.2824	intermediate - long	-0.090 [-0.23,0.050]	-0.74 [-1.7, 0.22]	0.2680	intermediate - long	-0.0091 [-0.11, 0.096]	-0.076 [-0.79, 0.64]	0.9724
	Absolute	GM	position	0.2372	short - intermediate	-0.0078 [-0.056, 0.040]	-0.087 [-0.53, 0.36]	0.9172	short - intermediate	-0.049 [-0.093, -0.0060]	-0.55 [-0.96, -0.15]	**0.0239**
			intensity	**<.0001**	short - long	0.0069 [-0.041, 0.055]	0.078 [-0.37, 0.52]	0.9317	short - long	-0.032 [-0.078, 0.014]	-0.36 [-0.78, 0.066]	0.2084
			position * intensity	**0.0151**	intermediate - long	0.015 [-0.032, 0.061]	0.16 [-0.27, 0.60]	0.7204	intermediate - long	0.017 [-0.024, 0.059]	0.20 [-0.18, 0.58]	0.5415
		SOL	position	0.8274	short - intermediate	0.050 [-0.078, 0.18]	0.46 [-0.52, 1.44]	0.6135	short - intermediate	-0.090 [-0.19, 0.012]	-0.83 [-1.6, -0.054]	0.0872
			intensity	0.5705	short - long	0.018 [-0.099, 0.13]	0.16 [-0.73, 1.1]	0.9273	short - long	-0.048 [-0.14, 0.046]	-0.45 [-1.2, 0.26]	0.3824
			position * intensity	**0.02617**	intermediate - long	-0.032 [-0.14, 0.073]	-0.30 [-1.1, 0.5]	0.7415	intermediate - long	0.042 [-0.040,0.12]	0.39 [-0.23, 1.0]	0.3956

Detailed statistical results for all parameters (i.e., ΔF, acceleration, brace height, attenuation, recruitment threshold and maxcimal discharge rate), for the Relative and Absolute contractions and the GM and SOL muscles. *P-values for F tests of main effects (i.e., position and intensity) and interaction (i.e., position*interaction) were computed with type III analysis of variance with Satterthwaite's method. Contrasts between the positions are inform with estimates and standardized effect sizes, with 95% confidence intervals and p-values. Pps : pulse per second ; MVC : maximal voluntary contraction.*

2. Annexe 2 : supplemental material for Study 2

2.A. Comparing muscle lengths at similar absolute contraction torque

Supplementary methods

In the core manuscript, to assess how motoneuron behavior adapts to muscle length, participants performed contractions at an intermediate muscle length (ankle at 0°) and at a short muscle length (20° plantarflexion). These triangular contractions reached 40% of the MVT at the respective joint position. However, because plantarflexion torque-generating capacity increases from short to intermediate muscle lengths, an additional contraction was performed at the intermediate position (0°), with torque matched to 40% MVT obtained at the short muscle length (20°). In addition, participants who were able to perform a contraction at 10° of dorsiflexion completed this condition at a torque matched to 40% MVT obtained at the short muscle length. This allowed comparison across a wider range of muscle lengths by including a long muscle length condition.

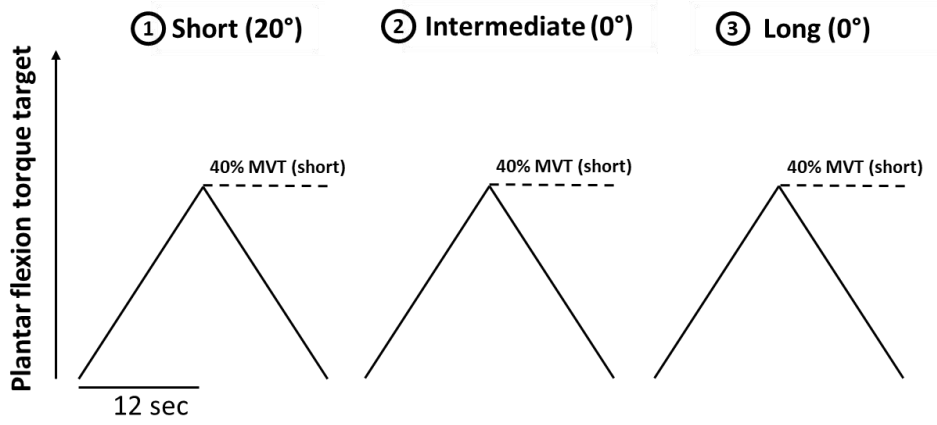

Supplementary Figure 1. Experimental setup. *Participants performed isometric submaximal plantarflexions at three ankle positions, corresponding to different plantar flexor lengths: 20° of plantar flexion(short muscle length position), 0° (intermediate muscle length position), and 10° of dorsiflexion. The intensity of the plantarflexions followed either the same absolute torque, which correspond to 40% of the maximal voluntary contraction (MVT) in the short muscle length position.*

Supplementary results

Recruitment threshold and rate coding

For the following results, the effects of interest are those involving interactions between group and muscle length (short, intermediate or long), including both group-muscle length interactions and group-muscle length-muscle interactions.

Participants did not perform maximal voluntary contractions at the long muscle length position, precluding determination of recruitment thresholds expressed as a percentage of MVT. Accordingly, in this condition, recruitment threshold was defined as the delay between contraction onset and the first firing. There was a significant interaction between group, muscle length, and muscle for recruitment threshold ($p > 0.0001$). Specifically, the control group showed a higher recruitment threshold in the GM at short compared with long muscle length by 1.9 s (95% CI: [0.9–3.0], $d = 0.67$, $p = 0.0002$). The incomplete SCI group showed higher recruitment threshold in the SOL at short than at long muscle length by 1.2 s (95% CI: [0.1–2.3], $d = 0.41$, $p = 0.0346$).

When considering firing rate at recruitment, there was a significant interaction between group and muscle length ($p = 0.0030$), with no significant interaction between group, muscle length, and muscle ($p = 0.9905$). Specifically, the control group showed a higher firing rate at recruitment at short compared with intermediate ($d = 0.72$, $p < 0.0001$) and long muscle length ($d = 0.90$, $p = 0.0001$), regardless of the muscle. Conversely, no difference between muscle lengths was observed in the incomplete SCI group (all $p > 0.1612$).

When considering firing rate modulation, there was a significant interaction between group and muscle length ($p = 0.0144$), with no significant interaction between group, muscle length, and muscle ($p = 0.0691$). Specifically, the control group showed a higher firing rate modulation at short compared to intermediate ($d = 0.51$, $p = 0.0019$) and long muscle length ($d = 0.92$, $p < 0.0001$), as well as a higher firing rate modulation at intermediate compared to long muscle length ($d = 0.41$, $p = 0.0203$), regardless of the muscle. Conversely, no difference between muscle lengths was observed in the incomplete SCI group (all $p > 0.1534$).

When considering peak firing rate, there was a significant interaction between group, muscle length, and muscle ($p = 0.0439$). Specifically, the control group showed a higher peak firing rate in the GM at short than at intermediate by 2.2 pps (95% CI: [1.3–3.0], $d = 1.5$, $p < 0.0001$)

and long muscle length by 2.8 pps (95% CI: [1.7–3.9], d = 2.0, p < 0.0001); and a higher peak firing rate in the SOL at short than at intermediate by 1.0 pps (95% CI: [0.3–1.7], d = 0.7, p = 0.0036) and long muscle length by 1.9 pps (95% CI: [1.1–2.7], d = 1.3, p < 0.0001), as well as at intermediate than at long muscle length by 0.9 pps (95% CI: [0.2–1.5], d = 0.6, p = 0.0118). Conversely, no difference between muscle lengths was observed in the incomplete SCI group (all p > 0.1500).

Estimates of synaptic inputs to motoneurons

There was a significant interaction between group and muscle length for acceleration (p = 0.0354), with no significant interaction between group, muscle length, and muscle (p = 0.2607). Specifically, the control group showed a higher acceleration at short compared with intermediate (d = 0.46, p = 0.0028) and long muscle length (d = 0.51, p = 0.0186), regardless of the muscle. Conversely, no difference between muscle lengths was observed in the incomplete SCI group (all p > 0.9727). There were no significant interactions involving the group factor for attenuation (all p > 0.2343) and brace height (all p > 0.1023).

When considering ΔF, there was a significant interaction between group and muscle length (p = 0.0203), with no significant interaction between group, muscle length, and muscle (p = 0.0765). Specifically, the control group showed a higher ΔF at short compared with long muscle length (d = 0.65, p = 0.0167), regardless of the muscle. Conversely, no difference between muscle lengths was observed in the incomplete SCI group (all p > 0.8960).

When considering normalized ΔF, there was a significant interaction between group, muscle length, and muscle (p < 0.0001). Specifically, the control group showed a higher normalized ΔF in the intermediate compared with the short (by 19%; 95% CI: [3–35], d = 0.79, p < 0.0001) and long (by 29% ; 95% CI: [11–47], d = 1.18, p < 0.0001) muscle lengths; and the incomplete SCI group showed a higher normalized ΔF in the short compared with the intermediate length (by 10% ; 95% CI: [0–19], d = 0.40, p < 0.0406).

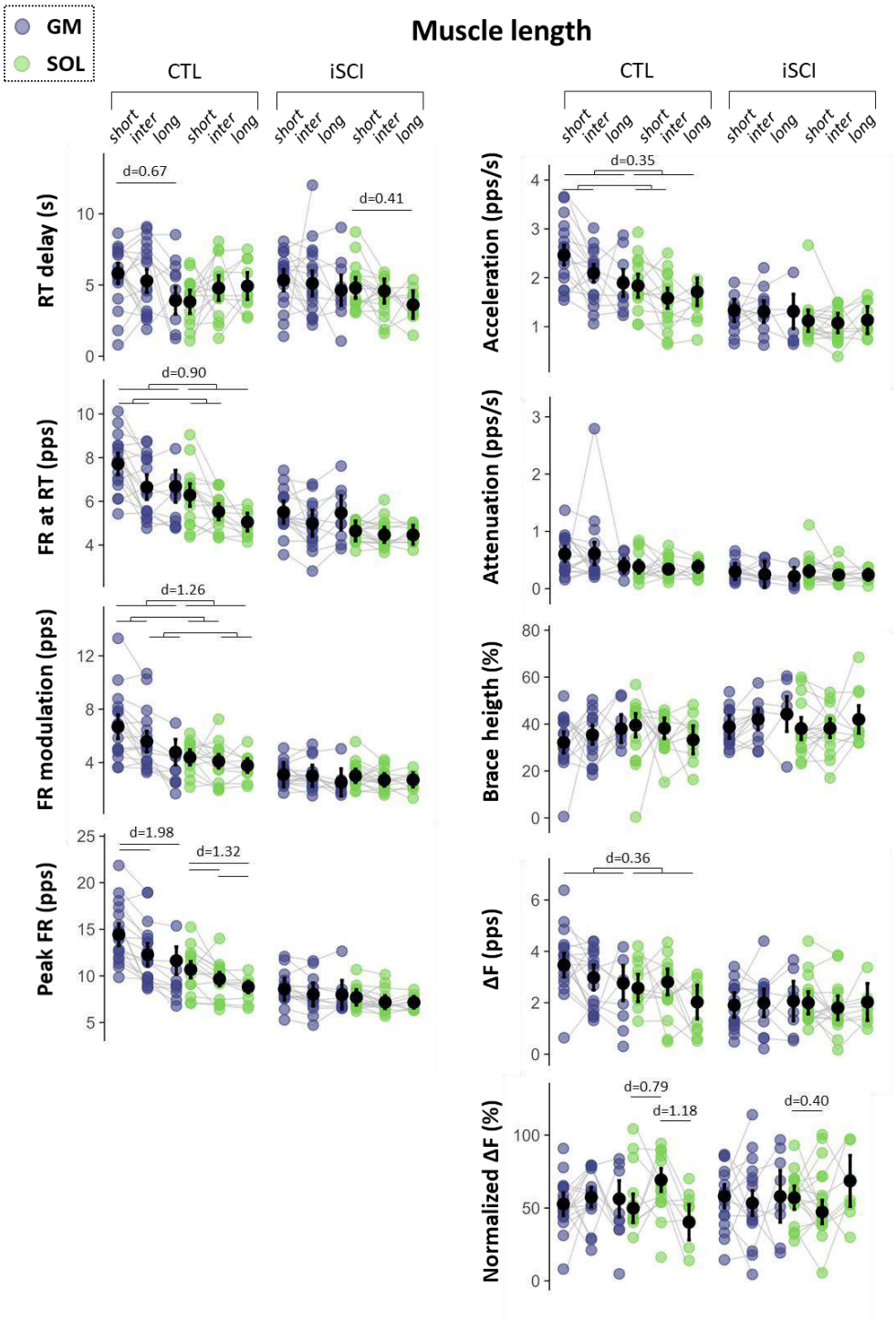

Supplementary Figure 2. Motoneuron recruitment thresholds, rate coding and estimates of synaptic inputs to motoneurons with changes of muscle lengths, at same absolute torque level. *The incomplete SCI (iSCI) and control (CTL) groups are compared at either the same absolute torque (40% MVT of the short muscle length position). Recruitment threshold (RT), firing rate at recruitment (DR RT), firing rate modulation (FR modulation), and peak firing rate (max DR), acceleration slope, attenuation slope, brace height, ΔF, and normalized ΔF were obtained from the gastrocnemius medialis (GM, purple) and soleus (SOL, green). Colored dots represent participant averages, while black dots and bars indicate the estimated marginal means with 95% confidence intervals predicted by linear mixed-effects models. Cohen's d is reported for significant differences.*

2.B. Comparing the effects of muscle length and vibration in tracked motoneurons

Supplementary methods 2

In the core manuscript, to assess how motoneuron behavior changed with changes in muscle length and the application of vibration, the entire set of decomposed motoneurons was used. This approach allows maximization of the number of motoneurons and participants included in the analysis. However, it may lead to comparisons between different motoneurons across conditions. Thus, we complemented our approach by tracking motoneurons across conditions (i.e., changes in ankle angle and application of vibration).

To achieve this, the motor unit filters identified at the short muscle length were applied to the extended and whitened EMG signals of the intermediate muscle length condition (Francic & Holobar, 2021). The resulting spike trains were compared with those initially obtained. A motor unit was considered tracked if at least 30% of the discharge times were shared. Only the motor units tracked across the two muscle lengths were included in the analyses. The same procedure was performed between contractions with and without vibration.

The statistical models used for these comparisons were adapted by adding a random intercept for each motoneuron [e.g., lmer(metric ~ positiongroupmuscle + (positiongroupmuscle|id_participant) + (1|id_participant:id_MU)].

Supplementary results 2

Recruitment threshold and rate coding

For the following results, the effects of interest are those involving interactions between group and condition (muscle length or vibration), including both group-condition interactions and group-condition-muscle interactions.

For the muscle length condition, there was a significant interaction between group, muscle length and muscle for recruitment threshold ($p = 0.0037$). Specifically, the control group showed a higher recruitment threshold in the GM at the intermediate than at the short muscle length by 5.5% MVT (95% CI: [1.8–9.1], $d = 1.0$, $p = 0.0037$), with no other significant differences (Fig. 3). When considering firing rate at recruitment, there were no significant interactions involving the group factor (all $p > 0.1372$). Conversely, there was an interaction between group, muscle length and muscle for firing rate modulation ($p = 0.0206$) and peak firing rate (p

= 0.0381). Specifically, the control group showed higher firing rate modulation by 0.86 pps (95% CI: [0.34–1.38], d = 0.80, p = 0.0019) and higher peak firing rate by 1.39 pps (95% CI: [0.79–1.98], d = 1.6, p < 0.0001) in the GM at short compared with the intermediate muscle length, while there was no difference in the SOL or in either muscle in the incomplete SCI group (all p > 0.0730).

For the vibration condition, there were no significant interactions involving the group factor for recruitment threshold (all p > 0.1722). There was an interaction between group and vibration for firing rate at recruitment (p = 0.0212) and for peak firing rate (p = 0.0007), with no significant interaction between group, vibration, and muscle (all p > 0.2815). Specifically, the control group showed a lower firing rate at recruitment (d = 0.75, p = 0.0071) and a lower peak firing rate (d = 1.1, p = 0.0003) in the presence of vibration; whereas the incomplete SCI group showed no significant changes with vibration. There were no significant interactions involving the group factor for rate modulation (all p > 0.1304).

Estimates of synaptic inputs to motoneurons

For the muscle length condition, there was no interaction between group and muscle length, nor between group, muscle length, and muscle for acceleration (p > 0.4480), attenuation (p > 0.0756), or brace height (p > 0.0684) (Fig. 4). When considering ΔF, there was an interaction between group, muscle and muscle length (p = 0.0096). Specifically, there were no significant changes in the incomplete SCI group (all p > 0.0783), whereas the control group showed higher ΔF at short muscle length in the GM by 0.43 pps (95% CI: [0.18–0.68], d = 0.62, p = 0.0017) and lower ΔF at short muscle length in the SOL by 0.65 pps (95% CI: [0.17–1.12], d = 0.94, p = 0.0076). By contrast, when considering normalized ΔF, there was no significant interaction between group and muscle length (p = 0.1004), nor between group, muscle length, and muscle (p = 0.6264).

For the vibration condition, there was no interaction between group and vibration, nor between group, muscle length, and muscle for brace height (all p > 0.0791), acceleration (all p > 0.0635), or attenuation (all p > 0.0855). When considering ΔF, there was a significant interaction between group and vibration (p = 0095) with no significant interaction between group, vibration, and muscle (all p > 0.0856). Specifically, there were no significant difference in the incomplete SCI group (p = 0.5155), whereas the control group showed higher ΔF without than with vibration, regardless of the muscle (d = 0.74, p = 0.0060). By contrast, when considering normalized

ΔF, there was no significant interaction was found between group and vibration (p = 0. 7497), nor between group, vibration, and muscle (p = 0.2307).

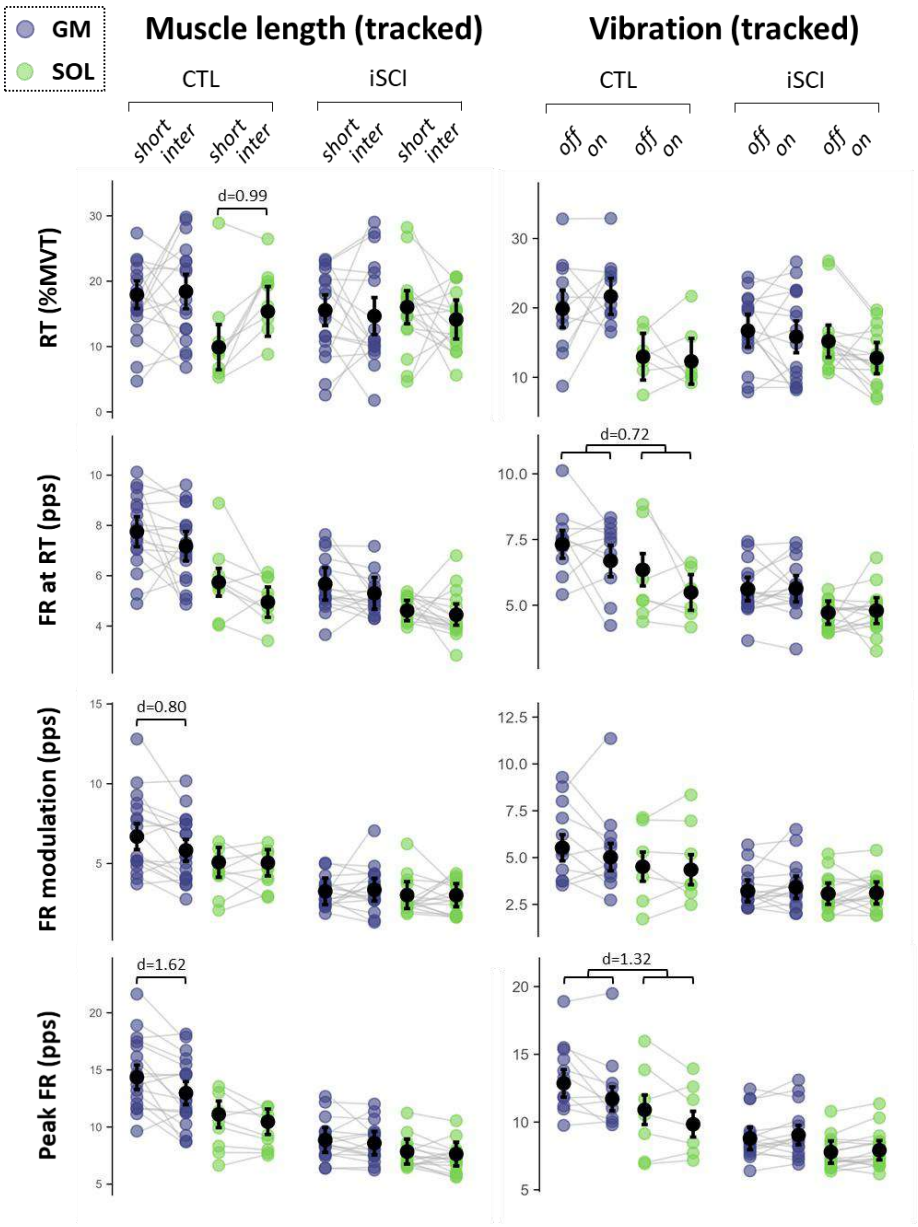

Supplementary Figure 3. Effect of muscle length and vibration in motoneuron recruitment threshold and rate coding, with tracked motoneurons across conditions. *The modulation of motoneuron rate coding and recruitment threshold between the incomplete SCI (iSCI) and control (CTL) groups are compared in response to changes in muscle length at the same relative torque (40% MVT), and the application of tendon vibration to antagonist muscles, at short muscle length (20° of plantarflexion). Recruitment threshold (RT), firing rate at recruitment (DR RT), firing rate modulation (FR modulation), and peak firing rate (peak FR), were obtained from the gastrocnemius medialis (GM, purple) and soleus (SOL, green). Colored dots represent participant averages, while black dots and bars indicate the estimated marginal means with 95% confidence intervals predicted by linear mixed-effects models. Cohen's d is reported for significant results (p < 0.05).*

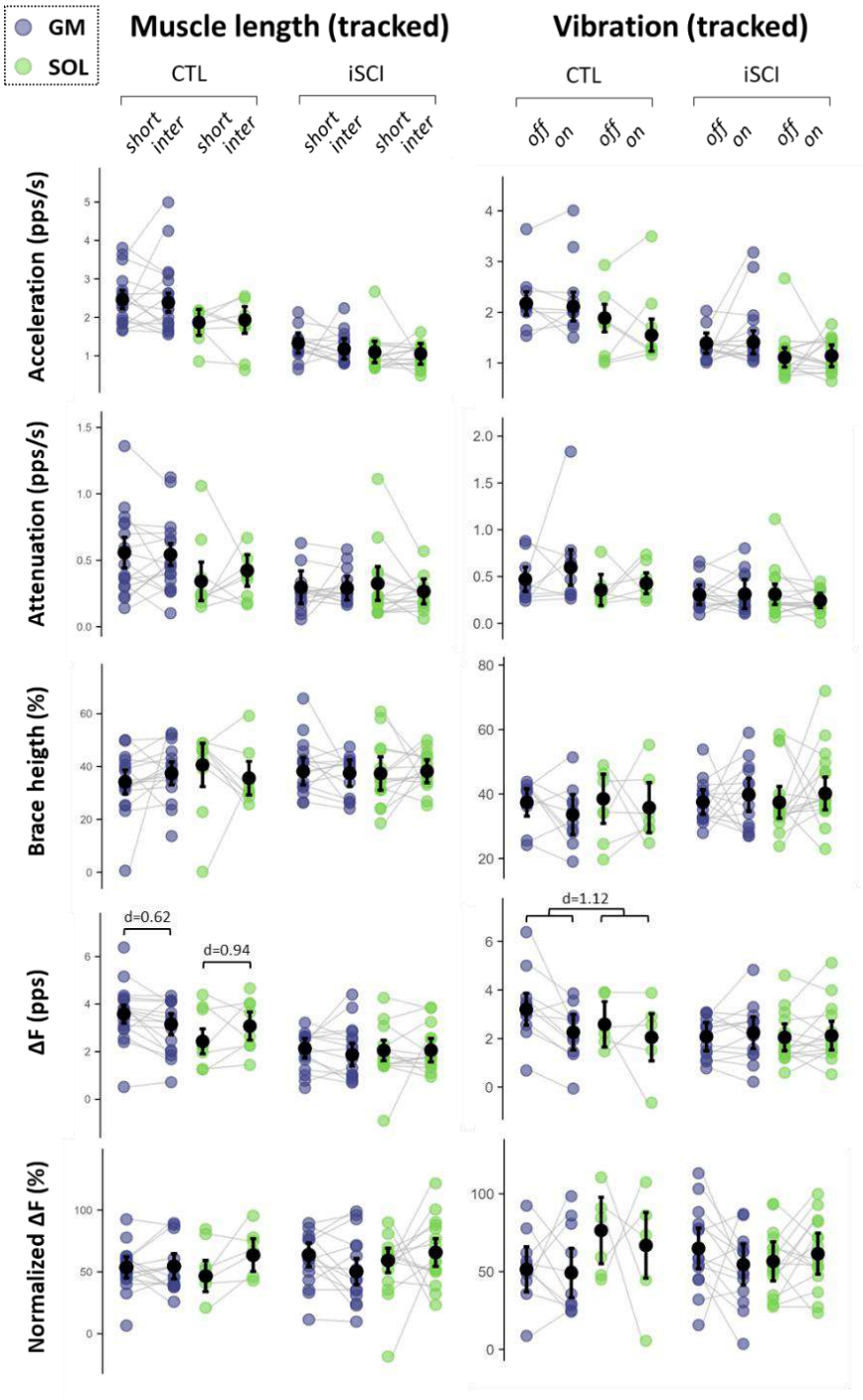

Supplementary Figure 4. Effect of muscle length and vibration in estimates of synaptic inputs to motoneurons, with tracked motoneurons across conditions. *The modulation of motoneuron estimates of synaptic inputs to motoneurons between the incomplete SCI (iSCI) and control (CTL) groups are compared in response to changes in muscle length at the same relative torque (40% MVT), and the application of tendon vibration to antagonist muscles, at short muscle length (20° of plantarflexion). The acceleration slope, attenuation slope, brace height, ΔF, and normalized ΔF were obtained from the gastrocnemius medialis (GM, purple) and soleus (SOL, green). Colored dots represent participant averages, while black dots and bars indicate the estimated marginal means with 95% confidence intervals predicted by linear mixed-effects models. Cohen's d is reported for significant results ($p < 0.05$).*

COLLEGE DOCTORAL PAYS DE LA LOIRE
ED EDUCATION, COGNITION, LANGAGES, INTERACTIONS, SANTE
Nantes Université

Titre : Estimation non invasive des entrées synaptiques des motoneurones α spinaux chez l'homme : effets de la position articulaire et des lésions du système nerveux central

Mots clés : unité motrice, parésie, inhibition, courants entrants persistants, neuromodulation

Résumé : Malgré la complexité des réseaux de neurones qui élaborent le mouvement volontaire, la contraction musculaire repose in fine sur un seul type de neurone, le motoneurone α. L'ensemble des influences qui s'exercent sur ce dernier peut être regroupé en trois grands types d'entrées synaptiques : excitatrices, inhibitrices et neuromodulatrices. Ces différentes entrées laissent des signatures caractéristiques dans l'activité des motoneurones α. En s'appuyant sur cette propriété, il est possible d'estimer les entrées synaptiques conduisant à l'activité des motoneurones α, qui peut elle-même être recueillie par décomposition des signaux d'électromyographie de surface. Sur cette base, les travaux de cette thèse visent à estimer les entrées synaptiques des motoneurones α lors de changements de position articulaire, ainsi qu'après un accident vasculaire cérébral (AVC) ou une lésion de la moelle épinière (LME). Ces travaux ont mis en évidence une augmentation des entrées inhibitrices après un AVC ou une LME, suggérant qu'elles contribuent à la diminution de la capacité à augmenter l'activité des motoneurones α. De plus, alors que les participants sains semblent adapter leurs entrées synaptiques à la position articulaire, notamment via une régulation des entrées inhibitrices, une telle adaptation n'est pas observée après un AVC ou une LME. Ces résultats indiquent que les entrées inhibitrices sont à la fois excessives et peu adaptables dans ces deux pathologies. Enfin, une augmentation des entrées neuromodulatrices n'a été observée qu'après un AVC, suggérant une organisation distincte des entrées synaptiques contribuant à la faiblesse musculaire, et appelant potentiellement à des stratégies thérapeutiques différenciées.

Title: Non-invasive estimation of synaptic inputs to human spinal α-motoneurons: effects of joint position and central nervous system injury

Keywords: motor unit, paresis, inhibition, persistant inward currents, neuromodulation

Abstract: Despite the complexity of the neural networks underlying voluntary movement, muscle contraction ultimately relies on a single type of neuron, the α-motoneuron. All the influences acting on it can be grouped into three main types of synaptic inputs: excitatory, inhibitory and neuromodulatory. These different inputs leave characteristic signatures in the activity of α-motoneurons. Based on this property, it is possible to estimate the synaptic inputs driving the activity of α-motoneurons, which can itself be obtained through decomposition of surface electromyography signals. On this basis, the work of this thesis aims to estimate the synaptic inputs of α-motoneurons during changes in joint position, as well as after stroke or spinal cord injury (SCI). This work has highlighted an increase in inhibitory inputs after stroke or SCI, suggesting that they contribute to the reduced ability to increase α-motoneuron activity. Furthermore, whereas healthy participants appear to adapt their synaptic inputs to joint position, notably via regulation of inhibitory inputs, such adaptation is not observed after stroke or SCI. These results indicate that inhibitory inputs are both excessive and poorly adaptable in these two pathologies. Finally, an increase in neuromodulatory inputs was observed only after stroke, suggesting a distinct organisation of synaptic inputs contributing to muscle weakness, and potentially calling for differentiated therapeutic strategies.